AFAPL-TR-64-135

HIGH TEMPERATURE THERMOELECTRIC RESEARCH

TECHNICAL REPORT NO. AFAPL-TR-64-135

15 DECEMBER 1964

AIR FORCE AERO PROPULSION LABORATORY
RESEARCH AND TECHNOLOGY DIVISION
AIR FORCE SYSTEMS COMMAND
WRIGHT-PATTERSON AIR FORCE BASE, OHIO

Project No. 8173, Task No. 817302-9

(Prepared under Contract No. AF 33(615)-1084 by Monsanto Research Corporation, Dayton, Ohio; C. M. Henderson, F. G. Ault, E. R. Beaver, D. H. Harris, W. H. Hedley, R. J. Janowiecki, Authors)

NOTICES

When Government drawings, specifications, or other data are used for any purpose other than in connection with a definitely related Government procurement operation, the United States Government thereby incurs no responsibility nor any obligation whatsoever; and the fact that the Government may have formulated, furnished, or in any way supplied the said drawings, specifications, or other data, is not to be regarded by implication or otherwise as in any manner licensing the holder or any other person or corporation, or conveying any rights or permission to manufacture, use, or sell any patented invention that may in any way be related thereto.

Qualified requesters may obtain copies of this report from the Defense Documentation Center (DDC), (formerly ASTIA), Cameron Station, Bldg. 5, 5010 Duke Street, Alexandria 4, Virginia.

This report has been released to the Office of Technical Services, U. S. Department of Commerce, Washington 25, D. C., for sale to the general public.

Copies of this report should not be returned to the Aeronautical Systems Division unless return is required by security considerations, contractual obligations, or notice on a specific document.

FOREWORD

This report describes work performed under Contract AF 33(615)-1084, Project No. 8173, Task No. 817302-9 during the period 15 September 1963 through 30 October 1964. The contract concerns development of high-temperature thermoelectric generators and was under sponsorship of the Flight Vehicle Power Branch, AF Aero Propulsion Laboratory, Research and Technology Division, Wright-Patterson Air Force Base, Ohio. For the Air Force, Mr. Charles Glassburn served as project engineer until May 1964 and was then succeeded by Captain R. B. Morrow, Jr.

Work on the contract has been conducted at the Dayton Laboratory of Monsanto Research Corporation, with C. M. Henderson as project leader. Working with him were R. G. Ault, E. R. Beaver, D. H. Harris, W. H. Hedley, H. B. Jankowsky, R. J. Janowiecki and L. J. Reitsma. Technical assistance was provided by R. R. Hawley, R. Hedges, D. Reinhardt, V. Ruzic, D. Sevy, D. Sheppard and D. Zanders.

This is the final technical report, unclassified, concluding the work on contract AF 33(615)-1084.

ABSTRACT

Nominal 50-watt(e) and 15-watt(e) laboratory model generators were designed, fabricated and subjected to sustained and thermal cycling tests at a hot-junction temperature of ~1200°C, and cold junctions of ~570°C in a vacuum of 10^{-5} - 10^{-6} torr. Both generators, constructed of solid-state, bonded, segmented, p- and n-type thermoelements showed good resistance to degradation under these conditions. The 50-watt(e) generator completed ~1200 hours of operation without degradation of its power output. The output of the 15-watt(e) model, after 2100 hours without degradation, decreased by 9% during an additional 1400 hours of sustained testing and a further 264 hours of thermal cycling tests. Degradation of the 15-watt(e) model appears to have resulted largely from deterioration of the electrical resistance of the ceramic insulation used to reduce its thermal shunt losses.

Improvements in the properties of thermoelectric materials and interface bonding techniques for thermoelements were achieved to yield p-n couples with 17% higher performance, relative to 1962-63 couples. Various techniques were investigated for screening p- and n-type thermoelements to 1200°C in a vacuum. Fundamental investigations of the thermoelectric materials and studies of hot-pressing and arc-plasma fabrication techniques indicated that significant further improvements in the performance of high-temperature thermoelements can be achieved.

Nuclear reactor, radioisotope, and solar-heated, high-temperature, thermoelectric, space-powered system concepts were proposed and preliminarily investigated. These studies showed that high-temperature (1200°C) thermoelectric space-type power units, ranging in size from a few watts to several hundred KW output, can be designed for performances from 335 lbs./KW(e) for a solar-concentrating type system to 15 lbs./KW(e) for 350 KW(e) or larger space power systems utilizing fast-reactor heat sources. High-temperature, radioisotope-heated, thermoelectric space-type units, of optimized design concepts and fabricated with state-of-the-art segmented p- and n-type thermoelements, are capable of 7-9.5 watt(e)/lb. (100-140 lb./KW(e)) performance, including the weight of the encapsulated isotope heat source.

TABLE OF CONTENTS

TABLE OF CONTENTS (Cont'd)

ILLUSTRATIONS

ILLUSTRATIONS (Cont'd)

ILLUSTRATIONS (Cont'd)

ILLUSTRATIONS (Cont'd)

ILLUSTRATIONS (Cont'd)

ILLUSTRATIONS (Cont'd)

TABLES

TABLES (Cont'd)

TABLES (Cont'd)

TABLES (Cont'd)

TABLES (Cont'd)

TABLES (Cont'd)

TABLES (Cont'd)

TABLES (Cont'd)

TABLES (Cont'd)

SYMBOLS

A	Atomic weight of lattice, g; area of thermoelement, $in.^2$; effective isothermal radiator area
A_I	Atomic weight of impurity, g
a	Interatomic distance, Å
b	Burger's vector, cm.
C	Specific heat
D	Grain diameter, cm.; cylinder diameter, cm.
d	Dispersed phase particle diameter, cm.
E	Difference in volume thermal expansion coefficients
E_L	Voltage output of generator under load, volts
E_{oc}	Open-circuit voltage, volts
I	Current, amperes
k	Thermal conductivity, watt/cm °C
L	Length of thermoelement, in.
ℓ	Phonon mean free path
N	Number of dislocations
OD	Outside diameter
P	Power output of generator under load, watts
P_{M_1}	Maximum power output of generator under matched resistance load at test conditions, watts
P_{M_2}	Maximum power output (P_{M_1}) of generator at any test condition, adjusted by ratio of the square of the average ΔT_{np} at a reference period to the square of the ΔT_{np} produced by the thermal conditions of any other period, watts
Q	Heat input to the generator, watts

SYMBOLS (Cont'd)

R	Resistance, ohms
S	Seebeck coefficient, μvolts/°C
TEC-1	Thermally emissive coating (Monsanto Research Corporation)
T	Temperature, °K
T_c	Cold junction temperature, °C or °K
T_{cn}	Average cold junction temperature of segmented n-type thermoelements, °C
T_{cp}	Average cold junction temperature of segmented p-type thermoelements, °C
T_h	Hot junction temperature, °C or °K
T_i	Intermediate junction temperature, °C or °K
T_{in}	Average intermediate junction temperature of segmented n-type thermoelements, °C
T_{ip}	Average intermediate junction temperature of segmented p-type thermoelements, °C
T_m	Melting point, °K
T_r	Temperature of an isothermal radiator, °K
T_s	Temperature of ambient space, °K
ΔT	Average temperature differential, T_h-T_c, across thermoelement, °C
ΔT_n	Average temperature differential, T_i-T_c, across n-type thermoelement, °C
ΔT_{np}	Average temperature differential, $(\Delta T_n + \Delta T_p)1/2$, °C
ΔT_p	Average temperature differential, T_i-T_c, across p-type thermoelement, °C
v	Phonon velocity

SYMBOLS (Cont'd)

X_1	Fraction of impurity
Z	Figure of merit, $10^{-12} \cdot S^2/\rho k$, $^\circ C^{-1}$ or $^\circ K^{-1}$
α	Constant (≈ 1)
η_{M_1}	Thermal efficiency of generator based on ratio of P_{M_1}/Q
η_{M_2}	Thermal efficiency of generator based on ratio of P_{M_2}/Q
ρ	Electrical resistivity, ohm-cm

I. INTRODUCTION

A. BACKGROUND

This is the final report on "High-Temperature Thermoelectric Research," presented under contract AF 33(615)-1084, covering work accomplished from 15 September 1963 through 30 October 1964. The overall program objective was to conduct applied research to establish the technical feasibility of utilizing high-temperature thermoelectric generators, powered with nuclear or solar heat sources, as long-lived power units for aerospace vehicles. This effort was the third phase of a program initiated in 1961 under contract AF 33(657)-7387.

The power output of electric power generators depends on the efficiency of the energy conversion device employed and on the quantity of thermal energy which can be drawn through the unit. As electrical power requirements increase for a given system, an increase in the thermal energy transferred through the conversion unit becomes necessary. Although generators employed in space vehicles can be conveniently heated by nuclear or solar heat, thermal radiation is the principal means of rejecting heat to accomplish thermal energy transfer through the device. The quantity of thermal energy rejected by radiation varies with the fourth power of the temperature of the radiating surface; consequently, increasing this temperature becomes extremely important. It is clear that high temperature is the key to improved performance [watts (e)/lb. or watts(e)/ft.^{2}] of most types of space power systems, including SNAP (Systems Nuclear Auxiliary Power) units. Until recently, it appeared that the high-temperature (1200°C) capabilities of the thermoelectric materials, investigated under this contract, exceeded the capabilities of the available heat source.

Recently, a nuclear fast reactor capable of core temperatures of 1600°C with reflector temperatures to 1200°C was displayed by the Russians[1], who were apparently not in a position to utilize fully the high-temperature capabilities of their reactor, since they employed silicon-germanium thermoelectric materials capable of only 900°C. Additionally, encapsulated isotope heat sources capable of providing hot-junction temperatures in excess of 1200°C are technically feasible.

During the first phase (1961-62) of the program, a laboratory-type, high-temperature generator was built and preliminarily tested.

Manuscript released by authors 30 October 1964 for publication as a RTD Technical Report.

The unit contained 1/2-inch diameter thermoelements of MCC 50, a p-type material originated by Monsanto Company and designed for use at 1200°C. The thermoelectric properties of MCC 50 remained relatively constant during a 100-hr. test at a hot-junction temperature of 1200°C, and the unit satisfactorily tolerated more than 100 thermal cycles between 200°C and 1200°C. Sublimation losses for MCC 50 at 1200°C in a vacuum of 10^{-5} torr were less than 1% in a 1000-hr. test period. It was indicated by Monsanto Research Corporation's thermoelement-module concepts used in the laboratory model generator, together with the low specific weight of MCC 50, that space-type generators capable of appreciably exceeding 2-3 watt(e)/lb. power output could be fabricated.

During the second phase (1962-63) of the program, the nominal 5-watt(e) laboratory model generator survived a 2556-hr. sustained performance test in a vacuum of $\sim 10^{-6}$ torr, at a hot-junction temperature of ~1200°C and a cold-junction radiator temperature of ~720°C with no degradation in thermoelectric properties. Specific performance of this device, employing only p-type MCC 50 thermoelements, was 2.75 watt(e)/lb. /364 lb./KW(e)/.

Monsanto Company made available to Monsanto Research Corporation other original p- and n-type thermoelectric materials in order to further increase the performance of space-type generators. These materials, known to exhibit low sublimation losses in vacuum, were characterized by property measurements at elevated temperatures. At the end of the second phase of the program, these thermoelectric materials were utilized, as shown below, in preparing segmented thermoelements for use in a nominal 50-watt(e) advanced laboratory model generator.

Polarity of Segmented Thermoelement	Hot-End Segment		Cold-End Segment	
	Material	Useful Temp. Range	Material	Useful Temp. Range
p-type	MCC 50	850-1200°C+	MCC 40p	400-950°C
n-type	MCC 60	850-1200°C+	MCC 40n	400-950°C

Design and fabrication of the nominal 50-watt generator were completed near the end of the second phase of the program. Solid-state, bonded, high-temperature, multi-segmented thermoelements (3/8-inch diameter) used for the first time in the fabrication of a generator, obviated the need for springs or other mechanical devices to maintain low-resistance contacts between thermoelectric segments and electrical and thermal leads. Lightweight central core construction, with radiators directly bonded to the segmented thermoelements, and high-temperature capability resulted in a

power output of 12.8 watt(e)/lb. /78 lb./KW(e)/, exclusive of heat source weight, with a hot junction temperature of 1200°C and a cold-junction temperature of 570°C in a vacuum of 10^{-5} to 10^{-6} torr. After 266 hrs. of sustained operation, generator performance became erratic, and inspection of the unit revealed that the safe operating temperatures at the intermediate junctions (T_i sites) of the n-type thermoelements had been exceeded by about 100°C, causing generator failure.

During the third and current phase of the program, the damaged 50-watt(e) generator was to be repaired and further evaluated. Additionally, an improved laboratory model generator of nominal 15-watt(e) output was to be designed, fabricated and tested. A test facility, similar to that used for evaluating the advanced laboratory model generator, was to be designed, fabricated, tested and delivered to the Air Force for evaluation of generators and components under simulated space conditions. Research was to continue on junction forming by hot-pressing, production of thermoelements by arc-plasma spraying, and fundamental studies directed toward correlating microstructure characteristics with thermoelectric properties of thermoelements. Finally, a preliminary investigation was to be made of advanced systems concepts involving the use of radioisotope, solar and nuclear heat sources in auxiliary power systems for space.

II. SUMMARY

A. RESULTS

This multiphase project was concerned with the design, building and testing of two laboratory type generators, applied research aimed at evaluating and improving high-temperature generator components, and a preliminary investigation of the performance of several system concepts using nuclear reactor, radioisotope and solar-type heat sources. The results of each phase are summarized below.

1. Advanced Laboratory Model Evaluation

The nominal 50-watt generator failed after 270 hours of operation at a hot-junction temperature of 1200 °C and a cold-junction temperature of 570 °C and 10^{-5} to 10^{-6} torr. Cause of failure was traced to operation of its n-type, 3/8 inch diameter, segmented thermoelements at ~100 °C above their design interface (T_i) temperature of 850 °C. The generator was completely disassembled following its failure, then rebuilt with new n-type thermoelements. Also, about 10% of the p-type thermoelements were replaced. The repaired generator then completed 1099 hours of sustained testing with its hot junction at ~1200 °C, its cold junction at ~570 °C and at 10^{-5} - 10^{-6} torr. It then was subjected to 105 thermal cycles (~100-hrs. further testing), without degradation of its power output. Performance of the generator during the sustained and thermal cycling tests ranged from 10.4 to 10.9 watt(e)/lb., with a short time peak of 11.8 watt(e)/lb., while its thermal efficiency ranged from 1.5% to 1.8%. Chief problems encountered were maintenance of the temperature monitoring thermocouples and the resistance heat source.

2. Improved Experimental Model Evaluation

Based on knowledge gained in building and testing the 50-watt(e) generator and in developing 1/4-inch diameter segmented thermoelements, a nominal 13-15 watt(e) generator weighing 1.3 lbs., exclusive of heat source, was designed, fabricated, and tested for 3508 hours (146 days) with its hot junction at ~1200 °C, cold junction at 575 °C and in a vacuum of 10^{-5} - 10^{-6} torr. Following the sustained performance test, this generator was subjected to 264 thermal cycles, under simulated space conditions in which peak heating and cooling rates to 250 °C/min. were reached. The power output of this generator, under matched load conditions, ranged from 12.4 to 17.3 watt(e), corresponding to 9.5 to 13.2 watt(e)/lb.

and thermal efficiencies of 2.0% and 2.8%, respectively. No degradation in power output was observed during the first 2160 hours (90 days) operation. Performance during this period climbed from 10.6 to 13.2 watt(e)/lb. Beyond this time, power output dropped slowly by 6% from 2160 hours to 3508 hours, and by an additional 3% during the 264 hours required for thermal cycling tests. Post-test examinations showed that the electrical resistance of the ceramic portion of the thermal insulation, used to minimize thermal shunt losses, had depreciated below its original value by a factor of ~100. A single broken n-type thermoelement was also found. Chief cause of degradation of this generator, therefore, appeared to be failure of its ceramic insulation, with no apparent damage having occurred to the segmented thermoelements. As with the 50-watt(e) generator, considerable difficulties were encountered in keeping temperature-monitoring thermocouples and the electrical resistance heater operating.

3. Test Facility

A versatile facility for evaluating thermoelements, p-n couples, and thermoelectric generators was designed, fabricated, and evaluated for the Air Force.

4. Component Research

a. Junction-Forming Techniques More than 600 3/8-inch and 1/4-inch diameter, segmented thermoelements were fabricated and evaluated under this phase of the contract for the purpose of evaluating junction-forming techniques, in repairing the 50-watt(e) generator and in building the experimental model. Considerable difficulties were encountered, particularly in producing 1/4-inch diameter, p- and n-types, segmented thermoelements needed for the experimental model. Daily yields of usable thermoelements frequently ran as low as 10%. Nevertheless, the mechanical strength and electrical conductivity of interface junctions between thermoelectric material segments were improved by 15-20% during the past 12 months. Electrical resistance measurements of segmented thermoelements were also made, and the base of knowledge concerned with solving junction-forming problems was extended.

b. Arc-Plasma and Flame-Spraying Studies Although efforts on this phase of the project were limited, due to extensive flame-spraying operations required for repair of the 50-watt(e) and experimental model generators, the following progress was made:

- Powder particle size and shape characteristics needed for uniform feeding of thermoelectric and junction-bonding powdered materials to arc-plasma and flame-spraying equipment were developed.

- It was determined that pre-reaction and conditioning of thermoelectric material components, prior to arc-plasma spray fabrication and post-spray treatment, gave better thermoelectric materials.

- It was learned that thermoelectric compositions, optimum for hot-pressing, must be modified for use in the arc-plasma spray fabrication of thermoelements.

- Segmented p- and n-type thermoelements were made and tested to ~1000-hrs.

- Promising solid-state microstructures capable of useful, oriented, and improved (relative to the properties of hot-pressed materials) thermoelectric properties were made.

- The possibility of substantially lowering the cost of producing high quality, single and multiple segment thermoelements, and in producing them in a wide variety of geometries, remains technically feasible and is economically quite attractive.

c. Screening and Sustained Performance Testing of Materials

This phase was largely concerned with the difficult problems of making useful measurements of thermoelectric properties at temperatures to 1200 °C in a vacuum. Considerable effort was devoted to developing a method for measuring T_j junction temperatures in fragile 1/4-inch diameter, double-segmented thermoelements required for the experimental model generator. More than 800 segmented thermoelements of 3/8-inch and 1/4-inch diameter were screened or performance-tested, as required for studies under the Fundamental Investigation, Junction Forming, and Generator Fabrication phases of the project.

A series of tests were performed to assist in determining the causes of failure at the MCC 40-graphite intermediate junction of p- as well as n-type thermoelements. These tests contributed to the diagnosis and solution of causes of the failure of the 50-watt(e) generator. Modifications were also made to the screening appartus in an effort to improve its accuracy and utility at 1200 °C.

A hot-pressed p-n couple, representative of the best p-n compositions made during 1963, was produced and tested at a T_h of

~1200°C, cold junction of 550°C and at 10^{-5} - 10^{-6} torr for 1012-hrs., without degradation of its output. The power output of the 1963-64 couple was found to be 17% higher than that for representative 1962-63 couples operating under nearly identical thermal conditions.

d. Fundamental Investigations A survey of possible mechanisms and microstructure examination techniques was made in an effort to explain the performance of Monsanto Research Corporation's high-temperature thermoelectric materials. This study, when correlated with measured properties of thermoelements, indicated that Monsanto Company's high-temperature thermoelectric materials approach is technically sound and that substantial improvement of thermoelectric properties is possible.

5. Preliminary Investigation of System Concepts

a. Nuclear Out-of-Pile and In-Pile Thermoelectric Space Power Systems Conceptual designs were proposed and investigated in a preliminary way for three types of fast reactor-heated high-temperature thermoelectric space power systems. Comparisons of their optimized performances with those of several SNAP systems are presented below:

System Performance	Power Level, KW(e)	SNAP* (2,8)	System Concepts: HORSE (out-of-pile, with loop) 1965	HORSE (out-of-pile, with loop) 1971-85	TIGER (in-pile, no loop) 1965	TIGER (in-pile, no loop) 1971-85	SWIFT (in-pile, with loop) 1965	SWIFT (in-pile, with loop) 1971-85
lbs./KW(e)	3	400	150	120	350	130	160	110
ft^3/KW(e)		-	14	14	21	19	15	15
$1000/KW(e)		16	89	86	680	68	118	100
lbs./KW(e)	30	>100	59	33	290	90	[illegible]	[illegible]
ft^3/KW(e)		4.7	3.5	2.2	4.3	2.9	1.9	1.6
$1000/KW(e)		2.6	17	14	830	22	92	39
lbs./KW(e)	350	-	55	26	-	-	43	15
ft^3/KW(e)		-	3.2	2.2	-	-	0.22	0.24
$1000/KW(e)		-	4.8	3.4	-	-	75	20

*The data for the SNAP systems do not include shield weight. The performance of the systems investigated on the project includes all components and shielding for an instrument payload.

These performance data were obtained using properties of MCC thermoelectric materials anticipated by 1964-1965 and by 1971-1985. Such performances, however, can only be attained with segmented thermoelements that are smaller than presently practical to produce. The performance of each of the three system concepts studied is quite sensitive to thermoelectric material parameters.

The performance of the HORSE and SWIFT systems could be further improved with 1964-1965 thermoelectric properties, and by the use of hybrid thermoelectric-dynamic (Rankine cycle with turbines) systems. Further improvements in thermoelectric and structural materials, anticipated during 1971-1985 could improve performance of SWIFT concept (without dynamic auxiliary power units) to approximately 15 lbs./KW(e).

b. Radioisotope Space Power Systems A performance and thermal efficiency study (based on 1964-1965 MRC materials) for a 25-watt(e) Cm^{242} heated (T_h of 1200°C) thermoelectric space power generator, utilizing 3/8-inch diameter segmented thermoelements, showed a maximum performance of 9.0 watt(e)/lb. [110 lb/KW(e)] at an element length of 1.7 cm (0.67 inch) and cold-junction temperature of 550°C. The thermal efficiency at optimum performance is 2.8%. The maximum thermal efficiency at a T_h of 1200°C is 3.75% at an element length of 2.7 cm (1.060 inch) and at a cold-junction temperature of 500°C. The design points for maximum performance and for maximum thermal efficiency do not coincide. The study also shows that generators can be designed with high performance of, for example, at least 7.0 watt(e)/lb. [143 lb/KW(e)] within a wide range of cold-junction temperatures and element lengths.

A comparison between the cylindrical, spherical and sandwich design generator concepts for a 25-watt(e) Cm^{242} heated (T_h of 1200°C) thermoelectric space power generator, with 3/8-inch diameter, segmented thermoelements operating at 600°C cold-junction temperature, showed the spherical concept to be superior in performance at 9.5 watt(e)/lb. [105 lb/KW(e)] vs. 3.2 watt(e)/lb. [122 lb/KW(e)] for the cylindrical concept. These performances are reached at an overall element length of 1.5 cm (0.59). The performances of the sandwich concept reach a maximum of only 3.8 watt(e)/lb. [263 lb./KW(e)] at an element length of 2.2 cm (0.88 inch).

A comparative study of 25-watt(e) thermoelectric space power generators with 3/8-inch diameter, segmented thermoelements heated with Po^{210}, Cm^{242} and Cm^{244} heat sources (T_h of 1200°C) and operating at 600°C cold-junction temperature showed the generator with the Po^{210} heat source to have superior performance at 9.3 watt(e)/lb. [108 lb/KW(e)] and 1.4 cm (0.55 inch) element length. The performance for the Cm^{242} heated system is somewhat lower at 8.8 watt(e)/lb. [114 lb/KW(e)] with the same element length.

The performance of the Cm^{244} heated system is again lower at 3.8 watt(e)/lb. [263 lb./KW(e)] at 1.5 cm (0.59 inch) element length.

Preliminary investigations showed that a Pu^{238} heated generator will have lower performance than one heated with Cm^{244}. This disadvantage does not offset the many advantages of the utilization of Pu^{238} with respect to availability and shielding. An investigation of Sr^{90} showed this isotope to be unsuited for space power applications. The low power density of this isotope and the heavy shielding requirements result in very poor performance values for space-type systems.

A preliminary study based upon the 1971-1985 thermoelectric parameters showed that at 1400°C hot-junction temperature, 1050°C interface temperature, and 550°C cold-junction temperature, a system's thermal efficiency of 9.0% can be reached and a performance of better than 50 lbs./KW(e) can be achieved with a Cm^{242} oxide heat source for a wide range of element lengths and cold-junction temperatures. A 25-watt(e) thermoelectric space power system, using a gadolinium-polonide^{210} heat source, can have a performance better than 40 lbs./KW(e), based upon 1971-1985 material property predictions.

c. Solar-Concentrating Thermoelectric Systems Based on the properties of MCC thermoelectric materials anticipated by 1964-1965, it was found that a high-temperature thermoelectric generator, operating in a near-earth orbit, and heated by a one-piece, 9-ft. diameter, parabolic mirror would be capable of 250 watt(e) and 335 lbs./KW(e). These performance figures take into account the weight of deployment and orientation hardware. The specific volume of this module was estimated at 240 ft^3/KW(e). Batteries are more practical than thermal storage devices for providing power during dark orbiting periods.

B. CONCLUSIONS

The results of this program support the following conclusions.

1. Laboratory Model Generators

The successful completion, without degradation of performance, of more than 1200 hours of sustained operation and thermal cycling tests at 10^{-5} - 10^{-6} torr on a 50-watt(e) generator operating between 1200°C and 570°C indicates that segmented 3/8-inch diameter thermoelements of Monsanto Company thermoelectric materials are capable of a year's operation with less than 10% degradation. This conclusion was supported by the results of concurrent sustained performance and thermal cycling tests of 3770-hrs. on a 13-15 watt(e) generator made from segmented 1/4-inch diameter thermoelements. No degradation was experienced with the smaller generator to about 2100-hrs. operation. Degradation which was encountered beyond 2100 hrs. and reached 6% at 3508 hrs. and a total of 9% after an additional 264-hrs. of thermal cycling, was apparently the result of deterioration of the electrical resistance of the ceramic thermal insulation used in this generator. A broken n-type thermoelement, found during a post-test examination, demonstrated the value of redundancy in generator circuits, but accounted for less than 10% of the degradation experienced. The mechanical and thermal stresses experienced by both laboratory-type generators during thermal cycling tests showed that the basic multi-segment thermoelement, multi-thermoelement module, and tier concepts used in their fabrication are sound and useful for future space power system designs.

2. Test Facilities

The versatile facility completed for the Air Force is capable of evaluating thermoelements and single, double, and higher multiples to 1200°C in a vacuum of 10^{-5} - 10^{-6} torr. This facility can also be used to evaluate multi-watt generators under simulated space conditions and a variety of thermal conditions.

3. Component Research

Further effort will be required to lower the contact resistance and improve the quality and reproducibility of the segmented thermoelements. Significant improvements in both the quality and reproducibility of MRC's high-temperature thermoelements are

technically feasible.

As demonstrated by the completion of the 1000-hr sustained performance and 250-cycle thermal shock tests, the potential for the achievement of high reliability and performance with arc-plasma fabricated thermoelements remains high. This method of fabrication continues to offer good possibilities for the low-cost mass production of thermoelectric space power units.

On the basis of knowledge gained under this program, it is likely that significant (10-30%) improvements in the performance of segmented thermoelements can be attained.

4. Preliminary Investigation of System Concepts

On the basis of present investigations of reactor-heated thermoelectric space power systems, it is concluded that:

a. The lbs./KW(e) performances (including shielding weights) of the HORSE (out-of-pile thermoelements with heating loop), SWIFT (in-pile thermoelements cooled by out-of-pile loop), and TIGER (in-pile thermoelements, no loop) concepts, based on 1964-1965 thermoelectric material properties and a PuC fast-reactor heat source, are higher than those for SNAP 10A, SNAP 2 and SNAP 8.

b. The performance of each of the three space power concepts studied is quite sensitive to the performance of the thermoelectric components. Thus, significant improvements in system performance could result from improvements in performance of the thermoelectric components.

c. Calculations indicate that system performances below 30 lbs./KW(e) could be attained for HORSE systems using values of thermoelectric parameters assumed to be attainable in the 1971-1985 time period.

d. SWIFT systems could approach a performance of 15 lbs./KW(e) and possibly surpass this figure if the high-temperature thermoelectric generator were combined with a low-temperature Rankine cycle turbine system. Additional conceptual design studies of such hybrid static-dynamic systems should be made.

e. The HORSE and SWIFT concepts with fluid heat transfer loops offer higher performances but lower reliability

than TIGER, which requires no fluids and is of simplified design.

f. Fuel cost in $/KW(e) for large HORSE systems appears competitive with that for the SNAP 8 system, while cost for large SWIFT systems is between those for SNAP 10A and SNAP 2.

g. The system volume in ft^3/KW(e) is lower for both the HORSE and SWIFT concepts than for SNAP 8.

h. Attainment of optimum performances in the 3 KW(e)-350 KW(e) ranges for each of the three high-temperature thermoelectric systems investigated will require development of production processes for making smaller segmented thermoelements than will be available by 1965. It is anticipated that the small thermoelements could be developed during 1965-1970.

i. Optimum performance of HORSE and SWIFT systems is attained at low to moderate (250-650°C) radiator temperatures. The SWIFT type of system could utilize present state-of-the-art coolant systems (such as mercury or water) for use at temperatures below 500°C.

Investigations of radioisotope heated space power systems, based on the use of heavy-walled isotope containers, as required for total isotope containment during reentry, or an aborted launch, led to the following conclusions:

a. High performance Cm^{242} or Po^{210} heated thermoelectric space power generators with 3/8-inch diameter elements at a power level of 25 watt(e) can be built utilizing a wide range of element lengths and operating over a wide range of cold-junction temperatures. Performances as high as 9.0 watt(e)/lb. [110 lbs./KW(e)] are feasible.

b. Cm^{242} or Po^{210} heated thermoelectric space power generators, with 3/8-inch diameter thermoelements, can be operated at thermal efficiencies as high as 3.75%.

c. Since the design points for maximum performance and maximum thermal efficiency do not coincide, practical generator designs will have to be a compromise between the two performance parameters. A high performance coincides with a low thermal efficiency, i.e., with a high isotope investment. A further study will have to be made of the trade-offs between performance and cost of the generator.

d. While the spherical design was found to be superior to the cylindrical design with respect to the performance of a 25-watt(e) generator and for 3/8-inch diameter thermoelements, the difference is too small to warrant the additional effort needed to successfully develop the inherently more complicated spherical design.

e. At the 25-watt(e) power level the Po^{210} is the best radioisotope heat source. While tentative computations show the performance of a Pu^{238} fueled generator to be lower than that of a Cm^{244} fueled one, the advantages of Pu^{238} are such that it must be considered to be the superior fuel.

On the basis of a brief, preliminary investigation of a solar-concentrating type of space power system, based on the assumption that a 9-ft. diameter parabolic mirror-thermoelectric generator module is of optimum size, it is concluded that:

a. A specific performance of about 335 lbs./KW(e) might be expected for mirror-thermoelectric generator modules of about 250-watt(e) output. This performance is based on properties of MCC thermoelectric materials, the availability of which is anticipated during 1964-65.

b. Batteries are more practical than thermal storage devices as a means of supplying power during dark orbital periods.

c. Increasing the power level of this type system does not appreciably improve its performance.

d. Thermoelements smaller than those that will be available during 1964-1965 are needed to reach optimum system performance.

e. Collector storage and high collector/thermoelectric generator weight ratios are major problem areas requiring attention for improved performance of this type system.

III. RESEARCH AND DEVELOPMENT

A. ADVANCED LABORATORY MODEL EVALUATION

Duration tests on this nominal 50-watt(e) generator were initiated during the last two weeks of the second (1962-63) phase of the program and extended into this, the third phase of the program. The results of duration and thermal cycling tests, as well as detailed post-test examinations made on this generator, are presented in this report section.

1. 1000-Hr. Sustained Performance Test

This generator, shown in the assembly drawing of Figure 1 and described in Table 1, weighed 3.86 lb., exclusive of its heat source. It utilized 46 series-connected stages of two p-type and two n-type segmented thermoelements, each 3/8-inch diameter by 0.65 inches long. These thermoelements were joined at their hot ends by molybdenum-graphite contacts and at their cold ends by finned copper radiators coated with TEC-1, a highly emissive proprietary Monsanto Research Corporation coating. An electrically powered, 0.5 inch O.D. tantalum tube, with 0.020 inch walls and equipped with solid tantalum ends that extended 1 inch into the central cavity at each end of the generator, was used as a heat source. An A.C. low-voltage high-current power supply, controlled by means of a single thermocouple located at the hot junction of a p-n couple at the approximate center of the generator, provided the thermal energy needed to maintain the tantalum resistor at operating temperature.

As shown in Figure 2, the generator was mounted within a water-cooled cylindrical protective shield which served as the primary heat sink for the radiatively cooled generator and protected the pyrex glass vacuum jar from thermal damage. The inside surface of the heat sink was coated with TEC-1.

Sustained testing of the generator was started with operation at 1217°C (T_h) in a vacuum of 0.8-0.9 x 10^{-6} torr. Initial observations indicated that the tiers of both ends of the generator were below their designed operating temperatures of 1200°C (T_h, hot-junction temperature), 850°C (T_i, intermediate-junction temperature between segments of high-and low-temperature thermoelectric materials), and 500°C (T_c, cold-junction temperature).

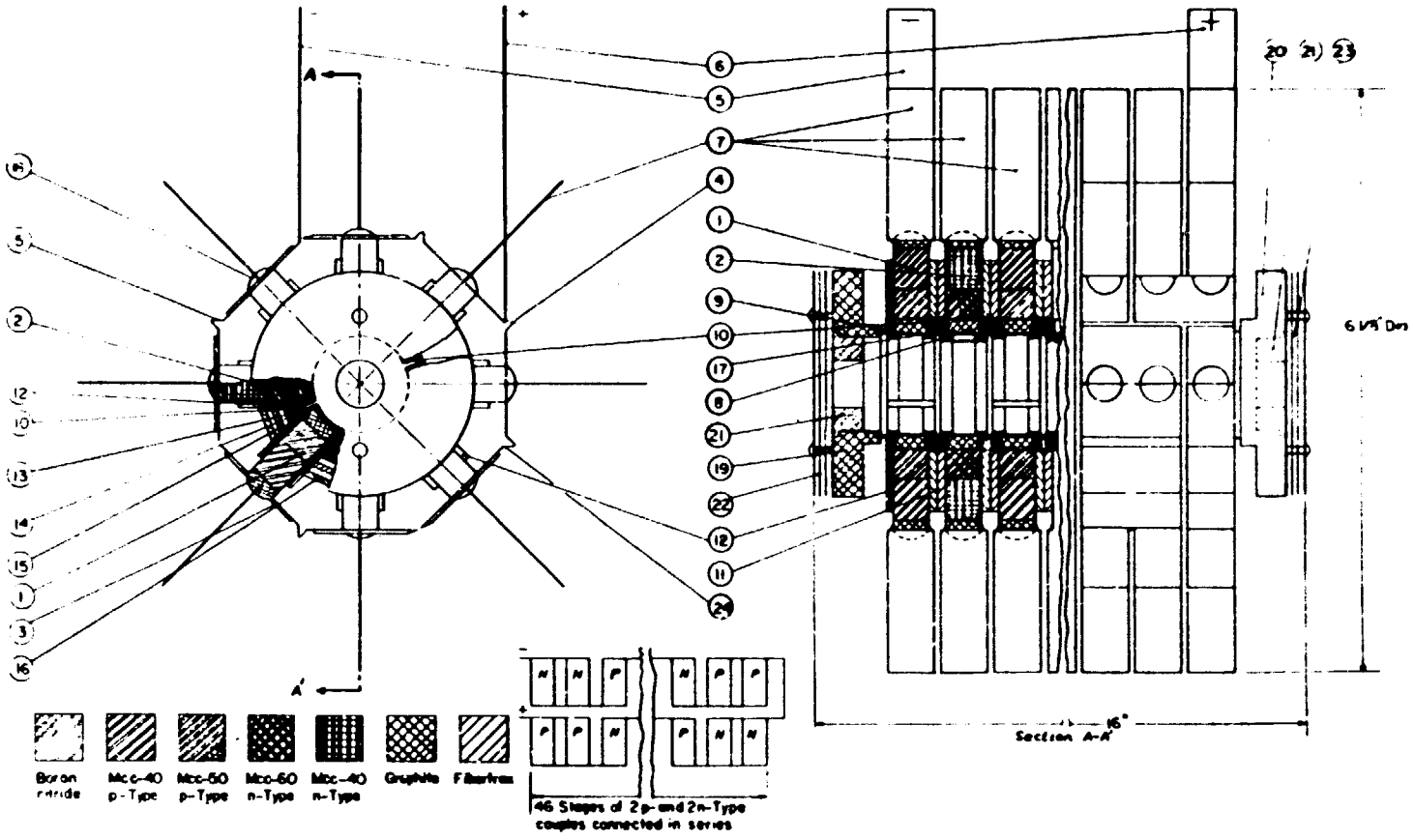

Figure 1. Assembly Drawing of Advanced Experimental Model Generator

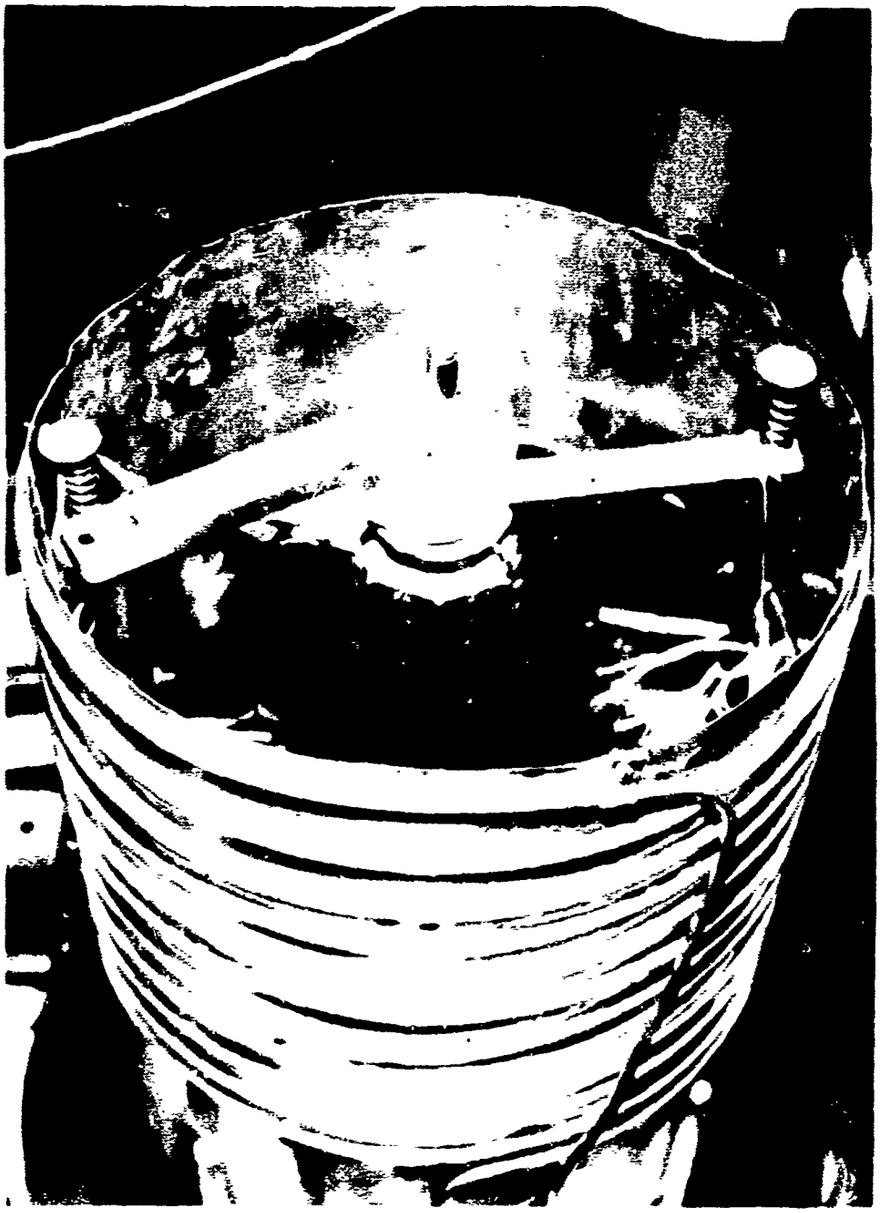

Figure 2. Advanced Experimental Model Generator in Test Stand Showing Water-Cooled Protective Shielding

As shown in Table 2, the first 144-hr. operation of the generator yielded an output of 46 watt(e) /11 9 watts(e)/lb./ at an overall thermal efficiency of 1.8%. Heat losses at the ends were severe, as was the temperature gradient (estimated at 100-200°C) between the central and end sections of the generator. To reduce these undesirable and harmful effects, a 0.5 inch O.D. tantalum heater, with a wall thickness of 0.015 inch and with shorter solid ends than the first heater, was installed in the generator and it was returned to operating conditions. An improvement in the uniformity of the temperature gradient (estimated at 25-50°C) between the central and end sections of the generator was noted with the new heater in place. Additionally, power output increased to about 50 watt(e) /12.8 watt(e) /lb./ at an improved overall thermal efficiency of 2%. This improvement in performance during the next 122-hr. operation of the generator is believed to have resulted from the more uniform temperatures and reduced heat losses obtained with the second heater.

Generator power output became erratic after 266 hrs. of operation, and further sustained tests on the generator were halted. A close inspection of the generator after it had cooled to room temperature revealed that four n-type thermoelements located in its central section had failed at their MCC 60-MCC 40 junction. This inspection failed to reveal more serious damage, so it was decided to electrically bypass the damaged thermoelements. Vacuum feedthrough facilities for 12 new thermocouples were also installed to permit monitoring of the junction temperatures of selected thermoelements. These efforts were, in effect, lost, when upon returning the repaired generator to operating conditions, its power output was again erratic and low.

2. Failure Analysis

An analysis of the generator performance relating to causes of failure and discontinuance of the sustained testing was immediately initiated. Initial examinations indicated that failure of the n-type thermoelements was due to unexpected high T_i temperatures between the MCC 60 and MCC 40, n-type thermoelectric segments. Previous screening of representative segmented thermoelements had indicated that T_i junction temperatures for n-type thermoelements would be in the 850-900°C range. In such screening tests T_i temperatures were measured by thermocouples inserted in holes machined radially from the surface to the center of selected thermoelements. Machining of such thermocouple holes at the MCC 60-MCC 40 junctions of thermoelements used in this generator was avoided in the interest of retention of maximum thermoelement strength and generator reliability.

Table 2

DATA FROM INITIAL TEST ON ADVANCED LABORATORY MODEL GENERATOR OPERATING AT $10^{-5} \times 10^{-6}$ TORR

Hrs Operation	Average T_h, °C	Average T_c, °C	ΔT, °C	I, amps	E_L, volts	P, watts	R, ohms	E_{oc}, volts	Max. P, watts	Q, watts*	η,%
2	1217	528	689	8.03	5.760	46.25	0.6965	11.353	46.26	2600	1.8
26	1215	527	688	8.02	5.764	46.23	0.6960	11.346	46.24	2600	1.8
50	1217	529	688	8.03	5.770	46.33	0.6940	11.350	46.40	2600	1.8
72	1214	526	688	8.01	5.760	46.14	0.6960	11.335	46.15	2600	1.8
80	1216	528	688	8.03	5.757	46.23	0.6956	11.343	46.24	2600	1.8
96	1215	527	688	8.03	5.749	46.17	0.6970	11.346	46.19	2600	1.8
104	1217	529	688	8.02	5.766	46.24	0.6965	11.352	46.26	2600	1.8
120	1216	528	688	8.00	5.778	46.23	0.6969	11.353	46.24	2600	1.8
128	1216	529	687	8.03	5.758	46.24	0.6965	11.351	46.25	2600	1.8
144	1215	528	687	8.01	5.770	46.22	0.6970	11.353	46.23	2600	1.8
				Shutdown to change resistance heater							
2	1216	569	647	8.11	6.150	49.88	0.7600	12.320	49.93	2500	2.0
8.5	1215	569	646	8.08	6.160	49.78	0.7610	12.309	49.78	2500	2.0
24.5	1216	570	646	8.11	6.152	49.95	0.7592	12.317	49.96	2500	2.0
32.5	1217	570	647	8.09	6.170	49.91	0.7571	12.295	49.92	2500	2.0
48.5	1215	569	646	8.11	6.150	49.88	0.7589	12.305	49.88	2500	2.0
56.5	1216	569	647	8.08	6.175	49.89	0.7594	12.311	49.89	2500	2.0
70.5	1215	569	646	8.11	6.150	49.85	0.7591	12.307	49.88	2500	2.0
102.5	1216	569	647	8.10	6.170	49.98	0.7580	12.310	49.98	2500	2.0
122.0	1217	570	647	8.11	6.154	49.91	0.7575	12.298	49.91	2500	2.0

*Corrected for energy losses in electric leads and terminals.

Better thermal insulating techniques used in the fabrication of the advanced laboratory model generator, as compared with those used for the sustained testing of the p-n couple [2], significantly reduced thermal leaks, but caused higher T_i temperatures in many thermoelements. For example, on the basis of the patterns observed during screening of thermoelements, for a T_h of 1200°C, a maximum temperature of about 880°C with a T_c of about 560°C should have been reached for thermoelements in the final generator. Subsequent actual measurements, made on several n-type thermoelements from the central section of the damaged generator, showed that for a T_h of 1200°C a T_i of 1000°C was reached with T_c at 560°C. Substantial (50-100°C) temperature differences between the center and the outside surface of thermoelements at the intermediate junction were also observed in tests run on thermoelements from the damaged generator.

Cold-junction temperatures were found to be reasonably uniform, having an estimated variance of less than ± 20°C over the entire generator. Hot-junction temperatures of 1200°C to 1300°C were measured during the test run that was made on the generator after its initial failure. Examination of the thermoelements after disassembly of the generator showed that this rather wide range of hot-junction temperatures was due to the following conditions:

1. Hot-junction thermocouples (inserted under difficult conditions while the generator was still on the test stand) placed in the assembled generator after it had failed were found to be implanted slightly deeper toward the heater than they should have been. Such positioning of the thermocouples would account for readings between 1250°C and 1300°C (higher than the true hot-junction temperatures).

2. The hot-junction thermocouples implanted during generator assembly, at the proper positions, recorded true temperatures and exhibited good uniformity except where failure of an adjacent thermoelement interrupted the normal thermal paths. Such failures resulted in an approximate 30°C temperature rise at the hot junction of the remaining thermally conducting thermoelements. The temperatures of normally functioning thermoelements were of satisfactory uniformity and were believed to have varied less than ± 20°C from operating temperature over the entire generator.

Vibration of the generator during sustained testing may also have contributed to failure of the n-type thermoelements. Such

vibration, resulting from oscillation of mechanical vacuum forepumps and from the building, had been observed to cause the generator to continuously vibrate on its test stand at low frequency (estimated at less than 100 cps) and 1/32-inch to 1/16-inch amplitude, despite application of vibration damping procedures. However, as evidenced by the successful 1000-hr. sustained performance test on the p-n couple, [2] where similar vibration was present, it is doubtful that such vibration in the absence of overheating of the intermediate junction would in itself have caused thermoelement failure.

Partial disassembly of the advanced laboratory model generator, as shown in Figure 3, disclosed an excellent condition of all components, except as noted in Figure 4, at the junctions between segments of the thermoelectric materials. All graphite structures were in excellent condition except for hairline cracks in two half-tiers at the hot-junction graphite ends. These cracks did not interfere with generator performance. All insulation and radiation shielding was in perfect condition. The TEC-1 emissive coating was in all cases adherent, intact, and functional in appearance. The flame-sprayed molybdenum joints, electrically and mechanically bonding the thermoelements to the graphite rings at the hot-end, and the copper radiators at the cold-end were examined minutely and found to be in perfect condition. The thermoelectric segments were found to be unaffected in appearance, as were both hot and cold junctions of all thermoelements.

It was concluded that the generator failure was largely the result of unknowingly operating the intermediate junctions of thermoelements located in the central section of the generator beyond their design limits. Vibration may have played a secondary role in causing the failure of the overheated n-type thermoelements. Exceeding the design limits in temperature was, in turn, the result of encountering temperature gradients not found in the screening of single thermoelements, the 1000-hr. operation of a p-n couple, or the 150-hr. operation of 3-ring generator subassembly modules, previously reported.[3]

Disassembly of the generator into individual tiers or rings revealed that none of the p-type elements had failed completely, but 13 out of 92 showed visible evidence of change at the intermediate junction. This was assumed to indicate incipient damage that might lead to failure and these thermoelements will be replaced if such damage is verified in re-testing. These elements were located in modules (half-tiers) where n-type thermoelements failed. The p-type thermoelements in such half-tiers would have operated hotter due to the reduced number of thermal paths remaining after failure of the n-type thermoelements. Thermoelement 187P in tier 9 of Figure 4 was fractured mechanically during disassembly. This fracture was not related to generator failure.

(a) side view

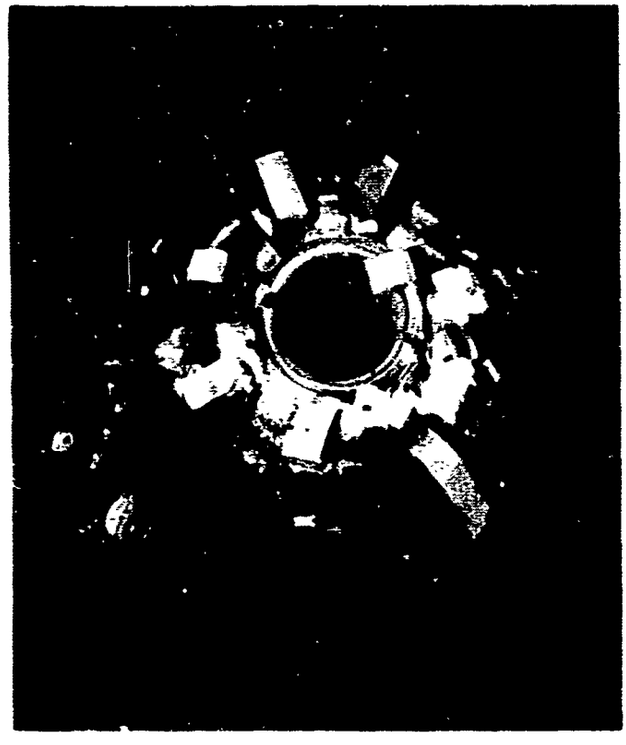

(b) top view

Figure 3. Bottom Portion of Advanced Laboratory Model Generator After Advanced Laboratory Model Was Cut into Halves for Inspection of Components

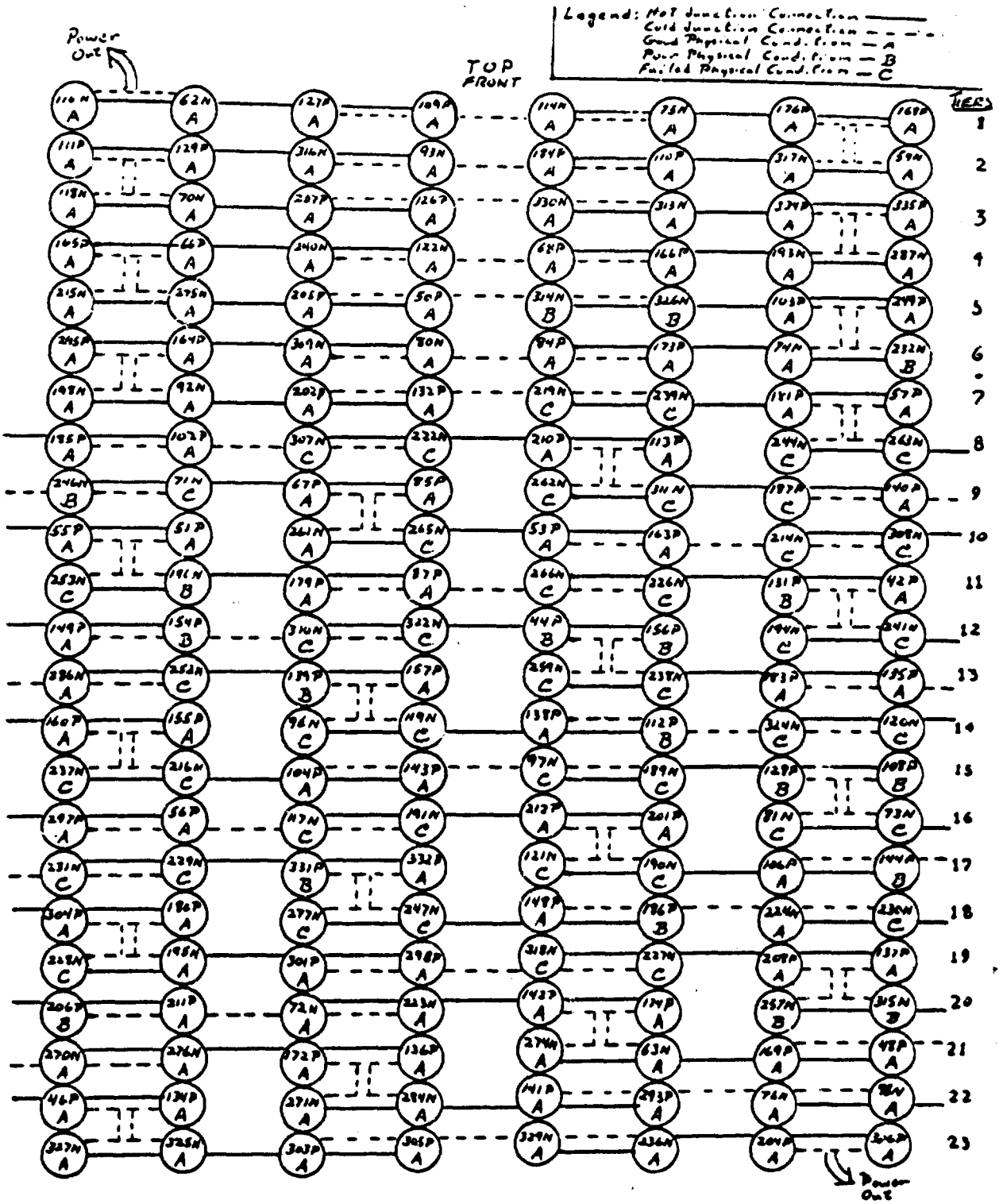

Figure 4. Diagram Showing Location and Condition of All Thermoelements in the Advanced Laboratory Model after Failure Analysis

Forty-four n-type thermoelements of the 92 present failed completely and seven others showed visible evidence of change at the intermediate junction, as described for the p-type elements. All physically intact thermoelements were retested to evaluate possible damage to their thermoelectric properties.

Figures 5 through 10 present individual photographs of generator tiers 1 through 23, showing each as it was removed from the advanced laboratory model. The background indicates the number of each individual thermoelement and its electrical and thermal circuitry. The inner graphite hot junctions show the connections of that area and the outer circle represents the copper radiators. The indicated breaks in the outer circles show where the circuit was interrupted in the generator. The arrows (↑) pointing upward represent connections to the adjacent tier above. Arrows (↓) pointing down represent connections to the adjacent tier below. Arrows (→) pointing outward indicate output leads from the generator.

Hairline cracks were present in the inner graphite connectors of tiers 3 and 11, but these did not affect performance in the generator. Tier number 11 was forcibly separated before photography to ascertain this.

Figure 11 shows a representative individual thermoelement in a more detailed manner and illustrates where the intermediate junction problem area is located in a typical n-type element.

On the basis of an examination of the entire generator, failure in the advanced laboratory model generator is believed to have proceeded as follows:

1. Due to unexpected high heat source temperatures encountered in the central section of the generator, the maximum operating T_1 temperature (950°C) was appreciably (50-100°C) exceeded, causing failure of the bond between the MCC 60 and MCC 40 segments. These T_1 temperatures were not monitored, due to a limitation in the maximum number of thermocouple throughputs from the vacuum environment chamber and to the omission of intermediate-junction thermocouple holes, in the interest of maintaining high mechanical strength in the thermoelements.

2. A previously unobserved temperature differential of 50-100°C existed, under generator operating conditions, between the center (axis) and surface at the intermediate junctions of the n-type thermoelements.

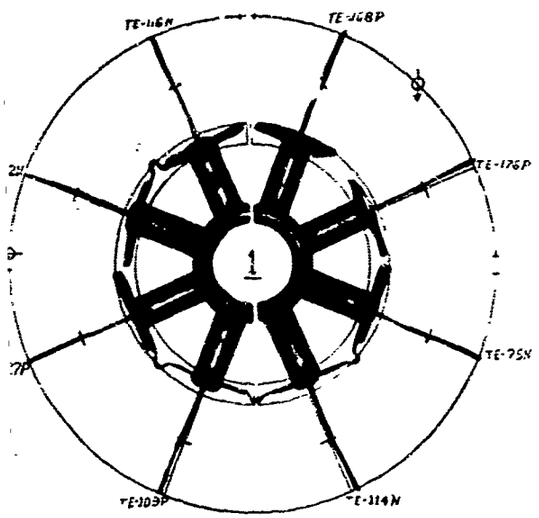

Tier 1

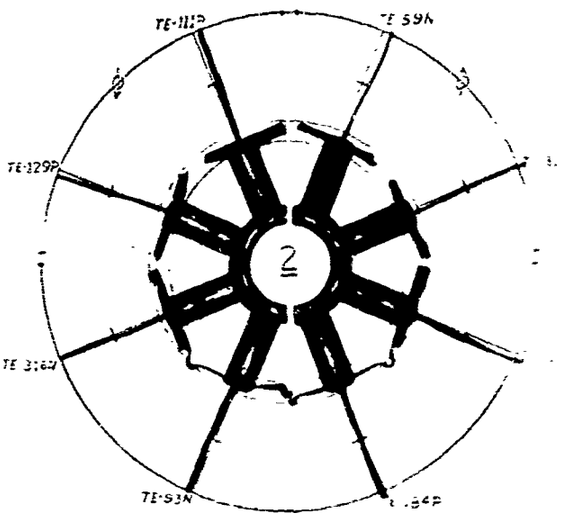

Tier 2

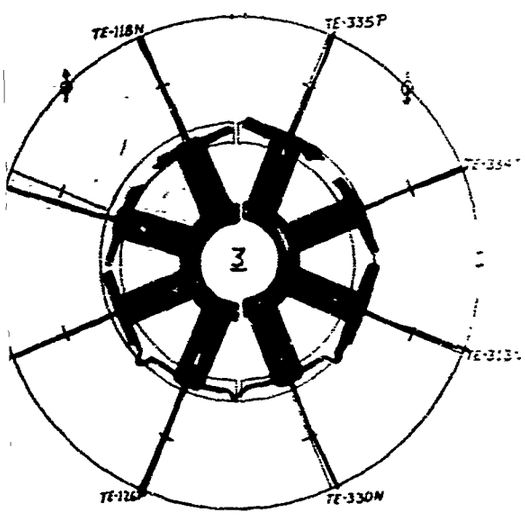

Tier 3

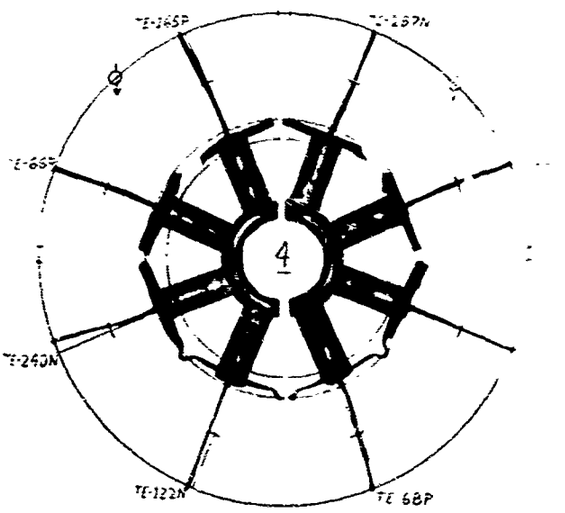

Tier 4

Figure 5. Top View of Tiers 1, 2, 3, and 4 Showing Thermoelement Numbers and Circuit Symbols of the Disassembled Advanced Laboratory Generator

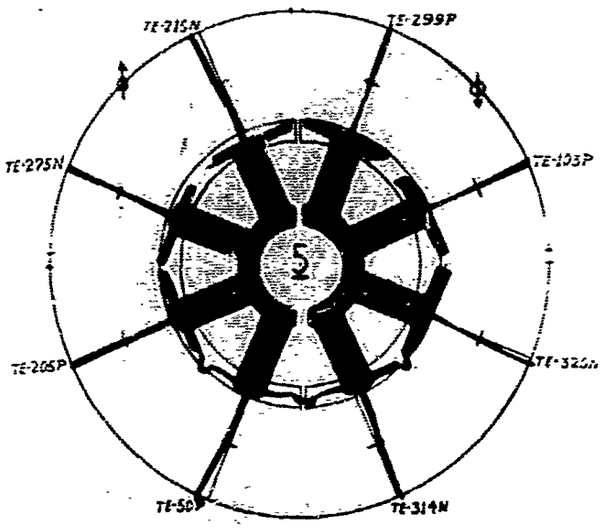

Tier 5

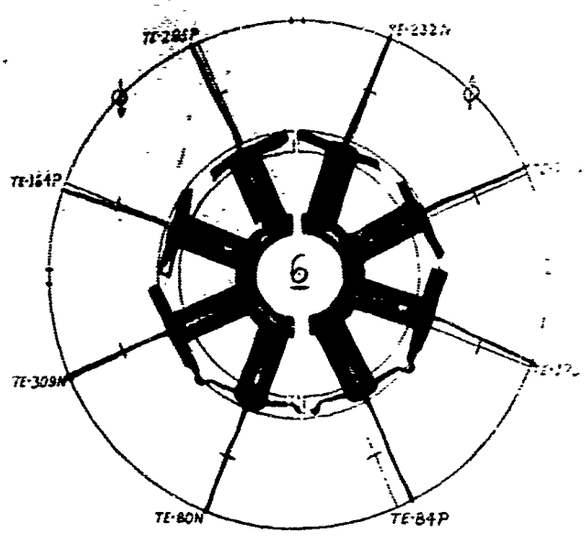

Tier 6

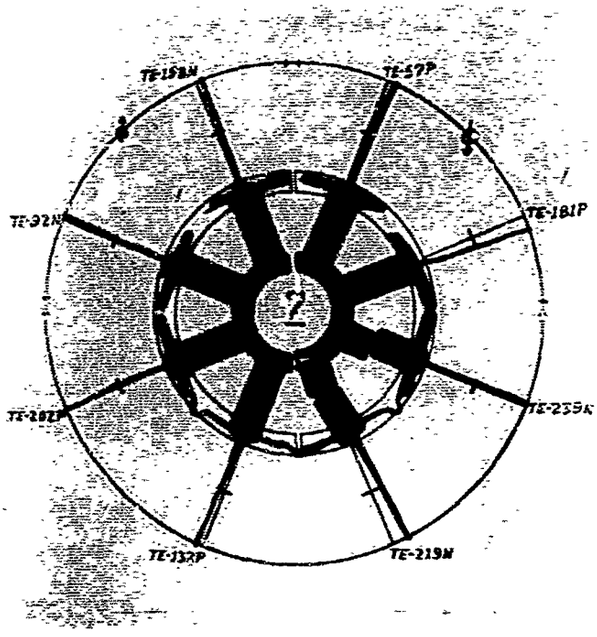

Tier 7

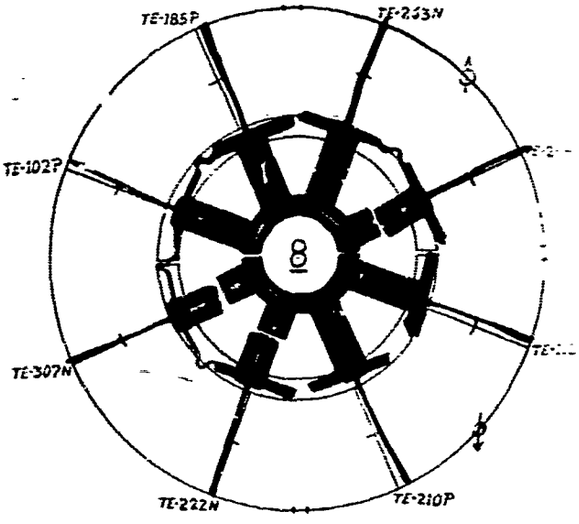

Tier 8

Figure 6. Top View of Tiers 5, 6, 7, and 8 Showing Thermoelement Numbers and Circuit Symbols of the Disassembled Advanced Laboratory Generator

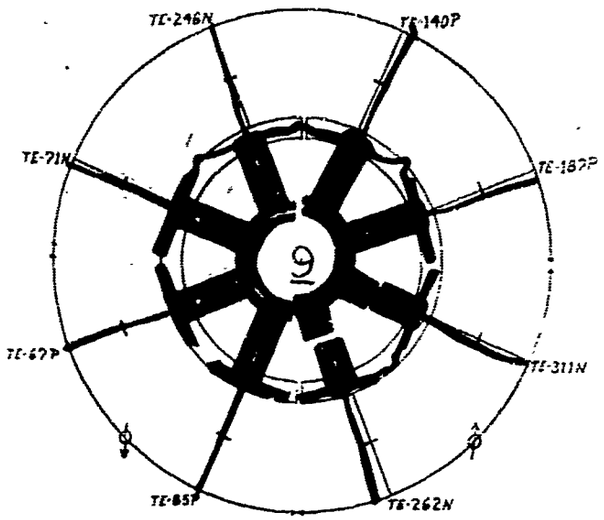

Tier 9

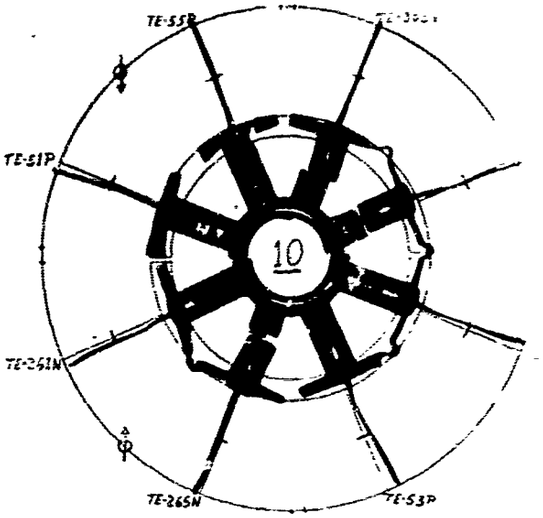

Tier 10

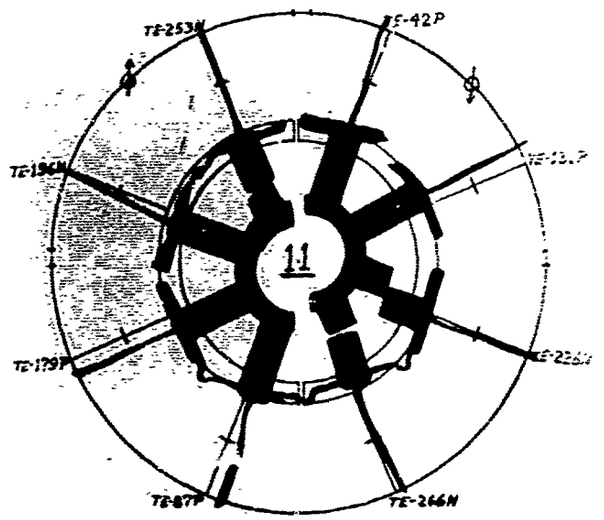

Tier 11

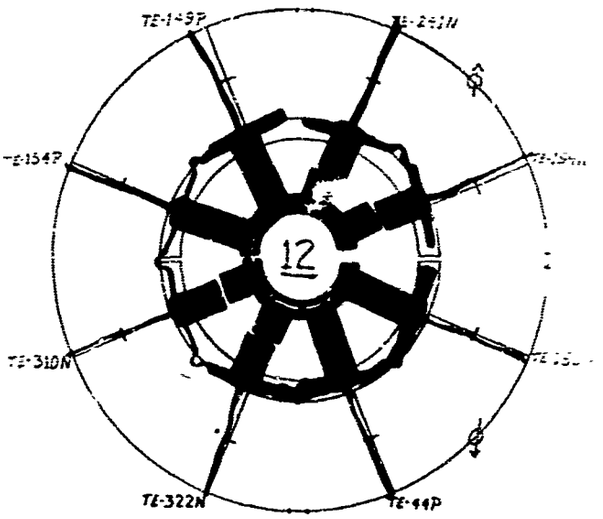

Tier 12

Figure 7. Top View of Tiers 9, 10, 11, and 12 Showing Thermoelement Number and Circuit Symbols of the Disassembled Advanced Laboratory Generator

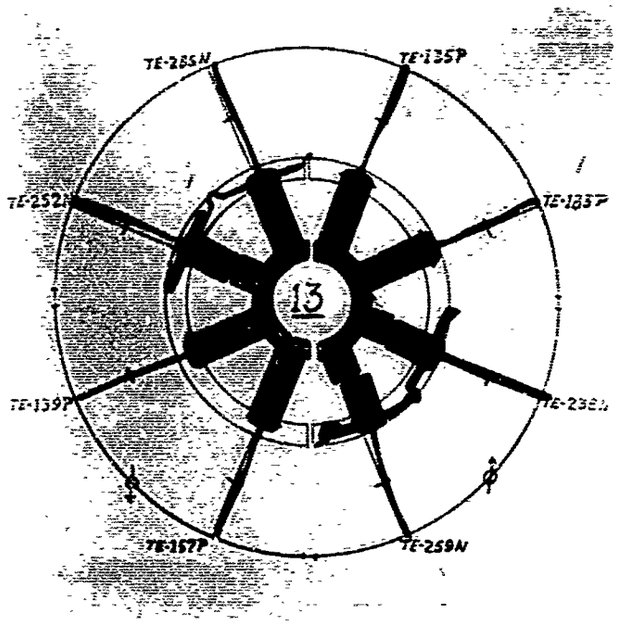

Tier 13

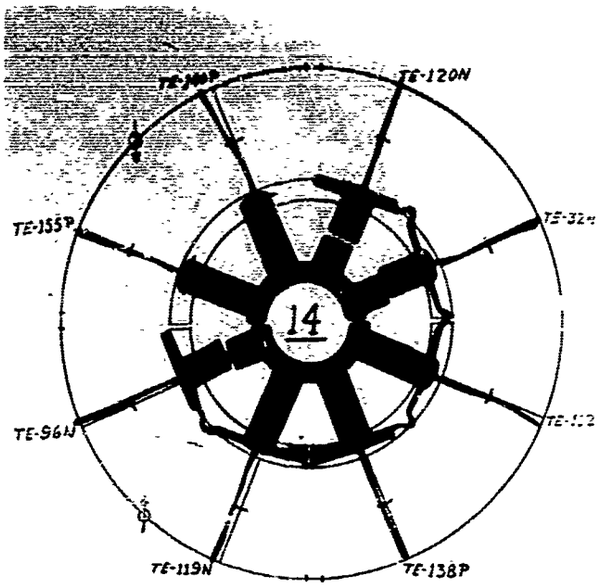

Tier 14

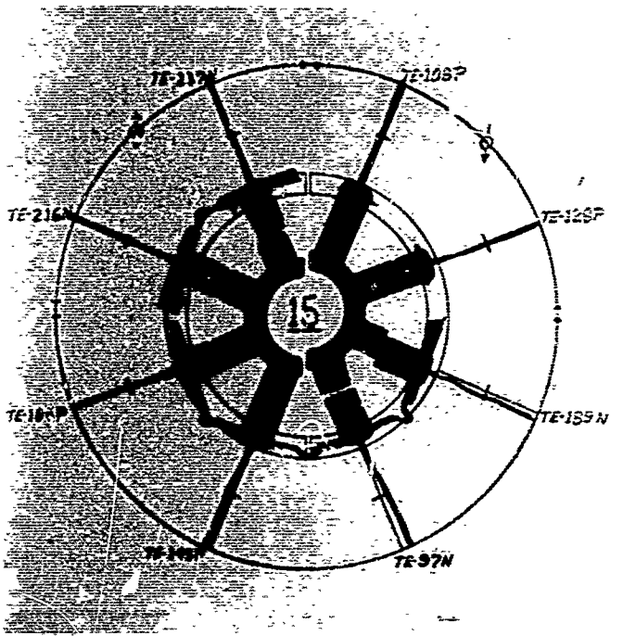

Tier 15

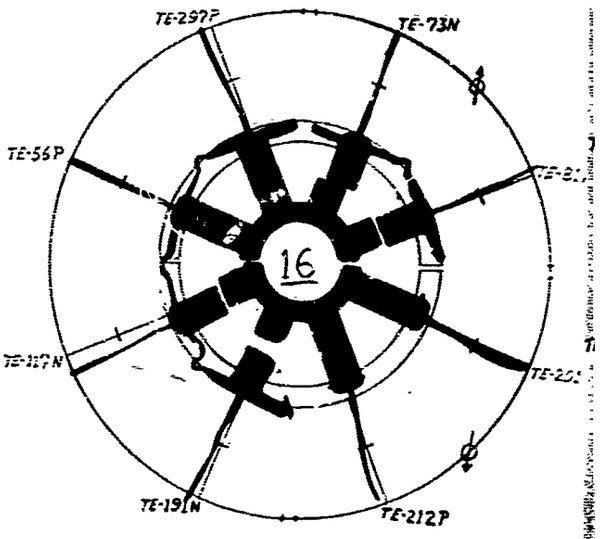

Tier 16

Figure 8. Top View of Tiers 13, 14, 15, and 16 Showing Thermoelement Numbers and Circuit Symbols of the Disassembled Advanced Laboratory Generator

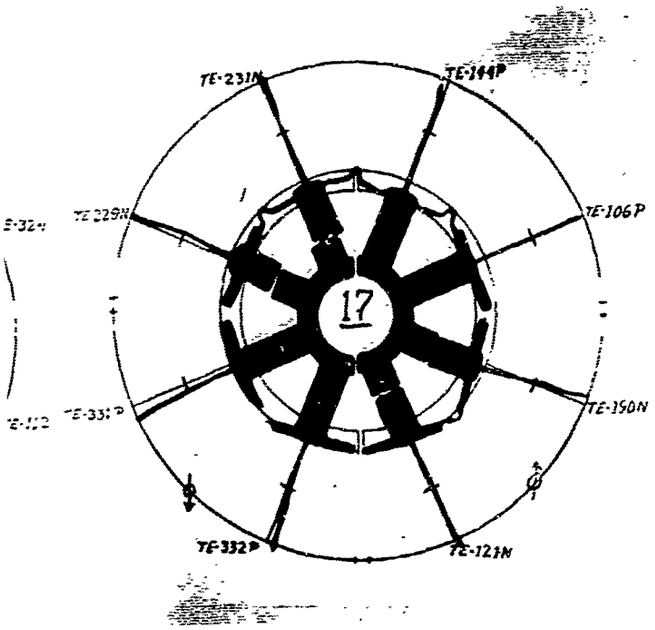

Tier 17

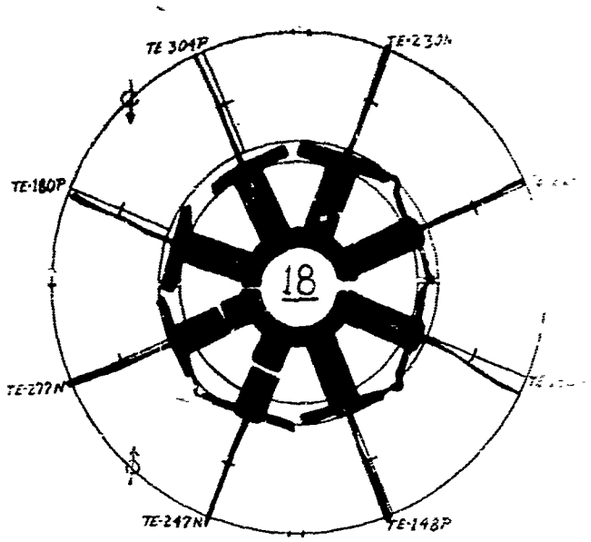

Tier 18

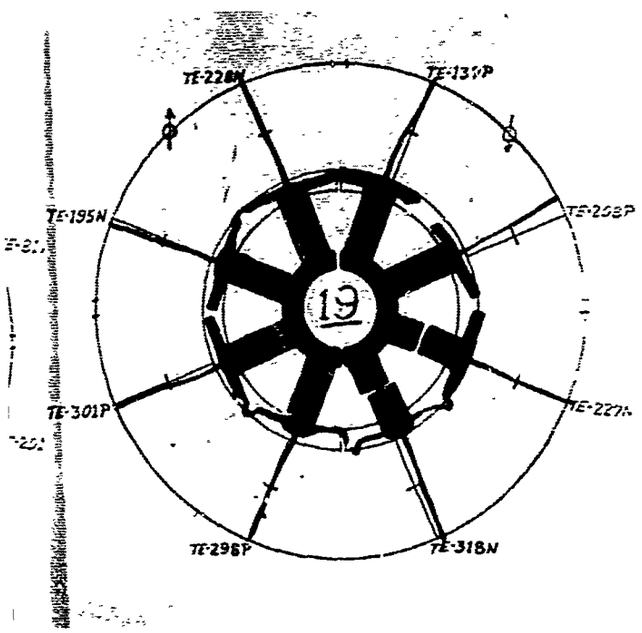

Tier 19

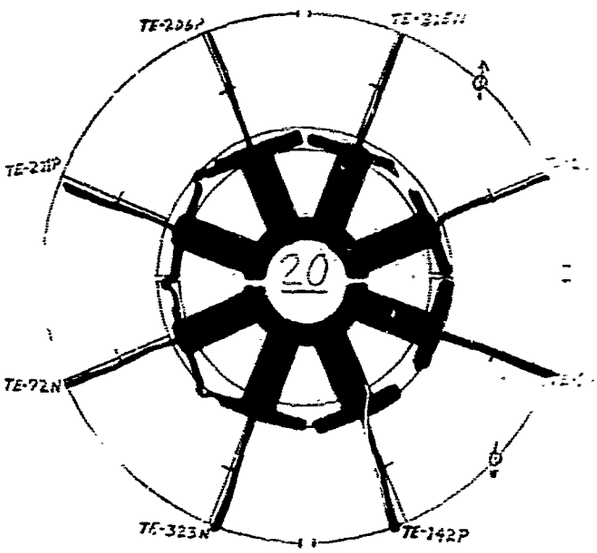

Tier 20

Figure 9. Top View of Tiers 17, 18, 19, and 20 Showing Thermoelement Numbers and Circuit Symbols of the Disassembled Advanced Laboratory Generator

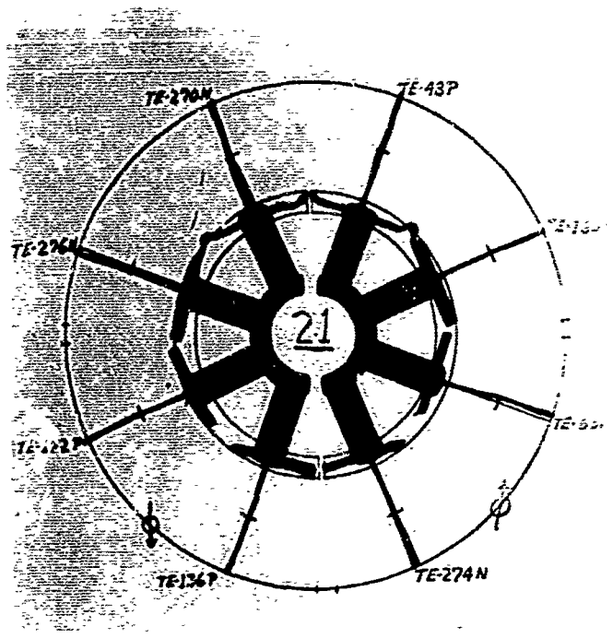

Tier 21

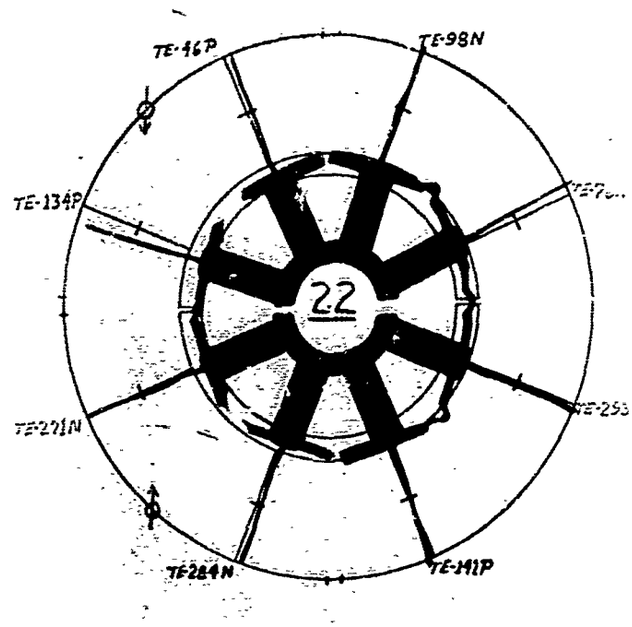

Tier 22

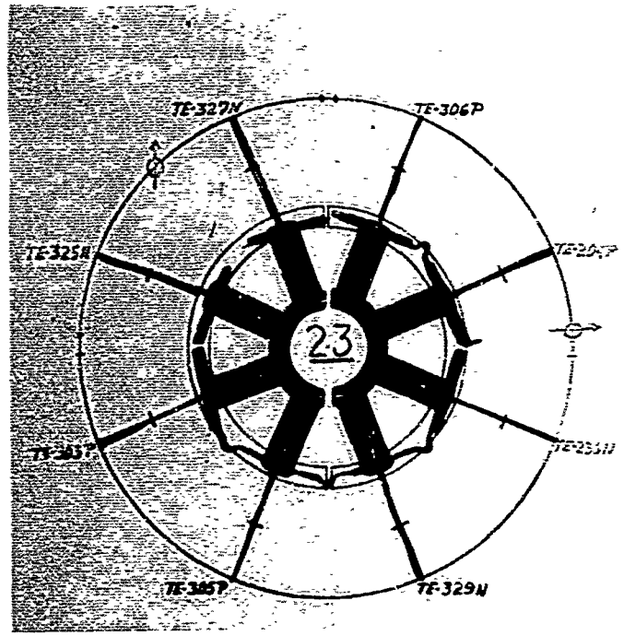

Tier 23

Figure 10. Top View of Tiers 21, 22, and 23 Showing Thermoelectric Numbers and Circuit Symbols of the Disassembled Advanced Laboratory Generator

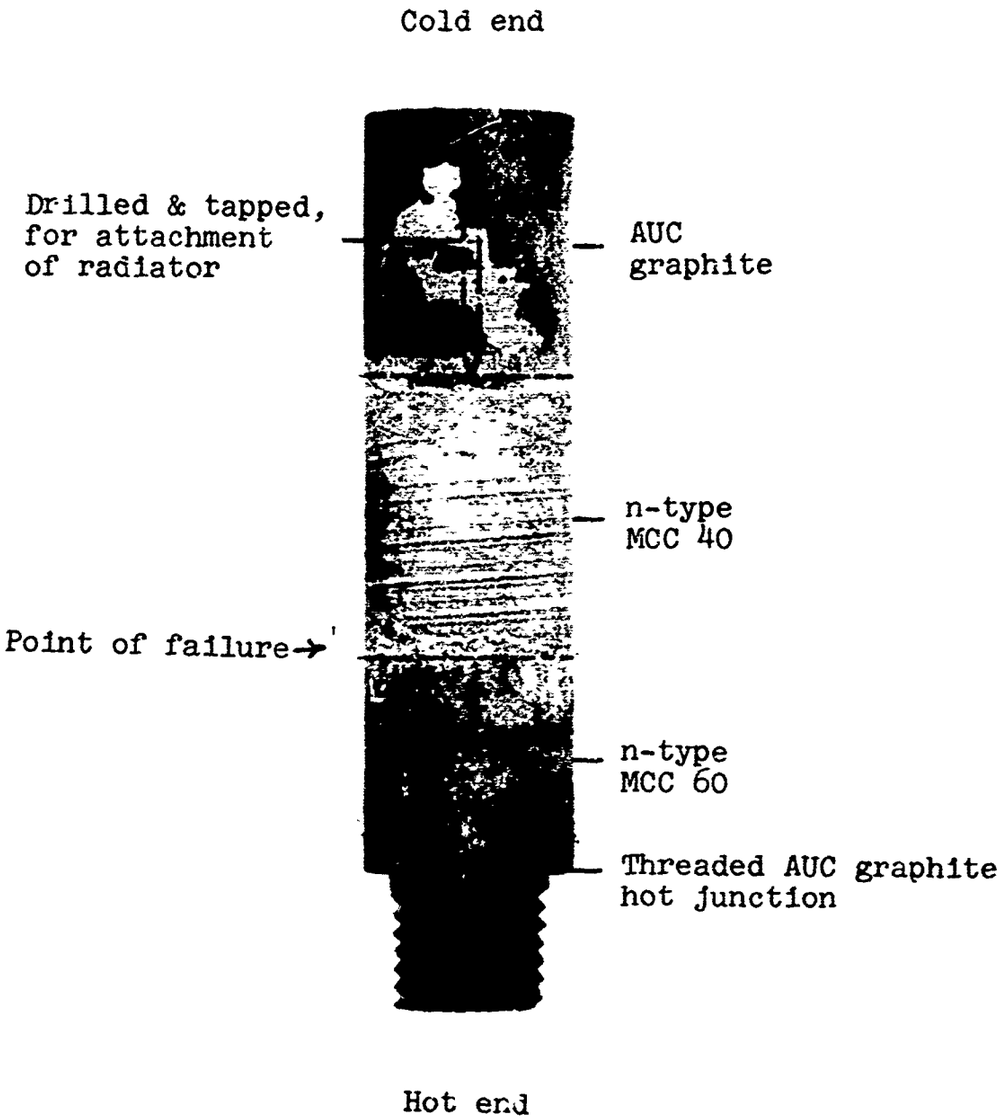

Figure 11. Typical Segmented Thermoelement Showing Point of Failure

3. The above conditions resulted in a borderline temperature at the junction between MCC 60 and MCC 40 segments of the n-type thermoelements. Normally, a fluctuation of a few degrees in heat source temperature would not affect the strength of n-type thermoelements. However, the borderline temperature conditions were exceeded, causing melting of the MCC 40 at its junction with the graphite interface transition material. Reaction of the higher melting alloy components of MCC 40 (from the liquid phase) with the graphite transition material at the intermediate junctions and subsequent diffusion with MCC 60 and other adjacent materials proceeded into the solid phase MCC 40 and outwardly to the thermoelement surface, progressively lowering melting points in the intermediate junction areas. After 266-hr. of this action, probably aggravated by the inherent vibration of the vacuum test stand, the first thermoelement intermediate-junction failures occurred.

4. Upon failure of the first thermoelement in a four-element half-tier, hot-junction temperatures rose in the remaining elements available to conduct the thermal energy present, and accelerated their failure.

5. Thermoelements in the top and bottom four or five tiers were unaffected due to the lower operating temperatures to which these units were exposed.

6. The n-type thermoelements were more affected than the p-type elements, due to the slightly lower melting point of the n-type MCC 40 formulation. Also, the better reproducibility and lower thermal conductivity of MCC 50, in relation to MCC 60, tended to minimize the rise in the T_i temperature of the p-type thermoelements.

It was concluded that the thermal conductivity of MCC 60 should be better established and its reproducibility improved. Preferably, the thermal conductivity of MCC 60 should be lowered without affecting its other thermoelectric properties. Improved techniques for detecting T_i temperatures in critically located thermoelements in prototype generators are needed for monitoring purposes.

3. Repair of the Generator

As repair of the damaged generator progressed, it became increasingly apparent that while its damage had been disconcerting, experience gained in recognizing the causes of trouble and in repairing the unit had cast much beneficial light upon the special problems connected with this pioneering attempt to use solid-state bonded multi-segment thermoelements in high-performance generators. As a result of this exploratory work, the importance and critical nature of the intermediate-junction temperature (T_i) between high-temperature (900-1200°C) thermoelectric segments and medium-temperature (400°C-950°C) segments were now recognized. Additionally, the need for and the difficulties of monitoring T_i temperatures, in research concerned with high-performance generators, were better appreciated.

Thermocouples had not been installed at the T_i sites for initial sustained performance tests on the 50-watt(e) generator because earlier tests, performed on what was believed to be representative p- and n-type thermoelements, had shown that for thermoelements operating between a T_h of 1200°C and a T_c of 500°C, the T_i's should be below 950°C. Further, the use of radially drilled thermocouple holes at the T_i sites had caused cracks to develop in the segmented 3/8-inch diameter thermoelements. Such cracking difficulties did not permit T_i measurements during production and selective screening of thermoelements for use in the advanced model generator.

This lack of information on T_i temperatures prevented detection of any large variations during routine production. Subsequent investigations, however, showed that T_i temperatures could vary widely (by as much as 100°C) in thermoelements made during production runs, despite the reasonable reproducibility in thermoelements S, R and E_{oc} observed during screening operations at a T_h of 1200°C.

When it was found that T_i temperatures in the 3/8-inch diameter, segmented thermoelements varied widely and were more critical from a long life viewpoint than the T_h temperatures of the generator, considerable effort was directed to developing a crack-free means for installing thermocouples at the T_i sites. Numerous attempts were made to drill thermocouple holes in the thin (1/16-inch) graphite barrier at the T_i site. In these efforts, acoustic, electric, and precision mechanical drilling techniques were investigated. Too frequently, the drilling device contacted the hard MCC 60 and MCC 50 segments, causing development of small and difficult-to-detect cracks. These cracks frequently became enlarged under thermal and physical stress, particularly in the case of n-type thermoelements, causing thermoelement failure.

After considerable experimentation, it was found that by using a 3/32-inch - 1/2-inch long graphite barrier, bonded between 3/8-inch diameter MCC 60 and MCC 40 segments, safe drilling of the desired radially oriented 0.036-inch diameter thermocouple holes could generally be accomplished at T_i sites. Accordingly, all p- and n-type thermoelements for use in repairing the generator were fitted with the longer (standard barriers were about 1/16-inch long) graphite barriers and thermocouple holes at the T_i sites. While the longer graphite barriers solved the problem of permitting thermocouple installation at the critical T_i sites, the resistance (R) of the modified thermoelements was 10-20% higher than for the earlier p - and n-type elements used in the 50-watt generator.

Each of the segmented p-type thermoelements from the damaged generator was re-evaluated at 1200°C for ρ, ΔT, S and R. It was found that thermoelement power output had been lowered by 10-20%, due to inadvertent operation at excessive T_i temperatures. The p-type thermoelements were physically sound and judged to be satisfactory for use in the repaired generator. To counter the reduced power output which could be expected from the damaged p-type elements and the high resistance n-type elements, the number of thermoelements in the repaired generator was increased by 20%. This increased the weight of the generator from 3.86 to 4.6 lb. exclusive of heat source and thermocouples which were installed at 117 different sites. The repaired and highly instrumentated generator is shown installed on its vacuum test stand in Figure 12 . Although 117 thermocouples were installed, only 41 couples could be used during a test because of vacuum feedthrough and switching limitations. The 72-contact, multi-deck switch used for thermocouple selection is shown near the lower end of the meter stick in Figure 12. The water-cooled cold wall shown at the lower left side of Figure 12 is normally used in a position surrounding the generator, switches ,and connection panel.

The 117 thermocouples were located in the generator as follows:

1. High-temperature tungsten-rhenium couples at 15 T_h sites.

2. Chromel-alumel couples at 46 T_i sites.

3. Chromel-alumel couples at 46 T_c sites.

4. Chromel-alumel couples located about the cold wall, on the multi-deck switch and thermocouple connection panel.

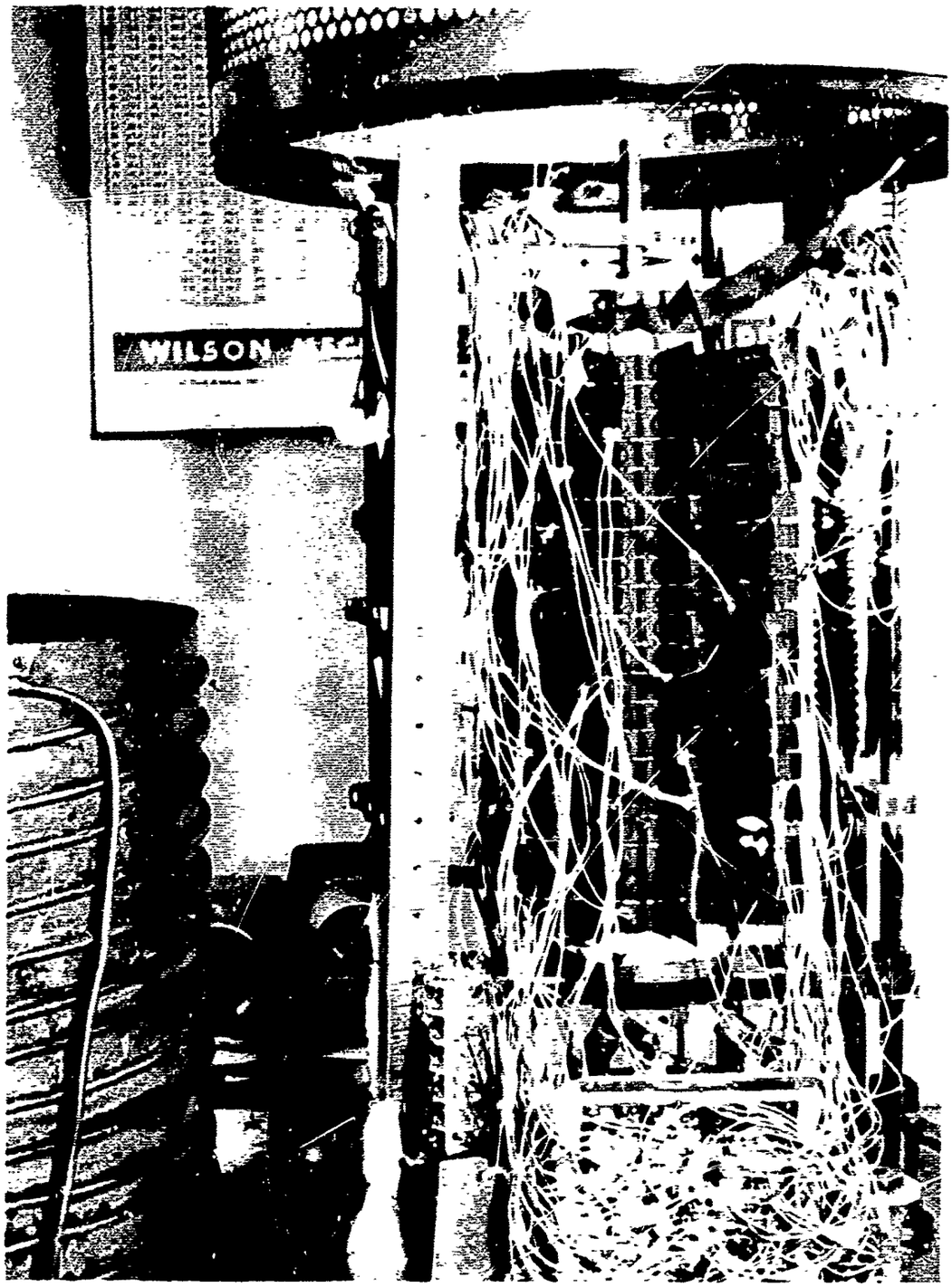

Figure 12. Advanced Laboratory Model Generator, Ready for Shakedown Tests, with Thermocouples Installed at 117 Sites

Prior to again starting the 1000-hr. sustained performance test, the repaired generator was subjected to a series of thermal tests to remove volatile material and to determine which of the monitored thermoelements would exhibit the highest T_i temperature as T_h approached 1200°C. These tests indicated that:

1. As many as 6-8 of the n-type thermoelements might appreciably exceed T_i temperatures of 900°C at a T_h of 1200°C. Such critical thermoelements were found in the central and hottest section of the generator.

2. The T_i temperatures of most n-type thermoelements would operate 15-50°C hotter than the T_i temperatures of adjacent p-type thermoelements of the same T_h.

3. A temperature differential of ~100°C existed between the hot-junction ends of thermoelements located in the center tiers and those located in the top and bottom tiers of the generator.

4. The smooth interior water-cooled cold wall, shown in place and surrounding the generator in Figure 2, was not capable (at 20°C) of dropping the T_c's of the generator to a sufficiently low level to keep the T_i's below the desired operating temperature of 900°C.

A schematic diagram of the repaired generator is presented in Figure 13, where its 248 3/8-inch diameter p- and n-type thermoelements are shown in 20 series-parallel connected tiers of 12 thermoelements each, with a 21st tier of 8 thermoelements at its top. In this diagram each segmented thermoelement is identified with a number and its polarity noted. The heavy lines shown at the bottom of each horizontal row (tier) of thermoelements represent the hot-junction straps between adjacent pairs of n- and p-type thermoelements. The lighter horizontal lines, shown connecting adjacent pairs of p- and n-type elements, represent the cold junction or radiator components. The small circles, with numbers in them, identify all of the remaining thermocouples that could be used at the end of the tests to monitor the performance and temperature of various segments of the generator. The smaller black dots on the periphery of the thermocouple circles indicate the thermoelement in which the thermocouple is located.

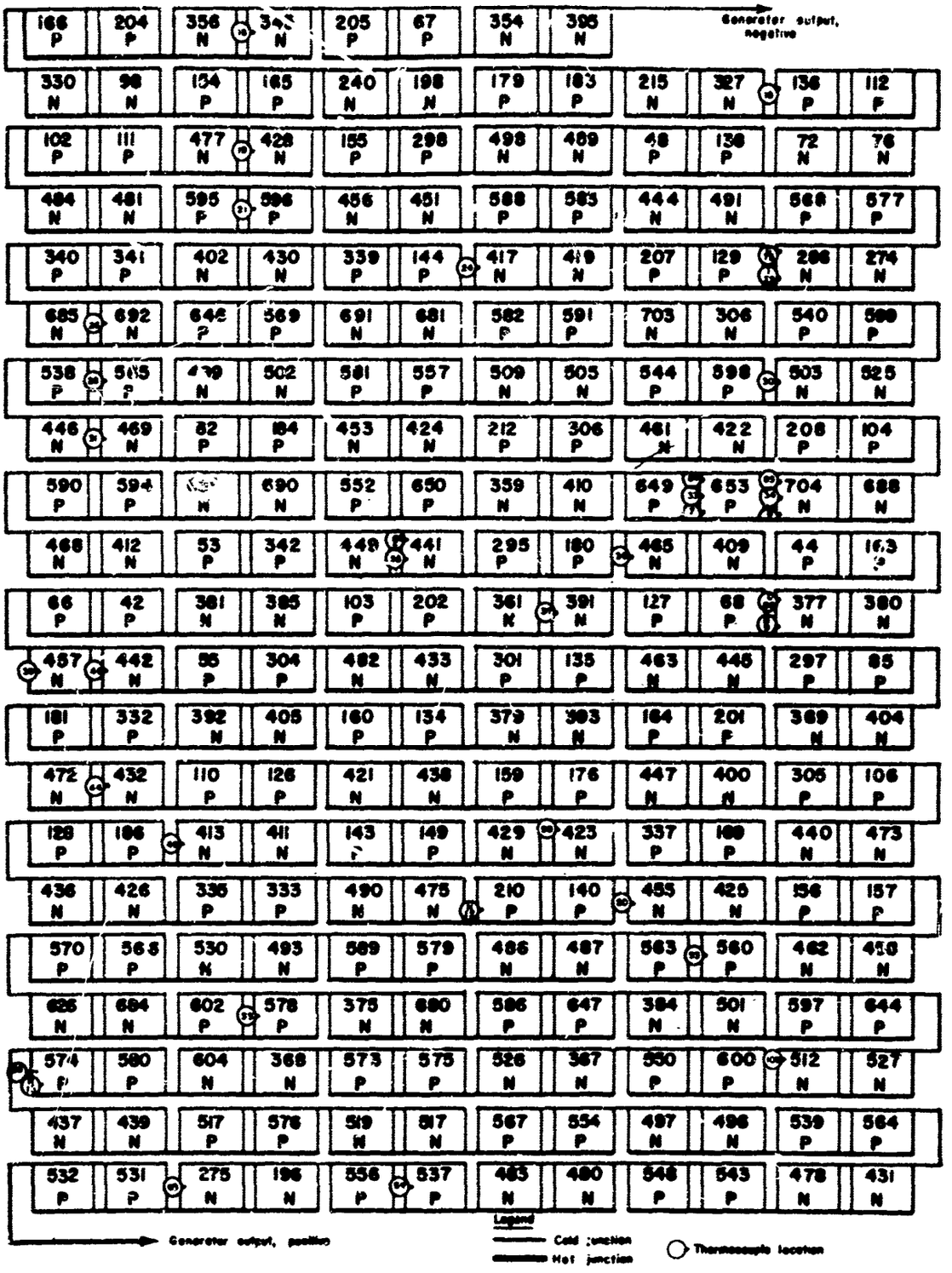

Figure 13. Schematic of Advanced Laboratory Model Generator Showing Thermocouple Locations

In an effort to lower T_i temperatures by decreasing the T_c temperatures of the generator, a new, internally finned, water-cooled, cold wall unit (not shown) was constructed. The fins of this unit, mounted on the inside surface of the heat sink, could be placed between the vertical rows of the generator fins. Despite use of this specially finned cold wall, it was not possible to operate the generator at a T_h of 1200°C without exceeding 900°C at T_i sites in the central thermoelements.

4. Second Sustained Performance

During preliminary thermoelement screening and shakedown tests, considerable difficulty was encountered in maintaining the integrity of the small gage thermocouples, and more than half of these couples were damaged. On the basis of the results of the shakedown test, it was decided to operate the most critical n-type thermoelements at a maximum T_i of 950°C in order to attain a T_h operating temperature during the 1000-hr. test. An n-type thermoelement which exhibited a T_i of 950°C at a T_h of 1200°C was chosen as the most critical thermoelement. This thermoelement (441 of Figure 13), located in the central (hottest) section of the generator, was equipped with thermocouples at its T_h and T_i sites. The temperature of the T_i site of this thermoelement was used as the reference temperature to control the power input to the tantalum heater source for the generator.

Data pertaining to the performance and operating conditions of the advanced model generator during its second sustained performance test was taken daily. This data is presented in Table 3 and shown graphically in Figure 14. It is important to note that with the exception of the T_h control temperature, temperatures presented in Table 3 and Figure 14 are average temperatures obtained from all thermocouples at T_h, T_i and T_c sites.

As shown in Table 3 and Figure 14, fluctuations in the temperatures (T_h, T_{in}, T_{ip}, T_{cp}, ΔT_{np}) of the generator occurred unpredictably. Such fluctuations are believed to have resulted from movement of the thermocouples due to vibration from the vacuum pumps of the test stand. Attempts to eliminate movement of the thermocouples by cementing them within the drilled thermocouple holes were unsuccessful. In this effort ceramic cements proved too brittle to maintain proper thermal contacts. Additionally, temperature fluctuations were caused by occasional losses of monitoring thermocouples, which altered the overall average of the affected group. An example of this condition is shown in the temperature change of T_{in}, noted in Figure 14, with respect to T_{ip}

Table 3

...NA Pt-M SUSTAINED PERFORMANCE AND THERMAL CYCLING TESTS IN ADVANCED LABORATORY M DEL GENERATOR OPERATED AT 1200°C AND 10^{-5} - 10^{-6} TORR

Hours Operation	Critical T_{hj}, °C	Avg. T_{hj}, °C	Critical T_{lj}, °C	Avg. T_{lj}, °C	Avg. T_{tp}, °C	Avg. T_{cp}, °C	Avg. ΔT_{hj}, °C	Avg. ΔT_{lj}, °C	Avg. ΔT_{tp}, °C	Avg. ΔT_{cp}, °C	I, amp	E_g, volts	P_g[1] watts	R_l, ohms	E_{out}, volts	P_{out} watts	P_{out}[2] watts	Input watts[3]	η_{th}, %	η_e, %
26	1204	1160	950	895	5[illegible]	578	554	582	578	585	5.65	7.71	43.60	1.35	14.[illegible]	44.32	45.40	3300	1.45	1.53
39	1204	1159	950	914	8[illegible]	5[illegible]	550	600	585	564	5.65	7.74	43.[illegible]	1.35	14.71	43.[illegible]	43.[illegible]	3000	1.[illegible]	1.4[illegible]
48	1204	1160	950	914	8[illegible]	5[illegible]	554	534	592	504	5.67	7.74	43.[illegible]	1.[illegible]	14.73	43.92	48.50	3000	1.4[illegible]	1.[illegible]
73	1204	1160	950	914	[illegible]	573	554	540	596	562	[illegible]	7.74	43.[illegible]	1.[illegible]	14.[illegible]	44.10	49.50	3300	1.47	1.[illegible]
104	1204	1160	950	905	876	573	558	540	595	562	[illegible]	7.74	43.[illegible]	1.[illegible]	14.[illegible]	44.10	49.50	3300	1.47	1.[illegible]
118	1201	1150	950	901	850	574	559	597	573	585	5.66	7.71	43.68	1.37	14.[illegible]	43.[illegible]	45.[illegible]	2450	1.47	1.51
133	1201	1147	950	888	861	572	555	582	565	572	5.64	7.68	42.71	1.37	14.[illegible]	42.80	46.[illegible]	2450	1.44	1.[illegible]
156	1202	1151	950	876	841	574	555	583	574	578	5.65	7.62	42.[illegible]	1.37	14.[illegible]	42.60	45.00	2480	1.43	1.51
179	1201	1143	950	874	860	575	554	570	560	566	5.62	7.60	42.[illegible]	1.29	14.[illegible]	42.82	47.50	2450	1.44	1.[illegible]
208	1200	1142	950	870	858	578	[illegible]	564	553	561	5.56	7.60	42.24	1.29	14.[illegible]	42.41	47.60	2480	1.42	1.[illegible]
232	1200	1142	950	870	865	578	554	564	557	561	5.56	7.60	42.24	1.29	14.60	42.41	47.60	2360	1.42	1.[illegible]
256	1200	1142	950	870	866	578	554	564	558	561	[illegible]	7.60	42.24	1.29	14.60	42.41	47.60	2490	1.42	1.[illegible]
280	1204	1144	950	873	863	581	557	563	555	563	5.57	7.63	42.41	1.29	14.91	42.64	44.30	2450	1.42	1.[illegible]
304	1204	1146	950	877	874	575	558	574	554	564	5.57	7.69	42.81	1.29	14.86	42.77	47.30	2480	1.43	1.58
327	1204	1147	950	872	863	571	558	570	556	563	5.57	7.63	42.58	1.29	14.82	42.58	47.30	2450	1.43	1.5[illegible]
360	1204	1144	950	871	863	573	555	566	550	559	5.54	7.61	42.24	1.29	14.80	42.40	49.20	2460	1.42	1.61
385	1204	1142	950	874	862	574	[illegible]	[illegible]	[illegible]	[illegible]	5.56	7.63	42.38	1.29	14.[illegible]	42.[illegible]	48.50	2490	1.42	1.63
409	1204	1142	950	874	862	574	[illegible]	[illegible]	[illegible]	[illegible]	[illegible]	[illegible]	42.23	1.29	14.[illegible]	42.23	48.50	2490	1.41	1.[illegible]
434	1204	1142	950	874	862	[illegible]	558	565	[illegible]	[illegible]	[illegible]	[illegible]	41.86	1.27	14.72	42.07	48.00	[illegible]	1.41	1.[illegible]
453	1204	1141	950	881	862	[illegible]	558	[illegible]	545	[illegible]	[illegible]	[illegible]	41.79	1.29	14.[illegible]	42.[illegible]	48.50	2480	1.41	1.[illegible]
483	1204	1143	950	870	872	580	559	564	[illegible]	[illegible]	[illegible]	[illegible]	42.20	1.29	14.50	42.30	48.50	2450	1.42	1.62
504	1204	1142	950	871	872	580	559	564	544	[illegible]	[illegible]	[illegible]	42.10	1.24	14.[illegible]	42.3[illegible]	48.50	2450	1.42	1.[illegible]
526	1204	1142	950	870	873	580	559	564	544	[illegible]	[illegible]	[illegible]	42.07	1.30	14.[illegible]	42.30	[illegible]	[illegible]	1.42	1.[illegible]
548	1204	1142	950	872	873	580	559	564	546	[illegible]	[illegible]	[illegible]	42.00	1.[illegible]	14.[illegible]	[illegible]	48.50	[illegible]	1.42	1.[illegible]
575	1204	1142	950	872	873	580	559	564	[illegible]	[illegible]	[illegible]	[illegible]	42.00	1.24	14.[illegible]	42.[illegible]	48.50	[illegible]	1.42	1.[illegible]
594	1204	1142	950	872	873	580	559	564	[illegible]	[illegible]	[illegible]	[illegible]	41.97	1.23	14.[illegible]	42.[illegible]	48.50	[illegible]	1.41	1.[illegible]
620	1204	1144	950	871	[illegible]	[illegible]	[illegible]	[illegible]	[illegible]	[illegible]	[illegible]	[illegible]	41.82	1.25	14.[illegible]	42.46	47.20	[illegible]	1.[illegible]	1.[illegible]
632	1204	1144	950	827	[illegible]	[illegible]	[illegible]	[illegible]	[illegible]	[illegible]	[illegible]	[illegible]	After Heater Repair							
[illegible]	[illegible]	[illegible]	[illegible]	825	[illegible]	[illegible]	[illegible]	[illegible]	[illegible]	[illegible]	[illegible]	[illegible]	44.[illegible]	1.[illegible]	14.[illegible]	44.71	50.00	[illegible]	1.[illegible]	1.[illegible]
[illegible]	[illegible]	[illegible]	[illegible]	822	[illegible]	[illegible]	[illegible]	[illegible]	[illegible]	[illegible]	[illegible]	[illegible]	42.[illegible]	1.[illegible]	14.[illegible]	42.[illegible]	[illegible]	[illegible]	[illegible]	[illegible]

[1] Assumed [illegible] as indicated above. [2] Maximum power output [illegible] the square of the voltage [illegible] the load to the square of the average [illegible] operation. [3] Input power was maximum [illegible] until heater failure. Additional explanation [illegible]

Table 3 (Cont'd)

DATA FROM SUSTAINED PERFORMANCE AND THERMAL CYCLING TESTS IN ADVANCED LABORATORY MODEL GENERATOR OPERATED AT 1200°C AND 10^{-5} - 10^{-6} TORR

Hours Operation	Critical T_h, °C	Avg. T_h, °C	Critical T_{in}, °C	Avg. T_{in}, °C	Avg. T_{ip}, °C	Avg. T_{cn}, °C	Avg. T_{cp}, °C	Avg. ΔT_n, °C	Avg. ΔT_p, °C	Avg. ΔT_{np}, °C	I, amp	EL, volts	P_o[1] watts	R, ohms	E_{oc}, volts	P_{o1} watts	P_{o2} watts	Input, watts[3]	η_1, %[4]	η_2, %[5]
711	1204	1129	950	921	868	582	564	547	546	546	5.53	7.61	42.45	1.30	14.98	42.45	50.10	2890	1.47	1.7[illegible]
735	1204	1127	950	921	858	580	564	577	546	546	5.55	7.58	42.09	1.30	14.[illegible]	42.1[illegible]	49.[illegible]	2890	1.4[illegible]	1.73
759	1204	1126	950	919	853	578	564	548	546	547	5.53	7.55	41.77	1.30	14.77	41.96	49.70	2890	1.45	1.71
787	1204	1126	950	920	861	568	566	559	544	551	5.54	7.57	41.91	1.30	14.80	41.92	49.60	2890	1.45	1.68
811	1204	1126	950	922	877	558	570	569	540	554	5.53	7.54	41.96	1.30	14.77	41.67	47.80	2890	1.44	1.65
835	1204	1126	950	920	877	557	570	570	540	555	5.50	7.52	41.38	1.31	14.72	41.69	47.60	2890	1.44	1.65
861	1204	1139	950	917	880	572	573	567	549	558	5.50	7.54	41.50	1.31	14.75	41.81	47.30	2890	1.44	1.61
883	1204	1139	950	917	880	572	573	567	549	558	5.50	7.54	41.50	1.31	14.75	41.81	47.30	2890	1.44	1.64
907	1204	1139	950	922	874	577	574	567	548	557	5.50	7.52	41.54	1.32	14.79	41.55	47.30	2890	1.44	1.64
922	1204	1139	950	922	870	577	575	567	547	557	5.50	7.52	41.54	1.32	14.79	41.55	47.30	2890	1.44	1.64
946	1204	1139	950	921	862	577	576	566	546	551	5.51	7.50	41.38	1.31	14.75	41.41	47.[illegible]	2[illegible]90	1.44	1.64
968	1204	1135	950	920	868	572	576	562	544	553	5.49	7.47	41.01	1.32	14.70	41.05	47.70	2890	1.42	1.60
972	1204	1135	950	921	869	575	577	561	545	553	5.50	7.49	41.20	1.32	14.75	41.21	47.80	2890	1.43	1.60
1004	1204	1135	950	920	869	575	577	561	545	553	5.50	7.49	41.20	1.32	14.75	41.21	47.80	2890	1.43	1.60
1051	1204	1126	950	919	853	578	564	548	546	547	5.53	7.55	41.77	1.31	14.77	41.96	49.70	2890	1.45	1.72
1099	1204	1138	950	922	870	577	575	567	547	557	5.50	7.5[illegible]	41.[illegible]	1.31	14.79	41.60	47.30	2890	1.44	1.61
							---- Thermal Cycling Tests ----													
1120 (Cycle 5)	1204	1135	950	921	869	575	577	561	545	553	5.50	7.49	41.20	1.32	14.75	41.21	47.80	2890	1.43	1.60
1140 (Cycle 29)	1204	1139	950	922	870	577	575	567	547	557	5.50	7.52	41.54	1.32	14.79	41.55	47.30	2890	1.44	1.64
1153 (Cycle 53)	1204	1135	950	920	869	575	577	561	545	553	5.50	7.49	41.20	1.32	14.75	41.21	47.80	2890	1.43	1.60
1166 (Cycle 77)	1204	1135	950	921	869	575	577	561	545	553	5.50	7.49	41.20	1.32	14.75	41.21	47.80	2890	1.43	1.60
1186 (Cycle 105)	1204	1135	950	920	869	575	577	561	545	553	5.50	7.49	41.21	1.32	14.75	41.21	47.80	2890	1.43	1.60

(1) Actual power output at indicated ΔT_{np}. (2) Maximum power output P_{o1} corrected by ratio of square of the average ΔT_{np} at each operating period to the square of the average ΔT_{np} at 39 hrs operation. (3) Calculated actual energy input to generator. (4) Based on power output maximum (P_{o1}) at thermal conditions when readings were taken. (5) Based on maximum power output (P_{o2}) adjusted as explained in note (2).

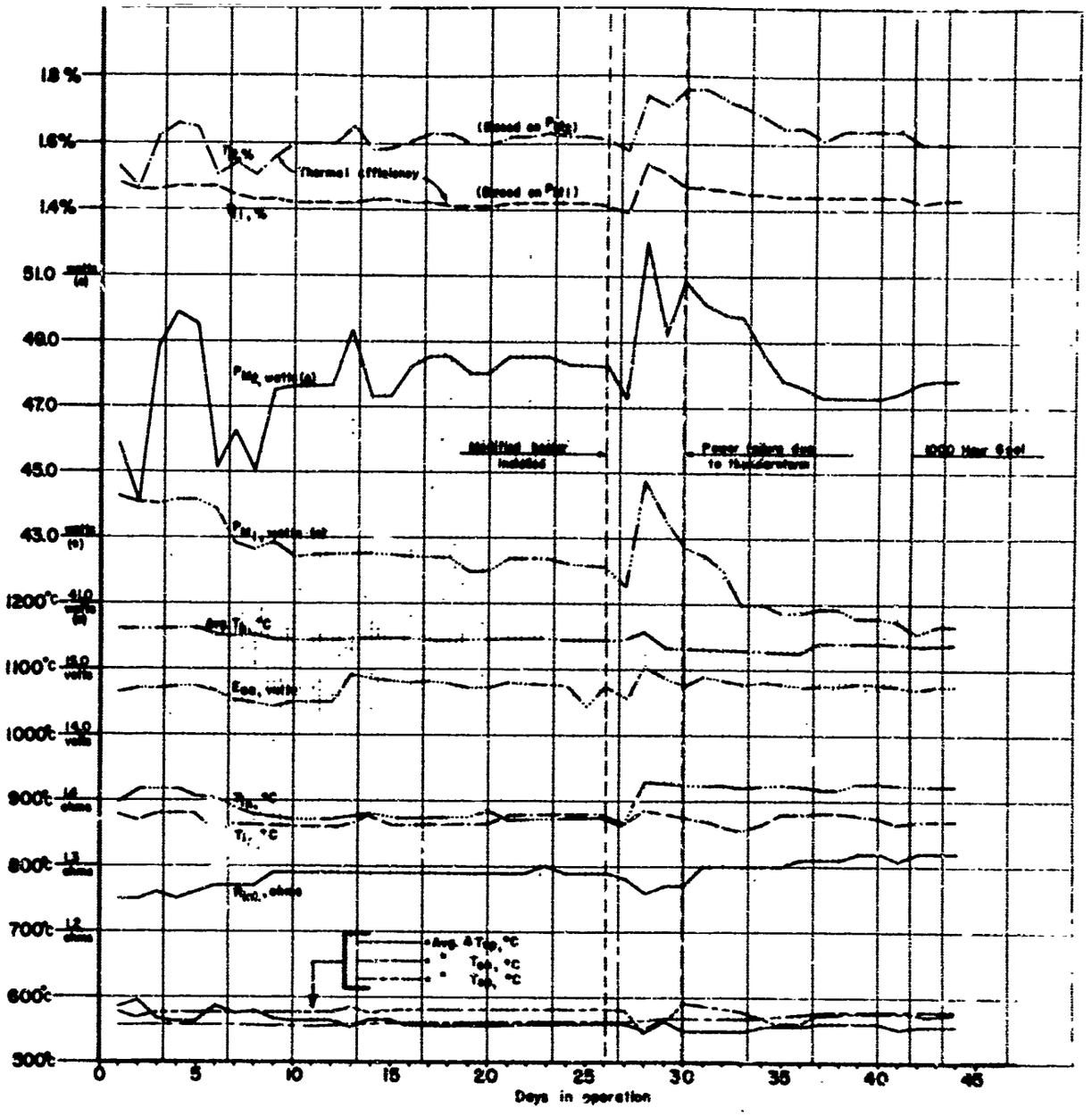

Figure 14. Performance Characteristics of Advanced Laboratory Model Generator

on the 21st day (500 hr.). At this time, two n-type T_i monitoring thermocouples simultaneously failed, altering the average T_{in} to a value below the average T_{ip}. Similar occurrences affected the average temperatures at various times throughout the 1000-hr. sustained performance test.

The fluctuations of thermocouple readings also contributed directly to the varying of E_{oc} and P_{M_1} (Figures 14 and Table 3), since the positional change of the T_h control thermocouple alters the input power slightly. The generator serves as a multiplier of minor thermal effects of input power fluctuation and responds by exhibiting greater fluctuation of E_{oc} and P_{M_1}. The remaining data presented (R_{int}, T_{M_2}, η_{M_1}, η_{M_2}) were affected by both input power, temperature, and thermocouple fluctuation with resulting compounded variations in their respective curves.

In addition to the thermocouple considerations noted, it was noticed that as the sustained performance test progressed beyond the 20th day (480 hrs.), P_{M_1} gradually decreased while the resistance to the heater unit increased. A study of the T_i and T_h temperatures indicated that the top and bottom seven tiers of the generator were operating at a temperature somewhat below that of the central section of the generator. The T_i temperatures in these end portions of the generator averaged 50-70 °C below those of the center section. This uneven temperature profile prevented the generator from operating at its full power potential.

The heater originally consisted of a tantalum cylinder of 0.5-inch O.D. and a wall thickness of 0.015 inch, but a check after its removal showed that the wall thickness in its center section had been reduced by an amount varying from 0.0015 to 0.002 inch during its more than 600-hr. use as a heat source.

Figure 15 presents a sketch of the modification that was made to the tantalum heater. It consisted of flame-sprayed molybdenum to a maximum depth of 0.005 inches on its central 5 inches, with a gradual taper toward the ends. This molybdenum coating decreased the resistance of the central portion of the heater, thus reducing the I^2R heating effect at its center, with resultant smoothing of the temperature profile of the generator.

During installation of the modified heater, a vapor shield was constructed and installed as a precautionary measure to minimize deposition of tantalum on the hot junctions of the generator. It consisted of a graphite cylinder mounted around the heater and positioned by boron nitride bushings, so that thermal contact was minimized and no electrical contact occurred between vapor shield, heater, and the hot junctions of the generator. The total operation required less than 4 hrs. of down time on the 26th day (620 hrs.) of performance testing.

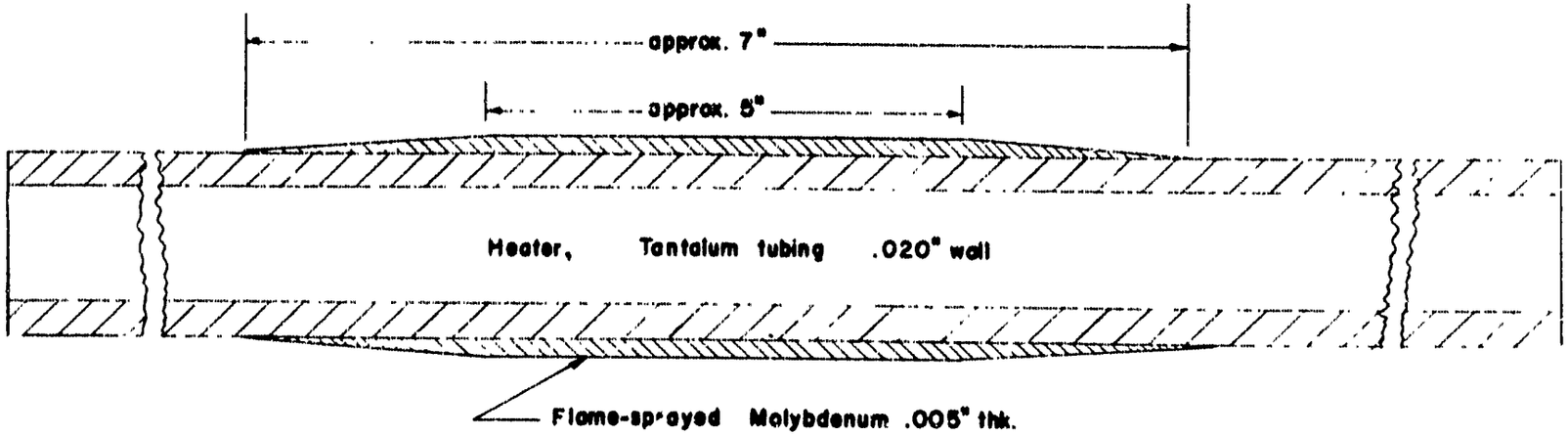

Figure 15. Sectional View of Improved Tantalum Heater

Initial performance of the generator, after heating to an operating T_h of 1200°C, indicated that repairs to the heater had been successful. The power peaks exhibited by the P_{M_1} and P_{M_2} of Figure 14 at 28 days (670 hrs.) were a direct result of the increased average T_h created by raising the end temperature of the generator. The average T_i variation over the generator length at 28 days did not exceed 10°C, but as the test proceeded, T_i variation between the end and center sections of the generator became progressively greater. At 687 hours, the temperature differential between the top and center sections of the generator had increased to 23°C, while that between the bottom and the center sections had increased to approximately 57°C, with the center section hotter in each case. Beyond this test time, further comparison of T_i temperatures was not significant, since several thermocouples located in n-type thermoelements were lost within the lower seven tiers. It is possible that much of the earlier fluctuation in T_i averages may have been caused by these slowly failing thermocouples.

However, as the test continued it became apparent that random hot spots were developing over the central area of the modified heater. After 750 hr., hot spots in the heater were encountered and T_i temperatures were not constant enough to be usable for control purposes. That is, the T_i's were so unstable that the generator's operating temperature could not be adjusted without fear of hot spots causing an interface temperature in excess of the critical 950°C limit. Accordingly, control of this generator was returned to a T_h thermocouple which had operated at about 1200°C when the critical T_i was at 950°C. It appeared that the generator power output values would have been considerably improved due to the heater modification, had not the erratic hot spot condition occurred.

It was believed at this time that the hot spots were caused by alloying of the molybdenum coating with the tantalum cylinder. Such alloying presumably formed a molybdenum-tantalum material which had resistance values considerably higher than either the molybdenum or the tantalum. These high-resistance areas created the random hot spots which prevented the generator from reaching maximum capability. Further evidence that alloying of the molybdenum was the cause of the heater hot spots was found in the fact that all of the T_i's that were fluctuating were located in the central section of the generator. This area received heat directly from the center section of the tantalum heater.

One other event, a power failure caused by a thunderstorm on the 30th day (720 hr.) of the test, is worthy of mentioning because it caused the generator to cool to 500°C. Maximum cooling rates of 250-260°C/min. were reached during this incident.

Two efficiency indexes, η_{M1}, and η_{M2}, were used during the sustained performance test. The first of these, η_{M1} was based upon the power output (P_{M1}) of the generator obtained under matched load conditions at the actual ΔT_{hp} encountered in the experiment. The second index, η_{M2}, was based upon the adjusted matched load power output (P_{M2}). The adjusted power output, P_{M2}, consists of P_{M1} normalized by the ratio of the square of the actual temperature differential (ΔT_{hp}) across the generator to the square of the temperature differential experienced by the generator at a reference point (39 hr. operation). The efficiency in each case was based on the ratio of P_M/Q, where Q (input) was estimated by subtracting the extraneous conductive and radiative losses of heat from the ends and supports of the generator. These losses were assumed constant during the test.

As indicated by the η_{M1} and η_{M2} columns in Table 3, the η_{M1}, thermal efficiency of the generator varied from a low of 1.46% at 39 hr. to 1.54% at 26 days (63 hr.). The more meaningful (because it was corrected for temperature variations) efficiency index, η_{M2}, increased from 1.46% at 39 hr. to a peak 1.76% between 687 and 711 hr. operation. It is significant that while fluctuations in both efficiency indexes occurred during the test, they did not decrease below the values at the start of the test.

The most meaningful power output index of generator performance vs time is presented in column "P_{M2}" of Table 3 and P_{M2} of Figure 14. This index gives the electrical power output of the generator under matched load conditions and adjusted to a standard thermal condition. The generator output after 39 hr. of operation was arbitrarily chosen as a standard performance for comparative purposes

While variations in P_{M2} occurred as the test progressed, the general trend, shown in Figure 14, was for the power to remain above 47 watt (e) after the first 50 hr. operation. A peak output value of 52 watt (e) /11.8 watt (e)/lb./ was reached on the 26th day (620 hr.). Lowest output was encountered between the 5th and 7th day when it dipped twice to about 45 watts (e). However, as shown in Figure 14, the adjusted power output (P_{M2}) remained above the reference condition (where $P_{M1}=P_{M2}$) at 39 hr. for the duration of the sustained performance test. Discounting the largest peaks and valleys shown in Figure 14, P_{M2} tended to improve somewhat with increasing time. On the basis of the improvement in P_{M2} with time, it could be concluded that the power-generating characteristics of the materials used in this generator improved rather than degraded with time under test conditions. A more conservative conclusion is in order: namely, that no apparent degradation of the thermoelectric

power-generating properties of these MCC materials used building the advanced model generator occurred during the sustained performance and thermal cycling tests.

5. Thermal Cycling Test

The thunderstorm that caused a power outage during the sustained performance test helped establish the maximum heating-cooling rate that could be attained by thermal radiation. Examination of the cooling curve of the generator after the power failure showed that peak rates of 240-250°C/min. were reached.

With regard to heating, it was assumed that the heat source would be a solar collector of fixed diameter, operating in an orbit of constant solar flux. Under these conditions, the heat input to the generator upon leaving the shadow of the earth was assumed to be 2890 watts(t), the same input used for the sustained performance test. To provide the desired cooling-heating cycling conditions, a temperature-time cam was machined and was used on a control instrument to govern the power input to the generator providing the typical thermal cycle curve shown in Figure 16. Peak cooling rates to 260°C/min. and heating rates of about 120°C/min. could be attained on a cyclic basis with this cam.

The generator was subjected to 105 consecutive thermal cycles of the type shown in Figure 16. Data from these tests is presented at the bottom of Table 3, and shows that no change in the power-generating characteristics of the generator developed during the thermal cycling tests.

6. Post-Test Examination

Upon completing the thermal cycling tests, the generator was cooled to room temperature and the bell jar opened for inspection. Since the bell jar could be swung aside, the test stand served as a secure mounting for examination. All thermocouples used for heat balance calculations and test-stand temperature monitoring were removed. Likewise, all protective insulation and reflective shields were removed in order to permit easier access to viewing of the generator. A careful inspection of all thermoelements available for viewing was made and no damage found.

Several radiator fins were slightly bent, and in several cases their emissive coating had been chipped off. This minor damage apparently resulted from removal of the close fitting, water-cooled heat sink. The bent radiators were straightened and the chipped coatings of TEC-1 emissive material were replaced.

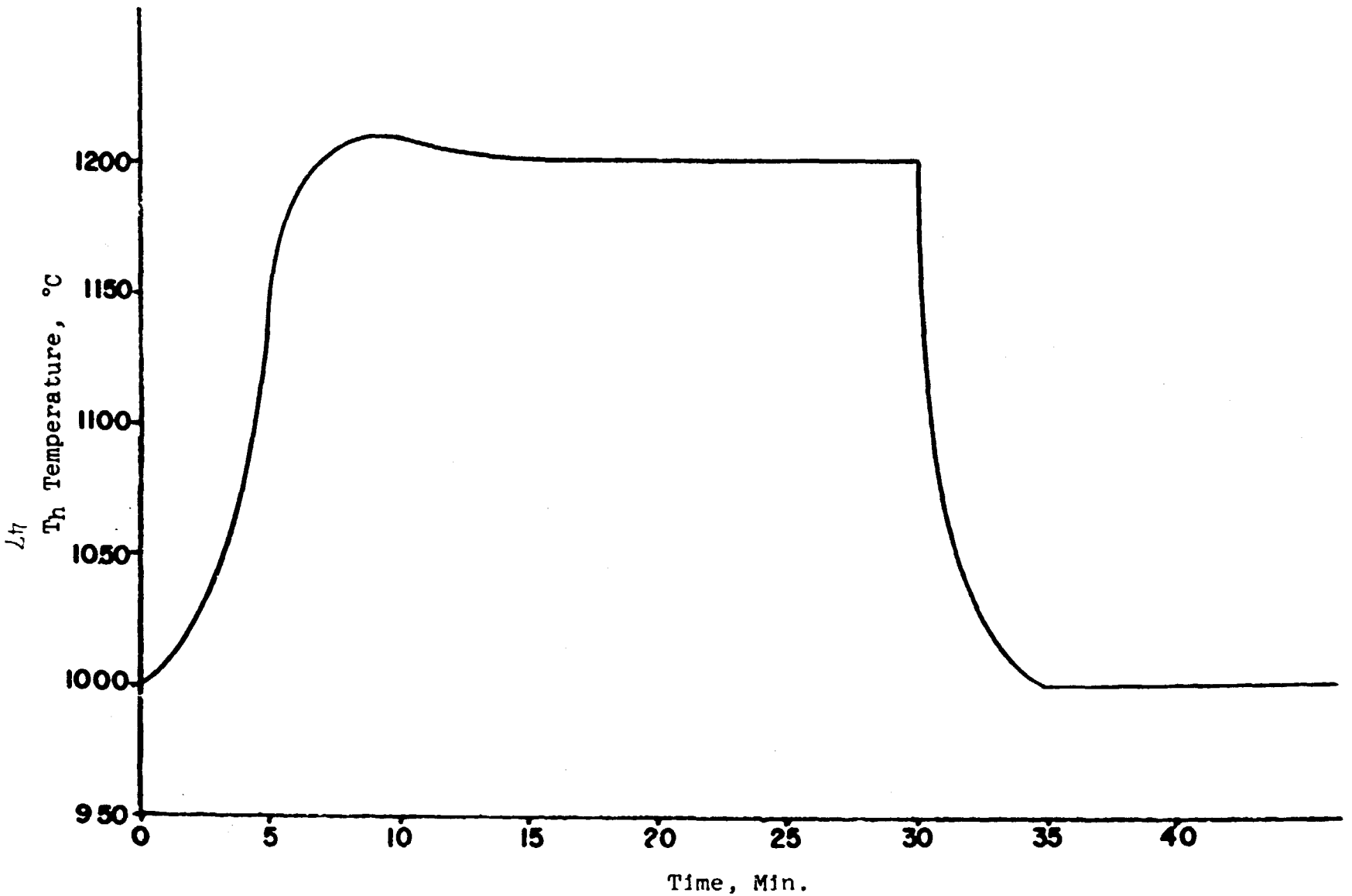

Figure 16. Typical Thermal Cycles of Advanced Laboratory Model Generator

It was noted that the molybdenum junctions were brittle, making movement of the generator quite risky. It was noted that the thermocouples were also brittle. Extreme care was taken wherever thermocouples and leads were involved so that no motion would entangle the lead about the radiator fins and cause flexure of the molybdenum.

After external inspection, the clamps attaching the current leads to the heater were taken off and the heater was removed. The heater, as shown in Figure 17, did indeed show evidence that hot spots had been produced during the latter stages of the sustained performance and the thermal cycling tests. Excessive and irregular grain growth was found on the surface of the heater, particularly in the center section of the generator. Hot spot areas were also found at each end of the heater where electrical contact between it and the power supply was made. The presence of such large, irregular areas in the surface of the heater was judged to be the result of molybdenum alloying with the tantalum and the effect of exposure of the heater to temperatures in excess of 1200°C.

Following a visual inspection of the heater cavity, which showed no change in mechanical appearance from the last inspection, the hold-down top cross bar was replaced to provide support to the generator structure during the remaining inspection. The graphite vapor shield, normally used to prevent vaporized heater material from plating on the hot junction of the generator, was removed. Removal of the vapor shield permitted viewing of the interior surfaces (hot-junctions) of the generator. Only a very light coating of tantalum, deposited during the first 620 hr. of the tests and prior to installation of the vapor shield, could be seen. This coating was apparently thin enough not to have appreciably short-circuited the generator.

On the basis of this examination, it was concluded that the segmented MCC thermoelements used in the construction of the generator were virtually unaffected by the 1186 hr. of sustained performance and thermal cycling tests. Since many of the thermoelements used in the fabrication of this generator had previously been exposed to about 270 hr. of the initial sustained tests, it can be concluded that the MCC thermoelements are capable of more than 1450 hr. of operation at the test conditions without degradation.

Generator components most affected by these tests were the molybdenum-copper-graphite junctions of its radiators and molybdenum -graphite hot-junctions. These components became brittle and sensitive to cracking from mechanical impact after more than 1200 hr. of exposure to simulated space-operating conditions.

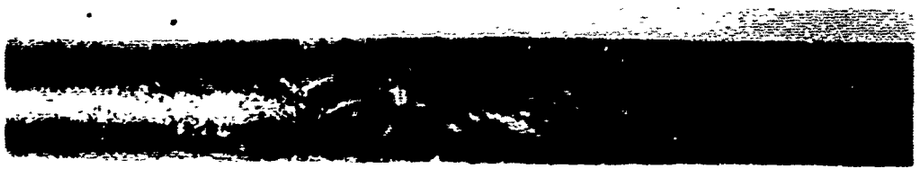

Top end

Center section

Figure 17. Molybdenum Sprayed Tantalum Heater Showing Grain Growth in Top End and Center Section

Additionally, the small (0.005 inch diameter) thermocouples used for monitoring purposes became brittle and were difficult to keep properly positioned.

It is not likely that serious embrittlement problems would be encountered with the molybdenum coatings of the radiators and hot-junctions on this type of generator during the essentially vibration- and impact-free post-launch period.

However, attention should be given to minimizing preflight tests for extended periods at elevated temperatures.

B. IMPROVED EXPERIMENTAL MODEL GENERATOR

The experience gained in designing, building, and initially testing the 50-watt advanced laboratory model was used in the design of the improved experimental model generator that is presented in this section. The design goals for the improved model were to make it more rugged, reliable, long-lived and capable of a higher performance ratio than the advanced laboratory model.

Because of the problems that occurred when the intermediate-junction design temperature (T_i) of the n-type thermoelements of the 50-watt model was unknowingly exceeded, particular attention was paid to solving this problem in the improved experimental model. To overcome the T_i monitoring problem it was planned to install thermocouples at the intermediate junctions of p- as well as n-type thermoelements located in the hottest central sections of the generator. Additionally, a spiral-wound, resistance-wire heater unit was used in place of the tubular one employed with the 50-watt generator.

In addition to the above tasks, a very difficult problem to be solved in designing and building an improved experimental model generator involved the reduction of the diameter of the segmented thermoelements from 3/8-inch to 1/4-inch without serious reduction in the quality and reproducibility of their thermoelectric properties. Considerable difficulties with these areas were encountered during the preceding year's efforts when it was necessary to reduce the diameter of segmented thermoelements from 1/2 inch to 3/8 inch to raise the watts/pound ratio of the advanced laboratory model. The task is even more difficult in reducing thermoelement diameter from 3/8 inch to 1/4 inch. Emphasis was placed by the Air Force on producing an improved experimental generator that could be operated for 3500 hours during this year's program.

1. Design Optimization

Prior to completing the preliminary design of the improved experimental model generator, a series of computer calculations was made to study the relative effects of changes in the generator design parameters on the overall watts/pound ratio. For these calculations a fixed thermoelement diameter of 1/4 inch was used and the thermoelement length and cold-junction (radiator) temperatures were varied over fairly large ranges (0.1 to 2.5 cm. for the total thermoelement length and 500°C to 750°C cold-end temperatures). The material properties of the thermoelectric segments were identical to those used for a similar calculation on the 3/8-inch diameter thermoelements as reported previously[4]. A hot-junction temperature of 1200°C and an intermediate-junction tem-

perature (T_i) of 850°C between p-type MCC 40-MCC 50 and n-type MCC 40-MCC 60 segments were used for the 1/4-inch diameter thermoelements.

Results of optimization calculations for 1/4-inch diameter thermoelements are shown in Figure 18. where the limiting effect of the radiator weight on the overall watts/pound ratios is apparent, just as it was for the 3/8-inch diameter thermoelements used in the advanced laboratory model study. It may also be seen from the curves of this figure that a definite improvement over the watts/pound ratio for the selected design of the improved experimental model could be made by using short thermoelements.

Although short thermoelements are definitely desirable from a high-performance ratio point of view, it is not feasible at this time to obtain the high degree of reproducibility in the length and thermal conductivity (or density) of thermoelectric segments needed if high watts/pound ratios are to be attained by closely approaching the critical T_i for each thermoelement.

The nature of the critical T_i temperature problem may be better appreciated if it is considered that for a design temperature of 700°C between the hot and cold ends of each thermoelement, an average temperature gradient of about 60°C/mm. would exist in 1.2 cm.-long by 1/4-inch diameter thermoelements. A 1.2 cm.-long thermoelement of 1/4-inch diameter corresponds to that which would result if the L/A ratio of the 1/4-inch diameter thermoelement were the same as that used for the 50-watt model. Even higher temperature gradients of 75-100°C/mm. would be encountered in segment areas immediately adjacent to the intermediate junction of the 1/4-inch diameter thermoelements. Thus, for 1/4-inch diameter MCC 50 or MCC 60 segments, only 0.5 mm. (0.0196 inch) shorter or longer than specified by design, the T_i in a segmented thermoelement could range from 30°C to 50°C higher, or lower, than the required T_i.

Variations in segment density also exert an effect on T_i with low and high segment densities in MCC 50 and MCC 60 segments contributing to low and high T_i temperatures, respectively. Low and high densities in MCC 40 segments would similarly affect the T_i temperatures.

Since it is not yet possible to reproduce the length and densities of the various segments with sufficient precision to meet design specifications for each material, the average temperature gradient down each thermoelement was decreased by making them longer. While this approach lowered the watts/pound ratio for the improved model, its thermal efficiency benefits from the longer lengths employed.

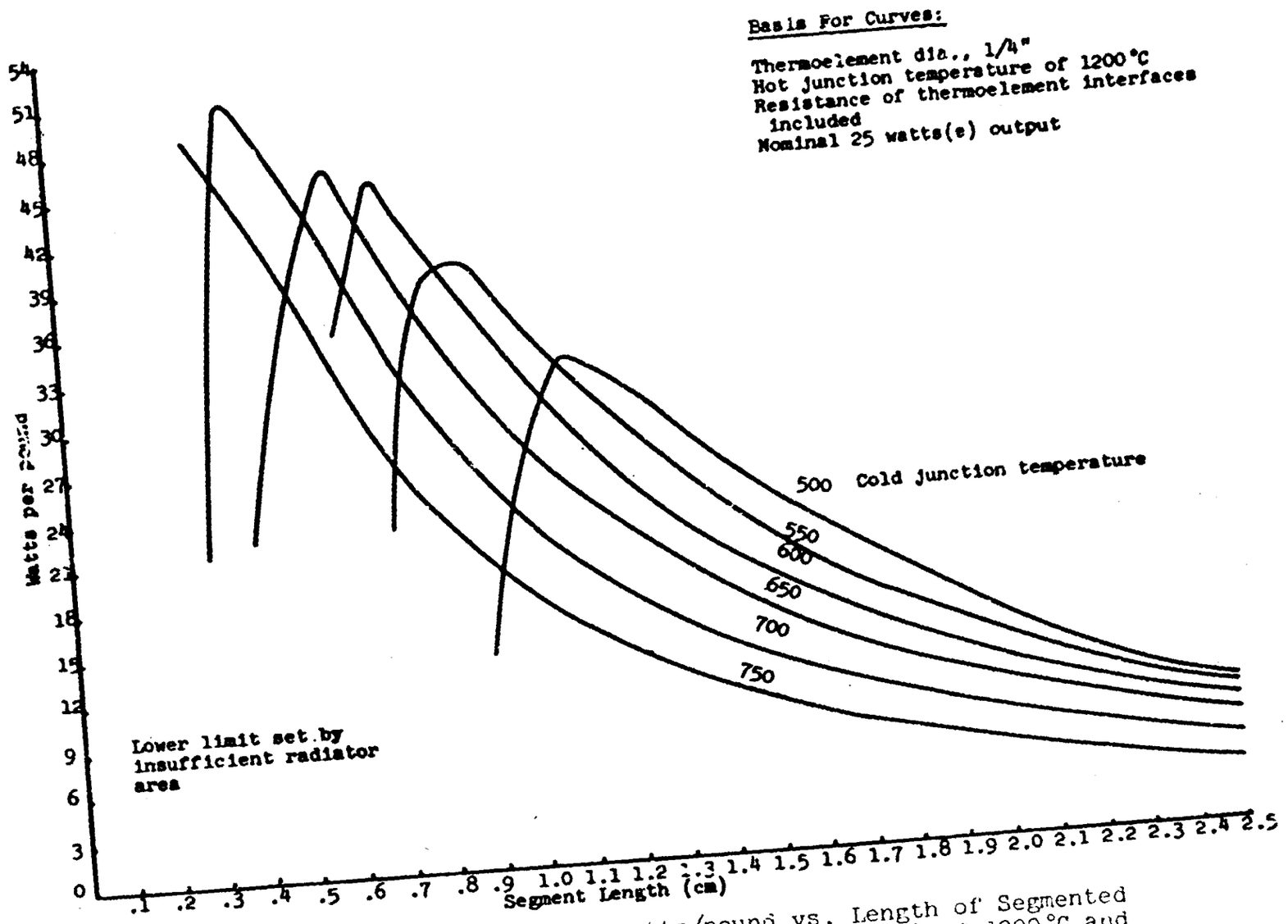

Figure 18. Variation of Generator watts/pound vs. Length of Segmented Thermoelements with Hot-End Temperature (T_h) of 1200°C and Various Cold-End Temperatures (T_c)

With the T_i problem in mind, the length of the 1/4-inch diameter thermoelements for the improved experimental model generator was arbitrarily set at 2 cm. On this basis, as shown in Figure 18, a watts/pound ratio of about 14.5 was computed for the improved experimental generator operating with a cold-junction temperature of about 500 °C.

The design of this generator was originally directed toward a nominal power output of ~25 watt (e). In addition to the smaller power output and diameter of its thermoelements, the following design features for the improved model differed from those of the 50-watt advanced laboratory model:

a. Each tier of the improved model was comprised of 16 rather than the 8 thermoelements used in the 50-watt unit. The use of more thermoelements per tier provided a shorter, more rugged generator geometry configuration.

b. Each tier is sectioned in quadrants rather than in halves. The use of quadrant tier sections, connected in series, permits generation of about 6 volts with the improved experimental model at approximately one-half of the total power of the 50-watt model.

c. The inner graphite quadrant sections are rigidized with a flame-coated refractory alumina bond. This new technique permitted significant increases in the mechanical strength of this generator geometry.

d. Use of 1/4-inch diameter thermoelements permitted close spacing of thermoelements and better utilization of the heat transfer area in the inner hot-junction graphite rings.

e. A spiral-type electrical resistance heater, rather than the tube-type used on the 50-watt model, was employed. This type heater provided a more uniform heat flux within the central cavity of laboratory-type generators.

f. Interface and T_c thermocouples were installed axially from the cold ends of the TE element.

Some similarities between the 50-watt advanced laboratory model and the improved experimental model generator are listed below:

a. A simple cylindrical generator geometry was used in each case.

b. Two p- and 2 n-type thermoelements were used per graphite hot-junction tier section to provide greater reliability of the power generating circuit.

c. Hot-pressed cylindrical thermoelements were used in both models.

d. Materials of construction were in general the same.

It was not possible to find optimum solutions to each of the problems, discussed in the next section, in time to permit fabrication of a 192-element generator, as originally proposed. Instead, a generator based on 144 segmented p- and n-type thermoelements and capable of 15-watt (e) output at 1200°C T_h and 500°C T_c, was fabricated.

2. Fabrication

The preparation of enough thermoelements of sufficient quality for generator fabrication proved quite difficult. The situation was similar to that encountered previously, when it became necessary to learn how to produce 3/8-inch diameter segmented thermoelements for the advanced laboratory model after having worked out useful production techniques for 1/2-inch diameter thermoelements.

A major difficulty encountered with the 1/4 inch diameter thermoelements involved the attainment of consistent thermoelectric properties during repetitive production. This difficulty was partially due to the very small quantities (each thermoelectric segment weighs about 1 g.) of powdered materials required per element. Additionally, small variations in hot-pressing conditions had a very significant effect on the density and, therefore, on the thermoelectric properties of 1/4 inch diameters. The smaller thermoelements also required thermal and pressure cycles which were different from those used for either 3/8 inch-or 1/2-inch diameter elements. Lastly, it was impractical to screen candidate thermoelements for critical T_i temperatures by inserting thermocouples at the T_i site, as was done for the larger diameter elements. More than 60 1/4-inch diameter thermoelements were lost during attempts to evaluate them by insertion of thermocouples at the T_i sites, and it was necessary to develop new screening techniques.

Figure 19 presents a view of a 16-thermoelement tier unit, without radiators and thermal insulation, essentially identical to those used in the fabrication of the improved experimental model. Nine such tiers, consisting of 8 p- and n-type 1/4-inch diameter segmented thermoelements, connected series-parallel, were used in the generator. As shown by the small white cylinders spaced at 90° intervals in the 1 3/8-inch I.D. x 1 3/4-inch O.D. graphite ring, each tier consisted of four sections, each containing 2 p- and 2 n-type thermoelements with like thermoelements connected in parallel. Each 4-thermoelement section was then connected in series with the 4-thermoelement sections on each side of it, or to a similar section on the tier above or below. Thus, the improved experimental model contained 36 series-connected 4-thermoelement parallel-connected sections. It was judged that test results obtained with such a 9-tier unit would be adequate for purposes of evaluating the operating characteristics of the design concept and for extrapolation purposes. The electrical scheme of the generator is presented in Figure 20 .

A 1 1/4-inch O.D. x 5-inch long graphite sleeve was inserted between the spiral-wound resistance heater and the hot-junction ends of the generator. The function of this sleeve was to prevent evaporated tungsten from electrically shorting the exposed hot ends of the thermoelements.

When completed, the improved experimental model measured about 5-inch O.D. by 5-inch high, excluding its ceramic insulating top and base plate, and weighed 1.3 lb., exclusive of heat source, thermocouples and nonfunctioning ends. A detailed assembly drawing is shown in Figure 21.

Figure 22 presents a view of the assembled generator without its cold-wall heat sink in place. This view was taken prior to starting shakedown tests on the generator. The white wires shown connected to the generator and to the panel at its base, are 41 thermocouples for monitoring T_h, T_i and T_c temperatures at strategic sites within the generator.

3. 3500-Hr. Sustained Performance Test

The sustained performance test was initiated on April 7, 1964. The method of operation and collection of data were identical to that described for the advanced laboratory model with the exception that a different heater configuration was used. For this generator, a spiral wound tungsten heater (0.050-inch diameter wire) was substituted for the cylindrical tantalum heater. The use of the coiled tungsten heater, with electrical leads at the bottom of the coil, permitted complete closure of the top end of

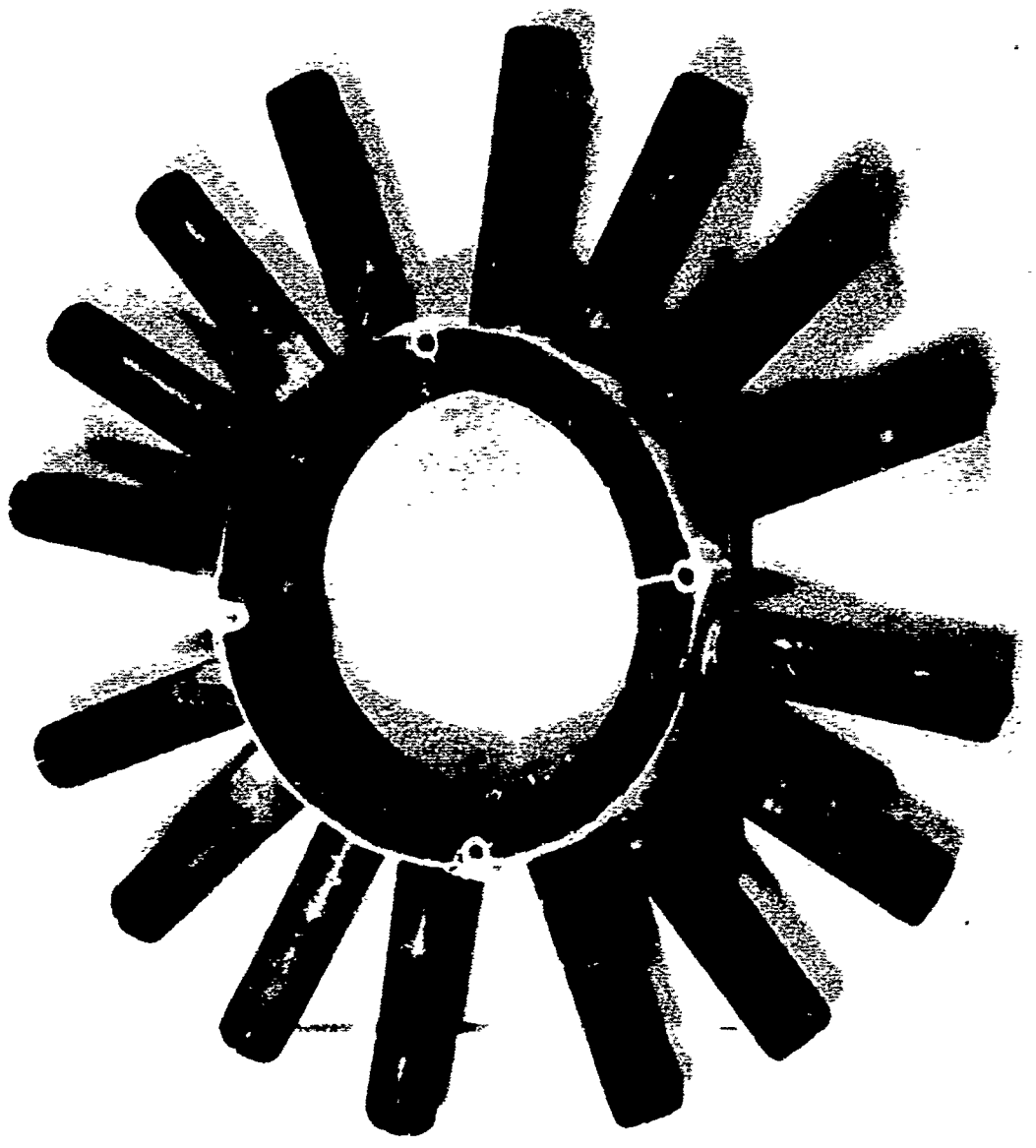

Figure 19. View of a Thermoelement Tier Unit, Without Radiators and Thermal Insulation

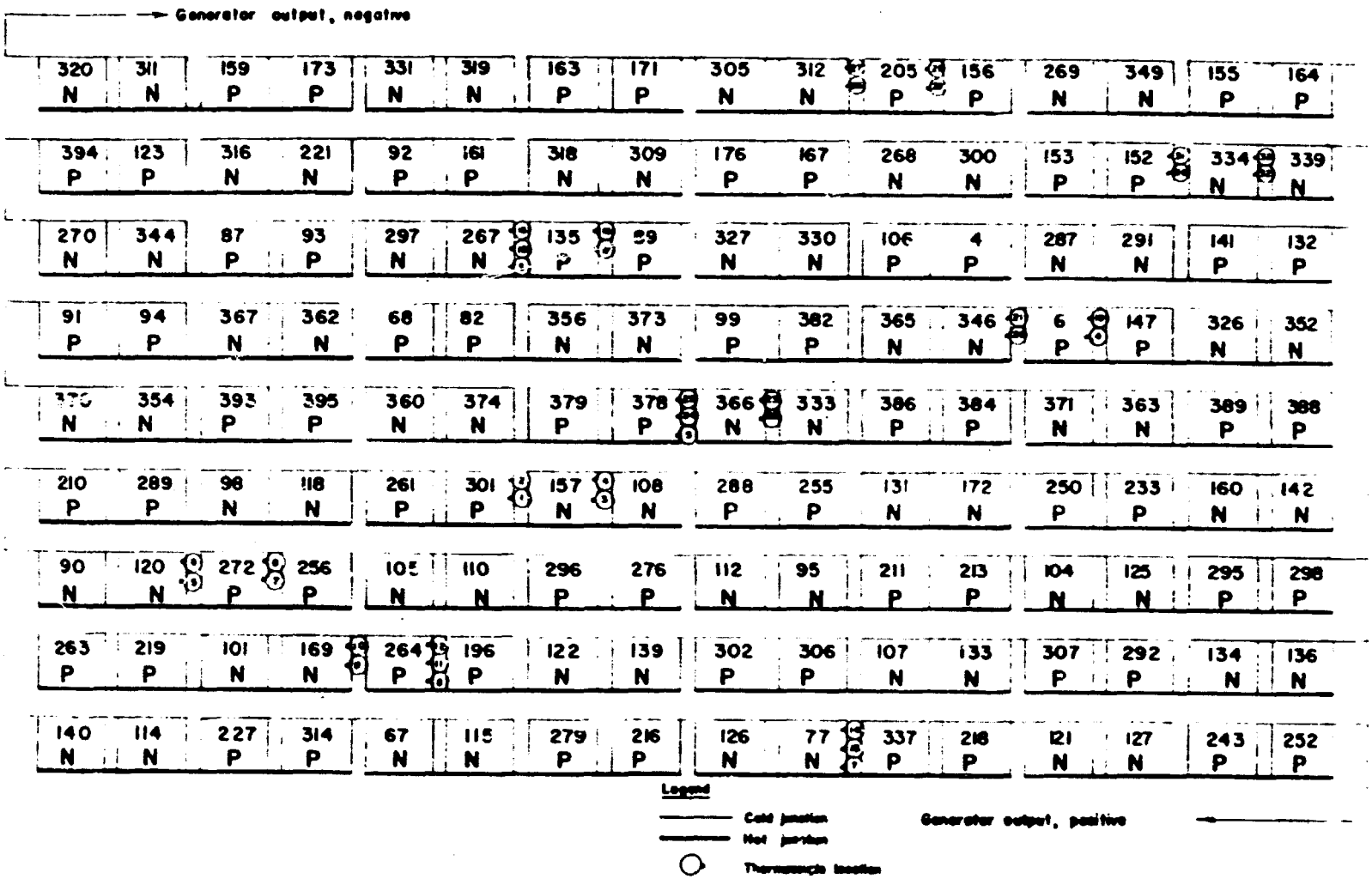

Figure 20. Schematic of Improved Experimental Model Generator Showing Thermocouple Locations

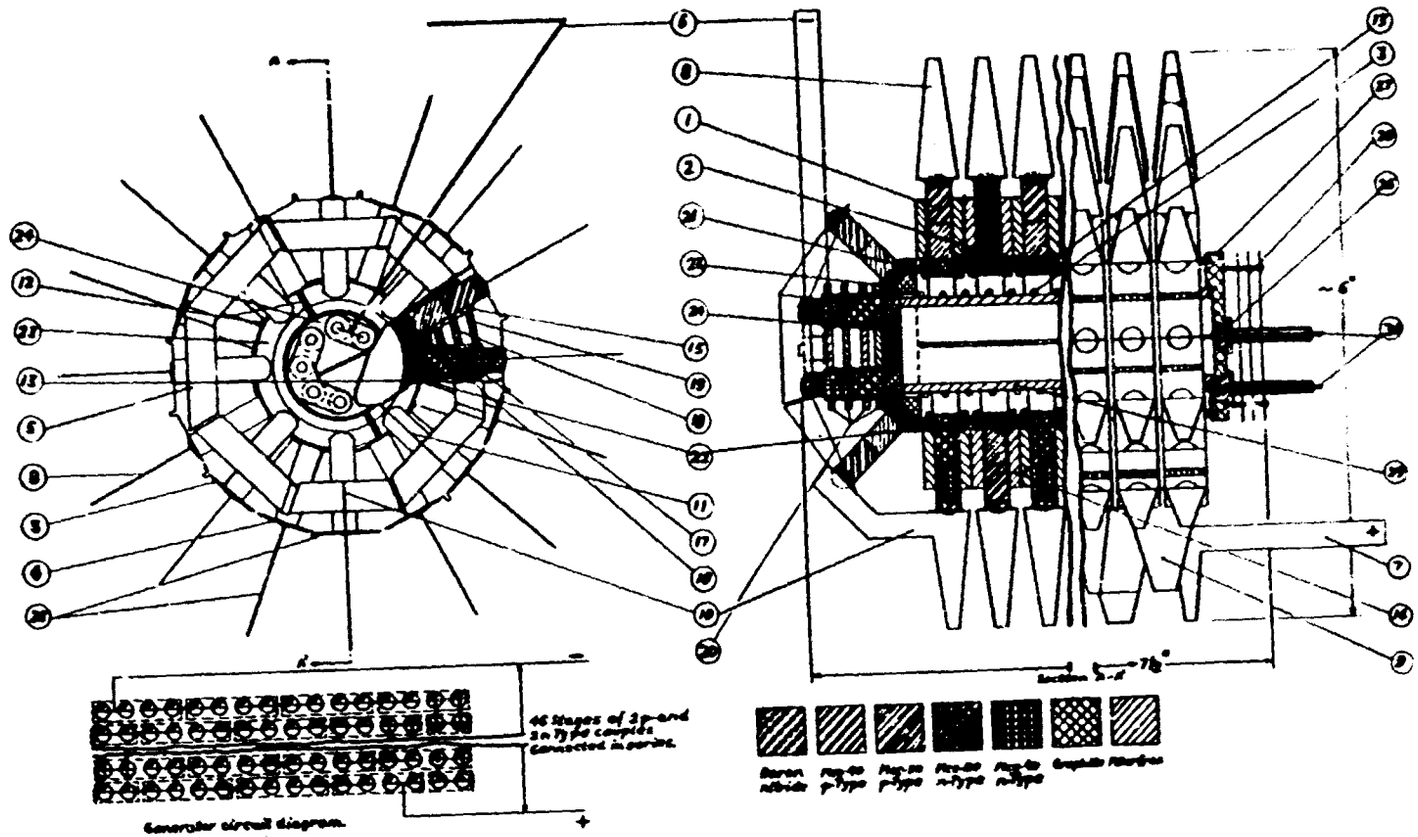

Figure 21. Assembly Drawing of the Improved Experimental Model Generator

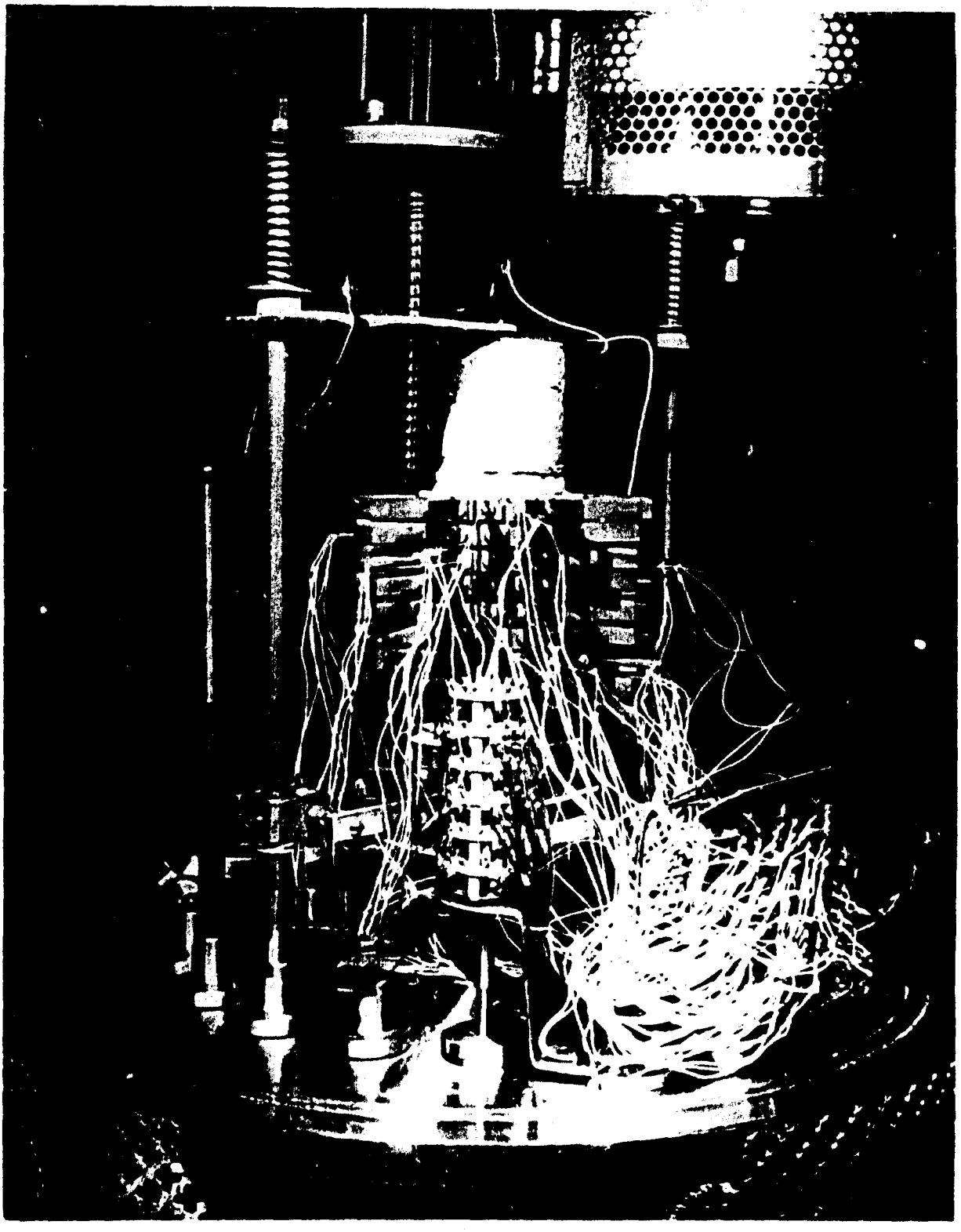

Figure 3.1. Improved Experimental Model Generator on Test Stand

this generator, tending to decrease its thermal losses.

Daily tabulations on this generator are presented in Table 4 and graphically in Figures 23, 24 and 25. As with the data for the advanced laboratory model, unpredictable fluctuations in temperatures occurred and undoubtedly affected the performance of the generator. Also, as in the sustained performance tests with the advanced laboratory model, losses of thermocouples by breakage and changes in their outputs occurred with this generator. On occasion, such thermocouple problems caused rather odd variations in the temperature averages. For example, it was observed that the average T_{in} and T_{ip} temperature curves of Figure 23 crossed several times. These events, which were noticeable from the 10th through the 38th day of the test, are believed to have been caused by changes in thermocouple readings resulting when solid contact was periodically made and lost between various thermocouples and the surfaces of their positioning holes. Such events are common occurrences when attempting to measure temperatures of solids in a high vacuum environment, and can be particularly troublesome in the range of temperatures encountered at the T_i sites. These temperatures are not quite high enough to achieve equilibrium by radiant heat transfer nor low enough in this case to permit the use of ceramic cements, since such cements tend to react with the thermoelectric and barrier materials.

Three efficiencies, η_{M1}, η_{M2}, and η_{M3}, defined in Table 4, are determined in this test. Only η_{M2}, corresponding to the power output (P_{M_1}) of the generator in a matched load circuit for the actual ΔT_{np} involved, and η_{M3}, the efficiency based on the normalized or adjusted power output (P_{M_2}), were plotted in Figure 23 through 25. The values of η_{M_1} and η_{M_2} were usually so close that it was impractical to distinguish between their plots.

As for the advanced laboratory model tests, the power input to this generator was determined by subtracting estimated conductive and radiative heat losses from the total power (bus bar) input. The resulting generator efficiencies, as shown in Table 4 and Figure 23, initially increased slightly with time. It is felt that improved generator test conditions, rather than improvement of MRC thermoelements, were responsible for this rise.

Figure 26 presents a top-to-bottom temperature profile of the average T_i temperatures in this generator, with the original tungsten heater of evenly spaced spiral coils in place. The rather large (220°C) difference in temperatures between its ends and center prevented the generator from reaching its full design capability. This generator could produce about 20 watts(e), with each tier operating with an average T_h of 1200°C and an average ΔT_{np} of 600°C.

Table 4

DATA FROM SUSTAINED PERFORMANCE TEST ON THE IMPROVED EXPERIMENTAL RADIOISOTOPE GENERATOR OPERATED AT 1200°C AND 10^{-5} - 10^{-6} TORR

Hours of Operation	Control T_{h_1}, °C	Avg. T_{h_2}, °C	Control T_{1a}, °C	Avg. T_{1b}, °C	Avg. T_{1c}, °C	Avg. T_{2a}, °C	Avg. T_{2b}, °C	Avg. ΔT_a, °C	Avg. ΔT_b, °C	Avg. ΔT_{a-b}, °C	I, Amp.	E_1, Volts	P, Watts	Rint, Ohm	E_{oc}, Volts	P_{R_1} (1), Watts	P_{R_2} (2), Watts	Input, Watts	η_T (3)	η_{R_1} (4)	η_{R_2} (5)
8	1201	1111	950	848	822	537	507	574	604	589	3.404	4.172	14.20	1.2262	8.353	14.30	-	626	2.25	2.28	-
32	1201	1109	950	849	828	544	508	565	601	583	3.409	4.189	14.28	1.215	8.331	13.84	13.84	626	2.26	2.21	2.21
----------Electricity failed at 40 hrs - thunderstorm. Unit cooled to room temperature.----------																					
56	1201	1109	950	853	831	544	508	565	601	583	3.412	4.190	14.30	1.215	8.339	13.73	13.73	626	2.28	2.195	2.195
80	1201	1100	950	852	818	541	505	559	595	577	3.359	4.120	13.84	1.236	8.272	13.62	14.0	626	2.21	2.238	2.235
104	1201	1102	950	846	821	543	507	559	595	577	3.373	4.088	13.79	1.239	8.251	13.79	14.10	626	2.20	2.20	2.25
128	1201	1101	950	842	813	543	507	558	594	577	3.356	4.067	13.65	1.235	8.215	13.71	14.05	626	2.18	2.19	2.242
152	1201	1102	950	835	814	544	506	558	596	577	3.383	4.100	13.87	1.214	8.28	14.11	14.50	628	2.21	2.241	2.315
176	1201	1102	950	820	757	542	505	560	597	578	3.346	4.054	13.56	1.237	8.189	13.55	13.8	626	2.162	2.162	2.2
200	1201	1101	950	820	757	542	505	559	596	577	3.346	4.054	13.56	1.237	8.189	13.56	13.9	626	2.162	2.162	2.211
224	1201	1099	950	816	817	537	506	562	593	577	3.361	4.065	13.66	1.231	8.21	13.70	14.05	626	2.18	2.19	2.242
248	1201	1097	950	813	831	544	507	555	592	573	3.361	4.065	13.66	1.233	8.21	13.70	14.21	626	2.18	2.19	2.28
272	1201	1100	950	802	812	545	508	555	592	573	3.378	4.087	13.806	1.236	8.265	13.817	14.38	626	2.21	2.21	2.295
296	1201	1100	950	802	810	545	508	555	592	573	3.368	4.077	13.731	1.243	8.265	13.738	14.22	626	2.195	2.195	2.28
320	1201	1084	905	796	809	546	508	538	576	557	3.34	4.054	13.54	1.185	8.0125	13.924	14.5	626	2.16	2.235	2.315
344	1201	1084	950	796	807	541	509	579	576	557	3.34	4.054	13.59	1.185	8.018	13.924	14.5	626	2.16	2.235	2.315
368	1201	1100	950	802	812	545	508	555	592	573	3.378	4.088	13.806	1.256	8.265	13.817	14.38	626	2.21	2.21	2.295
392	1201	1100	950	802	812	545	508	555	592	573	3.378	4.088	13.806	1.256	8.265	13.817	14.38	626	2.21	2.21	2.295
416	1201	1109	957	799	810	548	512	561	577	579	3.342	4.06	13.568	1.226	8.160	13.577	13.80	626	2.16	2.162	2.2
440	1201	1100	950	802	810	543	508	555	592	573	3.368	4.017	13.731	1.243	8.360	13.738	14.22	626	2.495	2.195	2.28
464	1201	1084	950	796	809	546	508	538	576	557	3.345	4.054	13.54	1.185	8.0125	13.924	14.3	626	2.16	2.235	2.315
488	1201	1109	950	799	810	548	512	561	597	579	3.342	4.06	13.568	1.226	8.16	13.577	13.80	626	2.161	2.162	2.2
512	1201	1108	950	795	805	548	510	560	598	579	3.32	4.03	13.79	1.239	8.145	13.86	14.2	626	2.2	2.21	2.27
536	1201	1084	950	793	809	546	508	536	576	557	3.344	4.055	13.54	1.185	8.0125	13.92	15.3	626	2.16	2.22	2.44
560	1201	1109	950	798	810	548	512	561	597	579	3.342	4.051	13.388	1.226	8.160	13.517	13.81	626	2.14	2.16	2.45
584	1201	1108	950	796	823	551	520	557	588	572	3.326	4.045	13.453	1.237	8.160	13.457	14.1	626	2.14	2.15	2.25
608	1201	1105	950	792	791	548	519	557	586	571	3.32	4.032	13.384	1.243	8.160	13.392	14.0	626	2.138	2.14	2.24
632	1201	1105	950	792	791	548	519	557	586	571	3.32	4.032	13.386	1.243	8.160	13.396	14.0	626	2.138	2.14	2.24
656	1201	1109	950	797	809	553	513	556	606	581	3.37	4.094	13.796	1.2169	8.195	13.796	14.0	626	2.2	2.2	2.24
680	1201	1117	950	799	817	558	515	559	602	581	3.366	4.095	13.783	1.234	8.250	14.125	14.15	626	2.2	2.26	2.265

(1) Maximum power output for the test condition noted. (2) P_{R_2} based on a ΔT of 583, through 876 hrs. Beyond this time, P_{R_2} is based on a ΔT of 600°C. (3) Calculated efficiency using P_L. (4) Calculated efficiency using P_{R_1}. (5) Calculated efficiency using P_{R_2}, based on a ΔT of 583°C, through 876 hrs. Beyond this time, P_{R_2} is based on a ΔT of 600°C.

Table 4, (Cont'd)

Hours of Operation	Control T_{in}, °F	Avg. T_{in}, °F	Control T_{in}, °C	Avg. T_{in}, °C	Avg. T_{clp}, °C	Avg. T_{cip}, °C	Avg. T_{cop}, °C	Avg. ΔT_m, °C	Avg. ΔT_p, °C	Avg. ΔT_{m-p}, °C	I, Amp.	E, Volts	P, Watts	Elec. Ohms	Rec. Volts	P_{HQ} (1) Watts	P_{HQ} (2) Watts	Input, Watts	η_T (3)	η_{HQ} (4)	η_{HQ} (5)
694	1201	1109	950	797	809	553	513	556	596	576	3.37	4.094	13.796	1.269	8.195	13.796	14.15	686	2.205	2.205	2.263
718	1201	1108	950	810	807	551	505	557	603	581	3.348	4.062	13.599	1.227	8.173	13.61	13.7	686	2.17	2.18	2.19
732	1201	1105	950	798	791	548	519	557	586	572	3.32	4.032	13.38	1.247	8.160	13.92	14.5	686	2.14	2.235	2.32
756	1201	1109	950	797	809	553	513	556	596	576	337	4.094	13.796	1.269	8.195	13.796	14.15	686	2.205	2.205	2.263
780	1201	1108	950	810	807	551	505	557	603	581	3.348	4.062	13.599	1.227	8.173	13.61	13.7	686	2.51	2.18	2.19
804	1201	1117	950	799	817	558	515	559	602	581	3.366	4.095	13.783	1.234	8.25	14.125	14.15	686	2.2	2.26	2.265
828	1201	1117	950	799	817	558	515	559	602	581	3.365	4.095	13.783	1.234	8.25	14.125	14.15	686	2.2	2.26	2.265
852	1201	1118	950	797	803	558	515	552	595	573	3.36	4.096	13.73	1.234	8.25	14.10	14.62	626	2.2	2.26	2.34
876	1201	1111	950	798	805	559	515	552	596	574	3.37	4.095	13.72	1.234	8.25	14.0	14.57	626	2.2	2.24	2.33
---- Installed modified heater for profile correction - P_{HQ} and η_3 now calculated on basis of a reference ΔT of 600°C --- -																					
900	1201	1118	950	774	888	556	516	562	602	582	3.366	4.101	13.824	1.247	8.3	13.81	14.9	626	2.21	2.32	2.385
924	1201	1132	950	773	834	559	518	573	614	593	3.446	4.195	14.45	1.205	8.35	14.46	14.9	626	2.31	2.32	2.385
948	1201	1132	950	773	834	559	518	573	614	593	3.446	4.195	14.45	1.205	8.35	14.46	14.9	626	2.31	2.32	2.385
972	1201	1132	950	773	834	559	518	573	614	593	3.446	4.195	14.43	1.205	8.35	14.46	14.9	626	2.31	2.32	2.385
996	1201	1127	950	779	820	559	516	566	611	589	3.472	4.072	14.137	1.217	8.30	14.156	14.75	626	2.26	2.265	2.36
1020	1201	1141	950	782	841	558	517	583	624	603	3.44	4.094	14.08	1.201	8.28	14.09	-	626	2.25	2.26	-
1044	1201	1141	950	780	846	567	526	574	615	594	3.547	4.224	14.98	1.194	8.125	14.98	15.35	626	2.39	2.39	2.46
1068	1201	1140	950	781	838	566	526	574	614	594	3.571	4.255	15.2	1.22	8.62	15.22	15.55	626	2.43	2.44	2.49
1092	1201	1139	950	780	835	565	527	574	612	593	3.598	4.29	15.43	1.295	8.95	15.463	15.9	626	2.47	2.475	2.54
1116	1201	1139	950	780	835	565	527	574	612	593	3.598	4.29	15.43	1.295	8.95	15.463	15.9	626	2.47	2.475	2.54
1140	1201	1139	950	772	851	566	526	573	613	593	3.609	4.30	15.518	1.341	9.14	15.57	15.9	626	2.48	2.49	2.54
1164	1201	1139	950	772	851	566	526	573	613	593	3.609	4.30	15.518	1.341	9.14	15.57	15.9	626	2.48	2.49	2.54
1188	1201	1137	950	760	834	561	525	576	612	594	3.59	4.285	15.383	1.305	8.97	15.413	15.75	626	2.41	2.465	2.52
1212	1201	1137	950	780	839	561	525	576	612	594	3.59	4.285	15.383	1.305	8.97	15.413	15.75	626	2.41	2.465	2.52
1236	1201	1131	950	777	832	561	522	5.70	609	589	3.62	4.304	15.581	1.335	9.14	15 64	16.25	626	2.495	2.5	2.6
1260	1201	1134	950	775	865	593	537	541	597	570	3.582	4.236	15.173	1.302	8.90	15.209	17.10	626	2.405	2.435	2.735
1284	1201	1134	950	775	865	593	537	541	597	570	3.582	4.236	15.173	1.302	8.90	15.309	17.10	626	2.405	2.435	2.735
1308	1201	1138	950	755	866	594	532	546	594	570	3.575	4.261	15.233	1.353	9.10	15.301	17.0	626	2.42	2.425	2.72
1332	1201	1138	950	775	866	594	532	546	594	570	3.575	4.261	15.233	1.353	9.10	15.301	17.0	626	2.42	2.425	2.72
1356	1201	1138	950	775	867	594	532	546	594	570	3.575	4.26	15.216	1.338	9.10	15.301	17.0	626	2.42	2.425	2.72
1380	1201	1136	950	776	868	597	532	539	594	566	3.587	4.280	15.35	1.329	9.05	15 406	17.3	626	2.426	2.432	2.77
1404	1201	1136	950	776	869	593	533	543	603	573	3.581	4.270	15.29	1.332	9.04	15.338	16.8	626	2.42	2.43	2.68
1428	1201	1134	950	802	867	593	532	541	601	571	3.652	4.265	15.191	1.345	9.04	15.246	16.9	626	2.415	2.42	2.70

(1) Maximum power output for the test condition noted. (2) P_{HQ} based on a ΔT of 583, through 876 hrs. Beyond this time, P_{HQ} is based on a ΔT of 600°C. (3) Calculated efficiency using P_i. (4) Calculated efficiency using P_{HQ}. (5) Calculated efficiency using P_{HQ}, based on a ΔT of 583°C. through 876 hrs. Beyond this time, P_{HQ} is based on a ΔT of 600°C.

Table 4, (Cont'd)

Hours of Operation	Control T_h, °C	Avg. T_h, °C	Control T_{in}, °C	Avg T_{in}, °C	Avg. T_{cp}, °C	Avg T_{cn}, °C	Avg. T_{cp}, °C	Avg. ΔT_n, °C	Avg. ΔT_p, °C	Avg. ΔT_{n-p}, °C	I, Amp.	R_L Volts	P, Watts	R_{int}, Ohm	E_{oc}, Volts	P_{M_1} (1) Watts	P_{M_2} (2) Watts	Input, Watts	η_{M_1} (3)	η_{M_2} (3)	η_{M_2} (4)
1452	1200	1134	950	802	867	593	532	541	598	566	3.562	4.265	15.19	1.343	9.05	15.25	17.15	626	2.43	2.44	2.74
1476	1200	1135	950	781	870	594	532	541	593	567	3.576	4.258	15.22	1.348	9.08	15.29	17.20	626	2.42	2.42	2.74
1500	1200	1135	950	777	873	593	533	542	598	567	3.555	4.257	15.13	1.362	9.10	15.20	17.03	626	2.41	2.42	2.73
							-- Operated with no load, for resistance studies, in this time interval --														
1692	1200	1131	950	777	866	595	531	536	600	568	3.517	4.272	14.63	1.372	9.00	14.76	16.50	626	2.35	2.36	2.64
1716	1200	1133	950	783	867	594	530	539	603	571	3.533	4.198	14.83	1.359	9.00	14.90	16.50	626	2.38	2.39	2.64
1740	1200	1135	950	806	868	593	530	542	605	573	3.533	4.196	14.82	1.376	9.06	14.91	16.40	626	2.37	2.40	2.62
1764	1200	1135	950	806	868	593	530	542	605	573	3.533	4.196	14.82	1.376	9.06	14.91	16.40	626	2.37	2.40	2.62
1788	1200	1135	950	806	868	593	530	542	605	573	3.533	4.196	14.82	1.376	9.06	14.91	16.40	626	2.37	2.39	2.63
1812	1200	1133	950	777	867	590	531	543	604	573	3.514	4.19	14.72	1.376	9.03	14.8	16.20	626	2.35	2.37	2.58
1836	1200	1133	950	778	867	590	531	543	602	573	3.514	4.19	14.72	1.376	9.03	14.8	16.20	626	2.36	2.37	2.58
1860	1200	1133	950	778	867	590	531	543	602	573	3.514	4.19	14.72	1.376	9.03	14.8	16.20	626	2.36	2.37	2.58
1881	1200	1140	950	778	868	593	531	547	609	578	3.512	4.18	14.68	1.38	9.03	14.77	15.85	626	2.35	2.36	2.54
1908	1200	1140	950	777	868	590	531	550	609	580	3.513	4.18	14.73	1.384	9.05	14.79	15.85	626	2.35	2.36	2.54
1932	1200	1141	950	778	869	593	531	548	610	580	3.514	4.19	14.72	1.380	9.04	14.78	15.80	626	2.35	2.36	2.52
1956	1200	1141	950	778	869	593	531	548	610	580	3.514	4.18	14.72	1.380	9.04	14.70	15.77	626	2.27	2.35	2.52
1980	1200	1141	950	778	869	593	531	548	610	580	3.480	4.16	14.47	1.390	9.0	14.56	15.8	626	2.32	2.33	2.46
2004	1200	1141	950	778	869	593	531	548	610	580	3.386	4.05	13.70	1.072	7.68	13.74	14.7	626	2.19	2.20	2.35
2028	1200	1141	950	778	869	593	531	548	610	580	3.315	4.01	13.29	1.082	7.60	13.34	14.3	626	2.12	2.13	2.29
2052	1200	1148	950	775	865	593	531	555	617	586	3.30	3.53	12.94	1.093	7.53	12.96	14.62	626	2.07	2.07	2.34
2076	1200	1141	950	775	869	593	531	548	610	580	3.298	3.93	12.94	1.093	7.53	12.06	13.85	626	2.07	2.07	2.22
2100	1200	1141	950	775	869	593	531	548	610	580	3.298	3.92	12.94	1.093	7.53	12.96	13.95	626	2.07	2.07	2.22
2124	1200	1141	950	778	869	593	531	548	610	580	3.315	4.01	13.29	1.082	7.60	13.34	14.3	626	2.12	2.13	2.29
2148	1200	1142	950	775	868	591	532	551	610	580	3.298	3.93	12.94	1.093	7.53	12.66	3.85	626	2.07	2.07	2.22
2172	1200	1141	950	777	867	591	533	550	611	580	3.278	3.93	12.94	1.093	7.53	12.66	13.85	626	2.07	2.07	2.22
							-- Modified vapor shield and replaced heater --														
2198	1200	1191	950	801	882	602	551	589	640	615	3.514	4.16	14.61	1.104	8.04	14.64	14.00	626	2.33	2.34	2.22
2222	1200	1191	950	801	882	602	551	589	640	615	3.514	4.16	14.61	1.104	8.04	14.64	14.00	626	2.33	2.34	2.22
2246	1200	1179	950	795	873	594	545	575	634	610	3.48	4.11	14.29	1.13	8.04	14.31	13.83	626	2.28	2.29	2.21
2260	1200	1179	950	795	873	594	545	575	634	610	3.479	4.11	14.29	1.13	8.04	14.31	13.83	626	2.28	2.29	2.21
2284	1200	1179	950	795	873	597	545	575	634	610	3.479	4.11	14.29	1.13	8.04	14.31	13.83	626	2.28	2.29	2.21
2308	1200	1173	950	791	867	597	546	577	627	601	3.479	4.11	14.29	1.13	8.04	14.31	14.3	626	2.28	2.29	2.28

(1) Maximum power output for the test condition noted. (2) P_{M_2} based on a ΔT of 583, through 876 hrs. Beyond this time, P_{M_2} is based on a ΔT of 600°C. (3) Calculated efficiency using P. (4) Calculated efficiency using P_{M_1}. (5) Calculated efficiency using P_{M_2}, based on a ΔT of 583°C, through 876 hrs. Beyond this time, P_{M_2} is based on a ΔT of 600°C.

Table 4. (Cont'd)

Hours of Operation	Control Th. °C	Avg. Th. °C	Control Tin. °C	Avg Tin. °C	Avg Tip. °C	Avg Ton. °C	Avg Top. °C	Avg ΔTn. °C	Avg ΔTp. °C	Avg ΔTn-p. °C	I, Amp.	E, Volts	P, Watts	Rint, Ohm	E, Volts	P_{M_1} (1) Watts	P_{M_2} (2) Watts	Input, Watts	η_e (3)	η_{M_1} (4)	η_{M_2} (5)
2332	1200	1181	950	791	867	597	547	584	634	609	3.443	4.086	14.08	.037	7.90	14.12	13.65	626	2.24	2.24	2.16
2356	1200	1180	950	790	867	595	546	585	634	609	3.44	4.08	14.04	.039	7.95	14.13	13.66	626	2.23	2.24	2.17
2380	1200	1179	950	789	866	594	547	584	631	607	3.4.0	4.09	13.99	.041	7.88	13.98	13.65	626	2.22	2.22	2.17
2404	1200	1175	950	788	865	593	548	582	627	604	3.401	4.054	13.79	.043	7.90	13.79	13.6	626	2.19	2.19	2.16
2420	1200	1174	950	787	863	592	547	582	627	604	3.372	4.020	13.63	.043	7.88	13.63	13.58	626	2.16	2.16	2.15
2452	1200	1173	950	785	862	592	548	581	625	603	3.38.	3.996	13.53	.042	7.73	13.53	13.38	626	2.15	2.15	2.12
2476	1200	1170	950	790	859	597	547	573	623	598	3.39	4.080	13.83	.044	7.90	13.85	13.90	626	2.19	2.20	2.21
2500	1200	1170	950	788	858	596	546	574	624	599	3.38	4.079	13.79	.041	7.90	14.02	14.05	626	2.19	2.22	2.23
2524	1200	1170	950	783	853	595	545	573	625	600	3.36	4.053	13.62	1.14	7.98	13.63	13.63	626	2.16	2.16	2.16
2548	1200	1170	950	779	852	594	544	576	626	601	3.35	3.96	13.30	1.16	7.86	13.30	13.27	626	2.11	2.11	2.11
2572	1200	1168	950	779	851	591	544	577	624	600	3.343	3.95	13.19	1.17	7.86	13.20	13.20	626	2.09	2.09	2.09
2596	1200	1170	950	781	853	593	544	577	626	601	3.333	3.975	13.24	1.17	7.87	13.28	13.27	626	2.10	2.11	2.11
2620	1200	1170	950	783	855	594	544	576	626	601	3.329	3.93	13.30	1.17	7.88	13.30	13.29	626	2.11	2.11	2.11
2644	1200	1170	950	782	855	594	544	576	622	601	3 338	3.99	13.31	1.13	7.76	13.32	13.31	626	2.11	2.11	2.08
2668	1200	1170	950	779	852	592	542	578	628	603	3.34	3.99	13.35	1.15	7.84	13.36	13.28	626	2.12	2.12	2.11
2692	1200	1170	950	777	852	592	542	578	628	603	3.369	4.00	13.29	1.15	7.81	13.29	13.22	626	2.11	2.11	2.10
2716	1200	1170	950	779	852	596	546	574	624	599	3.34	4.01	13.39	1.13	7.81	13.49	13.50	626	2.12	2.14	2.14
2740	1200	1170	950	780	853	595	545	575	625	600	3.35	4.00	13.40	1.13	7.80	13.46	13.42	626	2.13	2.14	2.14
2764	1200	1170	950	781	852	594	544	576	626	601	3.36	3.996	13.42	1.13	7.79	13.43	13.42	626	2.13	2.13	2.13
2788	1200	1170	950	780	851	593	544	577	626	601	3.38	3.996	13.30	1.13	7.81	13.51	13.50	626	2.14	2.14	2.14
2812	1200	1170	950	779	850	597	547	573	623	598	3.39	4.080	13.83	1.10	7.82	13.80	13.82	626	2.19	2.19	2.19
2836	1200	1170	950	778	852	596	546	574	624	599	3.39	4.05	13.73	1.11	7.82	13.74	13.75	626	2.18	2.18	2.18
2860	1200	1170	950	781	854	595	545	575	625	600	3.38	4.04	13.65	1.12	7.81	13.67	13.67	626	2.17	2.17	2.17
2884	1200	1170	950	782	855	595	545	575	625	600	3.40	4.05	13.77	1.10	7.82	13.79	13.79	626	2.18	2.19	2.19
2908	1200	1170	950	783	853	596	546	574	624	599	3.36	3.99	13.82	1.14	7.81	13.84	13.82	626	2.13	2.13	2.13
2932	1200	1169	950	784	854	591	544	578	625	601	3.37	4.08	13.74	1.11	7.80	13.79	13.77	626	2.18	2.18	2.18
2956	1200	1171	950	783	856	591	544	580	627	603	3.39	4.07	13.79	1.09	7.79	13.82	13.60	626	2.19	2.19	2.16
2980	1200	1170	950	780	850	596	546	574	624	599	3.37	4.10	13.81	1.10	7.82	13.66	13.66	626	2.19	2.20	2.16
3004	1200	1170	950	780	855	596	546	574	624	599	3.38	4.07	13.75	1.10	7.82	13.78	13.79	626	2.18	2.19	2.19
3028	1200	1170	950	781	858	595	545	575	625	600	3.39	4.08	13.83	1.10	7.83	13.86	13.86	626	2.19	2.20	2.20
3052	1200	1170	950	782	859	595	545	575	625	600	3.39	4.00	13.56	1.12	7.80	13.58	13.58	626	2.15	2.15	2.15
3076	1200	1170	950	782	855	595	545	575	625	600	3.38	4.04	13.77	1.10	7.82	13.79	13.79	626	2.18	2.19	2.19
3100	1200	1170	950	783	853	596	546	574	625	600	3.40	4.05	13.42	1.13	7.81	13.43	3.42	626	2.13	2.13	2.13
3124	1200	1170	950	784	854	591	544	578	624	599	3.36	3.99	13.74	1.10	7.81	13.79	13.77	626	2.18	2.18	2.18

(1) Maximum power output for the test condition noted. (2) P_{M_2} based on a ΔT of 583, through 876 hrs. Beyond this time, P_{M_2} is based on a ΔT of 600°C. (3) Calculated efficiency using P_e. (4) Calculated efficiency using P_{M_1}. (5) Calculated efficiency using P_{M_2}, based on a ΔT of 583°C, through 876 hrs. Beyond this time, P_{M_2} is based on a ΔT of 600°C.

Table 4, (Cont'd)

Hours of Operation	Control Th. °C	Avg. Th. °C	Control Tin. °C	Avg. Tin. °C	Avg. Tcp. °C	Avg. Tcn. °C	Avg. Tcp. °C	Avg. ΔTn. °C	Avg. ΔTp. °C	Avg. ΔTn-p, °C	I, Amp.	E, Volts	P Watts	Rint. Ohm	E, Volts	P_{M_1} (1) Watts	P_{M_2} (2) Watts	Input, Watts	(3) %	(4) %	(5) %
3148	1200	1175	950	788	865	593	548	582	627	604	3.401	4.054	13.79	1.106	7.71	13.79	13.60	626	2.19	2.19	2.16
3172	1200	1171	950	783	856	591	544	580	627	603	3.390	4.070	13.79	1.097	7.79	13.83	13.60	626	2.19	2.19	2.16
3196	1200	1176	950	788	858	591	544	578	624	599	3.360	3.996	13.74	1.106	7.81	13.78	13.77	626	2.18	2.19	2.18
3220	1200	1170	950	782	859	595	545	575	625	600	3.390	4.000	13.56	1.128	7.80	13.58	13.58	626	2.15	2.15	2.15
3244	1200	1176	950	788	865	593	548	582	627	604	3.401	4.054	13.79	1.137	7.71	13.79	13.60	626	2.19	2.19	2.16
3268	1200	1173	950	785	862	598	548	575	625	600	3.381	3.996	13.53	1.120	7.74	13.53	13.53	626	2.15	2.15	2.15
3292	1200	1170	950	783	853	596	546	574	625	600	3.400	4.050	13.42	1.135	7.81	13.45	13.42	626	2.13	2.13	2.13
3316	1200	1170	950	781	852	594	544	576	626	601	3.360	3.996	13.42	1.129	7.79	13.43	13.42	626	2.13	2.13	2.13
3340	1200	1170	950	780	853	595	545	575	625	600	3.350	4.000	13.40	1.130	7.80	13.46	13.46	626	2.13	2.14	2.14
3364	1200	1173	950	785	862	592	548	581	625	603	3.381	3.996	13.53	1.120	7.93	13.53	13.38	626	2.15	2.15	2.12
3388	1200	1170	950	782	855	594	544	576	626	601	3.338	3.996	13.31	1.130	7.76	13.32	13.31	626	2.11	2.11	2.08
3412	1200	1171	950	783	855	594	544	576	626	601	3.329	3.990	13.30	1.169	7.88	13.38	13.29	626	2.11	2.11	2.11
3436	1200	1170	950	782	856	595	547	580	628	604	3.329	3.990	13.30	1.168	7.83	13.38	13.20	626	2.11	2.11	2.10
3460	1200	1170	950	780	853	593	543	575	623	600	3.327	3.950	13.14	1.127	7.70	13.15	13.15	626	2.11	2.11	2.11
3484	1200	1173	950	783	862	598	549	575	625	600	3.325	3.910	13.00	1.142	7.71	13.01	13.01	626	2.08	2.08	2.08
3508	1200	1171	950	783	856	591	544	580	626	602	3.324	3.900	12.96	1.146	7.71	12.97	13.00	626	2.08	2.08	2.09
							Start thermal cycling test - peak cooling rate of 240-250°C/ min for a ΔT of about 200°C														
3532 (24 cycles)	1200	1171	950	783	856	590	543	581	627	602	3.324	3.905	12.96	1.146	7.71	12.97	13.00	626	2.07	2.08	2.08
3556 (48 cycles)	1200	1170	950	781	855	591	543	579	627	602	3.324	3.900	12.96	1.185	7.69	12.91	12.80	626	2.07	2.08	2.06
3581 (73 cycles)	1200	1170	950	782	862	595	545	576	625	600	3.310	3.850	12.74	1.150	7.68	12.82	12.82	626	2.05	2.06	2.06
3604 (96 cycles)	1200	1170	950	783	863	594	544	570	626	600	3.300	3.840	12.74	1.151	7.68	12.80	12.80	626	2.05	2.06	2.06
3629 (120 cycles)	1200	1170	950	781	853	600	550	570	620	595	3.280	3.880	12.37	1.160	7.60	12.43	12.62	626	2.01	2.00	2.03
3652 (144 cycles)	1200	1171	950	780	853	596	546	575	625	600	3.300	3.751	12.41	1.136	7.50	12.41	12.4.	626	1.98	1.98	1.98
3676 (168 cycles)	1200	1170	950	781	852	595	545	575	625	600	3.360	3.750	12.60	1.116	7.50	12.60	12.60	626	2.02	2.02	2.02
3700 (192 cycles)	1200	1172	950	780	853	597	552	575	620	598	3.330	3.760	12.53	1.129	7.52	12.53	12.60	626	2.02	2.02	2.02
3724 (216 cycles)	1200	1173	950	783	862	598	549	575	625	600	3.360	3.750	12.60	1.116	7.50	12.60	12.60	626	2.02	2.02	2.02
3748 (240 cycles)	1200	1171	950	783	855	594	544	576	626	601	3.300	3.751	12.41	1.136	7.50	12.41	12.42	626	1.99	1.99	1.99
3772 (264 cycles)	1200	1170	950	782	852	597	543	573	627	600	3.310	3.749	12.41	1.136	7.50	12.41	12.41	626	1.99	1.99	1.99

(1) Maximum power output for the test condition noted. (2) P_{M_2} based on a ΔT of 583, through 876 hrs. Beyond this time, P_{M_2} is based on a ΔT of 600°C. (3) Calculated efficiency using P. (4) Calculated efficiency using P_{M_1}. (5) Calculated efficiency using P_{M_2}, based on a ΔT of 583°C, through 876 hrs. Beyond this time, P_{M_2} is based on a ΔT of 600°C.

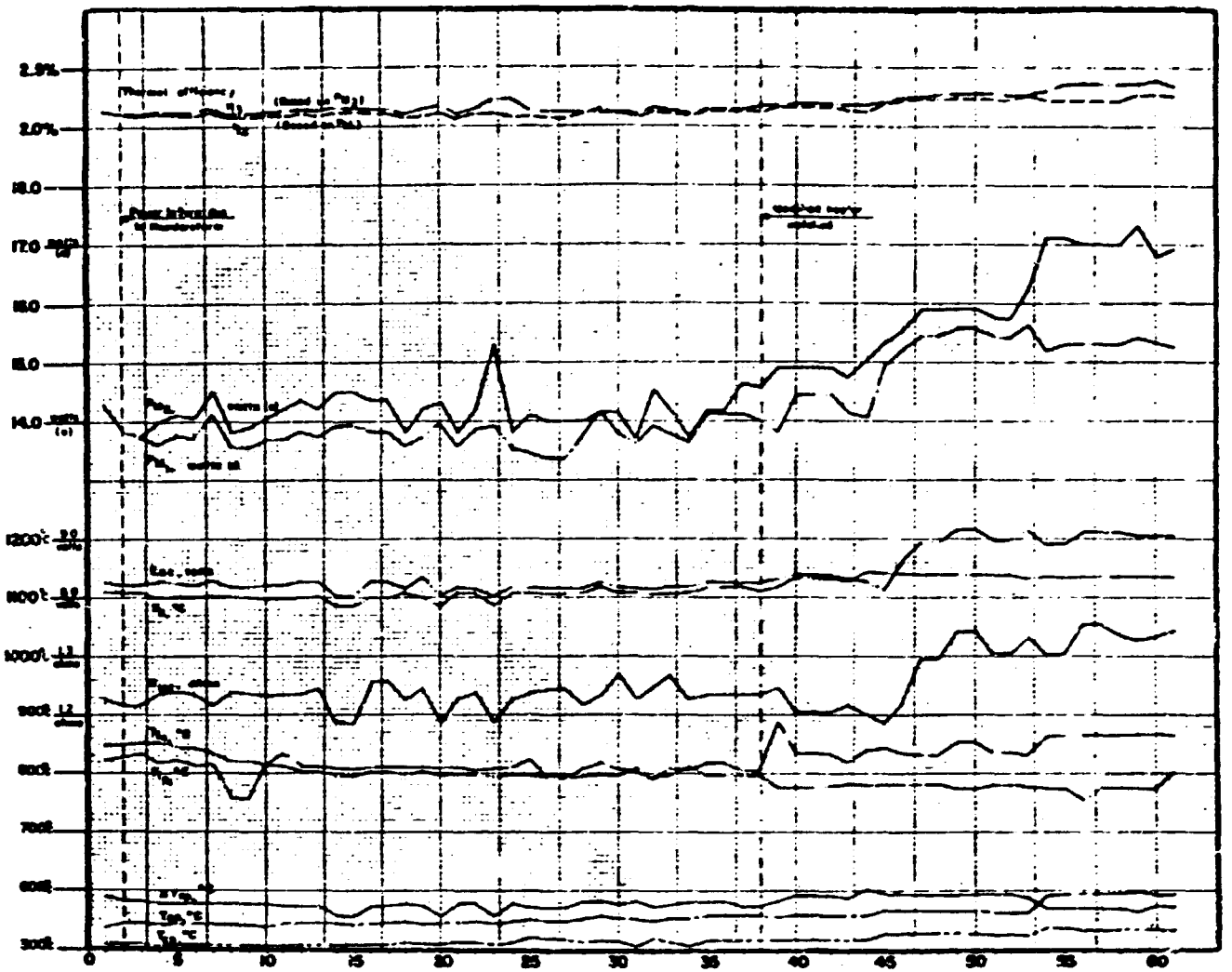

Figure 23. Performance Characteristics of Improved Experimental Model Generator for First 61 Days of Operation

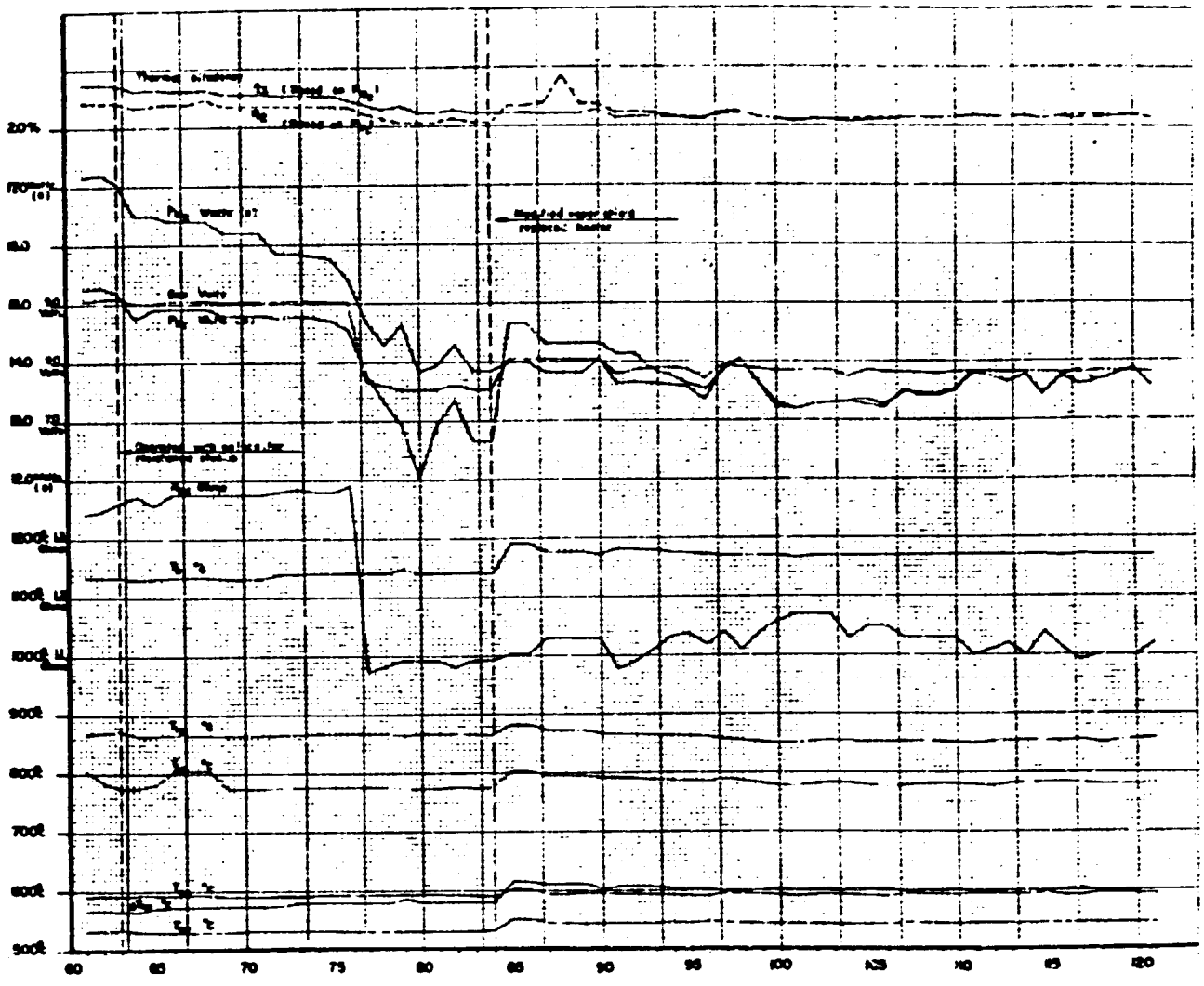

Figure 24. Performance Characteristics of Improved Model Generator from 62nd Through the 122nd Day of Operation

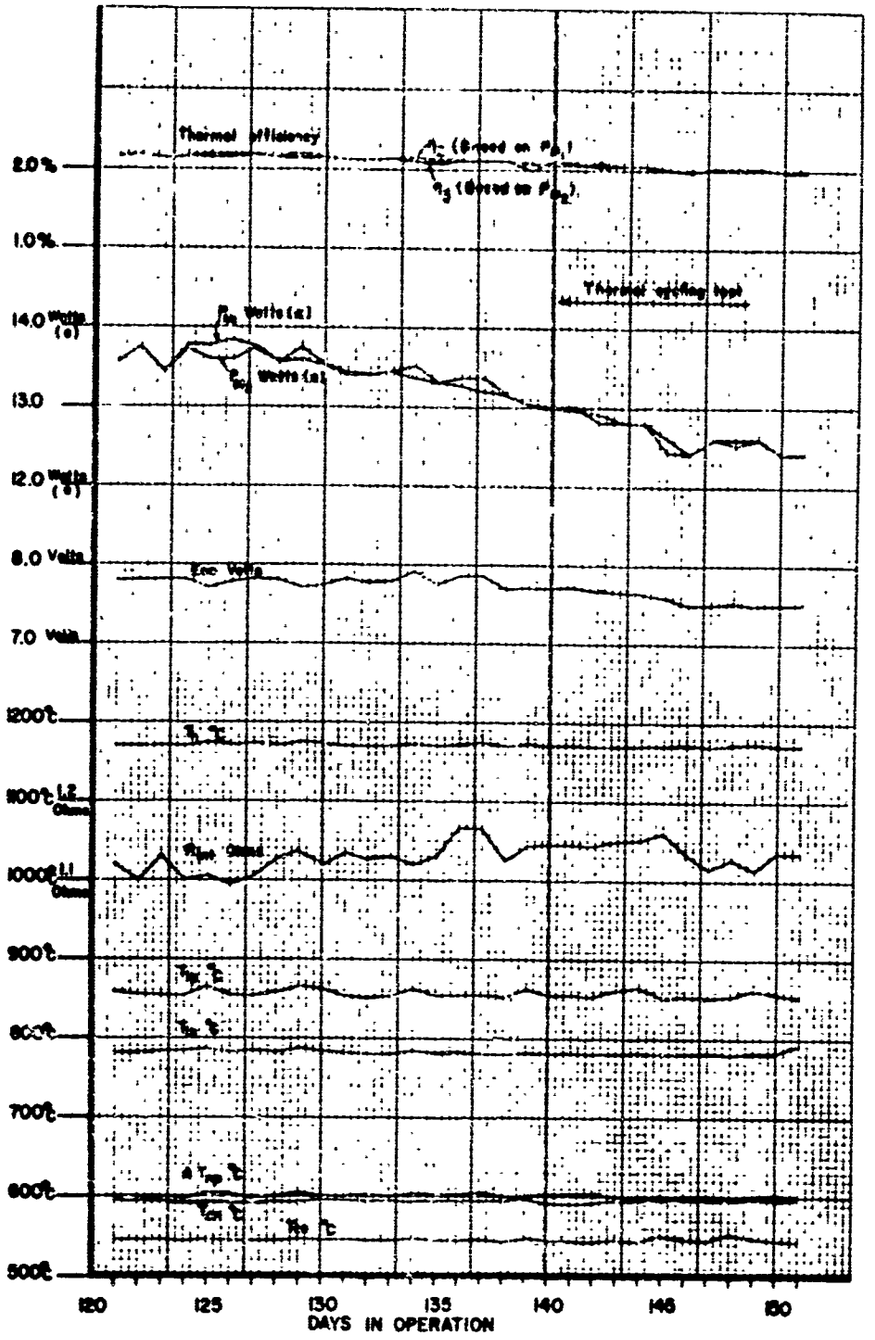

Figure 25. Performance Characteristics of Improved Model Generator from the 123rd Through the 157th Day of Operation

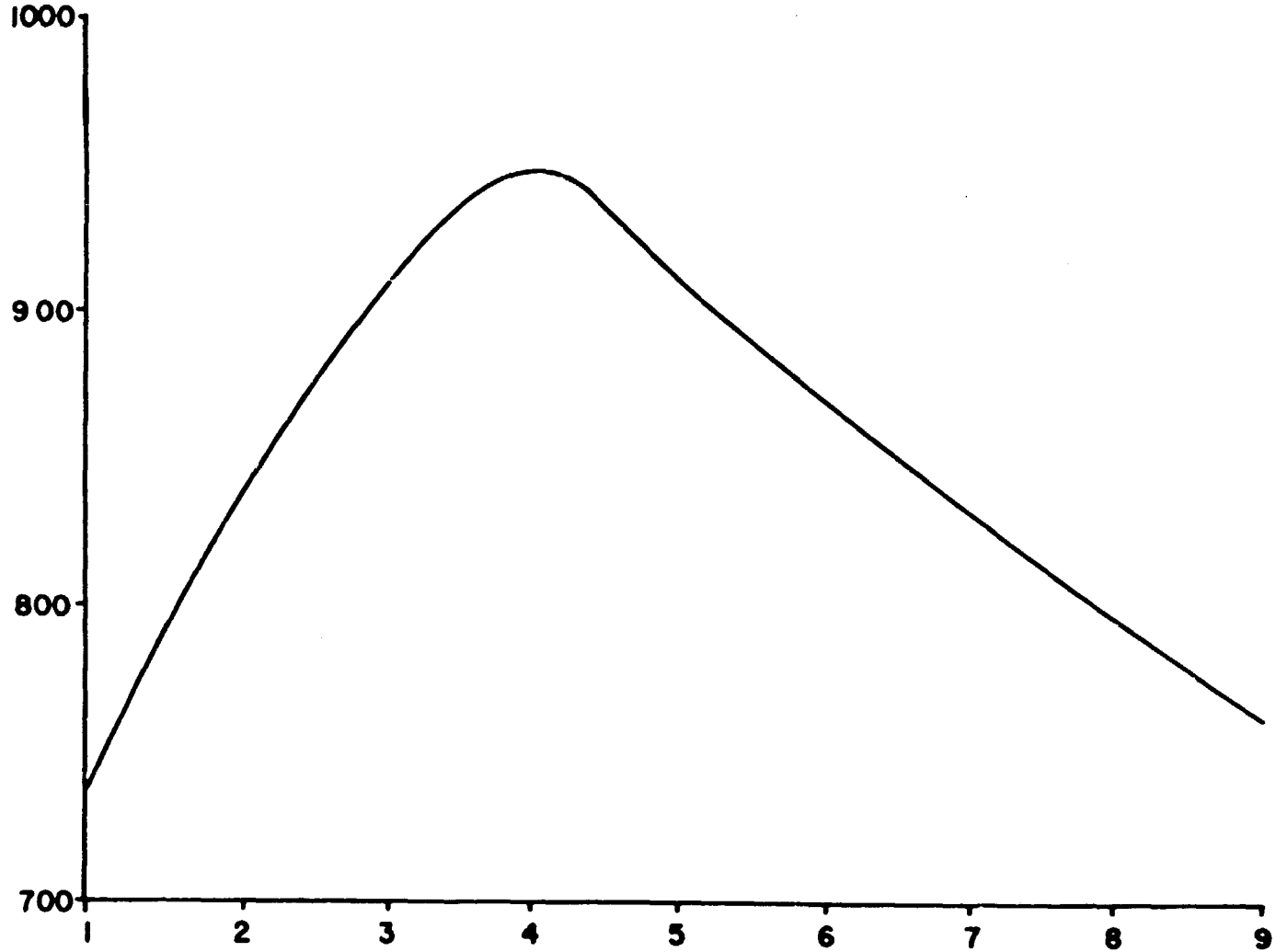

Figure 26. Thermal Profile for Improved Experimental Model Generator

In an attempt to smooth its temperature profile, a new spiral heater was made which employed fewer coils at its center and more at its ends. On the 38th day (910 hrs.) the generator was cooled to room temperature and the new heater was installed. At T_h temperatures below 1000°C the thermal profile was appreciably more even than it had been with the original heater. However, as the T_h temperature rose to 1200°C, the thermal profile again closely approximated that in Figure 26, for the original heater. It became apparent that the heat conducted from the ends of the generator via the heavy cross-section of the graphite vapor shield (between the heater and the hot-junctions), plus the cooling effect of radiant heat from ends of the generator, counteracted the gains made with the modified heater.

As shown in Figure 23, some gain in power output (P_{M_1} and P_{M_2}) appeared to result from installation of the modified heater. From the 43rd day of the test the improvement in P_{M_1} and P_{M_2} tended to parallel an increase in T_h, and a corresponding increase in the internal resistance of the generator was encountered.

The fact that the power output of the generator increased simultaneously with the internal resistance was somewhat mystifying until several radiator fins were noted to be in close proximity to the metal heat sink. It appears that prior to this time, they might have been touching the heat sink, producing an apparently low generator resistance and a correspondingly low power output. On resumption of tests, the gradual increase noted in the power output and resistance of the generator was probably the result of gradual separation of the radiator heat-sink component.

The power and internal resistance of the generator increased steadily to an adjusted peak value (P_{M_2}) of about 17 watts(e) and 1.35 ohms, 20 days (1308 hrs. of operation) after the attempt was made to correct the thermal profile problem. At 1500-hrs. (62nd day) of operation, a series of tests was conducted to determine, if possible, which section of the generator might have contributed to the increased internal resistance noted from the 1308th hr. (54th day). Tests consisted of operating the generator at carefully stabilized "no load" conditions and using the temperature-measuring thermocouples as voltage probes for resistance measurements. Calculations, based on the probe measurements of individual tiers, indicated no abnormalities in their resistances, so the increase in the resistance of the generator was judged to be the result of reducing electrical shorts between its fins and the heat sink unit.

At the conclusion of the no-load test, the generator was restored to approximate matched-load operating conditions. After

1956 hrs. the resistance of the generator increased to a peak value of about 1.39 ohms while the adjusted power (P_{M_2}) dropped to 15.4 watts(e).

The general rise in power and internal resistance which occurred to 1956 hrs. was similar to the performance exhibited by the advanced laboratory model generator (50-watt(e). Such changes in power and resistance were apparently due to improvements in the performance of various components (e.g., thermoelements, TEC-1 coating and contacts), which are not readily detected by present monitoring techniques but which do work to the advantage of generator power output over a long period of time.

Beginning at 1980 hrs., as shown in Figure 24, a sudden reduction in the internal resistance of the generator indicated that partial electrical shorting conditions were again being encountered. The generator was cooled to room temperature at 2172-hrs. and examined. It was found that the bottom part of the graphite vapor shield, used to protect the hot junctions of the generator from vaporized heater metal, was touching the junctions in one of the tiers of thermoelements. A new, thin-walled vapor shield was prepared and installed in an attempt to correct the electrical short condition and to reduce conduction heat losses from the central cavity of the generator.

In addition to replacing the heater vapor shield, a new tungsten resistance heater was installed. This heater was fabricated with fewer coils in its central section and with closely spaced ones at its ends.

While the generator was exposed at room temperature, measurements were made which showed that the electrical resistance of its thermal insulation had decreased by an order of magnitude or more. Such a loss of electrical resistance in the thermal insulation could account for the low internal resistance and reduction in power output of the generator. No changes in the electrical insulation were made at this time.

After reassembling the generator and returning it to normal (T_h of 1200°C) operating conditions, the corrected power output (P_{M_2}) was about 14 watts(e), with an internal resistance of 1.13-ohms. During the remainder of the sustained life test, random fluctuations continued to occur in the power output and internal resistance of the generator. Such fluctuations appeared to be the combined result of intermittent and partial electrical shorts between one or more radiator fins and the metal heat-sink shield, and degradation of the electrical properties of its thermal insulation.

At the conclusion of the life test, thi generator had successfully operated for 3508 hours in a vacuum of 10^{-5}-10^{-6} torr with its hot junction at about 1200°C. During the last 16 days of the test, output for the generator dropped by about 5%, or a total of 6% during the 3508 hours of its operation. Such a drop-off in power output of the generator after 3200 hours' operation is believed to be the result of further rapid deterioration of the electrical properties of its thermal insulation.

4. Thermal Cycling

Immediately following the conclusion of the sustained performance test, the heater control system was switched to a cam program control and thermal cycling initiated. The generator was subjected to 264 thermal cycles in which peak cooling rates of 240-250°C/min. were reached each cycle. Output of the generator decreased by 3% during the 250 hours of operation required to complete the thermal cycling tests. Total degradation of the generator, after 3772 hours of operation, including 264 thermal cycles, was about 9%.

5. Performance Analysis

Following completion of the duration and thermal cycling tests, the generator was partially disassembled and its various components examined. Figure 27 is a photograph of the generator during the process of disassembly. The top cap and top insulation have been removed, exposing the heater and vapor shield. All interior insulation has been removed prior to examination of the thermal elements.

The spiral wound tungsten heater on a thoria core may be seen in the center of the assembly in Figure 27. Concentric about the heater is a graphite vapor shield, which shows as a thin gray ring about the tungsten heater in the photograph. A boron nitride insulating ring, used to electrically insulate tiers, is visible as the white ring, concentric about the vapor shield and mounted upon the top graphite tier visible as a gray area on either side of the white ring. Insulating ceramic junctions between ring segments are shown at 2, 5, 8 and 11 o'clock positions in Figure 27. These are visible as raised, white surfaces on the outer surface of the central graphite ring. Inspection of these ceramic junctions showed that they had not been affected by the duration and thermal cycling tests. The top tier of 16 thermoelements is visible, joined to the graphite ring segments at their hot ends. At approximately the 7 o'clock position, a

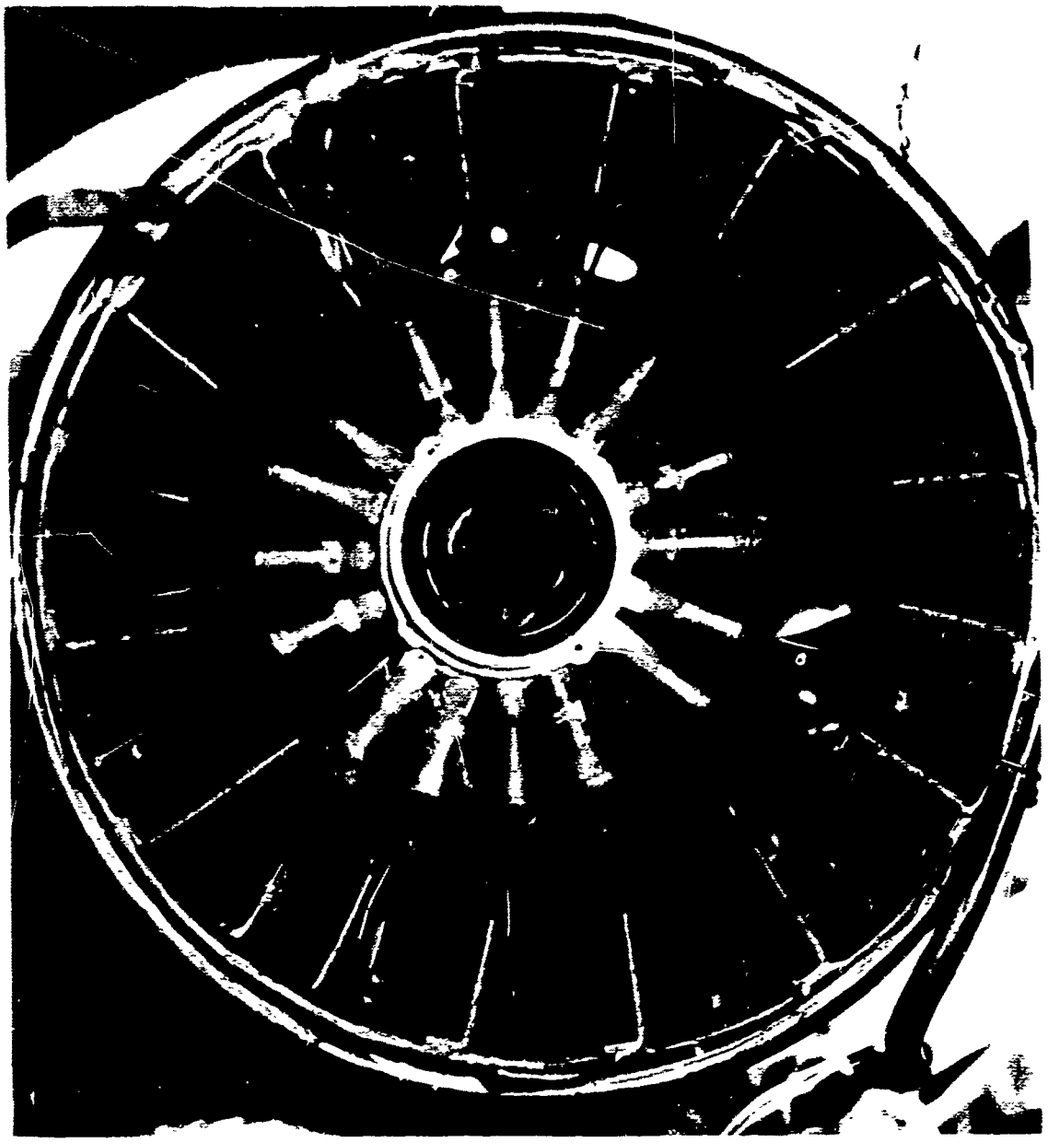

Figure 27. Partially Disassembled Generator Shown Within Water-Cooled Heat Sink and with its Top Ceramic Cap and Thermal Insulation Removed

small hole is seen at the hot end of a thermoelement. This hole was used for locating and insertion of a tungsten-rhenium thermocouple monitoring probe. Thermoelement segment interfaces can be seen in some cases by noting the innermost junction between the metallic-appearing bands of MCC 40 materials on the cold end of each leg and the dull grey segments near the center of the generator.

Affixed to the thermoelement cold ends are the copper radiator straps and radiator fins. The radiator fins normally extend between the heat-sink fins and are coated with TEC-1 for increased emissivity. The interior surfaces of the heat sink were also painted with TEC-1. The coated surfaces of the generator fins were not noticeably deteriorated by the generator testing. However, some sublimation of various materials was found condensed on these cold surfaces. The junctions between the copper cold straps (radiators) and the element cold ends appeared to be unaffected by the tests. Some radiator fins can be observed to be in direct contact to heat-sink fins, but this situation was caused by the generator's shifting position during its disassembly. T_c and T_i thermocouples can be observed as narrow,white,radiating lines at 6, 7, and 8 o'clock positions. Current and voltage straps, somewhat out of focus, are shown attached to the cold strap at the 10 o'clock position.

The photographs shown in Figures 28 and 29,respectively, show representative remnants of the thermal insulation and a close-up of representative portions of the thermal insulation (Fiberfrax) after it was removed from the generator. As indicated in Figure 28, the insulation was considerably more friable than when it was first installed in the generator. Additionally, it was badly discolored except where it was in close proximity to the hot (1200°C) sections of the generator.

Figure 29 shows a narrow,wavy band of light-colored material extending the length of representative strips of thermal insulation that was installed parallel with the vertical rows of thermoelements. The light-colored,wavy bands mark lines of constant temperature, showing how the thermal flux varied top-to-bottom and outwardly from the central hot sections of the generator.

In an earlier discussion in this text, the question of deterioration of the electrical insulating properties was raised. Further examination now discloses that the electrical resistance of the thermal insulation that was used to minimize thermal shunt losses in this generator had indeed degraded and probably created electrical shunt losses.

Figure 28. Remnants of Thermal Insulation Removed from the Improved Experimental Generator after 3772-hrs

Figure 29. Closeup of Representative Strips of Thermal Insulation Removed from the Improved Experimental Generator after 3772-hrs operation

With the exception of insulation immediately adjacent to the hot-strap portions of the thermoelements, the resistance of the thermal insulation had decreased from a value of about 20 megohms (for new insulation) to 10,000 to 200,000 ohms for insulation that had been subjected to operating conditions encountered during duration tests of the generator. When using conductive flat bar-type probes, placed parallel and 1/2 inch apart across the width of longitudinal strips, shown in Figure 29, resistance varied from 400-800 ohms. Since such measurements were made at room temperature, it is estimated that similar measurements made at the elevated temperatures encountered in the generator would show resistance values as low as 40-80 ohms. Such a large decrease in the electrical resistance of the insulating material, coupled with the fact that this insulation was generally in contact with as much as 40% of the surface of each thermoelement, suggests that a majority of the power losses experienced during the latter stage of the performance tests were, indeed, caused by electrical shorting between the thermoelements.

An additional factor, which will require future examination of the thermal insulation, is the possible deterioration of the thermal conductivity of this material. Lowered electrical properties suggest that the thermal insulating properties of the insulation may also have degraded significantly with a corresponding increase in thermal shunt losses.

An examination was made for broken thermoelements by visual and probe inspection. Element 363, an n-type thermoelement shown in the center tier of Figure 20, was found broken at the T_i site. Failure of this thermoelement did not appreciably affect the performance of this parallel-series connected generator, attesting to the value of redundancy in generator circuitry. Failure of this single element would account for less than 1% of the power loss experienced, leaving the deteriorated insulation and possibly some thermoelement degradation to account for the major power losses.

With the exception of the broken element and the degraded thermal insulation, all other components of the generator appeared unaffected by their prolonged exposure to vacuum and high-temperature conditions.

The results of this evaluation and performance analysis clearly show that there is a need for better long-lived thermal insulation for improved high-temperature, space-type power generating systems. Because of the significant effect that the degradation of its thermal insulation had in the power output of the generator, it is likely that degradation of its thermoelectric components was less than half of the 9% decrease experienced.

More specifically, it is estimated that the thermal insulation accounted for 5% of the loss in power output, with degradation from all other causes (including a broken thermoelement) amounting to about 4%.

C. TEST FACILITY FOR RTD

The test facility, as shown in the functional diagram of Figure 30, was designed with a capability for long (5000-hr.), sustained life tests and many (500) thermal cycling evaluations. The overall facility was patterned after one used at Monsanto Research Corporation for testing thermoelectric generators, thermoelements, and materials.

Essentially, the test facility consists of a high-vacuum bell jar apparatus (Veeco 401), shown in the center of Figure 30. Thermoelectric specimens or generators would be mounted within the 18-inch x 10-inch transparent bell jar for evaluation by sustained testing and thermal cycling. Electric power, providing energy to the required high-temperature heat sources, would be supplied by either the 2-KVA transformer built into the Veeco unit, or by the 10-KVA step-down transformer shown to the right of the Veeco 401 in Figure 30. The 2-KVA transformer may be controlled manually or automatically. The automatic control circuit consists of the Thermac, Regulator, Magnetic Amplifier, and Saturable Reactor shown to the right in Figure 30. The remaining two items in this grouping, the Data-Trak and Percentage Timer, are used to supply the desired thermal cycling or long-term life test programs to the control equipment. Two multipoint recorders (shown to the left in Figure 30) are used to collect data as the various tests are run. A selector switch is provided in order that individual data lines may be accurately sampled by a millivolt potentiometer.

Component selection for the test facility was based on reliability and compatibility with the task requirements. Additional attention was devoted toward making the test facility versatile. Several modifications, with respect to Monsanto Research Corporation's test facility, were made to insure safety to RTD personnel and equipment.

Further description of some of the features of the pieces of equipment shown in Figure 30 follows.

1. Veeco 401 Vacuum Unit

This unit is a high (10^{-7} torr) vacuum system comprised of an 18-inch x 30-inch bell jar, pumping system, Evapatrol, and a RG-3A Ionization Gauge Control. The Evapatrol consists of an autotransformer and a multiple tapped secondary step-down transformer with a 2-KVA capability. The 2-KVA unit can be used for miscellaneous filament and generator heat source demands.

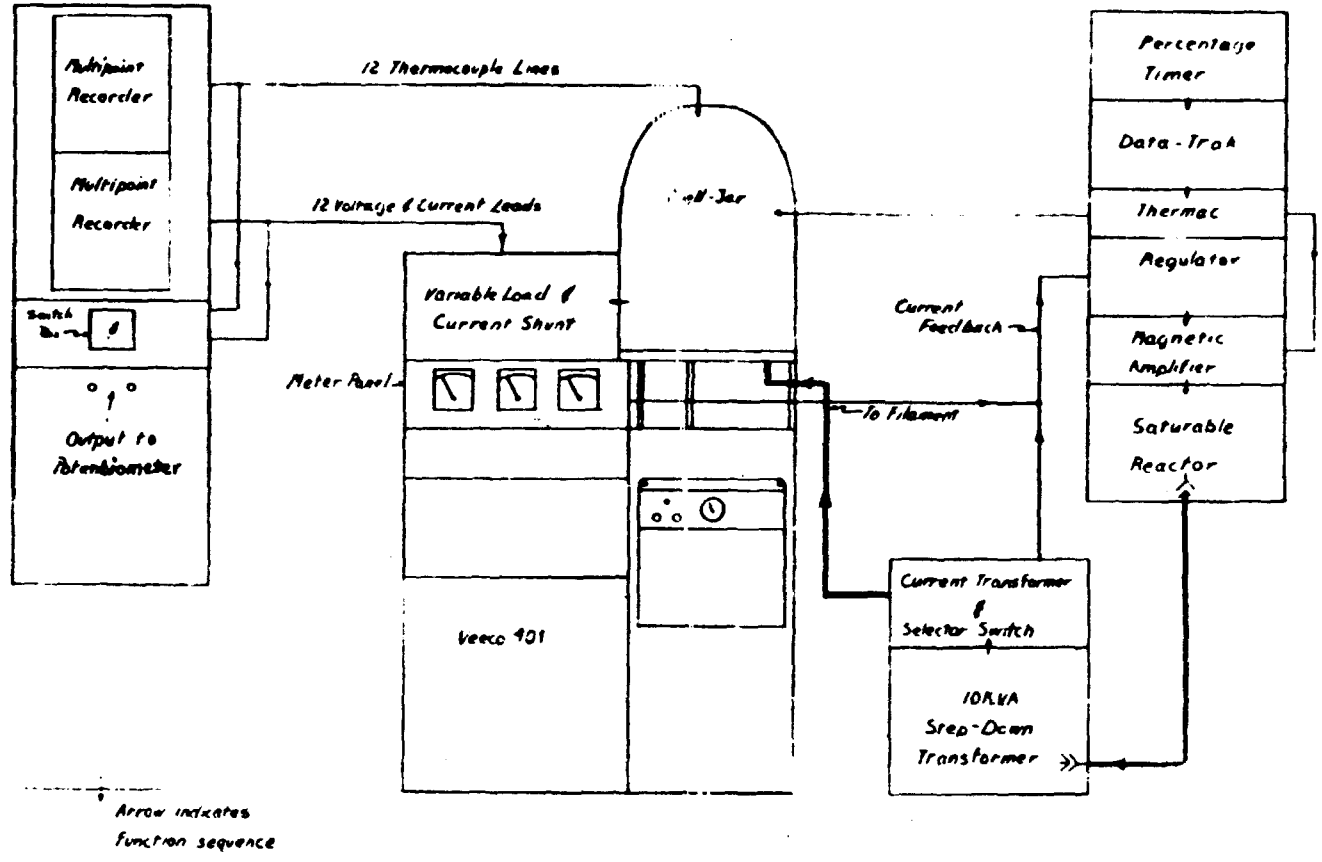

Note: All equipment to be in relay cabinet type modules
All mounted on casters

Figure 30. Functional Diagram of Test Facility for RTD

It is a convenient unit for both manual and automated control of heat sources used in testing generators. The versatility of the Veeco 401 unit was enhanced by the following modifications:

a. The vacuum bell jar and base plate can be mechanically raised to allow easy access to feedthroughs and octal headers.

b. Wiring changes provide heater element and heat source dropout, should power failure and subsequent loss of vacuum occur. A manual reset is required to restore the heater power supply.

c. Both the autotransformer and the step-down transformer (2-KVA system) were wired to Hubbell connectors on the front panel of this unit, allowing for full or partial interconnections for manual and automatic control. Automated control equipment is directly adaptable to either a 2-KVA unit or a 10-KVA power unit, both of which were provided.

d. An additional meter was supplied to record the voltage applied to the heat source.

e. A panel, comprising a variable 0-100 ohm load and a precision four terminal current shunt, was mounted on the rear of this unit.

2. Data-Trak and Percentage Timer

The Data-Trak, shown in the multiple unit panel at the right of Figure 30, offers a linear potentiometer output in response to a metallized paper program chart. Normally, the time variable is controlled by manual changing of gear ratios and/or motor drives. A remote control is available which applies DC braking bias to the drum motor, interrupting motion. By use of the Percentage Timer and this remote control feature, the program functions can be extended. Under these conditions, all ramp functions become multi-step functions. However, thermal inertia of the heater and surrounding media suppresses the multi-step input and creates a smooth thermal change. This whole feature allows many time pattern variations without having to alter program charts or gear ratios.

3. Thermac

This unit is also shown in the right panel of Figure 30. The device accepts the potentiometer output of the Data-Trak,

and by means of comparison to a sampling thermocouple, originates the heater control signal. The unit also has manual control (open end), set point control, and output limiting.

4. Magnetic Amplifier and Saturable Reactor

A Fincore magnetic amplifier and saturable reactor, as shown in the right panel of Figure 30, provide the final linkage to the 10-KVA or 2-KVA transformer. The magnetic amplifier accepts the control signal from the Thermac and supplies the control bias to the saturable reactor accordingly. The reactor will operate from a 220/440 volt source and be capable of a 10-KVA output.

5. 10-KVA Transformer

This unit is shown in the lower right of Figure 30, adjacent to the Veeco unit. The primary was wired for 220-440 VAC and the secondary tapped for 4, 10, 20, 40 VAC output. Connections between this unit and the saturable reactor were made by cable and Hubbell connectors. Selection of either the 10-KVA transformer or 2-KVA transformer was made at the base of the bell jar by means of bolt-on connections to the heater feedthroughs.

6. Regulator

This device is also shown in the right panel of Figure 30, and is a Barber-Coleman current regulator. Its purpose is to prevent excessive heater current during initial warm-up. Since heater element resistance increases with temperature, overloading of the equipment will occur at initial warm-up. However, the current egulator measures the heater current by means of a current transformer and modifies the input impedance of the magnetic amplifier. This unit has a manual set limit provided by an external control potentiometer.

7. Current Transformers and Switching

Two current transformers are necessary for feedback information to the Barber-Coleman unit just discussed. One is provided with the Veeco unit and housed within the vacuum unit. The second is mounted above the 10-KVA transformer (shown in same panel as 10-KVA transformer in Figure 30). The Veeco unit has taps for primary currents of 0-100 amperes and 0-400 amperes. The second current transformer has taps for 100, 200, 400 and 800 ampere ranges. In all ranges, for both current transformers,

secondary currents will be 5 amperes full scale. Since high potentials can exist across the secondary windings when unloading the transformer, a 3-pole, 2-position switch with self-shorting action is used for selection of either unit. A 0.5 ohm load is used across the unused current transformer at all times, preventing any lethal voltages.

8. Multipoint Recorder

Two Speedomax or similar units, shown in the left panel of Figure 30, having twelve-point capacity and strip chart drive, are required. One recorder is used for thermocouple monitoring. The other is equipped with voltage dividers for accurate reduction of any voltages which exceed the 50-millivolt recorder range. Easy access to both recorders allows for rearrangement of this concept.

9. Potentiometer Selection Switch

This switch is shown below the recorders in Figure 30. This 24-position, 2-pole, selector switch terminates in a pair of output terminals for monitoring with a manual laboratory-type millivolt potentiometer. The potentiometer is not supplied as part of the test facility.

The facility consists of two major circuits, the heater control and data recording circuits. Figures 31 and 32, respectively, illustrate the wiring details and interconnections of the various pieces of equipment which comprise the test facility.

The completed test facility, described in Figures 30, 31 and 32, is shown in Figure 33. After initial assembly and testing, the improved experimental model generator was installed in the unit. The RTD facility was in sustained operation for 3272 hours, maintaining a hot-junction temperature of about 1200°C and at a vacuum of 10^{-5} to 10^{-6} torr, providing thermal cycling conditions as required. The only problems encountered with the facility were centered about the temperature controller which failed in setpoint mode several times. The circuit board was returned to the factory and repaired each time. During repair of this component, the facility was operated in manual mode for approximately 500 hours.

Performance of the facility during the duration and thermal cycling tests of the improved experimental model generator proved its capability for long (5000-hr), sustained life tests and many (500) thermal cycle evaluations.

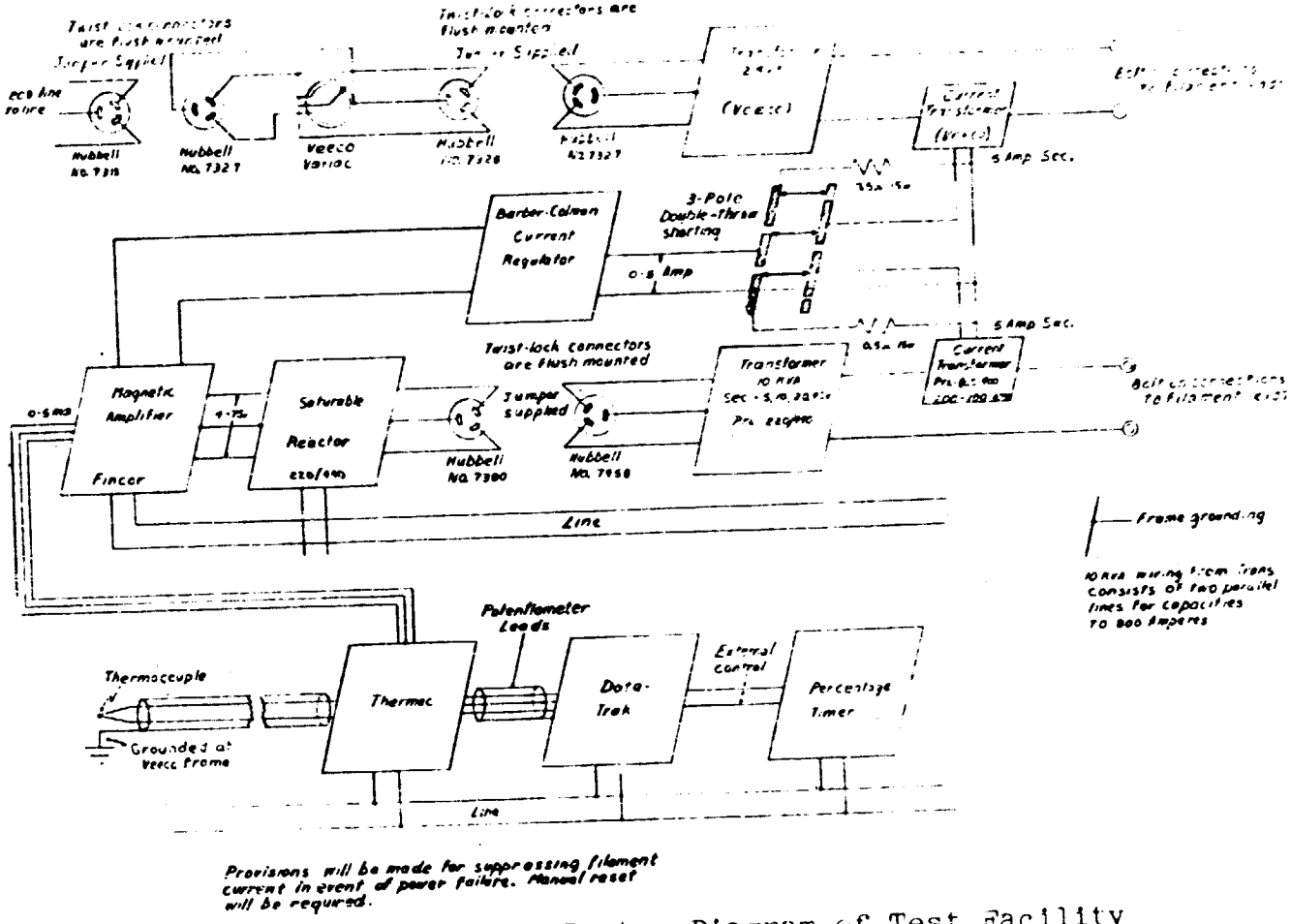

Figure 31. Heater Control System Diagram of Test Facility for RTD

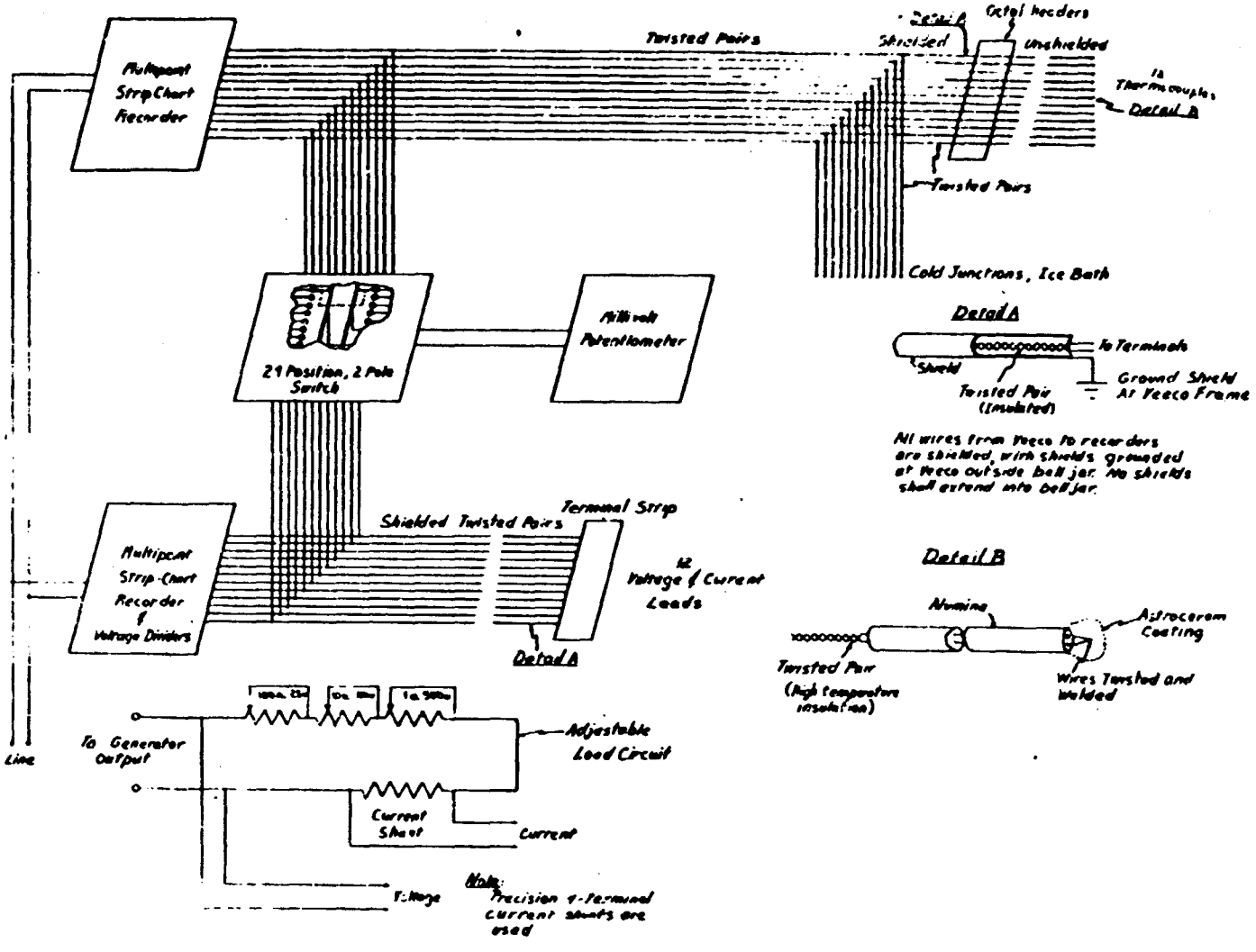

Figure 32. Recording and Load Circuit Diagram of Test Facility for RTD

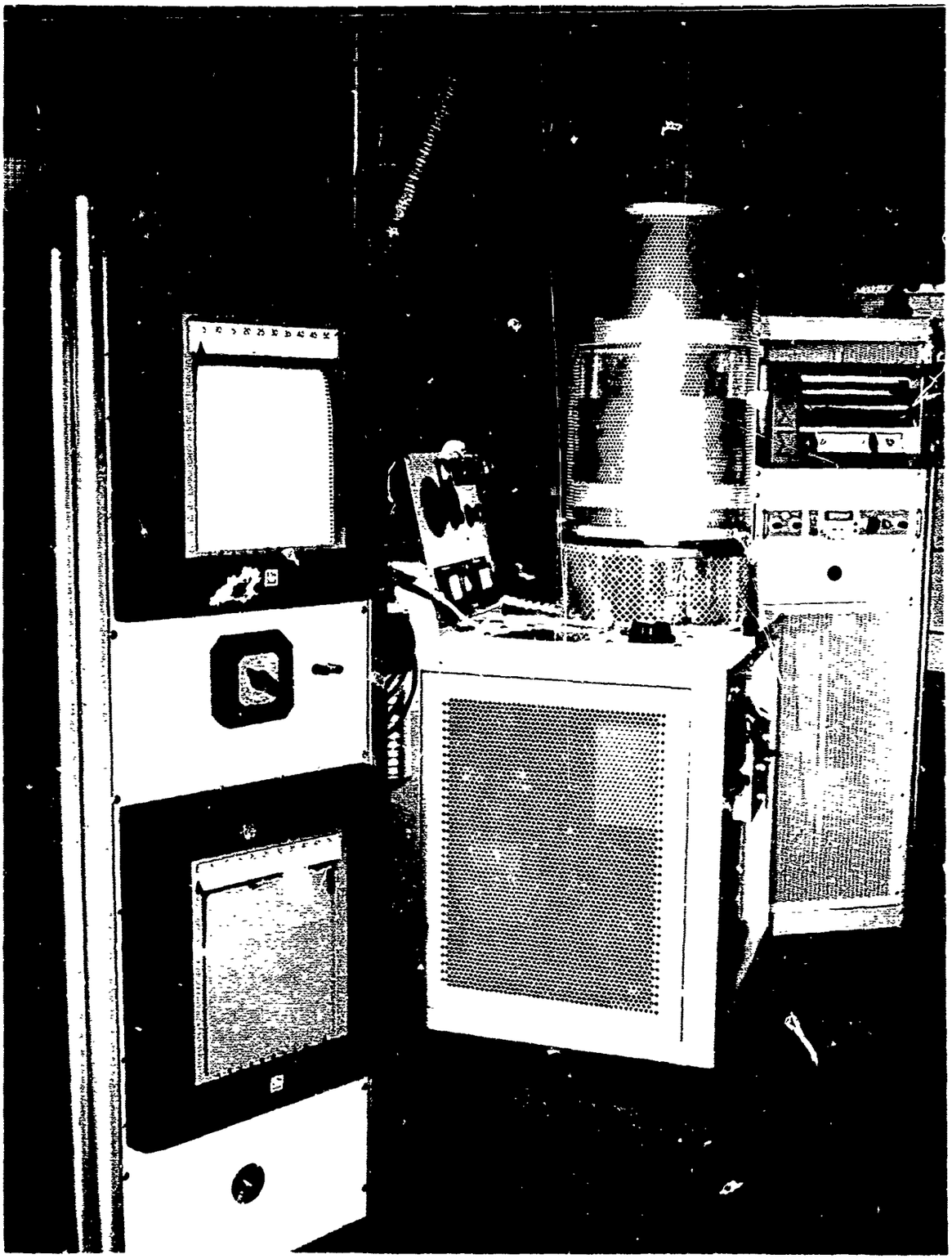

Figure 33. View of Completed Test Facility for RTD

D. COMPONENT RESEARCH

1. Junction-Forming Technique

It was necessary, due to unexpected problems encountered during operation of the improved laboratory model (50-watt) thermoelectric generator, to expend effort on portions of this phase in agnitudes not originally intended. Nevertheless, significant progress was made towards achieving project goals and advancing the state of the art.

Considerable effort was expended under this phase in an attempt to solve the problem of the intermediate-junction temperature limitations revealed wher they were exceeded in the 50-watt generator. Although single thermoelements and multi-element couples survived long-time (>1000-hrs.) duration testing, the incorporation of these elements into the ring-type generator design resulted in a change in thermal profiles along the thermoelement. These thermal changes resulted in operation of the MCC 40 segments at temperatures above their operating range and an early demise at their junction with the graphite intermediate. The mechanism of failure was found to be the chemical reaction of one component with the graphite. The melting point of the compounds formed by this reaction was found to be sufficiently lower in magnitude to cause an incipient melting condition at the bonds. Once this condition was initiated, it proceeded in a progressive manner and resulted in the catastrophic failure of the thermoelement at this junction. The immediate problem was solved by careful screening and fabrication control to insure safe operating temperatures at these potential sites of trouble.

Extensive effort was also expended to modify the fabrication equipment and technology in order to produce 1/4-inch diameter thermoelements for construction of the improved experimental generator. P-type segmented thermoelements were produced in diameters of 1/4 inch by direct extrapolation from the techniques used for production of 3/8-inch diameter thermoelements. The L/A ratios of the smaller thermoelements were increased to conform with radiator and efficiency goals for the improved experimental model (15-watt), as well as the necessity of limiting the intermediate-junction temperature to a safe operating level. The necessity for proper matching of thermoelectric material segments for incorporation into a device was graphically demonstrated by the considerable difficulty encountered when changing the n-type thermoelements from the 3/8-inch diameter used in the advanced experimental model generator to the 1/4-inch diameter required for the improved experimental model generator. The increase in

L/A ratio significantly aggravated the thermoelectric property mismatch between the n-type MCC 60 and MCC 40 segments. This mismatch in properties occurs when either the generated voltage or the internal electrical resistance deviates sufficiently between two series-connected material segments, and results in a decrease in power output. The assignment of primary effort to this problem resulted in an adequate solution by means of technique modifications and improved control in the fabrication of the elements. L/A ratios were successfully increased from 2.3 cm^{-1} to about 5.5 cm^{-1}.

The successive scaling down of thermoelements from 1/2-inch to 3/8-inch to 1/4-inch diameters during this period revealed a proportionate increase in the sensitivity of thermoelectric properties to the variables inherent in the fabrication techniques. The modification and control solutions developed were probably not optimum, due to time limitations, but permitted the production of 1/4-inch diameter thermoelements ranging from 0.1 to 0.2 watts power output for both p- and n-type segmented elements operating at the generator design temperatures of about 1200°C T_h, 850°C T_i and 500°C T_c.

One of the major fabrication variables controlled was that of material density. This problem of thermoelement density variations was traced to unpredictable variations in friction between hot-press die parts. In conjunction with the greater surface to mass ratio in 1/4-inch diameter thermoelements, this became such a large percentage of the total pressure required that it was no longer a negligible value as had been the case in consolidation of larger elements. Additionally, difficulties were encountered in reproducibly compounding the minute quantities (as 1 mole-% additive in a segment weighing less than 1 gram) of powdered materials required to produce 1/4-inch diameter thermoelements. Stringent efforts to better control of both these variables by technique refinement resulted in a sufficiently satisfactory means of producing the desired quantity of acceptable thermoelements to construct this generator.

Effort was also required to solve the problem of reproducing strong bonds in the more fragile 1/4-inch diameter elements. The greater L/A ratios in these elements produced greater leverages on the bonds between the thermoelectric material segments and their graphite contacts, resulting in separation problems in less-than-perfect bonds. Surface preparation of the graphite was found to be the critical factor and, after evaluation of several rather complicated machining methods, simple preparation methods evolved that resulted in segmented thermoelements which could not be broken by applying strong bending forces with the fingers.

The production of more uniform and shallow serrations in the graphite contact was found to result in improved (power) junction electrical resistance as well as high mechanical strength. Coarse emery cloth was found to produce the most satisfactory surface for the bonding of MCC 50 and MCC 60 to graphite at high fabrication temperatures. For the lower temperature bonding of MCC 40 materials to graphite, the best surface was produced by rubbing the graphite on an 8-inch double-cut bastard file, in a direction parallel to its teeth, to produce uniform grooves. Rotating the surface 90° and repeating the process produced the quality of surface required for good bonding.

An investigation was undertaken to determine the electrical resistance characteristics attributable to various portions of the thermoelements. The primary purpose of this study was to observe the range of resistance, including interface transition zones and bonds, of the individual thermoelectric material segments and the graphite end contacts by obtaining electrical profiles of multi-segment thermoelements in actual operation. Such profiles furnish indicative data on where work is needed to improve both quality and reproducibility in generator-type thermoelements. A number of 1/4-inch diameter thermoelements were measured in vacuum at T_h temperatures of about 1200°C, T_i of about 875°C and T_c temperatures of about 480°C. Temperature readings were obtained by thermocouples implanted at the T_h, T_i and T_c sites and corroborated by radiation pyrometry, where applicable. Values were measured using current probes across the total length of thermoelement and by attaching or implanting voltage probes (illustrated in Figure 34) at:

a. the output end of the graphite hot-end contacts;

b. the hot junction between the graphite contact and the MCC 50 or MCC 60 segment;

c. the graphite intermediate junction disc between MCC 50 or MCC 60 and MCC 40 p or MCC 40 n;

d. the cold junction between MCC 40p or MCC 40n and the cold-end graphite contact; and,

e. the output end of the graphite cold-end contact.

This pattern permitted assignment of resistance values to the specific points of interest along the element. Five p-type and fifteen of the more troublesome n-type 1/4-inch diameter thermoelements were measured in this study and the results are tabulated in Table 5.

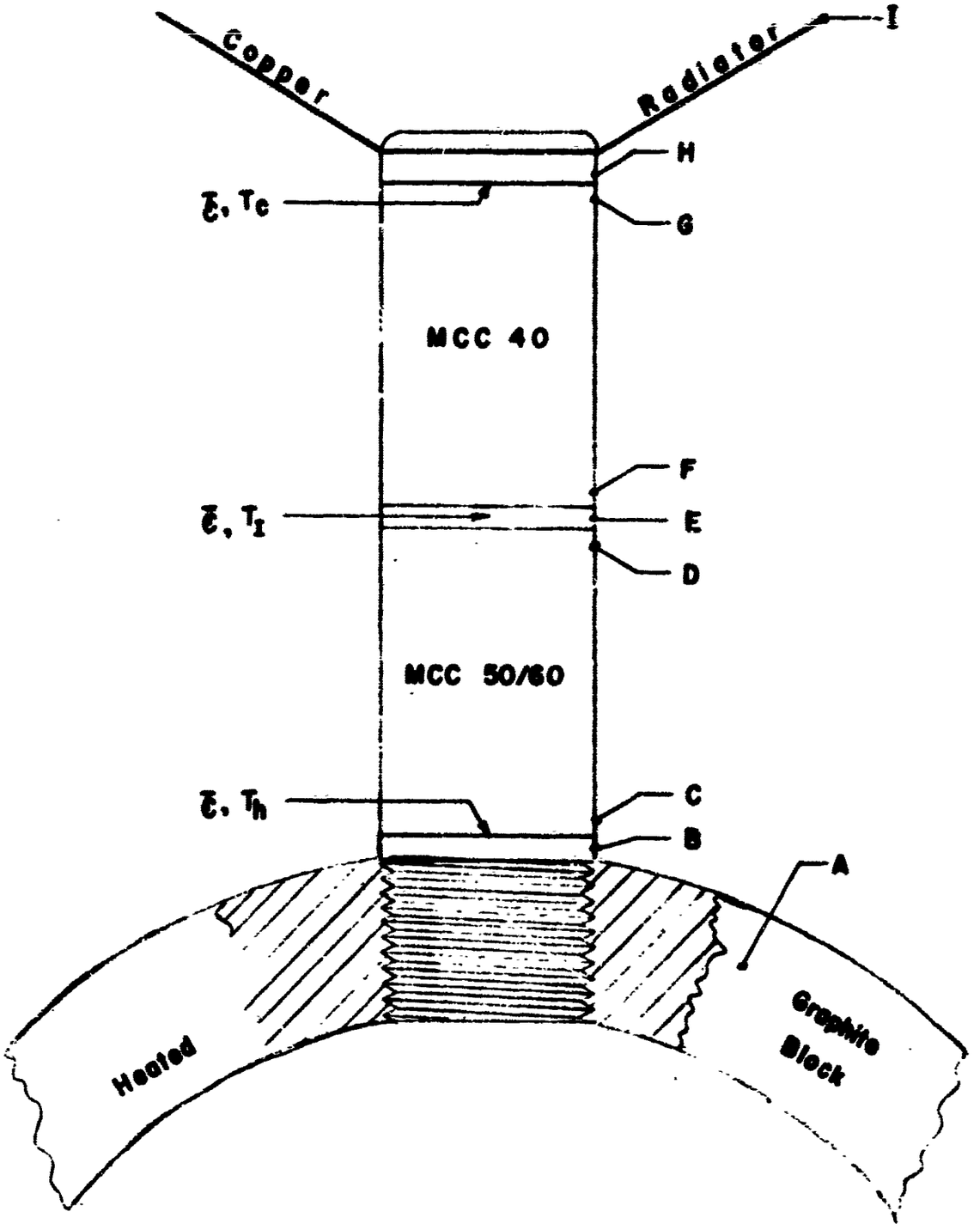

Figure 34. Diagram of a Typical Thermoelement Showing Sites of Thermocouples and Voltage Probes for Electrical Resistance Measurements

Table 5

ELECTRICAL RESISTANCE OF SEGMENTED
1/4 INCH DIAMETER THERMOELEMENTS

Element No. and Type	Resistance, ohms: Graphite Hot Contact(1)	MCC 50 or MCC 60 Segment(2)	MCC 40(n) or MCC 40(p) Segment(3)	Graphite Cold Contact(4)	Full Length Thermo-Element
1-p	0.0015	0.0145	0.0150	0.0033	0.0343
2-p	0.0016	0.0178	0.0203	0.0029	0.0426
3-p	0.0016	0.0120	0.0166	0.0026	0.0328
4-p	0.0017	0.0177	0.0106	0.0020	0.0320
5-p	0.0025	0.0132	0.0151	0.0027	0.0335
1-n	0.0022	0.0312	0.0181	0.0034	0.0539
2-n	0.0021	0.0254	0.0188	0.0026	0.0489
3-n	0.0037	0.0317	0.0294	0.0036	0.0684
4-n	0.0036	0.0273	0.0274	0.0030	0.0613
5-n	0.0034	0.0318	0.0141	0.0030	0.0523
6-n	0.0037	0.0183	0.0200	0.0031	0.0451
7-n	0.0025	0.0170	0.0309	0.0022	0.0526
8-n	0.0028	0.0183	0.0313	0.0029	0.0653
9-n	0.0057	0.0290	0.0252	0.0027	0.0626
10-n	0.0050	0.0126	0.0237	0.0021	0.0434
11-n	0.0060	0.0305	0.0239	0.0024	0.0528
12-n	0.0096	0.0121	0.0274	0.0023	0.0514
13-n	0.0017	0.0196	0.0240	0.0023	0.0476
14-n	0.0027	0.0115	0.0199	0.0026	0.0457
15-n	0.0013	0.0178	0.0308	0.0027	0.0526

(1) Approximate length of hot graphite contact, 1/4 inch
(2) Approximate length of MCC 50 and MCC 60 segments, 5/16 inch
(3) Approximate length of MCC 40p/40n segments, 3/8 inch
(4) Approximate length of graphite cold contact, 1/2 inch

Resistance profiles were also determined by the same methods for three p-type and three n-type multi-segmented thermoelements of 3/8-inch diameter. These results are tabulated in Table 6.

The electrical resistance was calculated, in all cases, from measurements of the current produced by and flowing through the operating thermoelement and measurements of the potentiometric voltage drop between two points along the element. Using two measured conditions with the circuit loading varied (usually open-circuit and matched-load conditions), the actual electrical resistance (or difference in resistance) between two points along the element was calculated by dividing the difference in measured voltage drop between these points by the difference in measured current. This four-point probe method, using the electrical output of the thermoelement, is more accurate and representative of thermoelectric behavior at temperature than such methods as the classical Kelvin technique of passing a measured current through a material.

In general, the total electrical resistance of n-type thermoelements was higher than that of p-type elements. It is believed that this was due in some part to diffusion of components of the n-type materials into the graphite contacts during fabrication. This hypothesis is supported by observed phenomena and reported under Fundamentals Investigations in this contract and by previous Monsanto Company-sponsored junction research. Variations in the electrical resistance of both p- and n-type thermoelectric material segments also appeared to generally correspond to density variations - mentioned earlier as a fabrication problem for 1/4-inch diameter thermoelements. The randomness of the high resistance points as to their occurrence at bonds, junctions, and contacts illustrates the complications in fabricating complex multi-material systems.

The resistance values reported in Table 5 are representative of values for single material segments tested in the past. The electrical resistance of graphite contacts, however, were previously measured for 1/2-inch diameter thermoelements and found to be negligible. As indicated by the data of Table 5, for 1/4-inch diameter thermoelements with L/A ratios of 5.5 cm^{-1} as compared with 1.9 cm^{-1} for 1/2 inch diameter thermoelements, the electrical resistance of the graphite contact is not negligible and accounts for about 10% of the total thermoelement resistance. The data of Table 6 indicates that the 3/8-inch diameter thermoelements, having an L/A ratio of 2.3 cm^{-1}, were unexpectedly worse in this respect with junction and contact resistance approaching and exceeding that of the thermoelectric material in some cases - at least 38% of total element resistance. While it should be noted that these elements were rejects from earlier

Table 6

TEMPERATURE AND ELECTRICAL RESISTANCE PROFILES*

Specimen	612N	630N	619N	549P	651P	654P
T_h, °C	1198	1201	1198	1200	1203	1197
T_i, °C	998	904	942	905	842	904
T_c, °C	595	562	580	592	613	565
R, A-I, ohms (overall)	0.0216	0.0600	0.0281	0.0436	0.0243	0.0333
R, A-B, ohms	0.0020	0.0136	0.0027	0.0047	0.0048	0.0071
R, B-C, ohms	0.0013	0.0224	0.0056	0.0058	0.0025	0.0119
R, C-D, ohms (MCC 50/60)	0.0033	0.0076	0.0054	0.0015	0.0059	0.0029
R, D-E, ohms	0.0028	0.0016	0.0018	0.0019	0.0025	0.0014
R, E-F, ohms	0.0002	0.0003	0.0032	0.0069	0.0006	0.0019
R, F-G, ohms (MCC $40_p/40_n$)	0.0071	0.0098	0.0074	0.0030	0.0059	0.0062
R, G-H, ohms	0.0044	0.0044	0.0018	0.0192	0.0017	0.0014
R, H-I, ohms	0.0005	0.0003	0.0002	0.0006	0.0004	0.0005

Note* Refer to Figure 34 for site locations.

generator construction, the primary reason for rejection was excessive interface temperature. This rejection factor and the high contact resistance are probably more than coincidence, but it is believed that a large part of the improvement that made the production of 1/4-inch diameter thermoelements feasible during the duration of this contract is the result of the extensive effort expended on junction improvement.

Some effort has also been expended on varying temperature-pressure cycles in the fabrication process and the modification of junction zone materials between thermoelectric material segments. While these efforts did not produce reproducible or useful thermoelements, the lattice structure and molecular compound combinations of the polycrystalline MCC-based thermoelectric materials appear to be sensitive to changes in fabrication technique. The techniques utilized in the fabrication of elements for the 50-watt generator permitted reasonable control of these variables and adequate matching of thermoelectric properties. The state of the art is not developed in sufficient degree to produce optimum properties in these materials, but, nevertheless, permitted satisfactory functioning of the devices in which they were used.

Attempts to improve the properties of the MCC-based thermoelectric materials by varying temperature-pressure cycles during hot-pressing of thermoelements resulted in a useful side-effect. It was discovered that the reaction between MCC 50 or MCC 60 and graphite could be produced at lower temperatures than normally used. Both materials were joined to graphite at temperatures as low as 1400 °C, producing metallurgically sound and mechanically strong bonds. This increase in potential range of cycle variation offered promise for the eventual exact matching of thermoelectric materials to device design requirements. Both MCC 50 and MCC 60 were subjected to examination under the 1400 °C fabrication temperatures. MCC 50, fabricated under these conditions, exhibited substantial density variations between the ends and the center when segment lengths in excess of 0.2 inches were attempted, ranging from about 85% of theoretical density at the ends to as low as 30% at the center. The variation in density resulted in high stress levels in the specimens, as manifested by high sensitivity to mechanical and thermal shock. This problem is less critical in the MCC 60 material. A few elements of excellent strength and stability were produced of both materials at 1400 °C. X-ray diffraction and spectrographic analyses indicated that compounds and structures similar to those produced by 2000 °C fabrication resulted, but, as tabulated in Table 7. parameter measurements revealed drastic changes in thermoelectric properties including electrical resistivity, Seebeck coefficient and thermal conductivity (indicated by ΔT).

Table 7

PROPERTIES OF MATERIALS FABRICATED BY HOT-PRESSING AT 1400 °C

Spec.	Material	T_h, °C	T_c, °C	ΔT, °C	S, μv/°C	ρ, ohm-cm.
LTE-33N	MCC 60	1205	764	441	38	0.076
LTE-35N	MCC 60	1145	741	404	18	0.020
LTE-44P	MCC 50	1188	608	580	309	0.159
LTE-23N	MCC 60	1199	720	479	202	0.052
LTE-76N	MCC 60	1198	1008	190	75	0.033

Since the properties produced were variable and, in general, below the performance of the units produced at higher temperatures, MCC 60 material was pressed at 2050 °C and crushed to powder. The resulting material was then pressed at 1400 °C in an attempt to gain a better understanding of the mechanisms involved. The resulting specimens exhibited properties similar to those of material that had not been treated at the higher temperature, indicating that a definite and permanent structural modification was produced by the fabrication temperature variation. While initial results are not conclusive, the great variations which can apparently be induced in the properties of MCC-type thermoelectric materials by modifications in formulation and fabrication techniques indicate great promise for the technology. With additional understanding of the art, it should be feasible to tailor-make a thermoelectric material to yield optimum performance in a defined application without real or significant limitations within characteristic ranges, which appear to be extremely wide in comparison to normal semiconductors. Useful devices are presently produced by cut-and-try methods, since present understanding of thermoelectric phenomena with this and other high-temperature materials is limited. Nevertheless, the technology of the foreseeable future appears to be amenable to improving and controlling thermal conduction, voltage output, electrical conduction, resistance to solid-state diffusion, and thermal cycling damage.

An investigation of techniques to prevent catastrophic failure of MCC 40-graphite bonds when exposed to high temperatures for long periods of time, was undertaken late in the program. Previous Monsanto Research Corporation-sponsored research on encapsulation of thermoelectrics indicated that containment of the junction within a thin refractory shell should be feasible. Evaluations were made of MCC 40 thermoelements hot-pressed in a graphite

die liner. Results of initial tests on both MCC 40N and MCC 60N, presented in Table 8 for shells of 0.010-0.020 inch wall thickness, indicate that this technique could improve junction stability and decrease the problem of electrically matching thermoelectric materials in multi-segment thermoelements.

Table 8

PROPERTIES OF ELEMENTS FABRICATED IN GRAPHITE SHELLS

Spec.	T_h, °C	ΔT, °C	S, μv/°C	ρ, ohm-cm	P, watts
783	903	198	236	0.0017	0.081
(MCC 40n)	997	215	233	0.0016	0.096
	1101	249	209	0.0014	0.117
	1204	259	184	0.0015	0.092
785	903	243	222	0.0022	0.089
(MCC 40n)	1000	279	213	0.0021	0.112
	1101	304	204	0.0019	0.133
	1203	328	187	0.0018	0.142
795	1204	313	133	0.0027	0.042
(MCC 60n)					

In summary, many 3/8-inch diameter and 1/4-inch diameter thermoelements were fabricated under this subphase of the contract for the purpose of evaluating junction-forming techniques and constructing the advanced and improved experimental model generators. While considerable effort was concentrated on the solution of unexpected MCC 40 junction failure problems in the advanced experimental model generator, substantial progress was made in the advancement of hot-press fabrication technology. The operating temperature limits of MCC 40-graphite junctions were established and techniques developed to keep these temperatures within safe limits and to protect the junctions against failure, in case of accidental generator overheating. Extensive modification problems were overcome in both equipment and tech-

niques, caused by an element size reduction from 3/8-inch to 1/4-inch diameters and the resultant increase in L/A ratio design. A sufficient number of good quality, smaller elements were produced to permit construction of the improved experimental model generator. A substantial improvement was made in material density control, refinement of thermoelectric powder formulation, and in the quality and reproducibility of junction bonds. Both mechanical strength and electrical conductivity were improved by an estimated 15-20% during this program. Electrical resistance profiles were investigated in thermoelements produced, and the sites for most effective improvement and the methods to best accomplish the improvement established. An investigation of the potential variations attributable to changes in fabrication techniques instituted and the potential scope determined. Progress in advancing the state of the art of junction-forming techniques, while not as extensive as would have been desired, succeeded in both solving all immediate problems submitted to this subphase and, simultaneously broadening the base of knowledge necessary to permit more effective use of thermoelectricity in the future.

2. Arc-Plasma and Flame-Spraying Studies

The overall objective of this phase of the contract was to continue investigation of the plasma spray technique for obtaining usable thermoelements of any desired configuration, with emphasis on encasing a cylindrical substrate with segmented thermoelectric materials, appropriate junctions and leads, for evaluation.

Although the arc-plasma and flame-spraying facilities were required in the repair of the 50-watt generator to a considerably greater degree than originally anticipated, all goals established initially for this phase of the experimental work were achieved during the contract period.

The large heat losses and high fabrication costs which are characteristic of thermoelectric generator designs employing radially mounted hot-pressed thermoelements could be significantly reduced if, for example, doughnut-shaped thermoelements could be produced by arc-plasma and flame-spraying methods. Spray techniques could also permit greater flexibility in the shape and capacity of thermoelectric generators. Thermoelectric coatings surrounding a central heat source could ultimately offer high current or voltage capability, as well as improved thermal efficiency, owing to a reduction in the heat losses which are experienced with radially mounted hot-pressed thermoelements.

The technical program for this phase of the project consisted of determining the spraying techniques required to produce generally acceptable coatings of individual p- and n-type thermoelectric materials on graphite cylindrical substrates, attaching electrical lead wires to such coatings, and screening specimens for thermoelectric characteristics, thermal shock resistance, and selected physical properties. Where possible, coating properties were to be correlated with process variables involved in the spraying and/or postspray thermal treatment of coated specimens. P- and n-type segmented thermoelements were to be produced by appropriately combining sprayed high- and low-temperature materials and promising segmented specimens were to be screened at a hot-junction temperature of 1200°C in a vacuum to determine thermoelectric characteristics, thermal shock resistance, and sublimation loss. Cutting techniques were to be considered for controlling the area-to-length ratio of sprayed thermoelements, and the effect of this ratio on thermoelectric properties was to be observed. Finally, a p-n couple, consisting of sprayed p- and n-type segmented thermoelements, was to be fabricated, evaluated for 1000 hours, and thermally cycled to observe overall performance.

In addition to fabricating sprayed thermoelements, arc-plasma and flame-spraying techniques were to be employed for producing low-resistance contact joints at the graphite terminals of hot-pressed thermoelements for screening, in the repair of the 50-watt advanced laboratory model generator, and the construction of the 15 watt improved experimental model generator.

Various types of equipment were utilized for the experimental work in this phase of the program. A 25-KW, Model SG-3, and an 80-KW, Model SG-2, arc-plasma spraying unit (Plasmadyne Corp) were used for producing coatings of MCC 40 (p and n), MCC 50 and MCC 60. Feed powders, transported in a carrier gas stream, were injected into the plasma stream through a feed port in the anode near the nozzle exit to induce melting. Feed powders of appropriate size were introduced into the carrier gas stream from a type 2MP volumetric powder feeder (Metco) or a canister-type feeder (Plasmadyne) employing a double tube venturi. A special MRC apparatus provided variable speed rotation and transverse movement of graphite cylindrical substrates during spraying. A type 4E metallizing gun (Metco), employing an oxygen-acetylene flame, was used to produce sprayed molybdenum joints in selected areas. Associated facilities utilized during this work included type 7B spray booths (Metco), a type 2CW wet collector (Metco), a type EN-2 blast cabinet (Pangborn), and a Model D industrial abrasive unit (S. S. White). Evaluation of sprayed thermoelectric elements at high temperatures was accomplished in a Model VE-401 (Veeco) or a Model BD-40V (Bon-De) vacuum system.

A water-cooled, controlled environment spray chamber, 30-inch I.D. x 48-inch long, was acquired by Monsanto Research Corporation to permit comparison of thermoelectric and physical properties of coatings produced in non-oxidizing environments with those of specimens prepared under normal spraying conditions in the atmosphere. The unit was installed and tested in the latter portion of the contract period. The gun-holding mechanism supplied with the unit was extensively modified to provide additional flexibility in adjusting substrate-spray gun positions. A remote-controlled, multi-specimen, rotating-transversing device was designed and fabricated for manipulating cylindrical substrates inside of the chamber. Small, isolated leaks in the system were located and sealed. Initial tests were completed in which the system pressure was reduced to about 50μ Hg, welding-grade argon added, and coating deposition accomplished in a positive-pressure, recirculating, inert atmosphere. Although the overall operation of the chamber was considered to be satisfactory, experimental efforts in this area could not be emphasized to the extent desired. Production of thermoelectric coatings on a regular basis was not accomplished

during this contract period and none of the individual coatings produced in initial work were considered to be of sufficient quality to justify determination of thermoelectric properties.

Various experimental studies were required to produce satisfactory coatings of MCC 40, MCC 50, and MCC 60 by arc-plasma spraying. A large number of feed powders in selected particle sizes were studied, including mechanical mixtures of elemental and/or reacted materials and sintered powders prepared from high quality and low grade elemental components. A description of feed powders utilized for producing sprayed specimens in this experimental work is shown in Table 9. In general, spray powders produced from crushing and sizing of completely prereacted components have yielded thermoelements with the most promising thermoelectric properties. The effect of using prereacted components, as compared to mechanical mixtures of elemental constituents plus dopants, will be observed later when thermoelectric properties of individual MCC 40, MCC 50 and MCC 60 coatings are presented as functions of feed powder compositions and test conditions. Additional studies appear necessary to more precisely define the prereaction cycle (time-temperature-pressure-atmosphere) which should be utilized to prepare the most promising feed powders for producing improved thermoelectric coatings of MCC 40, MCC 50 and MCC 60 by spraying techniques.

A large number of thermoelectric coatings were applied to hollow graphite cylinders (mostly 1/2-inch diameter, 5/8-inch long) using the 25-KW or 80-KW arc-plasma spray guns. To achieve satisfactory bonding of the coatings to the graphite substrates, the latter were outgassed at about 900°C for 1 hr. in vacuum. In early work a thin molybdenum coating was applied to the graphite substrate prior to deposition of individual thermoelectric materials; later, direct bonding of thermoelectric coatings to outgassed graphite was achieved with apparent improvement in bond strength. Most coatings were produced using argon or 5% hydrogen-argon arc gas, argon or helium powder carrier gas, and nitrogen gas for substrate cooling and plasmajet deflection. Plasma stream enthalpy was varied over a wide range to observe its effect on physical and thermoelectric properties of coatings. Powder feed rates were generally adjusted to achieve satisfactory melting and deposit efficiency for the operating conditions studied. The overall range of selected operating conditions which were found to be most satisfactory in this study is shown in Table 10.

Physical properties of selected coatings were determined during this program in an effort to correlate such properties with thermoelectric properties and with spray conditions. The

Table 9

FEED POWDERS USED FOR PRODUCING SPRAYED THERMOCHEMICS

Powder Designation	Constituents/Preparation	Particle Size of Major Components
MCC 40-3P	Mechanical mixture of elements and dopants	-325
MCC 40-3P-3.5%	Mechanical mixture of elements and dopants plus 3.5% "spray-aid"	-325
MCC 40-5P	Mechanical mixture of elements and dopants	-150 + 325
MCC 40-9P	Mechanical mixture of elements and dopants	-325
MCC 40-9P (sintered)	MCC 40-9P heated slowly to 1070°C, 1 hr., N_2, and cooled slowly	-325
MCC 40-11P (sintered)	Mechanical mixture of elements and dopants heated rapidly to 1450°C, 10 min., CO, and cooled rapidly	-150 + 325
MCC 40-4N	Mechanical mixture of elements and dopants	-325
MCC 40-4N (sintered)	MCC 40-4N heated slowly to 1070°C, 1 hr., N_2, and cooled slowly	-325
MCC 40-6N (sintered)	Mechanical mixture of elements and dopants heated slowly to 1070°C, 1 hr., then to 1200°C, 30 min., argon, and cooled slowly	-325
MCC 40-9N (sintered)	Mechanical mixture of elements and dopants heated rapidly to 1450°C, 10 min., CO, and cooled rapidly	-150 + 325
MCC 50-15 (sintered)	Mechanical mixture of quality elements and dopants heated rapidly to 2000°C, 20 min., CO, and cooled rapidly	-325
MCC 50-18-1	Mechanical mixture of partially reacted components and dopants	-325
MCC 50-19A (sintered)	Mechanical mixture of low grade elements and dopants heated rapidly to 2000°C, 15 min., CO, and cooled rapidly	-200
MCC 50-20 (sintered)	Mechanical mixture of quality elements and dopants heated rapidly to 2000°C, 20 min., CO, and cooled rapidly	-325
MCC 50-21	Mechanical mixture of quality elements and dopants	-325
MCC 50-22	Mechanical mixture of quality elements and dopants	-150 + 325
MCC 50-23 (sintered)	Mechanical mixture of quality elements and dopants heated rapidly to 2000°C, 15 min., CO, and cooled rapidly	-325
MCC 60-2	Mechanical mixture of prereacted components and dopants	~ 7 μ
MCC 60-2-3.5	Mechanical mixture of prereacted components and dopants + 5% "spray-aid"	~ 7 μ
MCC 60-3	Mechanical mixture of prereacted components and higher concentration of dopant	~ 7 μ
MCC 60-3-3.5	Mechanical mixture of prereacted components and higher concentration of dopant + 5% "spray-aid"	~ 7 μ
MCC 60-5	Mechanical mixture of elements and higher concentration of dopants	-150 + 325
MCC 60-5 (sintered)	MCC 60-5 heated rapidly to 1450°C, 10 min., CO, then to 2000°C, 10 min., CO, and cooled rapidly	-150 + 325
MCC 60-6	Mechanical mixture of elements and higher concentration of dopants	-325
MCC 60-7	Prereacted components without dopants	~ 7 μ
MCC 60-8	Mechanical mixture of elements without dopants	-325
MCC 60-15 (sintered)	Mechanical mixture of elements and higher concentration of dopants heated rapidly to 1350°C, 15 min., CO, then to 2000°C, 15 min., CO, and cooled rapidly	-325
IN-6	Intermediate material: 50% MCC 50-19A (sintered) 50% MCC 40-9P (sintered)	-325
IN-7	Intermediate material: 50% MCC 50-3-3.5%, MCC 40-4N	-325
IN-8	Intermediate material: 50% MCC 50-3-3.5% MCC 40-9N (sintered)	-325

Table 10

SUMMARY OF SPRAYING CONDITIONS STUDIED

	MCC 40 (p-type)	MCC 40 (n-type)	MCC 50 (p-type)	MCC 60 (n-type)
No. of specimens sprayed	21	19	47	59
Arc gas	A	A	A;5% H_2-A	A;5% H_2-A
Powder carrier gas	A;He	A;He	A;He	A;He
Substrate cooling + deflecting gas	N_2	N_2	N_2	N_2;A
Spraying distance, inch	0.875 3.500	0.625 2.000	1.250 2.875	0.875 4.000
Power level, KW	5-15	4-13	19-30	6-39
Plasma stream enthalpy, Btu/lb.	1810- 5500	1550- 5700	2100- 8190	2540- 8160

volume of coatings having uniform thickness was readily calculated from linear measurements, while the volume of coatings having varying thicknesses was determined, in many cases, using a displacement type densitometer, which employed fine glass beads, instead of liquids, as displacement fluid. Coating density, obtained from coating volume and weight, was found to vary from approximately 70 to 95% of theoretical, depending on spray conditions and feed powder type and particle size. Thickness of uniform coatings was obtained from linear measurements; average thickness of non-uniform deposits was calculated from measured coating volume and length. In general, coating thickness ranged from several mils to approximately 1/8 inch during this program. Knoop hardness measurements were made on several specimens using a 100-gram load and these results are discussed and presented later (Table 24) in conjunction with microstructure observations of sprayed materials.

Thermoelectric properties of sprayed cylindrical deposits were determined for most of the satisfactory coatings prepared in this study. To obtain such measurements, current and voltage leads had to be provided on the hot and cold portions of the coating, and installation of thermocouples was required for determination of hot- and cold-junction temperatures. Originally, molybdenum was flame-sprayed over the thermoelectric coating which had previously been deposited on an outgassed graphite cylindrical substrate. A thin copper strap was wrapped circumferentially over and bonded to the molybdenum outer coating to provide current and voltage leads at the cold junction. Hot-junction current and voltage leads were provided by small diameter molybdenum wire spray bonded to a hollow graphite adapter, which surrounded a resistance-type heating element. The coated specimen was threaded onto the graphite adapter and firmly positioned for testing. During initial testing of thin thermoelectric coatings at 1200°C hot-junction temperature, only small temperature drops were realized through the deposits, thus resulting in excessive and intolerable temperatures in the vicinity of the cold end copper straps. Some melting of copper was observed

Measurement of thermoelectric properties was then attempted directly on "as sprayed" coatings, and on molybdenum coatings applied over thermoelectric coatings, by using special contact probes. However, excessive and usually inconsistent interface resistances were observed. The unsatisfactory results obtained with these original techniques caused further study for a more reliable measuring procedure and resulted in the finally selected method of spray-bonding a double molybdenum wire to the outer molybdenum coating at the cold junction for use in current and voltage measurement. For this purpose, the wire was grit-blasted with

alumina, degreased with trichloroethylene, and bonded by flame spraying. A small-gage, chromel-alumel thermocouple, for measurement of cold-junction temperature, was also spray-bonded to the outer molybdenum coating. Essentially all sprayed specimens were prepared for testing in this manner. For specially selected specimens, thin copper fins, located radially, were spray-bonded to the outer coating to permit achievement of greater temperature differences through the coating wall during screening, and in such cases an emissive coating (TEC-1) was also applied over the exposed molybdenum outer layer and over the radial copper fins. The effect of adding radiator fins and an emissive coating to a sprayed thermoelement can be observed for a selected specimen in Table 11. Although temperature differential and power output were usually considerably enhanced by this technique, it was deemed sufficient for screening purposes to compare characteristics of coatings having only a thin molybdenum layer with thermocouple and lead wires over the thermoelectric coating instead of the more elaborate radiator design.

Table 11

EFFECT OF RADIATORS AND EMISSIVE COATING ON THERMOELECTRIC PROPERTIES OF SPRAYED MCC 50

Spec.	Outer Surface of Coating	T_h, °C	ΔT, °C	Actual Max. Watts/lb. TE Material
253	Molybdenum + lead wires + cold-end thermocouple	1204.5	100.5	0.88
253A	Molybdenum + copper radiators + emissive coating + lead wires + cold-end thermocouple	1205.5	372.0	8.01

Thermoelectric properties of sprayed, individual coatings on cylindrical graphite substrates were routinely determined by rapidly heating the specimen to 1200°C (for MCC 50 and MCC 60) or about 900°C (for MCC 40) hot-junction temperature, and measuring hot- and cold-junction temperatures as well as open circuit voltage, load voltage and current. From these measurements, specimen resistance, power and S were calculated. A tungsten wire

or rod, positioned axially through the center of the sprayed specimen, provided a hot-junction temperature of 1200°C, which was measured by a tungsten-rhenium thermocouple. Cold-junction temperatures were normally measured by chromel-alumel thermocouples, as mentioned above, or by optical pyrometer. The overall measuring technique appeared to be reasonably reliable for a relative comparison of the thermoelectric characteristics of sprayed specimens.

Since coating thickness and weight were arbitrary and not identical for all specimens, appropriate experimental data were normalized to permit comparison of thermoelectric properties of sprayed materials. Specifically, open-circuit voltage, E_{oc}, was adjusted to a ΔT of 500°C, and maximum power output, based on adjusted E_{oc}, was determined per unit weight of thermoelectric material. This normalization was intended to resolve differences in coating thickness and quantity of deposit, which influence the ΔT across the coating and the power output.

Thermoelectric properties of individual sprayed coatings prepared and evaluated during this program are shown in Tables 12 through 15. These data are intended to provide a relative comparison of TE properties of sprayed thermoelements as influenced by feed powder properties, spraying variables, and post-spray thermal treatment. On the basis of these considerations, the following general conclusions were made regarding the production of satisfactory, sprayed, thermoelectric coatings.

MCC 40 (p- and n-type): Coatings produced by spraying a mixture of elemental components plus dopants were generally unstable with time and usually exhibited a low power output per unit weight with gradual degradation in power with time. The most promising coatings were produced with powder obtained by prereacting elemental components with dopants at elevated temperature in a controlled environment, then crushing and sizing the resultant material for spraying. Additional studies are necessary, however, to precisely determine the prereaction conditions (time, temperature, atmosphere) necessary to prepare powders which will yield coatings possessing stable, improved thermoelectric characteristics. Appropriate use of post-spray thermal treatment on p- and n-type coatings produced from prereacted powders appears to show promise for enhancing power output and reducing degradation with time.

Table 12

THERMOELECTRIC PROPERTIES OF SPRAYED MCC 40 (p-TYPE) SPECIMENS

Spec.	Powder Type	Avg. Coating Thickness, mil.	Area/ Length, in.	Test Time, Min.	Th, °C.	ΔT, °C.	R, ohm	Seebeck, μ volts/°C.	Est. Max. Watts/in. TE Material
300	MCC 40-9P	9.2	104.2	60	900.0	63.8	0.00531	115.1	4.40
302PT	MCC 40-9P	4.3	223.0	60	899.0	56.6	0.01000	95.5	2.10
303	MCC 40-9P	4.8	190.0	45	900.0	53.0	0.00900	94.5	2.04
303	MCC 40-9P	4.8	190.0	4020	882.0	50.8	0.00956	91.4	4.30
304PT	MCC 40-9P	31.5	32.2	60	899.0	58.5	0.00822	89.6	1.13
304PT	MCC 40-9P	31.5	32.2	1050	894.0	53.0	0.00978	92.4	2.10
317PT	MCC 40-9P (sintered)	64.0	16.2	60	900.0	53.2	0.00500	140.1	24.30
317PT	MCC 40-9P (sintered)	64.0	16.2	4000	904.0	58.9	0.00551	154.0	24.90
318	MCC 40-9P (sintered)	ND	ND	10	752.0	39.5	0.00409	70.8	13.00
320	MCC 40-9P (sintered)	38.3	25.9	10	900.5	47.3	0.00500	82.9	1.44
320	MCC 40-9P (sintered)	38.3	25.9	944	909.5	40.3	0.01500	15.8	0.20
352	MCC 40-11P (sintered)	21.3	58.6	60	852.0	124.8	0.00500	45.5	8.90
352	MCC 40-11P (sintered)	21.3	58.6	6820	895.5	133.0	0.00588	41.4	6.30
353A(1)	MCC 40-11P (sintered)	22.8	53.7	60	853.0	19.2	0.01142	95.3	12.90

ND = not determined.
PT = postspray thermal treatment.
(1) molybdenum applied to graphite substrate prior to deposition of TE coating.

Table 13

THERMOELECTRIC PROPERTIES OF SPRAYED MCC 40 (N-TYPE) SPECIMENS

Spec.	Powder Type	Avg. Coating Thickness, mil.	Area/ Length, in.	Test Time, min.	T_h, °C.(1)	ΔT, °C.	R_e, ohm	Seebeck, μ volts/°C.	Adj. Max. Watts/ in. TE Material
321 PT	MCC 40-4M	16.8	58.3	10	946.5	44.4	0.00613	35.6	4.60
321 PT (Retest)	MCC 40-4M	16.8	58.3	10	953.0	62.3	0.0066	29.6	4.15
310	MCC 40-4M (sintered)	ND	ND	10	702.5	27.3	0.0084	245.1	29.60
312 PT	MCC 40-4M (sintered)	36.5	27.3	10	752.0	35.2	0.0021	54.1	15.20
341A	MCC 40-4M (sintered)	55.8	18.1	10	599.0	121.0	0.00720	40.3	6.11
351	MCC 40-8M (sintered)	39.0	32.3	10	899.5	32.5	0.00528	177.6	15.60

ND = not determined.
PT = postspray thermal treatment.
(1) hot-junction temperature at maximum power output.

Specimen 341A contained radiators and emissive coating over molybdenum cold-end material.

Table 14

THERMOELECTRIC PROPERTIES OF SPRAYED MCC 50 SPECIMENS

Spec	Powder Type	Avg. Coating Thickness, mil	Area/ Length, in.	Test Time, Min	T_H, °C	ΔT, °C	α, ohm	Seebeck, mvolts/°C	Avg. Power Output at T_H Max., w
254	MCC 50-19 (sintered)	49.3	20.6	1680	1255.5	242.4	0.013470	31.[illegible]	1.[illegible]
254PT	MCC 50-19 (sintered)	49.3	[illegible]	[illegible]	1201.0	75.5	0.00[illegible]	[illegible]	.0[illegible]
254TT	MCC 50-19 (sintered)	49.3	[illegible]	1185	1251.7	60.8	0.00[illegible]	[illegible]	[illegible]
57	MCC 50-19 (sintered)	7.2	133.9	140	1207.5	88.7	0.01[illegible]	[illegible]	[illegible]
71	MCC 50-18-1	80.3	13.9	60	1205.0	119.0	0.01[illegible]	[illegible]	[illegible]
75	MCC 50-18-1	80.3	13.9	150	1229.5	137.5	0.01[illegible]	[illegible]	[illegible]
79	MCC 50-18-1	87.5	13.2	60	1201.0	166.0	0.01[illegible]	[illegible]	[illegible]
79	MCC 50-18-1	87.5	13.2	150	1218.5	196.0	0.01[illegible]	[illegible]	[illegible]
80	MCC 50-18-1	71.2	14.7	60	1207.1	170.6	0.01[illegible]	[illegible]	[illegible]
82	MCC 50-18-1	71.2	14.7	300	1237.0	221.0	0.01[illegible]	[illegible]	[illegible]
84	MCC 50-18-1	86.6	12.4	60	1219.5	214.5	0.01[illegible]	[illegible]	[illegible]
87	MCC 50-18-1	86.6	12.4	150	1224.1	251.6	0.01[illegible]	[illegible]	[illegible]
247	MCC 50-19A (sintered)	39.5	25.2	60	1205.0	95.5	0.00[illegible]	16[illegible]	2.[illegible]
247A	MCC 50-19A (sintered)	39.5	6.3	10	1177.0	1[illegible]	0.00418	[illegible]	1.[illegible]
247A	MCC 50-19A (sintered)	39.5	6.3	420	1194.0	[illegible]	0.00[illegible]	[illegible]	1[illegible]
247A-PT	MCC 50-19A (sintered)	39.5	6.3	30	1202.5	[illegible]	0.00[illegible]	[illegible]	[illegible]
248	MCC 50-19A (sintered)	70.7	14.6	65	1200.0	151.[illegible]	0.00[illegible]	1[illegible]	[illegible]
249	MCC 50-19A (sintered)	55.0	18.5	10	1199.1	1[illegible]	0.00[illegible]	14[illegible]	3[illegible]
250	MCC 50-19A (sintered)	62.0	16.3	10	1196.5	124.5	0.00[illegible]	[illegible]	[illegible]
251	MCC 50-19A (sintered)	50.0	14.6	10	1203.0	109.[illegible]	0.01305	1.1[illegible]	1[illegible]
251	MCC 50-19A (sintered)	69.0	14.6	1715	1245.0	259.0	0.02[illegible]	[illegible]	[illegible]
51A	MCC 50-19A (sintered)	69.0	14.6	60	1239.5	370.3	0.01[illegible]	1[illegible]	[illegible]
253	MCC 50-19A (sintered)	50.[illegible]	20.4	10	1204.5	100.5	0.01970	1[illegible]	[illegible]
253A	MCC 50-19A (sintered)	[illegible]	20.4	[illegible]	1205.5	3[illegible]	0.06[illegible]	3[illegible]	18.[illegible]
238	MCC 50-20 (sintered)	54.5	18.9	60	1201.8	157.[illegible]	0.00750	[illegible]	[illegible]
238	MCC 50-20 (sintered)	54.5	18.[illegible]	5145	1203.0	283.[illegible]	0.00[illegible]	[illegible]	[illegible]
239	MCC 50-20 (sintered)	86.8	10.1	30	1192.[illegible]	1[illegible].5	0.013[illegible]	[illegible]	5.[illegible]
240	MCC 50-20 (sintered)	109.2	9.9	10	1203.5	1.1[illegible]	0.01105	14[illegible].1	13.[illegible]
242	MCC 50-20 (sintered)	110.0	9.9	60	1197.5	198.5	0.02[illegible]	4[illegible]	[illegible]
242	MCC 50-20 (sintered)	110.0	9.9	120	1199.0	206.5	0.00[illegible]	4[illegible]	[illegible]
242PT	MCC 50-20 (sintered)	110.0	9.9	40	1[illegible].0	1[illegible]	0.01[illegible]	42	1.[illegible]
243	MCC 50-20 (sintered)	101.0	10.[illegible]	10	1201.0	[illegible]	0.00[illegible]	[illegible]	[illegible]
244	MCC 50-20 (sintered)	ND	ND	30	1184.5	100.[illegible]	0.01[illegible]	[illegible]	2.[illegible]
245	MCC 50-20 (sintered)	102.0	10.6	10	1201.5	115.6	0.011[illegible]	56.0	4.[illegible]
245	MCC 50-20 (sintered)	102.0	10.6	840	1210.5	278.5	0.01[illegible]	62.1	2.[illegible]
245PT	MCC 50-20 (sintered)	102.0	10.6	10	1201.0	30.[illegible]	0.00[illegible]	155.[illegible]	4.[illegible]
245TT	MCC 50-20 (sintered)	102.0	10.6	1800	1211.0	73.[illegible]	[illegible]080	65.[illegible]	5.20
246	MCC 50-20 (sintered)	[illegible]	18.0	10	1202.5	186.0	0.01[illegible]	93.	9.[illegible]
258	MCC 50-20	[illegible]	15.5	100	1201.0	[illegible]	0.0[illegible]	[illegible]	[illegible]
259	MCC 50-20	[illegible]	15.5	5280	1198.0	[illegible]	0.01[illegible]	[illegible]	[illegible]
260	MCC 50-20	[illegible]	14.[illegible]	60	1201.5	10[illegible]	0.01[illegible]	11[illegible]	1
260	MCC 50-20	[illegible]	14.[illegible]	3010	1204.0	251.[illegible]	0.01[illegible]	[illegible]	[illegible]
261	MCC 50-20	[illegible]	[illegible]	10	1196.5	23[illegible]	0.0[illegible]	11[illegible]	[illegible]
262	MCC 50-20	[illegible]	[illegible]	3900	1203.5	280.[illegible]	0.01[illegible]	[illegible]	[illegible]
263	MCC 50-20	[illegible]	[illegible]	[illegible]	1205.0	23[illegible]	0.01[illegible]	[illegible]	[illegible]
263	MCC 50-20	40.0	[illegible]	3300	1208.5	211.[illegible]	0.01[illegible]	[illegible]	[illegible]
264	MCC 50-20	31.5	31.[illegible]	10	1200.[illegible]	[illegible]	0.01[illegible]	[illegible]	[illegible]
264	MCC 50-20	31.5	31.[illegible]	900	1[illegible].5	[illegible]	0.01[illegible]	1[illegible]	[illegible]
264 (Retest)	MCC 50-20	31.5	31.[illegible]	3[illegible]	1197.0	[illegible]	0.01[illegible]	109.5	[illegible]
250	MCC 50-19 (sintered)	19.0	28.1	10	1201.0	74.[illegible]	0.00[illegible]	[illegible]	1[illegible]
250	MCC 50-19 (sintered)	19.0	[illegible]	[illegible]	1202.0	[illegible]	[illegible]	[illegible]	[illegible]
252	MCC 50-19 (sintered)	19.0	28.1	[illegible]	1204.5	134.[illegible]	[illegible]	[illegible]	[illegible]

ND = not determined.
PT = postspray thermal treatment.
Specimens 253A and 253A contained radiators and Ti[illegible] emissive coating.
Specimen 247A was sectioned into 4 wedge-shaped [illegible] segments, connected in parallel by clip-type radiator.
Specimen 253A-PT contained no radiator but [illegible] emissive coating.

Table 15

THERMOELECTRIC PROPERTIES OF SPRAYED MCC (n) SYSTEMS

Spec.	Powder Type	Avg Coating Thickness, mil	Area/ Length, in	Test Time, min.	T_h, °C	ΔT, °C	P_o, Mw	Seebeck μ volts/°C	Adj. Max. Watts/ ft. TE Material
294	MCC 60-2	ND	ND	30	1202.5	33.3	0.00926	76.4	30.4
302PT	MCC 60-2	ND	ND	60	1199.0	128.2	0.02933	195.7	(1)
302PT	MCC 60-2	ND	ND	120	1195.0	126.5	0.03123	198.3	(1)
272-1	MCC 60-2-65	ND	ND	75	1197.0	70.0	0.00769	71.2	32.40
274	MCC 60-2-65	ND	ND	30	1201.5	7.5	0.00733	47.5	8.10
274 (Retest)	MCC 60-2-65	ND	ND	10	1196.0	31.5	0.01000	32.0	2.70
274 (Retest)	MCC 60-2-65	ND	ND	60	1200.5	34.0	0.00500	30.2	4.90
295	MCC 60-2-65	27.0	36.8	10	1200.0	8.8	0.01131	381.0	108.00
295	MCC 60-2-65	27.0	36.8	1060	1198.5	26.0	0.01259	198.8	50.40
338	MCC 60-3	ND	ND	60	1201.0	59.0	0.00600	50.3	4.32
338	MCC 60-3	ND	ND	240	1202.0	62.5	0.00611	55.8	4.20
338PT	MCC 60-3	ND	ND	60	1201.0	173.8	0.03596	114.1	3.69
338PT	MCC 60-3	ND	ND	990	1198.5	163.0	0.04136	114.8	3.24
281PT	MCC 60-6	11.5	95.6	90	1205.2	57.2	0.00813	26.4	11.37
281PT	MCC 60-6	11.5	95.6	150	1200.0	56.0	0.01009	25.3	8.33
286	MCC 60-7	25.3	38.6	10	1200.0	15.5	0.00714	105.2	62.70
286	MCC 60-7	25.3	38.6	120	1199.0	15.5	0.00858	96.0	62.70
293	MCC 60-7	74.0	14.3	60	1196.5	56.0	0.00389	138.5	20.70
293	MCC 60-7	74.0	14.3	1315	1199.0	63.5	0.01486	211.0	32.20
298PT	MCC 60-8	5.5	176.0	60	1200.5	50.0	0.00750	15.0	9.40
298PT	MCC 60-8	5.5	176.0	180	1198.5	48.5	0.01000	5.7	2.36

ND = not determined
PT = postspray thermal treatment
(1) = coating weight not determined; actual maximum power at 60 and 120 min. was 5.4 and 4.8 x 10^{-3} watts.

MCC 50: Coatings produced from prereacted elements plus dopants were readily deposited as dense coatings, and exhibited some improvement in actual power output and stability with time, when compared to coatings prepared by spraying unreacted or partially reacted mixtures of appropriate components. To improve thermoelectric properties, the most suitable condition for prereacting elements and dopants in this system should also be more precisely determined. Further improvement in power output and more stability in thermoelectric characteristics during prolonged performance appear possible with appropriate post-spray thermal treatment of particular, prereacted powders.

MCC 60: The most satisfactory coatings of this material were apparently produced late in the program using a completely prereacted powder. Most early studies utilized an elemental mixture or a partially reacted powder in very fine particle size, but essentially all of these products appeared to be inferior. However, the use of controlled high-temperature post-spray treatment, with additional study, could convert MCC 60 coatings, readily prepared from mechanical mixtures of elements and dopants, into physically and chemically stable thermoelectric coatings of satisfactory power output. The alternate route of preparing acceptable MCC 60 coatings, through deposition of completely reacted feed powders, will also require further effort to define the most suitable reaction conditions for converting a mixture of elemental components plus dopants into a useful spray powder.

In general, evaluation data obtained to date indicate that sprayed thermoelements with satisfactory properties can be produced by plasma-spraying techniques. Basic spraying procedures have been defined for producing physically satisfactory coatings of MCC 40, MCC 50 and MCC 60. However, it appears that thermoelectric properties could be considerably improved through use of properly reacted spray powders, use of appropriate post-spray thermal treatment, control of area-to-length characteristics, employment of more efficient overall thermoelement design, and other related considerations.

The thermal shock resistance of sprayed thermoelements was observed during routine heating of specimens to appropriate hot-junction temperatures for screening and during cooling of

tested specimens to room temperature. In general, coatings remained intact and bonded when subjected to the typical cycle shown in Table 16 for heating and cooling, although several specimens did experience cracking and bond failure.
MCC 50 and MCC 60 coatings were heated to 1200°C hot-junction temperature as shown; however, p- and n-type MCC 40 specimens were generally heated to only 900°C for testing, although heating and cooling rates were as shown below:

Table 16

TYPICAL THERMAL CYCLES USED DURING SCREENING OF SPRAYED THERMOELECTRIC COATINGS

Typical Heating Cycle To T_h = 1200°C		Typical Cooling Cycle from T_h = 1200°C.	
Elapsed Time, Min.	Temp., °C	Elapsed Time, Min.	Temp., °C
3	70	3	1190
6	200	6	1060
9	450	9	925
12	620	12	750
15	750	15	620
18	925	18	450
21	1060	21	200
24	1190	24	70
27	1200	27	room temp.

As noted in Tables 12 through 15, gradual changes in thermoelectric properties of some sprayed specimens were observed as a function of test time. In an effort to stabilize the chemical composition and crystalline structure of the sprayed material and to optimize thermoelectric properties, selected coatings were subjected to a high-temperature, post-spray treatment in a controlled environment. A globar-heated furnace containing mullite tubes was used for treating some coated specimens to 1400°C in a helium atmosphere. Higher temperatures were achieved by low-frequency induction heating of the coated graphite substrate in a slightly reducing atmosphere. This was accomplished by mounting the coated specimen on a graphite stud and inserting the latter into a graphite cylinder. After central positioning of the coated specimen, the graphite cylinder was tightly closed at both ends and the residual air inside of the enclosure provided a slightly reducing (CO) atmosphere around the specimen during high-temperature exposure.

The effect of high-temperature post-spray treatment on physical and thermoelectric properties could not be conclusively determined owing to the large number of feed powder compositions and operating conditions employed. Results obtained in this study are presented in Table 17. Although some materials were found to be favorably affected while others were apparently adversely affected by exposure to a particular thermal treatment, the overall findings did appear to be worthy of further study. In view of progress made in defining basi feed powder compositions and spray conditions during this contract period, more intensive investigation of a limited number of sprayed thermoelements appears possible in future work, and such additional studies should provide sufficient information to conclusively determine the value of post-spray thermal treatment on thermoelectric properties of sprayed thermoelements.

Although the significant effect of area/length ratio on thermoelectric properties of thermoelements was realized, this ratio was not normally controlled during routine preparation of sprayed coatings. For cylindrical coatings, the area term employed in this ratio corresponds to the average circumferential coating area through which the temperature gradient exists, while the length term corresponds to the sprayed coating thickness. On this basis, area/length ratios were calculated for most coated specimens prepared and, in general, these ratios were considered to be much larger than required for obtaining maximum thermoelectric output. Calculated area-to-length ratios, corresponding to specimens screened during this program, were tabulated earlier in Tables 12 through 15 together with thermoelectric data from screening tests.

In a brief study regarding the control of area-to-length ratio, an abrasive cutting technique was used to section the coating of a previously screened MCC 50 specimen onto four wedge-shaped coating segments and the effect of area-to-length ratio on thermoelectric properties was experimentally observed. The coating segments remained bonded to the graphite cylindrical substrate for parallel connection at the hot junction and a disc-type radiator, flame-sprayed to the surface of all coating segments, formed parallel cold-end connections. The effect of area-to-length ratio for this particular specimen can be observed in Table 18.

Segmented p- and n-type cylindrical thermoelements were produced by spray-bonding concentric layers of thermoelectric materials to outgassed graphite cylinders. Initially, a coating of high-temperature material was applied to the graphite substrate. Molybdenum or a mechanical mixture of 50 wt.% high-temperature material-50 wt.% low-temperature material was then sprayed over the initial coating. A coating of low-temperature material was added over the intermediate deposit.

Table

EFFECT OF POSTSPRAY TREATMENT ON THERMOELECTRIC PROPERTIES OF SPRAYED THERM ELEMENTS

Spec.	Powder Type	Postspray Treatment	Effect (Observation)
308PT	MCC 40-9P	1000°C, 60 min., He	Poor thermoelectric properties when compared to untreated Spec. 300 prepared under essentially same conditions.
30APT	MCC 40-9P	1200°C, 30 min., He	Poor thermoelectric properties when compared to untreated Spec. 300 prepared under similar spray conditions.
317PT	MCC 40-9P (sintered)	1200°C, 30 min., He	Significant improvement in adjusted max. power output/lb TE material when compared to untreated Spec. 320 prepared under essentially same conditions.
321PT	MCC 40-AH	1200°C, 30 min., He	Effect uncertain. TE properties of coating not measured prior to postspray thermal treatment. Comparable untreated specimen not available.
312PT	MCC 40-AH (sintered)	1200°C, 30 min., He	Decrease in thermoelectric properties when compared to Spec. 310 prepared under approximately same conditions.
313PT	MCC 40-AH (sintered)	1400°C, 60 min., He + 1450°C, 10 min., He	Coating cracked, spalled.
25APT	MCC 50-15	2050°C, 8 min., CO	Considerable increase in adjusted maximum power output/lb TE material.
233PT	MCC 50-18-1	2000°C, 8 min., CO	Increase in secondary phase observed in microstructure. Hardness increased 1142 to 2090 (Knoop Scale, 100 gram load).
235PT	MCC 50-18-1	2050°C, 8 min., CO	Coating separated intact from graphite substrate.
236PT	MCC 50-18-1	2050°C, 8 min., CO	Coating separated intact from graphite substrate.
247A-PT	MCC 50-19A (sintered)	2050°C, 8 min., CO	Apparently slight degradation in overall TE properties.
242PT	MCC 50-20 (sintered)	2050°C, 8 min., CO	Apparent decrease in power output.
245PT	MCC 50-20	2050°C, 8 min., CO	Considerable increase in adjusted max. power output/lb TE material.
259PT	MCC 50-21	2050°C, 8 min., CO	Coating cracked and separated from graphite substrate.
340PT	MCC 60-2	1400°C, 60 min., A	Effect on TE properties not certain since coating weight not initially determined. Color change observed.
337PT	MCC 60-3	1450°C, 30 min., A	Thick coating cracked and separated from graphite substrate.
338PT	MCC 60-3	1400°C, 30 min., A	Considerable increase in actual max. power / lb. TE material. Fine longitudinal cracks observed.
280 PT	MCC 60-5	2000°C, 10 min., CO	Blisters observed on surface. Coating separated from graphite during effort to remove specimen from sample holder.
281PT	MCC 60-6	1400°C, 30 min., then 2050°C, 10 min., CO	Poor thermoelectric properties of treated specimen. Untreated coating not screened.
297PT	MCC 60-8	2000°C, 10 min., CO	Hard outer shell, soft inner core in coating. Coating crushed during effort to remove specimen from sample holder.
298PT	MCC 60-8	1400°C, 60 min., A+ 2040°C, 10 min., CO	Effect inconclusive. Comparable specimen with untreated coating not available. Definite color change observed.
295PT	MCC 60-8	2000°C, 10 min., CO	Hard, thin outer shell, soft inner core in coating. TE properties could not be measured.

Table 18

EFFECT OF AREA/LENGTH RATIO ON THERMOELECTRIC PROPERTIES OF SPRAYED MCC 50 THERMOELEMENT

Spec.	Powder Type	Area/ Length, in.	T_h, °C	ΔT, °C	Test Time, min.	R, ohm	Actual Max. Watts/ lb, TE Material
247	MCC 50-19A (sintered)	25.2	1205.0	95.5	60	0.00561	1.60
247A	"	6.3	1198.0	229.0	420	0.00560	2.55

Finally, a molybdenum outer coating was applied, as well as current and voltage leads, copper (14 mil) radiators, and cold-junction thermocouples, using flame-sprayed molybdenum. Emissive coating TEC-1 was applied over the radiators and the exposed molybdenum surfaces, and the specimen was screened at T_h of about 1200°C to determine S, R, ΔT and thermal shock resistance. Thermoelectric properties of sprayed segmented thermoelements, screened during this program, are presented in Table 19. Properties measured at the beginning and end of sustained testing are summarized. Continuous performance characteristics for one p-type and one n-type segmented thermoelement are presented in Tables 20 and 21, respectively. Small variations in thermoelectric properties of specimens, as noted in continuous performance data, may possibly be attributed to marginal precision of millivolt recorders used for overnight and weekend data collection, compared to quality potentiometers utilized during normal working hours. By control of area-to-length ratio and use of more stable and properly reacted feed powders, production of considerably improved segmented thermoelements, by spraying techniques, should be possible.

Heating elements used during initial, continuous testing of the p-type segmented thermoelement (Spec. 252B) were of the same type as employed in screening thin individual coatings and were found to be unsatisfactory for maintaining the hot-junction temperature at 1200°C during the entire test period. As noted in Table 20, the initial heating element failed after 28 hours and a second heater failed after 80 hours of testing, rapidly cooling the specimen each time from about 1200°C to room temperature. Thermal shocks resulting from these failures were approximately 130°C/min. during the first 5 minutes and approximately 55°C/min. during the next 5-minute period. To subject the segmented thermoelement to a third thermal shock test, the heating element power was abruptly terminated at the end of the nomina

Table IV

THERMOELECTRIC PROPERTIES OF SPRAYED SEGMENTED THERMOELEMENTS

Spec.	Polarity	Hot-End Material	Intermediate Material (IM)	Cold-End Material	Avg. Coating Thickness Hot-End, mil	IM, mil	Cold-End, mil	Test Time, Min.	T_h, °C	ΔT, °C	R, ohm	E_{oc}, mv	Seebeck, watts/°C	Adj. Max Watts/lb TE Mat'l	Remarks
2509	p	HCC 50-19A (sintered)	IN-6	HCC 40-9P (sintered)	78	15	62	10	1200.0	468.8	0.00683	68.35	137.3	9.41	6 radiators, 1 7/8"x1/2"x .014"
2509	p	HCC 50-19A (sintered)	IN-6	HCC 40-9P (sintered)	78	15	62	60	1198.5	452.4	0.00647	64.86	143.2	9.44	
2509	p	HCC 50-19A (sintered)	IN-6	HCC 40-9P (sintered)	78	15	62	6100	1201.0	413.0	0.00731	63.50	152.6	7.29	
358B	p	HCC 50-8J (sintered)	Mo	HCC 40-11P (sintered)	41	1	69	10	1200.0	433.0	0.00233	39.80	91.9	1.43	6 radiators, 1 7/8"x1/2"x .014"
358B	p	HCC 50-8J (sintered)	Mo	HCC 40-11P (sintered)	41	1	69	60	1200.0	445.2	0.02187	41.26	92.7	1.45	
358B	p	HCC 50-8J	Mo	HCC 40-11P	41	1	69	5540	1200.5	524.9	0.00411	42.36	80.7	1.63	
339C	n	HCC 60-3	IN-8	HCC 40-6N (sintered)	90	31	150	115	1204.5	321.3	0.00500	15.45	48.0	1.64	8 radiators, 1 7/8"x1/2"x .014"
339C	n	HCC 60-3	IN-8	HCC 40-6N (sintered)	90	31	150	380	1201.0	342.2	0.00594	14.79	43.2	1.12	
339C	n	HCC 60-3	IN-8	HCC 40-6N (sintered)	90	31	150	4510	1160.0	290.0	0.00644	18.00	61.0	2.05	
345C	n	HCC 60-15 (sintered)	Mo	HCC 40-8N sintered)	36	2	30	10	1198.0	309.0	0.00507	20.31	67.7	3.39	6 radiators, 1 7/8"x1/2"x .014"
345C	n	HCC 60-15 (sintered)	Mo	HCC 40-8N (sintered)	36	2	30	1040	1134.0	339.0	0.00720	20.93	94.0	11.34	
345C	n	HCC 60-15 (sintered)	Mo	HCC 40-8N (sintered)	36	2	30	6680	1196.5	346.7	0.00724	31.84	91.8	10.80	

Table 2[illegible]

THERMOELEMENT PROPERTIES OF SEGMENTED p-TYPE THERMOELEMENT (SPECIMEN 2[illegible])

Elapsed Test Time, hr.	Hot-Junction Temperature, °C	Actual ΔT, °C	R, ohm	Seebeck μvolts/°C	Maximum Power, watts	Adj. Max. watts/ TE Material
0	1200.0	468.8	0.00688	137.3	0.1503	8.4[illegible]
[illegible]	1198.5	452.[illegible]	0.00657	143.2	0.1537	9.44
2	1199.5	448.2	0.00371	143.2	0.2770	16.94
6	1198.0	436.7	0.0048[illegible]	148.8	0.218[illegible]	14.[illegible]
14	1177.5	421.0	0.0065[illegible]	154.4	0.161[illegible]	11.23
18	1189.3	425.5	0.0067[illegible]	151.0	0.1537	10.43
20	1188.0	426.7	[illegible]	152.3	0.1290	8.7[illegible]
26	1176.5	416.5	0.0066[illegible]	152.2	0.1455	10.4[illegible]
27	1170.0	411.0	0.0072[illegible]	154.4	0.1367	10.17
27.58 (heater failure)	1177.5	413.7	0.0044[illegible]	157.2	0.2150	1[illegible].50
29	1207.5	424.5	0.0062[illegible]	151.6	0.1643	11.32
35	1203.0	417.5	0.00768	1[illegible]3.8	0.134[illegible]	9.3[illegible]
4[illegible]	1211.0	422.[illegible]	0.0078[illegible]	152.2	[illegible]	9.2[illegible]
47	1211.0	418.2	0.0067[illegible]	153.0	0.150[illegible]	10.67
52	1217.0	421.0	0.00725	148.[illegible]	0.1350	9.44
58	[illegible].5	419.5	0.00610	152.1	0.1669	11.7[illegible]
64	1224.0	425.2	0.00509	15[illegible].3	0.20[illegible]	13.[illegible]
70	1224.0	421.5	0.00679	151.[illegible]	0.1507	10.57
73	1223.5	419.0	0.00722	149.2	0.1353	9.45
76	1211.0	414.5	0.006[illegible]	152.[illegible]	0.1462	10.45
80.08 (heater fai[illegible])	1211.0	412.2	0.00848	154.0	0.1135	8.64
82	1200.0	420.[illegible]	0.00952	152.6	0.1020	7.55
88	1200.5	416.2	0.00712	152.7	0.1417	10.13
94	1200.5	416.2	0.01070	154.3	0.0962	6.89
98.5	1196.0	410.2	0.00928	153.0	0.1064	7.81
[illegible].5 (abrupt heater shutdown)	1201.0	413.0	0.00991	152.[illegible]	0.1002	7.28

Table 21

THERMOELECTRIC PROPERTIES OF SEGMENTED n-TYPE THERMOELEMENT (SPECIMEN 345C)

Elapsed Test Time, hr.	Hot-Junction Temperature, °C	Actual ΔT, °C	R, ohm	Seebeck, μvolts/°C	Maximum Power, watts	Max. Watts/lb. TE Material
0	1198.0	300.0	0.00509	67.7	0.0203	8.39
17.3	1184.0	329.0	0.00720	94.0	0.0332	11.34
24.0	1181.0	327.8	0.00659	94.8	0.0368	12.72
40.0	1173.5	323.0	0.00773	97.5	0.0321	11.44
48.5	1196.0	335.0	0.00826	93.2	0.0295	9.76
63.75	1195.0	338.0	0.00655	92.8	0.0375	12.20
70.80	1199.0	341.0	0.00744	91.8	0.0328	10.48
87.05	1197.0	343.5	0.00632	91.8	0.0392	10.53
95.18	1197.5	344.0	0.00674	91.7	0.0368	11.53
111.30	1196.5	346.7	0.00724	91.8	0.0350	10.80

100-hr. test, instead of following the less severe cooling rate generally utilized. During the abrupt heater shutdown, the coated specimen was subjected to a thermal shock cooling rate of about 140°C/min. for the first 5 minutes and 40°C/min. during the next 5 minutes. No apparent physical damage to the coatings or bonds could be attributed to these thermal cycling conditions. No significant change was noted in the appearance of two small radial cracks through the coatings which were earlier observed after post-spray treatment of the specimen and prior to the 100-hr. test. A reinforced, improved heating element was used for the evaluation of the n-type segmented thermoelement (Spec. 345C) and no heater failures were encountered during sustained performance testing of that specimen.

Weight losses, resulting from sublimation at elevated temperatures in vacuum, were determined for several individual and segmented sprayed coatings. These are shown below

Table 22

SUBLIMATION LOSS OF SPRAYED THERMOELEMENTS

Spec.	Coating Type	Avg. Th, °C	Accumulated Test Time, hr.	Increment wt. Loss, g.	Increment wt.Loss, %	Cum. Wt. Loss, %
339C	Segmented n-type, MCC 60-3 + IM-8+ MCC 40-6N (sintered)	1200	1.33	0.0794	0.250	0.25
			5.33	0.0058	0.018	0.27
			20.03	0.0198	0.063	0.33
			75.00	0.0110	0.035	0.37
353A	MCC 40-11P (sintered)	850	1.00	0.0032	0.641	0.04
357	MCC 50-23 (sintered)	1200	37.00	0.0400	0.760	0.76

A p-n couple, consisting of plasma-sprayed segmented thermoelements, was produced and evaluated. Concentric layers of appropriate high- and low-temperature thermoelectric materials were applied to outgassed graphite cylinders (1/2-inch OD, 3/8 inch ID, 5/8-inch long). Each cylindrical thermoelement contained a female thread, and the couple was assembled by screwing a p- and an n-type thermoelement over a threaded, hollow, graphite holder (3/8-inch OD, 3/16-inch ID). A resistance heater was fitted with difficulty inside the 3/16-inch ID graphite holder.

The total length of the p-n couple was 1 1/3 inch. Rectangular copper fins were attached radially to each thermoelement and covered with TEC-1 emissive coating to provide a suitable temperature drop across each element. The thickness of the sprayed MCC 60-intermediate-MCC 40(n) coatings on the n-type thermoelement was about 9/32 inch, and that of the MCC 50-intermediate-MCC 40(p) element was about 9/32 inch. These coatings yielded length-to-area ratios of 0.048 cm^{-1} and 0.068 cm^{-1} for the p- and n-type thermoelements, respectively. At a control temperature of 1200°C, average T_h of 1161°C, and average T_c of 814°C, the output of this couple remained constant at 0.1225 watt(e) for 819 hours in a vacuum of 10^{-5} to 10^{-6} torr. A gradual decline in power output was then observed, as shown in Table 23, to a value of 0.0662 watt(e) after 1030 hours, at which time the test was terminated. Photographs of both thermoelements, after completion of sustained testing, are shown in Figure 35. Thermal cycling tests, performed upon completion of sustained performance evaluation, appeared to have no significant detrimental effect on overall p-n couple performance. Reasons for degradation in power output with time are not yet certain. Use of incompletely reacted spray powders and production of unstable coating compositions, or diffusion of individual coating components may be responsible for this behavior. While microstructure of each thermoelement (shown later in Figure 40) shows distinct layers of high-temperature, intermediate, and low-temperature materials, definite conclusions regarding diffusion of various components do not seem possible at this time.

The microstructure of several sprayed, individual and segmented, coatings was examined using an optical metallograph in an effort to correlate structural properties with physical and thermoelectric characteristics. Plasma-sprayed specimens were arbitrarily selected for microstructure study and do not necessarily represent typical structures of coatings prepared under optimized spraying conditions. In general, "as sprayed" coatings demonstrated a distinct laminar effect, due to the spraying process. Specimens 208C and 241, shown unetched in Figure 36, were produced from feed powders containing prereacted elemental components and additives. Specimen 210B was prepared from a feed powder consisting of mechanically mixed elemental components plus additives. From a comparison of these microstructures with that of Spec. TE200, produced by hot-pressing, and also shown in Figure 36, the following observations were made

a. The sprayed coatings contain more undissolved dispersed particles than does hot-pressed material.

DATA PERTAINED PERFORMANCE TEST OF A [illegible]
[illegible] MADE BY PLASMA DYNAMICS

Cycle No.	Control T_{hi} °C	Avg. T_{hi} °C	Avg. T_{lo} °C	Avg. ΔT °C	Amps	Volts	Watts	P_{hi} psia	P_{lo} psia	Q Btu/cycle	Net Energy Btu	Cycle Time sec	Net Power Watts
Vacuum leak - shut down for repair													
834	1200	1201	853	348	0.244	73.01	[illegible]	[illegible]	[illegible]	[illegible]	[illegible]	[illegible]	[illegible]
908	1202	1191	831	360	0.[illegible]	72.70	[illegible]	[illegible]	[illegible]	[illegible]	[illegible]	[illegible]	[illegible]
966	1204	1197	851	346	0.244	72.70	[illegible]	[illegible]	[illegible]	[illegible]	[illegible]	[illegible]	[illegible]
996	1203	1190	844	321	0.238	74.43	[illegible]	[illegible]	[illegible]	[illegible]	[illegible]	[illegible]	[illegible]
[illegible]	1200	1197	841	286	0.244	72.70	[illegible]	[illegible]	[illegible]	[illegible]	[illegible]	[illegible]	[illegible]
[illegible]	1200	1200	858	302	0.270	[illegible]	72.65	[illegible]	[illegible]	[illegible]	[illegible]	[illegible]	[illegible]
1059	1201	1194	903	299	0.272	[illegible]	[illegible]	[illegible]	[illegible]	[illegible]	[illegible]	[illegible]	[illegible]
1082	1201	1178	873	305	0.258	64.91	68.73	[illegible]	[illegible]	[illegible]	[illegible]	[illegible]	[illegible]
1010	1200	1171	870	347	0.240	61.30	64.84	[illegible]	[illegible]	[illegible]	[illegible]	[illegible]	[illegible]
1033	1200	1165	873	293	0.244	61.25	[illegible]	[illegible]	[illegible]	[illegible]	[illegible]	[illegible]	[illegible]
Thermal cycling tests - 24 cycles/day in which cycling rates of 250-250°C/min. were reduced on 1 cycle for a temperature drop per cycle of 25°C													
1054 (54 cycles)	1200	1193	873	305	[illegible]	61.30	69.[illegible]	[illegible]	[illegible]	14.89	[illegible]	225	[illegible]
1078 (78 cycles)	1200	1197	864	293	[illegible]	61.30	[illegible]	[illegible]	9.[illegible]	15.[illegible]	[illegible]	232	
1102 (102 cycles)	1200	1189	861	287	[illegible]	[illegible]	63.44	[illegible]	[illegible]	[illegible]	[illegible]	256	[illegible]
1126 (126 cycles)	1201	1171	870	300	0.240	61.40	[illegible]	[illegible]	8.811	[illegible]	[illegible]	255	[illegible]
1150 (150 cycles)	1200	1167	869	297	0.244	60.23	64.16	[illegible]	[illegible]	[illegible]	[illegible]	243	[illegible]
1174 (174 cycles)	1200	1170	877	293	0.242	59.85	[illegible]	[illegible]	[illegible]	[illegible]	[illegible]	238	[illegible]
1198 (198 cycles)	1200	1169	[illegible]	298	0.240	59.22	[illegible]	[illegible]	[illegible]	[illegible]	[illegible]	[illegible]	[illegible]
1222 (222 cycles)	1200	1193	863	290	[illegible]	[illegible]	65.16	[illegible]	[illegible]	[illegible]	[illegible]	224	[illegible]
1246 (246cycles)	1200	1171	870	347	0.240	61.30	64.89	[illegible]	8.811	[illegible]	[illegible]	[illegible]	[illegible]
[illegible] (270 cycles)	1201	1140	831	309	[illegible]	[illegible]	[illegible]	[illegible]	[illegible]	[illegible]	[illegible]	[illegible]	[illegible]
[illegible] (294 cycles)	1200	1168	[illegible]	287	[illegible]	[illegible]	[illegible]	[illegible]	[illegible]	[illegible]	[illegible]	[illegible]	[illegible]

DATA FROM ISOTHERMAL PLANE RUPTURE TEST ON A GRAIN STEER P-N C UPIK MADE BY FLAME PLASMA TECHNIQUE

Duration of Irradiation	Inter T D_{T_1} °C	Surf. D_{T_2} °C	Avg. D_T °C	Avg. ΔT °C	α Amp.	λ_{max} eV	E_{max} eV	E_{max} Max	E_{max} Im	E_{max} Ave	Max. E_{max} Watt	α^2	Life
95	1203	1161	814	347	0.360	78.15	84.37	4.478	0.644	14.176	0.1225	240	
115	1203	1161	814	346	0.360	78.15	84.37	4.478	0.644	14.176	0.1225	240	
135	1203	1161	814	346	0.360	78.15	84.37	4.478	0.644	14.176	0.1225	240	
154	1201	1161	814	346	0.360	78.14	84.37	4.480	0.643	14.176	0.1225	240	
Heater failure. Couple cooled to room temperature and a new heater installed.													
159	1203	1162	815	347	0.368	78.20	84.40	4.474	0.643	14.175	0.1226	240	
183	1203	1161	814	347	0.368	78.19	84.39	4.479	0.643	14.176	0.1225	240	
180	1200	1160	814	346	0.367	78.14	84.37	4.480	0.643	14.178	0.1225	240	
Heater failure. Couple cooled to room temperature and a new heater installed.													
207	1203	1161	814	347	0.368	78.19	84.39	4.479	0.643	14.176	0.1225	240	
231	1203	1161	814	347	0.368	78.19	84.39	4.479	0.643	14.176	0.1225	240	
257	1203	1161	814	346	0.368	78.19	84.39	4.479	0.644	14.176	0.1225	240	
280	1203	1162	815	347	0.368	78.19	84.40	4.474	0.643	14.175	0.1225	240	
304	1203	1161	814	346	0.368	78.19	84.39	4.479	0.644	14.176	0.1225	240	
327	1201	1161	814	347	0.367	78.15	84.37	4.477	0.643	14.175	0.1224	240	
Heater failure. Couple cooled to room temperature and a new heater installed.													
347	1203	1162	815	347	0.368	78.19	84.40	4.474	0.643	14.174	0.1225	240	
374	1201	1160	814	346	0.367	78.16	84.37	4.479	0.644	14.176	0.1224	240	
400	1201	1161	814	346	0.368	78.19	84.39	4.479	0.643	14.176	225	240	
421	1202	1161	814	346	0.368	78.19	84.39	4.479	0.644	14.176	0.1225	240	
434	1200	1160	814	346	0.366	78.10	84.33	4.488	0.643	14.176	0.1224	240	
448	1201	1160	814	346	0.367	78.14	84.35	4.483	0.644	14.176	0.1224	240	
472	1199	1160	814	346	0.366	78.10	84.33	4.488	0.644	14.176	0.1224	240	
Heater failure. Couple cooled to room temperature and a new heater installed.													
496	1201	1159	814	346	0.364	78.05	84.30	4.313	0.643	14.180	0.1219	240	
520	1204	1162	815	347	0.368	78.19	84.39	4.479	0.643	14.175	0.1226	240	
543	1201	1160	814	346	0.366	78.15	84.37	4.478	0.644	14.176	0.1225	240	
567	1200	1160	814	346	0.366	78.15	84.36	4.478	0.644	14.176	0.1224	240	
591	1203	1162	815	347	0.368	78.18	84.39	4.479	0.643	14.175	0.1225	240	
615	1199	1160	814	346	0.366	78.13	84.35	4.478	0.644	14.176	0.1225	240	
639	1199	1160	814	346	0.366	78.15	84.37	4.478	0.644	14.176	0.1225	240	
Heater failure. Couple cooled to room temperature and a new heater installed.													
650	1200	1161	814	347	0.366	78.15	84.37	4.478	0.644	14.175	0.1225	240	
677	1204	1162	815	347	0.367	78.20	84.40	4.473	0.643	14.173	0.1227	240	
701	1200	1160	814	346	0.365	78.07	84.32	4.487	0.644	14.177	0.1224	240	
725	1204	1162	815	347	0.368	78.19	84.40	4.479	0.643	14.176	0.1225	240	
746	1201	1161	814	347	0.367	78.14	84.36	4.479	0.644	14.176	0.1225	240	
771	1201	1160	814	346	0.366	78.13	84.34	4.487	0.644	14.177	0.1224	240	
795	1201	1161	814	346	0.366	78.15	84.37	4.478	0.644	14.176	0.1225	240	
819	1200	1160	814	346	0.366	78.13	84.37	4.478	0.644	14.176	0.1225	240	

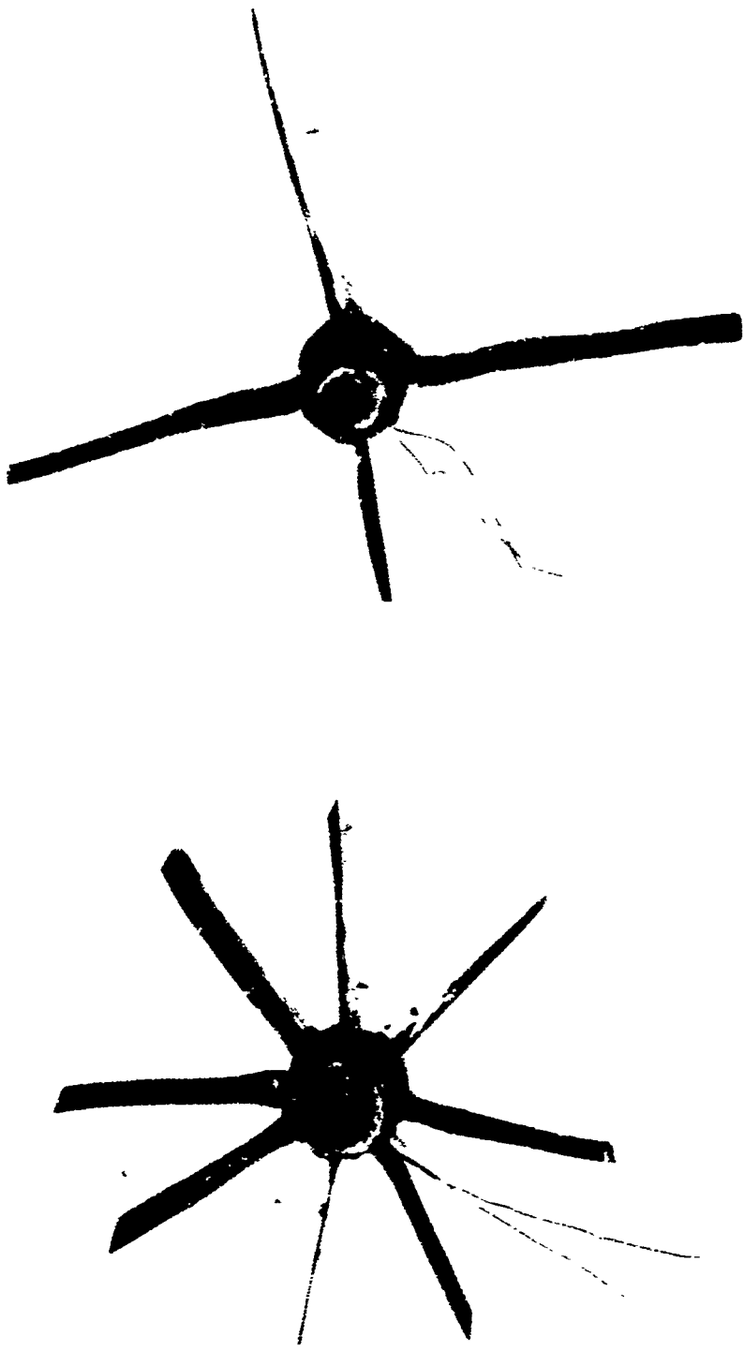

Figure 35. Sprayed Thermoelements from p-n Couple, After Sustained Performance Testing

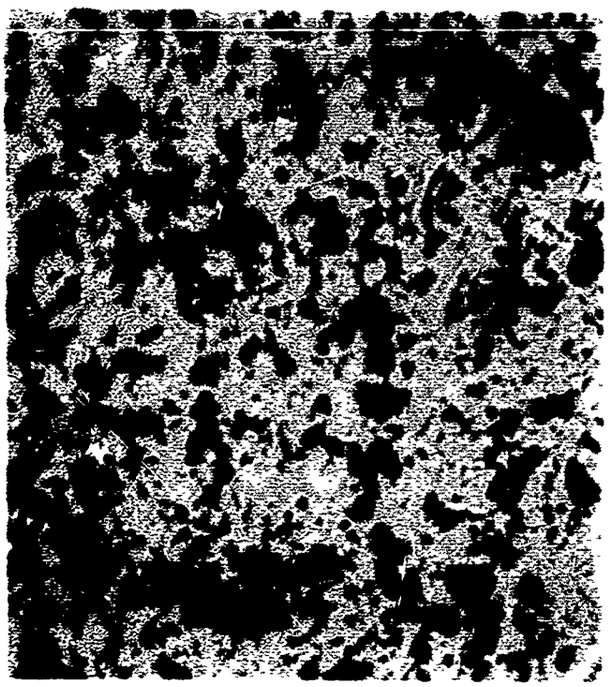

Spec. 208C. Plasma sprayed MCC 50, unetched, 600X

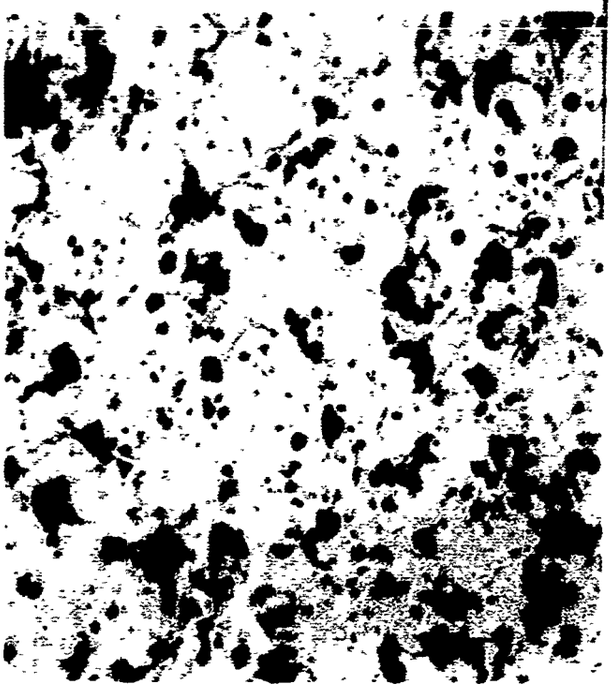

Spec. 241. Plasma sprayed MCC 50, unetched, 600X

Spec. 210B. Plasma sprayed MCC 50, unetched, 600X

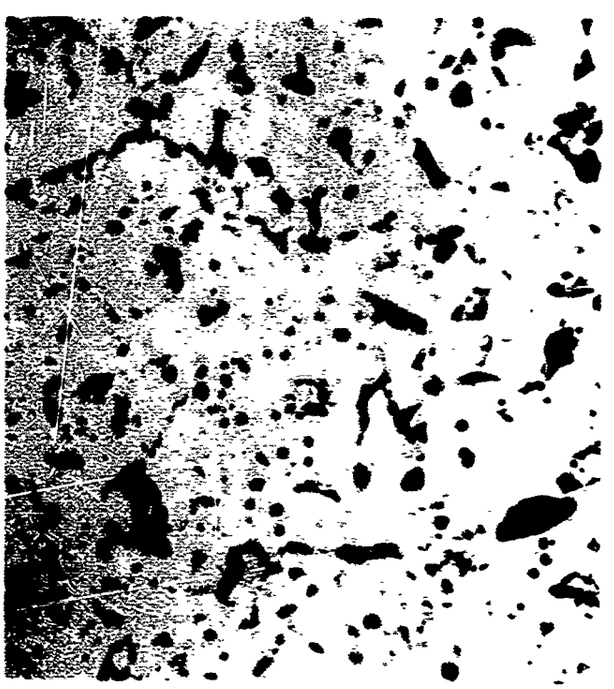

Spec. TE 200. Hot pressed MCC 50, unetched 600X

Figure 36. Microstructure of Plasma-Sprayed and Hot-Pressed Thermoelements

b. The apparent porosity of sprayed coatings appears to be more uniform and of smaller pore size than that of hot-pressed material.

c. The grain size of the MCC 50, under polarized light, appears to be generally very fine in both sprayed and hot-pressed materials.

Only two phases were evident in sprayed coatings produced from prereacted powder, whereas three phases and a distinct uniform laminar effect were observed in the sprayed material prepared from mechanically mixed powders. The microstructures shown in Figure 37 were obtained after etching all specimens electrolytically using 10% HCl. As observed under polarized light earlier with unetched specimens, the grain size in all materials is quite fine, appearing finer in sprayed materials than in typical hot-pressed MCC 50 material. The extremely fine grains present in the sprayed materials may have prevented observation of twinned phases, if present.

The microstructure of a sprayed MCC 50 specimen after exposure to thermal post-spray treatment is compared to that of the original "as sprayed" material in Figure 38, and the effect of high-temperature (2050°C) exposure can be readily observed from the increase in secondary phase of the treated material. Other MCC 50 coatings, after completion of screening tests, are shown in Figure 39. All specimens displayed orientation and some appeared to contain small quantities of white, unidentified material not observed in hot-pressed material. Knoop hardness measurements, using a 100-gram load, indicated that "as sprayed" coatings were generally softer than hot-pressed materials, but the hardness of the former could be increased by high-temperature post-spray treatment. Photomicrographs of screened individual coatings are presented in Figure 39, while corresponding observations are noted in Table 24.

Microstructures of the p- and n-type segmented thermoelements used to form the sprayed p-n couple, described earlier, are shown in Figures 40 and 41. The interfaces between the intermediate material and both the high- and low-temperature adjacent coatings were of special interest to observe whether solid-state diffusion of materials had occurred as a result of high-temperature sustained testing. Although distinct layers of each coating material can be readily observed, positive presence or absence of diffusion in these areas could not be determined owing to the difficulty in interpreting and precisely identifying individual components from each layer.

Spec. [illegible]. Plasma sprayed [illegible], etched. [illegible]X

Spec. 241. Plasma [illegible]. [illegible]. [illegible]X

Spec. [illegible]. Plasma sprayed [illegible], etched. [illegible]X

Spec. [illegible]. [illegible]. [illegible]X

Figure [illegible]. Microstructure of Plasma-Sprayed Metal-Ceramic Thermocouples

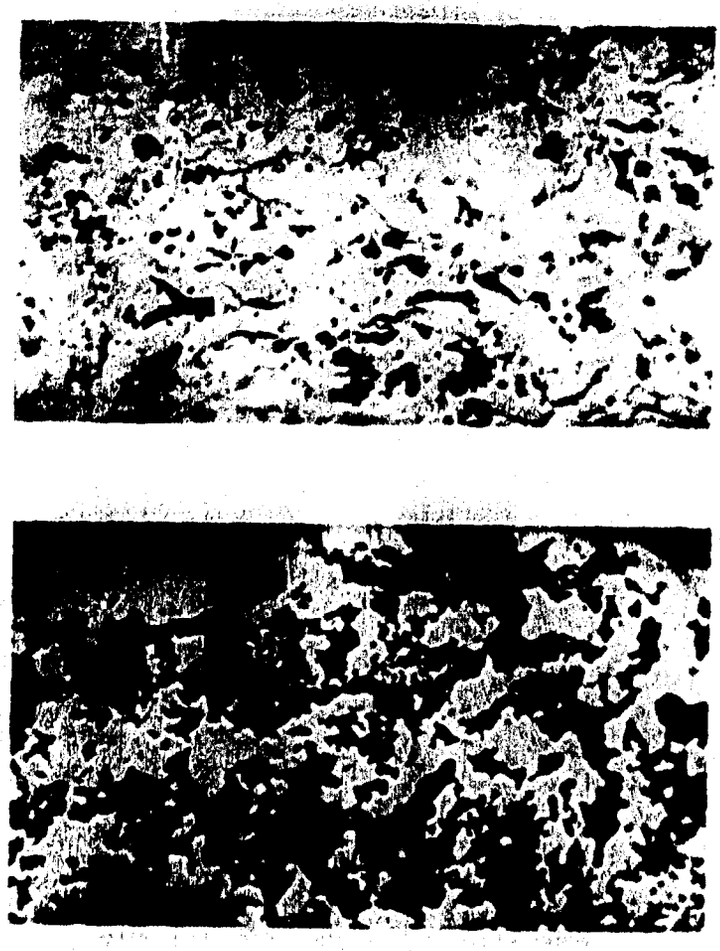

Figure 38. Effect of Post-Spray Thermal Treatment on Microstructure of Sprayed MCC 50

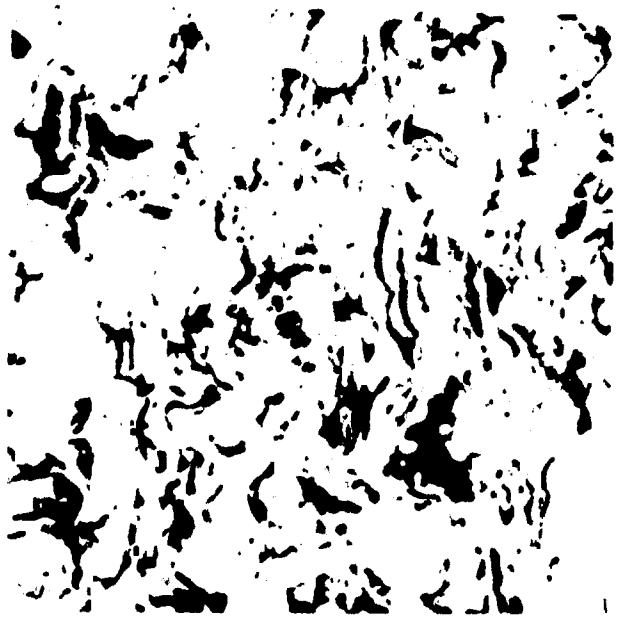

Spec. 261, (C-MCC 50-21) after 60 hr screening at T_h = 1200°C, unetched, 600X

Spec. 244, (C-MCC 50-20) (Sintered), after 1 hr screening at T_h = 1200°C, and 1 hr at 1300° in helium, unetched, 600X

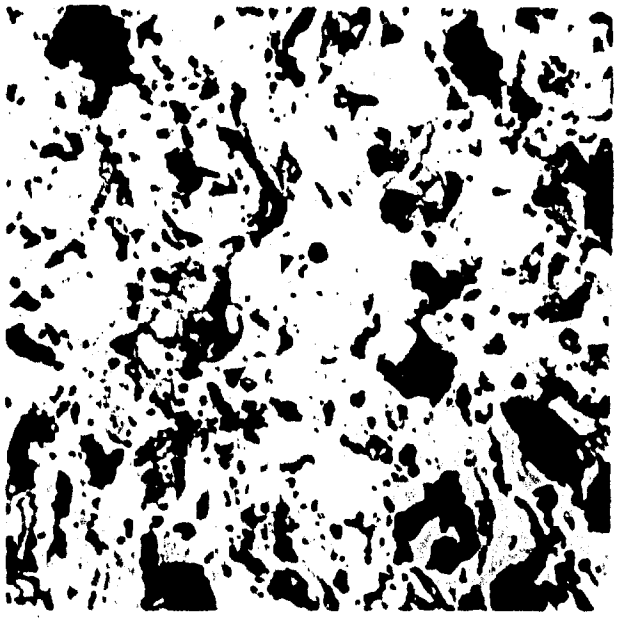

Spec. 234, C-MCC 50-18, after 150 min screening at T_h = 1200°C, and 1 hr heat treatment at 1400°C in helium, unetched, 600X

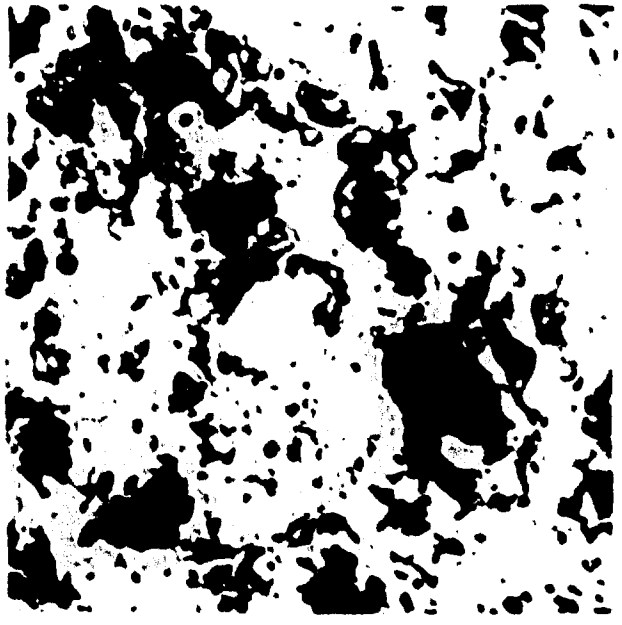

Spec. 251A, (C-MCC 50-19A) (Sintered), after 29 hr screening at T_h = 1200°C, unetched, 600X

Figure 39. Microstructure of Plasma-Sprayed MCC 50 Thermoelements After Screening

Table 24

MICROSTRUCTURE OBSERVATIONS AND HARDNESS READINGS FOR SPRAYED AND HOT-PRESSED MCC 50 AFTER SCREENING

Spec.	Thermoelectric Material	Sample History	Hardness, Knoop Scale (10^3 gram load)	Microstructure Analysis
261	MCC 50-21 (mechanical mixture of elements and dopants)	After 60-hr screening at T_h = 1200°C	2.38	Appears to be mechanical mixture of elements (apparent reason for poor thermoelectric properties observed earlier).
244	MCC 50-20 (sintered) (elements and dopants prereacted at 2000°C)	Screened 1 hr at T_h = 1200°C, then heated to 1300°C in He	1398	Laminar effect apparently reduced by heat treatment.
254	MCC 50-16 (mechanical mixture of partially reacted components and dopants)	Screened 150 min at T_h = 1200°C, then heated to 1400°C in He	2360	Heat treatment apparently caused secondary phase to agglomerate and reduced laminar effect.
251A	MCC 50-19A (sintered) (low grade elements and dopants prereacted at 2000°C)	Screened 24 hrs at T_h = 1200°C	460	Softness apparently due to low grade raw elements and equipment employed.
TE200	Hot-pressed MCC 50 (mechanical mixture of elements and dopants reacted at 2050°C)	Screened 1 hr at T_h = 1200°C	3704	Secondary phase present in much greater amount than in sprayed specimens.

Figure 40. Microstructure of a Sprayed Segmented p-type Thermoelement Used for Sustained Performance Testing

Figure 41. Microstructure of a Sprayed Segmented n-type Thermoelement Used for Sustained Performance Testing

In addition to the production of individual and segmented thermoelements a large portion of the plasma and flame-spraying effort was expended in support of the repair of the 50-watt generator and the fabrication of the improved experimental generator. This effort was used in preparing hot-pressed thermoelements for screening and in producing a variety of sprayed joints and coatings required in the fabrication of both generators.

Hot-pressed thermoelements were prepared for testing by flame-spray bonding copper radiators, after abrasive blasting and degreasing, to the graphite cold-end contacts of each thermoelement.

In repairing the 50-watt generator, thermoelements were inserted into a central graphite ring which served as the hot junction for each tier of the generator. Thermoelements were joined to the graphite rings with flame-sprayed molybdenum to improve electrical and thermal conductivity at the hot junctions. A thin molybdenum undercoating and a final alumina outer coating were applied to the surfaces of the rings, for thermal and electrical insulation, using plasma-spraying techniques. Graphite rings were split into four individual sections, for electrical circuitry, and the sections were later cemented together with electrically insulating (plasma-sprayed) alumina to produce integral composite rings capable of maintaining structural rigidity, proper ring segment spacing, and orientation during generator assembly.

3. Screening and Sustained Performance Testing of Materials

Screening and performance tests were conducted on 350 new elements and 144 used 3/8-inch diameter segmented elements, taken from the advanced experimental model (50-watt) generator for rebuilding. Tests were also conducted on a large number of new 1/4-inch diameter, hot-pressed, multi-segment thermoelements for use in this improved experimental model (15-watt) generator. Test services were also supplied on a continuing basis on arc-plasma sprayed thermoelements with the results presented under that section of this report.

A series of tests were performed on segmented 3/8-inch diameter n-type thermoelements of the type used in the 50-watt generator to investigate the possible mode and temperature of junction failures. These tests were run with the thermoelements in a horizontal position to simulate conditions that were encountered in the sustained performance test of the 50-watt generator. Six thermoelements were exposed to T_h temperature between 1183°C and 1450°C and to T_j temperatures (MCC 60-MCC 40) between 957°C and 1208°C. Each element was held for about 1 hr. at temperatures which ranged from 1180°C to 1450°C in increments of about 100°C, as shown in Table 25 . Four of the six elements reported in Table 25 neither failed nor decreased in power output, despite reaching junction (T_j) temperatures as high as 1190°C for short periods. Specimens TE-268 and TE-269 failed when their T_j temperatures reached 1187-1189°C after exposure of 21.5 hr. to T_j's well above the maximum recommended T_j temperature of 950°C. This data indicates that 3/8-inch diameter thermoelements can withstand severe overheating conditions for short (less than 5 hr.) times without damage. This finding tended to refute the possibility that brief overheating of the generator could have caused its failure, and strongly pointed to other factors - - such as the harmful effect of vibration in combination with excess temperatures on thermoelement life. Vibration, with the exception of launching operations, would probably not be a factor affecting the life of static-type space power systems.

An additional segmented n-type thermoelement was subjected to a 112-hr. duration test in a vertical position. The T_h temperature during this test was about 1230°C with the MCC 60-MCC 40 junction (T_j) temperature at 940-950°C. The data given in Table 26, under the vertical test position heading, showed a definite increase in resistance and a decrease in power output. After termination of the test, it was found that the thermoelement itself was sound but the molybdenum coating of its copper radiator had started to peel off. Thus, loss of bond between the radiator and the element,

Table 25

DATA FROM SHORT TERM TESTS OF SEGMENTED 3/8" DIAMETER n-TYPE THERMOELEMENTS EXPOSED TO MCC 60-MCC 40 JUNCTION TEMPERATURES BETWEEN 957°C AND 1208°C

Element No.	Time at Temperature, Hrs	T_h, °C	Junction* Temperature T_j, °C	T_c, °C	ΔT, °C	I, amps	E_L, mv	P, watts	R, ohms	E_{oc}, mv	Max. P, watts	$E_{oc}/\Delta T$, μv/°C	Pressure, 10⁻⁵ torr
TE-278	1.5	1197	957	518.0	679	3.278	97.6	.320	.0293	180.7	.323	266.1	2.9
	1.0	1297	1071	565.0	752	3.296	113.5	.374	.0239	192.3	.337	255.7	8.2
	1.0	1365	1131	567.0	798	3.460	117.9	.408	.0236	199.6	.422	250.1	10.8
	1.0	1430	1184	582.0	848	3.546	119.6	.424	.0249	207.9	.433	245.1	75.0
TE-94	1.5	1196	1039	534.0	662	2.224	81.0	.180	.0204	126.4	.196	190.9	3.9
	1.0	1302	1116	569.0	733	2.412	88.2	.213	.0193	136.4	.234	186.0	9.2
	1.0	1367	1164	588.0	779	2.596	96.3	.231	.0180	139.4	.270	178.9	10.3
	1.0	1425	1208	605.0	820	2.528	99.9	.253	.0182	146.0	.293	178.0	70.0
TE-255	1.0	1202	1003	507.0	696	3.100	102.9	.318	.0260	183.2	.323	263.5	6.3
	0.8	1249	1044	531.0	728	3.290	107.9	.352	.0248	188.7	.359	259.2	6.0
	0.8	1306	1089	536.0	768	3.394	114.0	.387	.0234	193.5	.400	251.9	10.5
	0.8	1347	1121	551.0	796	3.502	116.9	.403	.0233	196.4	.422	249.2	24.0
TE-319	1.0	1205	1006	471.0	734	2.866	101.4	.291	.0266	177.7	.297	242.0	6.0
	0.8	1250	1045	487.0	765	3.160	100.5	.318	.0258	182.0	.321	237.9	9.0
	0.8	1300	1086	502.0	798	3.252	102.7	.334	.0255	185.9	.339	232.9	11.5
	0.8	1348	1132	519.0	829	3.201	109.5	.351	.0251	190.9	.360	229.1	99.0
TE-268	1.0	1183	1023	579.0	604	2.734	84.0	.234	.0234	163.1	.234	270.0	3.4
	1.0	1299	1109	618.0	681	3.114	93.1	.290	.0265	175.6	.291	257.8	6.2
	1.0	1336	1135	629.0	707	3.060	101.3	.310	.0253	178.9	.316	253.0	50.0
	4.5	1405	1179	652.0	753	3.206	105.2	.337	.0238	181.6	.346	241.1	50.0
	14.0	1187	failed	498.0	689	2.390	63.2	.151	.0413	165.2	.159	236.8	40.0
	2.0	1441	failed	578.0	863	2.210	87.3	.193	.0499	197.6	.196	228.9	70.0
TE-269	1.0	1196	973	537.0	659	1.914	109.2	.209	.0271	161.1	.239	244.4	3.4
	1.0	1324	1069	577.0	747	2.504	111.4	.279	.0253	174.8	.302	234.0	6.6
	1.0	1357	1105	587.0	770	2.601	112.4	.292	.0251	177.9	.315	231.0	50.0
	4.5	1438	1189	611.0	827	1.470	147.0	.216	.0244	182.3	.343	221.1	50.0
	14.0	1189	failed	416.0	773	1.070	57.2	.061	.0678	129.8	.062	167.9	40.0
	2.0	1450	failed	489.0	961	1.776	64.9	.115	.0596	170.9	.121	177.8	70.0

*Junction between the MCC 60-MCC 40 segments.

Table 26

DATA FROM SUSTAINED TEST OF SEGMENTED 3/3" DIAMETER n-TYPE THERMOELEMENT

Vertical Test Position

Hrs Operation	T_{hj}, °C	Junction Temp. T_{cj}, °C	T_{cc}, °C	ΔT, °C	I, amps	E_1, mv	P, watts	R, ohms	E_{oc}, mv	Max. P, watts	$E_{oc}/\Delta T$, uv/°C	Vacuum, 10^{-5} Torr
1	1223	938	453	770	4.40	87.20	.384	.02473	196.0	.388	254.5	.00
18	1231	945	454	777	4.40	87.30	.394	.02527	198.5	.390	255.5	.50
39.5	1230	946	455	775	4.33	86.50	.370	.02619	198.9	.378	256.6	.28
63.0	1231	946	455	776	4.43	81.60	.362	.02650	199.0	.374	256.4	.46
72.0	1230	944	464	776	4.40	82.10	.361	.02661	199.2	.373	256.[illegible]	.25
87.0	1230	946	455	775	4.46	79.40	.354	.02695	199.6	.370	256.[illegible]	.30
112.0	1229	947	456	773	4.45	79.10	.352	.02710	199.7	.368	258.3	.34

Horizontal Test Position

[illegible]	1167	950	404	763	4.30	81.30	.350	.02879	205.1	.365	268.8	4.0
21	1165	949	404	761	4.32	80.00	.346	.02900	205.3	.363	269.7	3.0
37	1173	954	405	768	4.39	81.80	.353	.02888	206.6	.369	269.0	4.0
48	1174	953	403	771	4.[illegible]	83.10	.352	.02919	206.6	.366	267.9	1.05
65	1176	952	404	772	4.26	81.20	.346	.02946	206.7	.363	267.7	.68
88	1177	950	403	774	4.21	82.60	.348	.02959	207.2	.363	267.7	.34
114	1187	947	404	783	4.19	84.40	.354	.02959	208.4	.367	266.1	.60
128	1185	946	404	781	4.[illegible]	82.10	.350	.02976	208.9	.367	267.4	.52
152	1184	944	402	781	4.17	83.70	.349	.03004	209.0	.363	267.6	.32
177	1184	939	402	782	3.91	91.50	.358	.03053	210.9	.364	269.6	.40
200	1184	933	403	781	4.48	75.22	.332	.03019	208.7	.361	267.2	.40
224	1185	928	403	782	4.47	[illegible].60	.329	.03020	208.6	.361	266.7	.48
256	1184	923	403	781	4.35	76.20	.331	.03043	208.6	.357	267.0	.30
281	1182	918	401	781	4.66	85.05	.345	.03062	209.4	.358	268.1	.30
296	1183	915	402	781	3.92	89.20	.350	.03066	209.4	.357	268.1	.30
320	1182	914	401	781	3.94	88.40	.348	.03066	209.2	.356	267.8	.28

at the copper/molybdenum interface, caused the change in thermoelement properties. The cause of separation was found to have been that the wrong size sandblasting grit was used in preparing the copper substrate. The radiator was replaced, so that the thermoelement could be subjected to further sustained testing in a horizontal position. Initial data of the repaired thermoelement shows that its power output was as high as noted in the first test, thus confirming that the decrease in power was due to loss of electrical bond between the radiator and the thermoelement.

The thermoelement was removed from the apparatus used for testing it in a vertical position and installed in new apparatus that permitted its testing in a horizontal position. In making the transition from the vertical to the horizontal test apparatus, more thermal insulation was placed around the thermoelement than had been used for its tests in the vertical position. As shown by the data in the second, or horizontal test position, section of Table 26, a T_1 of about 950°C was reached with the T_h of the thermoelement at about 1170°C. The somewhat lower power output recorded for the thermoelement in the horizontal position can be credited to the lower T_h and smaller T_h-T_1 difference experienced in the horizontal position tests.

Data from 320 hr. operation of the thermoelement in a horizontal position show that soon after the beginning of the horizontal tests, the power output and the T_1 temperature started to drop slowly with time. Attempts were made at first to maintain a constant T_1 by raising the T_h temperature. Soon after 177 hr. operation, the rate of drop of T_1 with time increased, but the power output stayed relatively constant as T_h was held relatively constant. The rapid drop in T_1 without apparent effect on the power output, as the length of the test increased, indicated something had happened to the thermocouple used to monitor the T_1 temperature. The test was halted after 320 hr. The element by this time had been exposed to 122-hr. testing in a vertical position and 320 hr. in a horizontal position, or a total of 444 hr. exposure to generator temperatures.

Upon examining the thermoelement and the monitoring thermocouple, it was found that the thermocouple was in perfect condition. However, it was found that a small crack had developed near the drilled thermocouple hole in the intermediate junction between the MCC 40 and MCC 60 segments. This small crack, possibly initiated during the drilling of the thermocouple hole, seemed to have slowly widened and lengthened during the test. Since the crack involved only a small area of the intermediate junction between the MCC 60 and MCC 40 segments, its effect on the power output was small. The presence of even a small expanding crack between the thermocouple (largely imbedded in the MCC 40 material) and the hot MCC 60 segments, could provide sufficient thermal resistance to account for the lowering of the T_1 temperature experienced.

On the basis of this experiment, it appeared that the original decision to omit inserting thermocouples at the intermediate junction was a sound one. Not only would the drilling of these holes within the junction have weakened the thermoelements, but the temperatures so obtained could have been quite misleading. This problem was eventually solved by including a sufficiently thicker graphite intermediate disc to permit insertion of the T_1 site thermocouple in the graphite and by the surface preparation improvements reported in the junction-forming techniques section of this report. The increase in disc thickness consisted of about 1/16 inch, from 1/32-inch thick to 3/32-inch thick. When more graphite length than this was used, the increase in thermoelement electrical resistance increased prohibitively, partly as a result of excessive infusion of thermoelectric material into the graphite.

Severe problems were also encountered in trying to reproducibly measure T_1 temperatures in 1/4-inch diameter thermoelements. One of the knottiest problems, in addition to the harmful effect of radially-drilled T_1 thermocouple holes on element breakage, was that thermal gradients in excess of 50°C/mm were encountered in the T_1 areas. Such steep gradients make the location of reference thermocouples in this zone quite important and difficult in terms of reproducing thermoelement performance tests and ratings.

The high rate of thermoelement breakage dictated against the use of radially-drilled thermocouple holes at the T_1 site of 1/4-inch diameter thermoelements. For the screening of individual thermoelements, it was possible to attain reproducible test data by using a disappearing wire type of optical pyrometer sighted (under near-black body conditions) upon the surface of each element at its T_1 site. Thermocouples were simultaneously used at the T_h and T_c sites. All p- and n-type thermoelements were then screened for T_1, ΔT, P, S and R.

Since it was not feasible to use optical methods for measuring critical T_1 sites in the assembled improved experimental model, further attempts were made to find a practical method for drilling thermocouples from the T_c to the T_1 sites along the center axis. After experiencing considerable difficulty in the breakage of both thermoelements and drills, it was found that intermittent pressure with high-speed (1500-200 rpm) carbide drills permitted sinking of the required 0.036-inch diameter axial holes at the T_1 sites for both p- and n-type thermoelements. Thermocouples were inserted and the T_1 temperature measured for several thermoelements by optical and thermocouple means. The results of these tests demonstrated useful reproducibility of the thermocouple readings. While this approach reduced the cross-sectional area and increased resistance of each drilled thermoelement, it offered a workable and timely solution to the problem of measuring T_1 for screening and monitoring of 1/4-inch diameter thermoelements.

The difficulties inherent in drilling the thermocouple holes to the required depth and implanting thermocouples with sufficient precision to insure that the T_j site is being actually measured resulted in discard of the system. In the generator application, only the bead of the thermocouple was cemented into a small, shallow, radially-drilled hole in the intermediate graphite disc.

After screening more than 300 hot-pressed, 3/8-inch diameter thermoelements, it was found necessary to rebuild the testing apparatus before evaluating additional materials and junctions. It was decided to further modify the apparatus while rebuilding in order to permit achievement of more reproducible measurements than had been available. It was also considered desirable to add the potential for determining thermoelement efficiency, since this property could be obtained only in apparatus constructed for that specific purpose. This screening apparatus design borrowed extensively from the successful potted furnaces developed for induction-unit hot-pressing. This can be seen in Figure 42, which shows the cast ceramic exterior in the test stand and the thermoelements protruding from radially located holes. A detailed drawing of the internal configuration of the apparatus is presented in Figure 43. While the design shows positions for four thermoelements, only two of the elements would be in test. The remaining two positions are intended for comparison-type standard thermoelements which would be left in place throughout a series of tests to insure that conditions do, indeed, remain constant. This should contribute substantially to the consistency of the screening measurements. The apparatus thus permits testing of two n-type elements, two p-type elements, or one p- and one n-type element in the p-n couple configuration most representative of generator conditions. The deep holes and controlled conditions permit better measurements of heat throughput, with resultant better efficiency estimates as described in an earlier report (TDR No. ASD-TDR-62-896, Pt. II, Page 80, October, 1963). Initial testing of the electrical characteristics of several thermoelements proved the feasibility of the apparatus, but difficulties were encountered on these "shakedown runs" due to excessive outgassing of the cast ceramic thermal insulation in high vacuum. The insulation otherwise appeared to be a sound solution of the problem of minimizing extraneous heat losses. High-temperature pre-firing of the ceramic diminished the outgassing, but any duration of exposure to atmosphere reintroduced a pump-down problem on the succeeding run. No adequate solution was seen for this problem, so a more complicated multi-layer metal foil insulation was fabricated. This insulation was found to approach the ceramic in thermal properties and eliminated the problem of outgassing. A close-fitting, tapered joint was tried in place of the threaded graphite hot contact

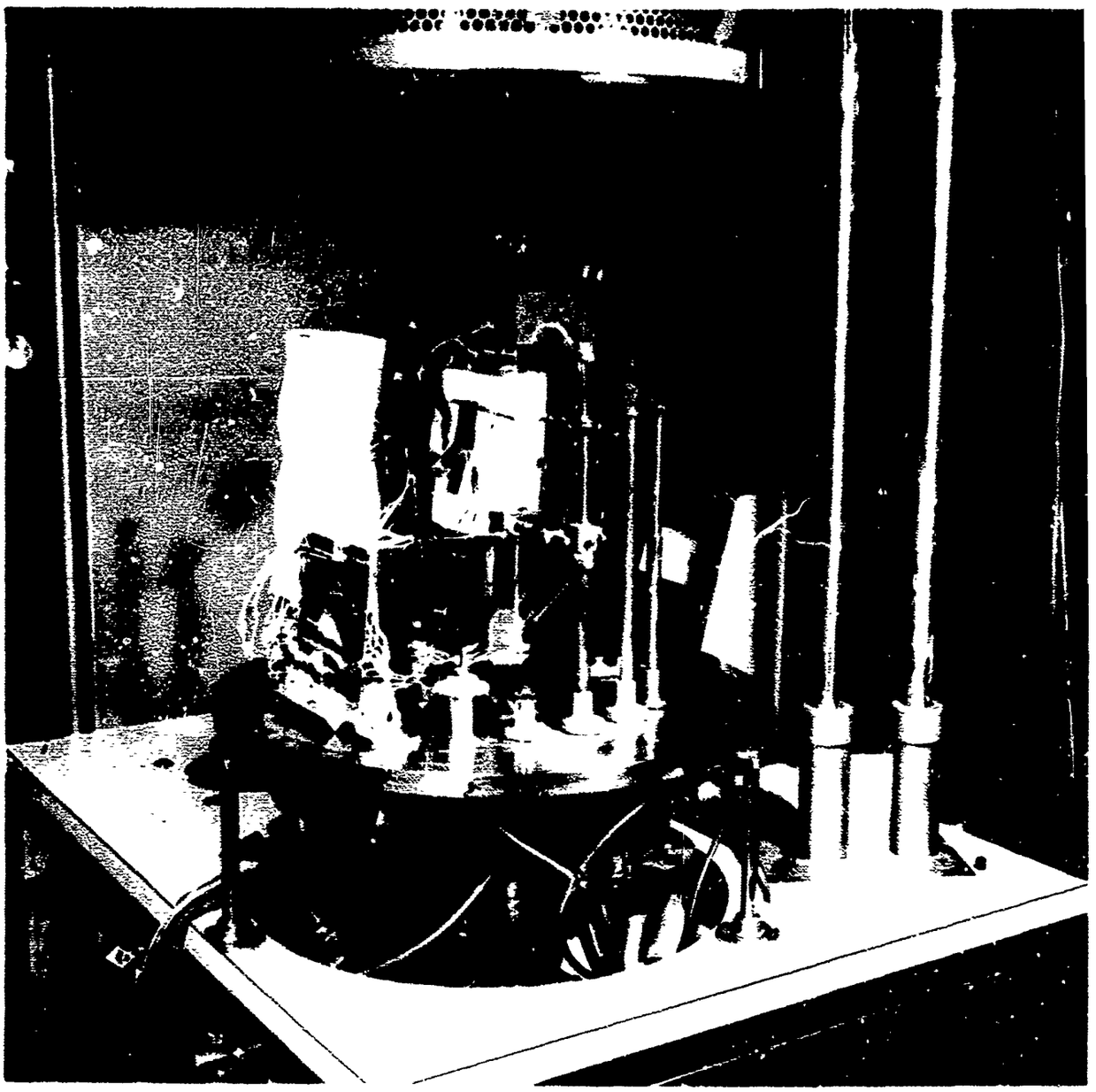

Figure 42. Modified Apparatus for Comparative Screening of Hot-Pressed Thermoelements

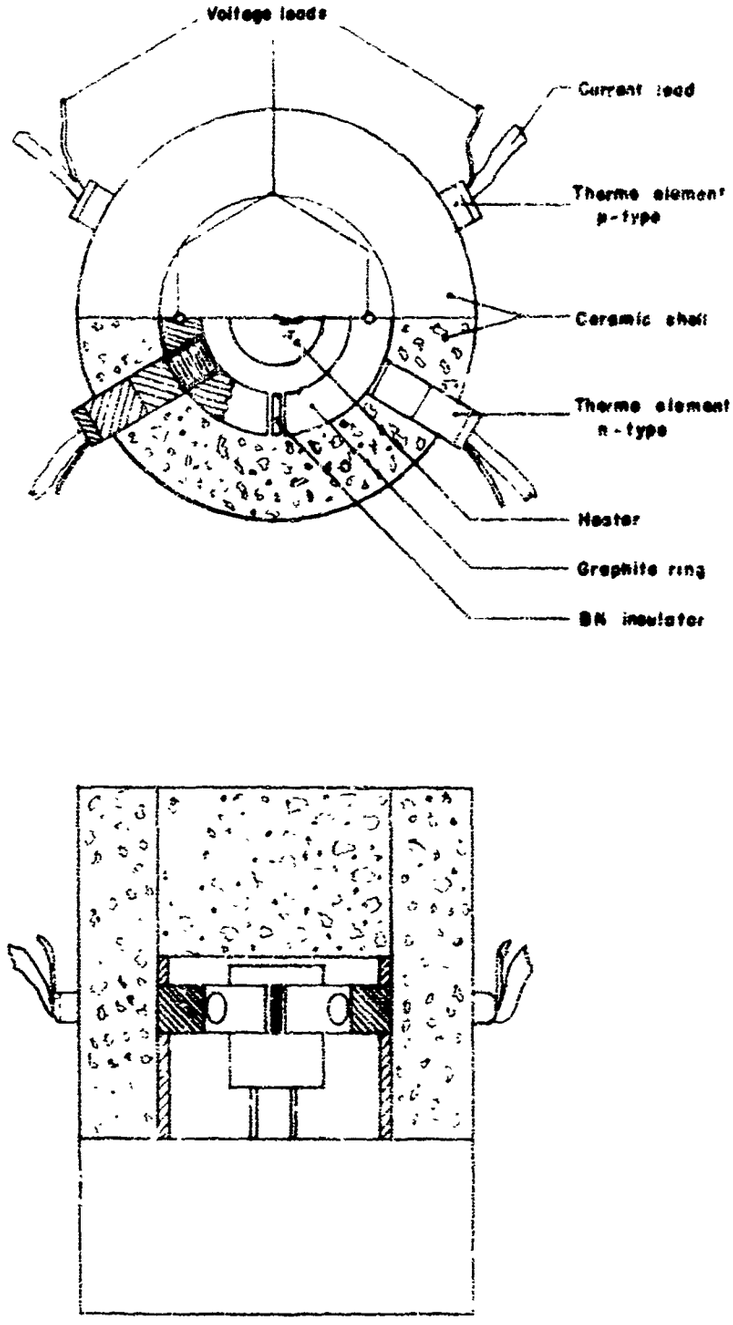

Figure 43. Cross-Sectional View of Modified Screening Apparatus

used on thermoelements. The tapered joint functioned equally well and offers an increase in ease and speed in loading where the final desired thermoelement configuration permits use of this shape. Refinements in the resistance heater, voltage leads and thermocouple placement were also obtained in this apparatus design.

The sustained performance test on a hot-pressed p-n couple of 3/8 inch diameter segmented thermoelements reached 1012 hr. At the end of 1012 hr. sustained testing at a T_h of 1194-1198°C, the couple was subjected to 278 thermal cycles in which peak cooling rates of 240-250°C/min. were reached each cycle. The power output (column "P_t", as shown in Table 27) varied only slightly throughout the test. A comparision of the performance of this 1964 state-of-the-art p-n couple is presented below:

	Performance of 3/8-Inch Diameter Hot-Pressed p-n Couples, Representative of:	
Operating Conditions	1963 State-of-the-Art	1964 State-of-the-Art
Vacuum, torr x 10^{-5}	0.1	0.1
Hot junction, T_h, °C	1200	1198
Average intermediate junction T_i, °C	904	937
Average cold junction, T_c, °C	532	550
Average ΔT, °C	668	648
Open circuit voltage, mv	282	290
Couple resistance, ohms	.047	.042
Current amps	3.23	3.26
Matched load output adjusted to same ΔT, watts(e)	0.422	0.495

The above data indicates that an improvement of about 17% has been achieved for p-n couples made from 3/8-inch diameter segmented thermoelements during the 1963-64 period.

In summary, at least one screening or performance test was conducted on 350 new 3/8-inch diameter, 144 used 3/8-inch diameter, and 351 new 1/4-inch diameter thermoelements for a total of over 845 element tests under this contract. This total included generato construction thermoelements as well as elements for evaluation, unde

Table 27

TEST DATA ON A REPRESENTATIVE P-N COUPLE OF HOT-PRESSED 3/8" DIAMETER SEGMENTED THERMOELEMENT, AUGUST 1964

[illegible]	Avg. Th, [illegible]	Average Temperature [illegible]		Avg. [illegible]	Avg. ΔT, [illegible]	[illegible] Approximately Matched Load Conditions					Average [illegible]	[illegible]
		[illegible]	[illegible]			I, Amps	E, Mv	Ei, Mv	Ri, Ohm	Pm, Watts		
[illegible]	1[illegible]	[illegible]	[illegible]24	[illegible]	64[illegible]	[illegible]	[illegible]	[illegible]	.0427	[illegible]	432	[illegible]
[illegible]	[illegible]	[illegible]	[illegible]	[illegible]	64[illegible]	[illegible].26[illegible]	[illegible]	[illegible]	[illegible]	0.4[illegible]	430	[illegible]
[illegible]	[illegible]	[illegible]	[illegible]26	[illegible]2	646	[illegible].26[illegible]	2[illegible]	[illegible]	[illegible]	[illegible]	[illegible]	[illegible]
[illegible]	[illegible]	862	[illegible]	552	642	[illegible].26	2[illegible]2	[illegible]	[illegible]	[illegible]	[illegible]	[illegible]
[illegible]	[illegible]	[illegible]2	[illegible]	552	[illegible]	3.26[illegible]	2[illegible]	[illegible]	[illegible]	[illegible]	[illegible]	[illegible]
[illegible]	[illegible]	[illegible]	[illegible]2[illegible]	[illegible]2	[illegible]	[illegible]	[illegible]	[illegible]	.046[illegible]	[illegible]	[illegible]2	[illegible]
[illegible]	[illegible]	[illegible]	[illegible]	[illegible]2	[illegible]	[illegible].26[illegible]	[illegible]	[illegible]	[illegible]	[illegible]	[illegible]	[illegible]
[illegible]	[illegible]	[illegible]	[illegible]	[illegible]2	[illegible]	[illegible]	2[illegible]	[illegible]	[illegible]	[illegible]	[illegible]2	[illegible]
[illegible]	[illegible]	[illegible]	[illegible]	[illegible]	[illegible]	[illegible].26[illegible]	[illegible]	[illegible]	[illegible]	[illegible]	[illegible]2	[illegible]
[illegible]	[illegible]	[illegible]	[illegible]	[illegible]2	[illegible]	[illegible]	[illegible]	[illegible]	[illegible]	[illegible]	[illegible]2	[illegible]
[illegible]	[illegible]	[illegible]2	[illegible]	[illegible]2	[illegible]	[illegible]	[illegible]	[illegible]	[illegible]	[illegible]	[illegible]	[illegible]
[illegible]	[illegible]	[illegible]	[illegible]	[illegible]	[illegible]	[illegible]	[illegible]	[illegible]	[illegible]	[illegible]	[illegible]	[illegible]
[illegible]	[illegible]	[illegible]2	[illegible]	[illegible]	[illegible]	[illegible]	[illegible]	[illegible]	[illegible]	[illegible]	[illegible]	
[illegible]	[illegible]	[illegible]	[illegible]	[illegible]2	[illegible]	[illegible]	[illegible]	[illegible]	[illegible]	[illegible]	[illegible]	
[illegible]	[illegible]	[illegible]	[illegible]	[illegible]2	[illegible]	[illegible]	[illegible]	[illegible]	[illegible]	[illegible]	[illegible]	[illegible]
[illegible]	[illegible]	[illegible]	[illegible]	[illegible]2	[illegible]	[illegible]	[illegible]2	[illegible]	[illegible]	[illegible]	[illegible]	
[illegible]	[illegible]	862	[illegible]	[illegible]	[illegible]	[illegible]	[illegible]	[illegible]	[illegible]	[illegible]	[illegible]	
443	[illegible]	[illegible]	[illegible]	[illegible]	[illegible]	[illegible]	[illegible]	[illegible]	[illegible]	[illegible]	[illegible]	
467	[illegible]	[illegible]	[illegible]	[illegible]	[illegible]	[illegible]	[illegible]	[illegible]	[illegible]	[illegible]	[illegible]2	
[illegible]	[illegible]	[illegible]	[illegible]	[illegible]2	[illegible]	[illegible]	[illegible]	[illegible]	[illegible]	[illegible]	[illegible]	
[illegible]	[illegible]	[illegible]	[illegible]	[illegible]2	[illegible]	[illegible]	[illegible]	[illegible]	[illegible]	[illegible]	[illegible]	
[illegible]	[illegible]	[illegible]	[illegible]	[illegible]2	642	[illegible]	[illegible]	[illegible]	[illegible]	[illegible]	[illegible]	[illegible]
[illegible]	[illegible]	[illegible]	[illegible]026	[illegible]2	642	[illegible]	[illegible]	[illegible]	[illegible]	[illegible]	[illegible]	[illegible]
[illegible]	[illegible]	[illegible]	[illegible]	[illegible]	[illegible]	[illegible].262	[illegible]	[illegible]	[illegible]	[illegible]	45[illegible]	[illegible]
[illegible]	[illegible]	[illegible]	[illegible]	[illegible]2	642	[illegible]	2[illegible]	[illegible]	.0460	[illegible]	452	[illegible]
636	[illegible]	[illegible]	[illegible]	[illegible]2	[illegible]	[illegible]	[illegible]	[illegible]	[illegible]	[illegible]	[illegible]	[illegible]
661	[illegible]	86[illegible]	[illegible]	[illegible]2	[illegible]	[illegible].262	28[illegible]	[illegible]	.04[illegible]	[illegible]	[illegible]	[illegible]
[illegible]	[illegible]	862	[illegible]	[illegible]2	[illegible]	[illegible]	2[illegible]	[illegible]	[illegible]	[illegible]	452	[illegible]
[illegible]	[illegible]	86[illegible]	[illegible]026	[illegible]2	[illegible]	[illegible].26[illegible]	[illegible]	[illegible]	[illegible]	[illegible]	[illegible]2	[illegible]
743	[illegible]	[illegible]	[illegible]	[illegible]2	642	[illegible]	[illegible]	[illegible]	[illegible]	[illegible]	[illegible]	[illegible]
[illegible]	[illegible]	862	[illegible]	[illegible]2	[illegible]	[illegible]	[illegible]	[illegible]	[illegible]	0.462	[illegible]	[illegible]
[illegible]	[illegible]	[illegible]	[illegible]	[illegible]	642	[illegible]	[illegible]	[illegible]	.0460	[illegible]	[illegible]	[illegible]
[illegible]	[illegible]	[illegible]	[illegible]	[illegible]2	[illegible]	[illegible]	[illegible]	[illegible]	[illegible]	[illegible]	[illegible]	[illegible]

Table 2?, (Cont'd)

TEST DATA ON A REPRESENTATIVE P-N COUPLE OF HOT-PRESSED 3/8" DIAMETER SEGMENTED THERMOELEMENT, AUGUST 1964

Hours at Temperature	Avg. T_H °C	Average Temperature °C		Avg. T_C °C	Avg. ΔT °C	Couple Characteristics Under Approximately Matched Load Conditions					Avg. α /ΔT, μv/°C	Observed Power Output, watts
		T_1 20/80	65/35			I, Amps	E_{oc}, mv	E_L, mv	W_i, new	W_o, watts		
944	1194	862	1026	552	642	3.261	292	142	.0460	0.468	455	
968	1195	862	1026	552	643	3.262	292	142	.0460	0.468	455	
992	1194	861	1025	552	642	3.261	291	141	.0459	0.467	454	
016	1193	861	1024	552	641	3.260	290	140	.0458	0.466	452	
040	1193	861	1024	552	641	3.260	290	140	.0458	0.466	452	
064	1195	862	1026	552	643	3.261	292	142	.0460	0.468	455	
088	1194	861	1025	552	642	3.260	291	141	.0459	0.467	454	
112	1194	861	1024	552	642	3.260	291	141	.0459	0.466	454	

Thermal cycling tests - 24 cycles/day in which cooling rates of 200-240°C/min. were reached each cycle for a temperature drop per cycle of 200°C.

1036 (36 cycles	1194	861	1024	552	642	3.260	292	140	.0460	0.468	451	
1060 (60 cycles)	1193	860	1025	552	643	3.259	291	142	.0459	0.465	453	
1084 (84 cycles)	1195	861	1024	552	642	3.[illegible]	291	140	.0459	0.466	453	
1108 (108 cycles)	1192	861	1024	552	642	3.2[illegible]	289	140	.0459	0.466	453	
1132 (132 cycles)	1193	860	1023	552	641	3.[illegible]	290	141	.0458	0.465	[illegible]	
1156 (156 cycles)	1194	861	1024	552	642	3.260	290	140	.0460	0.466	[illegible]	
1180 (180 cycles)	1192	861	1024	552	641	3.261	290	140	.0460	0.459	[illegible]	
1206 (206 cycles)	1194	860	1024	552	642	3.[illegible]	291	140	.0458	0.466	[illegible]	
1230 (230 cycles)	1194	862	1025	552	642	3.[illegible]	291	142	.0457	0.463	458	
1254 (254 cycles)	1195	860	1024	552	643	3.261	290	140	.0460	0.459	452	
1278 (278 cycles)	1194	861	1024	552	642	3.[illegible]	290	140	.0460	0.459	452	

the junction-forming techniques and fundamental investigation phases of the project. Some elements served both purposes in order to provide better efficiency in expenditure of effort. Test services were also provided on the arc-plasma sprayed thermoelements produced under that phase of this contract.

A series of tests was provided to assist in determining the causative factors for failure of the MCC 40-graphite intermediate junctions in the initial advanced experimental model thermoelectric generator. These tests contributed to the diagnosis and solution of the problem.

A substantial effort was provided to effect solution of the problem of measuring intermediate junction temperatures in the smaller, fragile, 1/4-inch diameter, multi-segmented thermoelements, and contributed to the construction and safe operation of the improved experimental model thermoelectric generator.

After completion of generator screening tests, the testing apparatus was rebuilt with the additional aim of attaining measurements with better reproducibility and accuracy. The equipment was so designed as to include a potential for measuring efficiency and thermal conductivity which were not possible previously. Extensive problems with outgassing of the desired cast ceramic insulation in vacuum resulted in final substitution of multi-layered metal foil insulation in the same physical shape. The resultant apparatus minimized extraneous heat losses and achieved more reliable energy balances capable of permitting meaningful efficiency and thermal conductivity measurements.

A hot-pressed thermoelectric couple was successfully subjected to duration tests of 1012 hr. and 272 thermal cycles. A comparison between these test results and the 1963 state of the art was made.

An arc-plasma sprayed thermoelectric couple was successfully subjected to duration tests of 1030 hr. and 294 thermal cycles. The results of these tests are presented under Section III D, 2 of this report.

4. Fundamental Investigation

The aim of this investigation was to more fully establish the operating mechanisms involved in MCC 40, 50 and 60 thermoelectric materials. This included establishment of the effect of nonsoluble dispersed materials on electrical and thermal conductivity, strength, Seebeck coefficient, sublimation and solid-state diffusion.

As one facet of the Monsanto approach, nonsoluble dispersed phases are used to control the flow of electrons and phonons in a matrix of selected thermoelectric materials. Properly sized and spaced particles cause appropriate strain in the crystal lattice of the matrix material. Such strain can be intensified on heating if the dispersant expands more than the matrix. The major result of this strain is an impedance of phonon flow which lowers the thermal conductivity. In our experience, electrical conductivity and Seebeck coefficient are generally not appreciably affected. The presence of the dispersant also tends to improve the strength of the thermoelectric material through impedance of grain growth. Additionally, sublimation effects and solid-state diffusion damage are inhibited.

Efforts to improve thermoelectric materials have been based on an increase in the thermoelectric figure of merit, Z, which is related to the major thermoelectric parameters:

$$Z = \frac{S^2}{\rho k}$$

where S = the Seebeck coefficient
ρ = the electrical resistivity
k = the thermal conductivity

In Monsanto Company's dispersed-phase approach, an improvement in Z is obtained by decreasing the thermal conductivity with only slight changes in the Seebeck and electrical resistivity through the use of doping and dispersed insoluble particles.

Thermal conductivity in a solid occurs when energy is transferred by phonons, free electrons, holes, electron-hole pairs, excitons and photons. It is decreased when these energy carriers are scattered. Phonons are most affected by the dispersed particles with some photon scattering also occurring from the boundaries of fine grained phases caused by the dispersed particles.

Consideration of mechanisms responsible for phonon scattering indicates the importance of the dispersed phase particle to the thermal conductivity of materials. By definition:

$$k = 1/3\ Cv$$

where C = specific heat
v = phonon velocity
ℓ = phonon mean free path in which $1/\ell = 1/\ell_1 + 1/\ell_2 + \ldots$ where ℓ_1, ℓ_2, are the phonon mean free paths for various scattering mechanisms.

Therefore, for a decrease in k, small mean free paths are desired.

Since phonons are scattered by various mechanisms, such as, other phonons, static imperfections, isotopes, alloys, dislocations, grain boundaries and electrons, the effect of each of these mechanisms on the mean free path of phonons was briefly considered below.* Phonon-phonon scattering in a single phase material is of great importance at high temperatures. The phonon mean free path from this mechanism can be approximated by the following relation:

$$\ell \approx 7a\ (T_m/T)$$

where a = the interatomic distance, Å
T_m = the melting point, °K
T = the temperature, °K.

On the basis of this equation, mean free paths of 0.2μ between phonon-phonon interactions would be expected for MCC 50, MCC 60 and MCC 40 materials.

Static imperfections are effective as a phonon scattering mechanism, and are probably the most effective from the dispersed-phase approach. An approximate relation for dilute dispersions follows:

$$\ell \sim a/2(1 - A_I/A)^2 X_1$$

where a = interatomic distance of the matrix materials, Å
A_I = the atomic weight of the impurity, gms.
A = the atomic weight of the lattice
X_1 = the fraction of impurity.

*This study is largely based on ideas advanced by R. W. Keyes and J. E. Bauerle, Thermoelectricity: Science and Engineering, Interscience Publishers, New York, 1961, and D. Dew-Hughes (a technical note) in Acta Metallurgica, Vol. 8, 1960, pp. 816-17.

Because lattice imperfections and phonon scattering resulting from isotope scattering tend to be quickly removed (annealed) at high temperatures, this mode of scattering was not considered for this study. Additionally, alloy (solid-solution) scattering as a phonon-scattering mechanism was not considered in this study, since it was confined, for the present, to learning more about the effect on phonon scattering of insoluble dispersants.

Dislocation scattering is affected by dispersed phases. An equation for the phonon mean free path from dislocations is:

$$\ell = a/\alpha\, Nb^2$$

where α = constant (≈ 1)
N = the number of dislocations
b = Burger's vector, cm

The number of dislocations, even in highly stressed materials where as many as $10^{12}/cm^3$ may be produced, is not sufficient to do much scattering. However, this number can be increased by using dispersants with large differences in thermal expansion coefficients between the dispersant and the parent lattices, according to the following relation:

$$\Delta N = \frac{4E}{3b}\,(T_m - T)d$$

where E = the difference in the volume thermal expansion coefficients,
d = the dispersed phase particle diameter, cm.

Boundary scattering also will be enhanced by dispersed phases since they produce fine-grained materials. The mean free path of the phonon is related to grain size as follows:

$$\ell \approx D$$

where D = the average grain diameter, cm.

As mentioned before, phonons are also scattered by grain boundaries, so attainment of fine-grain size in high-temperature thermoelectric materials is doubly important.

Phonon scattering by electrons is usually small for thermoelectric materials so it was neglected for the materials and thermal conditions of this study.

On the basis of the above considerations, static imperfections, dislocations and grain boundaries stand out as the major phonon scattering mechanisms apt to be affected by Monsanto Company's dispersed-phase approach. General conclusions are:

a. The dispersants should have higher atomic weights and different volume thermal expansion coefficients than the matrix or thermoelectric material.

b. Dispersants should also inhibit matrix grain growth.

More closely spaced (0.1u) uniform dispersions of more insoluble particles were sought as a means of further improving MCC thermoelectric materials, but experimental verification techniques are not yet sufficiently refined to make a definitive evaluation possible.

Considerable effort was directed toward determining the microstructure of MCC-based thermoelectric materials. Phase efforts were initially impeded by a serious tendency of the specimens to crack during preparation. For easier handling, specimens to be polished for microstructure evaluation were mounted in a bakelite plastic and cured under 3500 psi pressure at 135°C. This technique apparently exerted substantial tensile forces on the ceramic-like thermoelectric specimen, resulting in crack formation. When this mechanism was discerned, ASTRO-MET cold-mount resin was substituted for the bakelite plastic and the problem successfully circumvented. Figure 44 uses macrophotographs of a typical MCC 40 n-type specimen at 8.5X to illustrate the problem and solution. Both specimens were cut from the same thermoelectric segment and processed in a similar manner except for mounting technique. The upper photo is that of the bakelite-mounted specimen and the lower photo is of the "cold-mounted" sibling. The cracking phenomenon seen in the upper photo is completely eliminated in the specimen presented in the lower photo.

When this problem was solved, it was necessary to develop techniques for polishing MCC-based specimens in a manner that would permit viewing and measuring of the size and spacing of the dispersed particles used to control characteristics. This attempt was necessary in order to gain a better understanding of the mechanisms involved and, thus, yield improvement in materials through better controls. This proved to be a difficult task, in itself, since the polishing of such hard, brittle materials produced surface pitting which effectively masked observations of the size and spacing of the dispersed particles. The larger grit-size abrasives (> 6 microns) necessary to level the specimens prior to final polishing invariably caused this pitting effect. Better methods of

Mounted in bakelite plastic

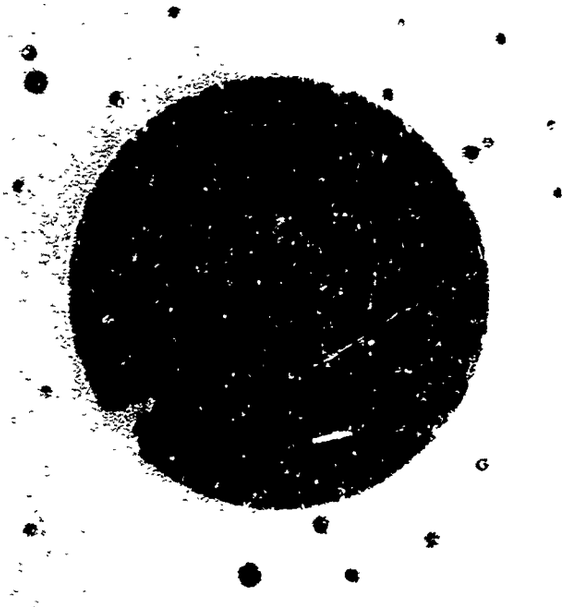

Mounted in Astro-met cold mount resin

Figure 44. n-Type MCC 40 Specimen Mounted in Different Resins, Unetched, 8.5X

preparing specimens of the MCC-based thermoelectric materials for microstructural examination were evolved. Successful preparation of MCC 50, MCC 60 and p- and n-type MCC 40 specimens was finally achieved in the following manner:

a. If necessary, the thermoelement was sectioned with a diamond cut-off saw.

b. The sectioned piece was then mounted in cold-mount resin, and leveled by surface grinding with a diamond abrasive wheel. Extreme care was taken during the grinding operation to obtain the best possible surface.

c. The specimen was smoothed on a 180-grit silicon carbide belt sander until no further improvement resulted.

d. The final step for each of the MCC thermoelectric materials was a preliminary polish on a 1μ diamond abrasive lap. This operation was continued until no further change in the surface was obtained. The specimen was then ready for initial evaluation under an optical microscope.

e. Final polishing on MCC 50 and MCC 60 materials was accomplished on a cloth lap with 0.5μ diamond abrasive and 0.3μ alumina abrasive, respectively. Etching, where desired, was done electrolytically with a 10% aqueous HCl solution.

f. Final polishing on p- or n-type MCC 40 materials was best accomplished on the 0.5μ diamond abrasive lap. Etching was accomplished at room temperature with the following solution:

10 ml. HNO_3
8 ml. HF
79 ml. $C_2H_4O_2$.

Microscopic observations made on specimens prepared by the above procedures provided evidence to show that the existing microstructures were far from the desired goal of closely spaced, uniform dispersions. A photomicrograph of an MCC 50 specimen, presented in Figure 45, clearly shows the calcium oxide dispersed phase. This sample was unetched and photographed at 500X magnification. The smaller, more numerous, dark particles in this

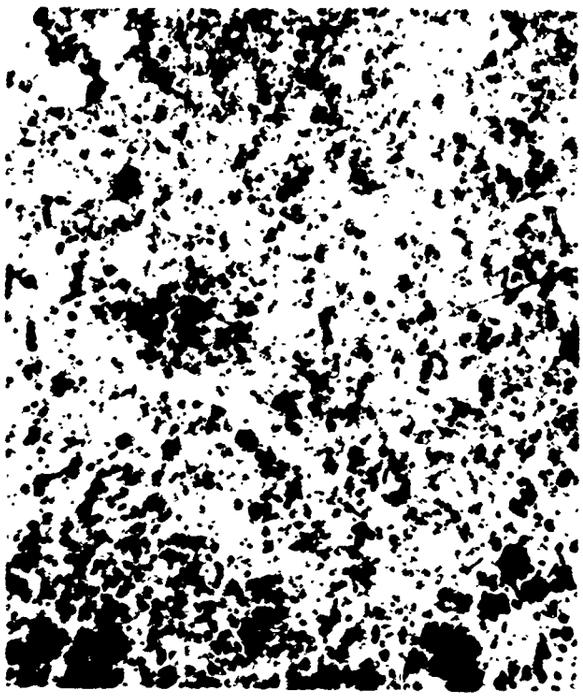

Figure 45. Microphotograph of MCC 50 Showing Dispersed Phase, as Polished, 500X

phot ere identified as calcium oxide. They appear to be appr mately 1-2 microns in diameter and fairly well dispersed. The ger black areas in this figure appear to be either voids resulting from earlier polishing procedures or porosity present in the "as produced" MCC 50 segment. The occasional white particles that can be observed are believed to be reaction products, possibly caused by a partial solubility of the calcium oxide with constituents of the matrix material. Other samples of MCC 50 that were examined showed dispersants of widely varying size and spacing, although all appeared quite fine-grained when viewed with polarized light. Both p- and n-type MCC 40 exhibited small dispersed particles; however, the dispersion distribution was poor in all cases. No dispersions were detectable in MCC 60 specimens up to the optical microscope limit of 1700X. The electron microscope was pressed into service for an examination at 20,000X and a few particles were observed having diameters less than 0.5μ.

Microscopic observations made on specimens prepared by the above procedures provided evidence to show that present microstructures were far from our desired goal of closely spaced, uniform dispersions. The hot-pressed MCC 50 material showed dispersants of widely varying size and spacings. Some similar flame-sprayed samples exhibited larger quantities of dispersed phases and a substantial degree of material orientation due to spraying. All samples when viewed with polarized light were fine-grained. Both p- and n-type MCC 40 exhibited small dispersed particles that were poorly distributed. No dispersants were detected in the MCC 60 specimens with the optical microscope up to 1700X. Viewing specimens of MCC 60 to 20,000X under the electron microscope showed that the number of dispersed particles were few and generally less than 0.5μ.

Specimens of the MCC 60, MCC 50, p- and n-type MCC 40, prepared as indicated above, were each examined with electron microscope to 20,000X. Replicas of the final polished surfaces were obtained in the following manner:

a. A piece of cellulose acetate tape was softened with acetone and pressed firmly on the specimen surface with a rubber applicator.

b. After the tape was dry, it was stripped from the specimen surface and placed in an evaporator where it was coated with a 100Å layer of carbon and shadowed at 45° with chromium.

c. Small squares were then cut from the coated tape and placed, carbon side down, on 400-mesh copper grids in an acetone wash dish. After the cellulose acetate was dissolved, the replica was ready for examination with the electron microscope.

An electron micrograph (5500X) of a typical hot-pressed MCC 50 specimen is presented in Figure 46. It shows particles of a large range of sizes (0.1 to 2μ) fairly well dispersed. The spacing between particles ranged from <0.1μ to about 1μ, or reasonably close to the <0.2μ interparticle spacing desired for high-quality, high-temperature thermoelectric material.

As shown in Figure 47 at 9000X, the number of particles per unit volume of a hot-pressed p-type MCC 40 specimen was appreciably less than that for the MCC 50 material. The average particle size determined by examining the total specimen area was about 0.5μ, with spacing of 1-10μ between particles.

The n-type MCC 40, as shown in Figure 48, also exhibited widely scattered particles. Average particle size was judged to be about 0.2μ, with interparticle spacing of 0.2μ to 6μ. This specimen exhibited large areas containing phases that could not be identified.

It was concluded that both p- and n-type MCC 40 specimens indicate a need for reduction in size and spacing of dispersants.

Figure 49 shows a typical electron micrograph of hot-pressed MCC 60 at 9000X. The microstructure of this material exhibited at least three different phases ranging in size from about 0.3μ to 30μ. These phases appeared to occupy 50-70% of the volume of the MCC 60 material. The extremely complicated structure makes identification and interpretation of the importance of these phases to the thermoelectric properties of MCC 60 a subject for future major efforts.

The metallographic examination, in general, uses the optical metallograph, the electron microscope and the microhardness tester, and is one of the most important diagnostic tools available for improving the Monsanto dispersed-phase thermoelectric materials. The presence of the desired small, relatively insoluble, well-dispersed particles must be observed in the microstructure of a thermoelement before an attempt can be made to correlate the structure with measured thermoelectric properties. The observed correlations then furnish the best available guide to permit attainment of the best structure and resultant best properties.

Figure 46. Electron Micrograph of MCC 50 Showing Dispersed Particles, Unetched, 5500X

Figure 47. Electron Micrograph of p-type MCC 40 Showing Dispersed Particles, Unetched, 9000X

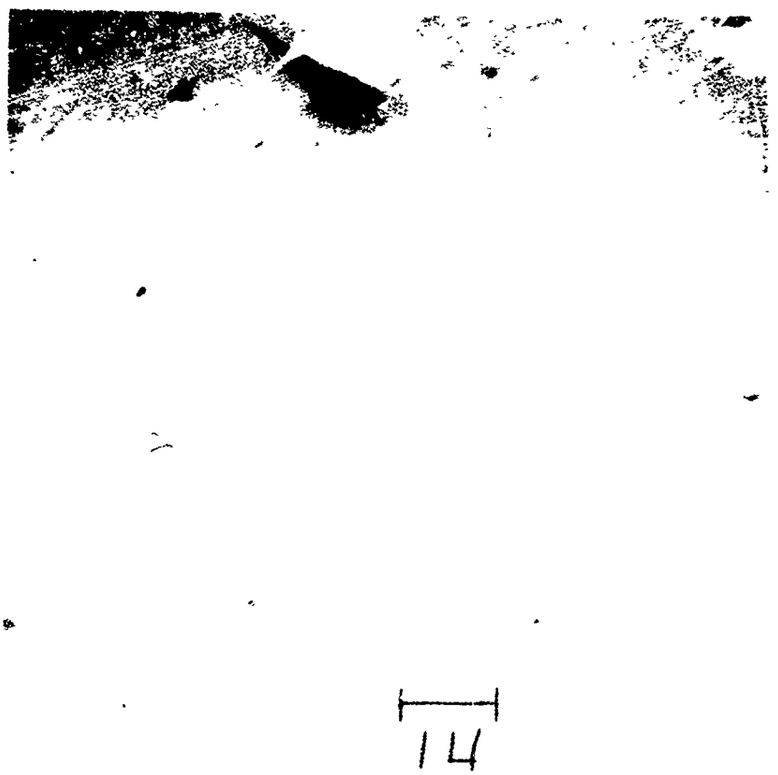

Figure 48. Electron Micrograph of n-type CC 40 Showing Dispersed Particles, Unetched, 13,500X

Figure 49. Electron Micrograph of MCC 60 Showing Dispersed Particles, Unetched, 9000X

Several derivations in structure noted during technique development appeared to have considerable significance in relation to problems that occurred in model generator construction and operation. Accordingly, effort was expended to follow these lines of inquiry and effect solutions.

The microstructure of hot-pressed MCC 40 did not appear to be that expected for a solid-solution alloy. Homogenization treatments were attempted by heating specimens to 1100°C in an inert atmosphere furnace for 100 hours. Although little homogenization was observed, there did appear to be some grain growth and dissolution of a secondary phase. The most interesting change, however, was the appearance of a small amount of a previously unobserved material at one junction of MCC 40P with graphite. This material was grey in color and contrasted with the white MCC 40P and dark graphite, as shown in Figure 50. This micrograph also shows white spheroidal particles of MCC 40P and black voids in the grey material. Careful observations also revealed a few darker grey particles of unknown composition. A microhardness survey of the unidentified material phase indicated that it was slightly softer than MCC 40.

A micrograph of a similarly exposed MCC 40N specimen, shown in Figure 51, required a more difficult analysis, but showed what appeared to be rather extensive amounts of the newly observed material. The apparently scattered distribution (compared with MCC 40P) and masking by the white MCC 40N, the dark-grey graphite, and the light-grey MCC 60 made positive identification more difficult.

Since some of the segmented thermoelements incorporated in the original version of the advanced experimental model thermoelectric generator had failed at the MCC 40 graphite interface due to incipient melting, the observed material was postulated as being the cause of these failures. An attempt to induce such failure was made by heating segmented thermoelements to a uniform 1000°C in a vacuum furnace for 24 hours. Nodes of the observed material, similar to those of Figure 50, were formed at the interfaces.

An extensive examination of existing specimens of thermoelements that had been held at relatively high temperatures (900-1100°C) during screening or endurance tests revealed many more examples of the material that had not been noticed in previous examinations. This examination indicated that the material itself was composed of at least three distinct phases, but this could not be definitively established.

Although a positive identification of the observed material could not be made, a causative hypothesis for the junction failure

Figure 50. Photomicrograph of MCC 40p Structure Showing Newly Observed Material (see descriptive text), Unetched, 50X

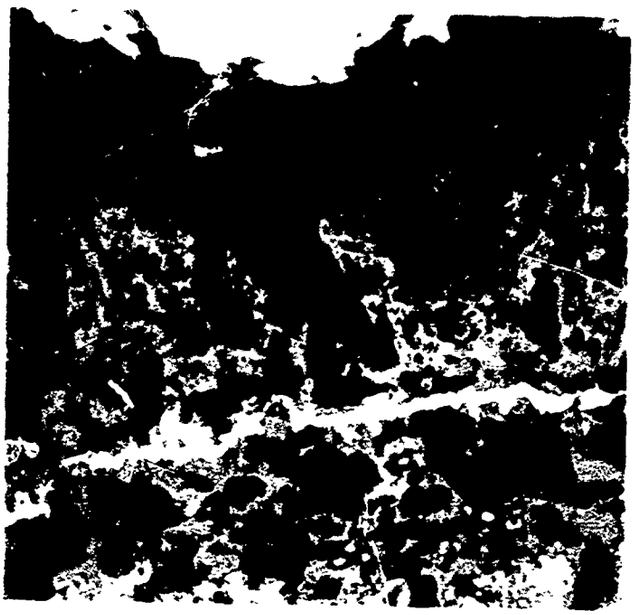

Figure 51. Photomicrograph of MCC 40n Structure Showing Newly Observed Material (see descriptive text). Unetched. 200X

between graphite and MCC 40 thermoelectric material was postulated from the observations. If a progressive reaction between a major component of MCC 40 and graphite removed that component from a local area of the material, then the deficient material remaining (the unknown material observed) could be expected to have a lower melting point. This reaction could then proceed across the bonded zone until mechanical separation and catastrophic failure of the thermoelement occurred.

A few standard comparison materials were prepared in order to expedite identification of unknown materials by microscopic and microhardness comparative techniques. This technique, while very useful and promising, could not be carried to completion within this contract period because there was not sufficient time or funding to permit analyses of the considerable number of unidentified constituents appearing in MCC-type thermoelectric materials. The unidentified phase remains so defined.

An effort was made to examine three p-type and three n-type 3/8-inch diameter segmented thermoelements on which an evaluation of electrical resistance profiles had been made and which exhibited irregularities in electrical contact resistances. These specimens were sectioned longitudinally in order to scan structures along the element axis. Figure 52, shows a MCC 40 graphite junction which was found to have a much lower electrical resistance than the similar junction represented in Figure 53. Both photomicrographs show representative views of the MCC 40-graphite cold junction, with the white MCC 40 and dark graphite materials easily recognizable. A correlation appears to exist between the greater penetration of MCC 40 into the graphite during fabrication and the higher electrical resistance measured on the junction illustrated in Figure 53. Examination of the MCC 40-graphite intermediate junction (at the T_1 site) revealed a similar situation. In all cases, the junction having the greatest MCC 40 penetration into the graphite also had the higher measured electrical resistance. The alteration of the penetrated MCC 40 structure in the graphite of the n-type specimens was also of interest. Figure 54 shows a higher magnification of the white MCC 40 material in the black graphite matrix. The grey material in this photo appears to be a reaction product between the MCC 40 material and either the graphite matrix or MCC 60 material penetrating from the other (hotter) side of the graphite intermediate disc. Since the reaction appears to be more complete as the MCC 60 segment is approached, this could be construed to support the latter hypothesis, but a temperature-dependent reaction variation towards the hotter end of the thermoelement during operation could be assumed to have equal validity. A definitive analysis would require knowledge of whether the reaction occurred primarily during fabrication at a uniform temperature or during thermoelement operation when a temperature

Figure 52. MCC 40-Graphite Junction, Unetched, 50X

Figure 53. MCC 40-Graphite Junction, Unetched, 50X

Figure 54. MCC 40-Graphite Junction with Graphite Intermediate Between MCC 40 and MCC 60, Unetched, 600X

gradient was in existence.

The MCC 60-graphite junctions also showed observable relations between structure and measured properties. Figure 55 shows a sharp transition between the white MCC 60 and the grey graphite matrix. This specimen exhibited a high electrical resistance. Figure 56 shows a similar junction, but with a broader, gradual transition zone and a lower electrical resistance. The broader transition zone appears to indicate a better metallurgical bond between the thermoelectric material and its junction in this case. While the photomicrographs are of the junction between the MCC 60 segment and the intermediate graphite disc, examination of the element hot junctions showed a similar relation between the same microstructure and electrical resistance. A cursory examination of the junctions between MCC 50 and graphite revealed no appreciable variance in structures or electrical resistance.

One of the advantages realized from Monsanto Company's dispersed-phase thermoelectric approach is the stabilization of grain size in materials exposed to high temperatures for long periods of time. Availability of specimens which had been operated in duration testing at high temperatures for periods in excess of 1000 hours offered an excellent opportunity to validate this on a microstructure basis by direct comparison with "as pressed" specimens. Figure 57 presents photos of the microstructures representative of p- and n-type MCC 40 specimens, before and after 1000-hrs. exposure in a vacuum under a 950 °C-500 °C temperature differential. The structures shown in this figure were representative of those for the entire volume of each specimen, showing that the dispersed-phase approach prevents grain growth for at least 1000 hours at temperatures to 950 °C.

In summary, an extensive survey of mechanisms potentially assignable to Monsanto's dispersed-phase MCC-type thermoelectric materials was made and the results analyzed. Efforts were simultaneously expended to provide microstructure examination techniques for correlation of mechanisms, measured properties and material microstructure. These techniques involved development of special mounting procedures as well as surface preparation and etching techniques. Some correlation was achieved between microstructural phenomena observed and measured thermoelectric properties. An initial analysis of the relationship between theoretical potential and state-of-the-art achievements indicated substantial room for improvement of MCC-based materials in all areas. The mechanism responsible for failure of thermoelements in the advanced experimental model (50-watt) thermoelectric generator was identified during development of techniques to observe microstructure, and a basis laid to prevent occurrence in the

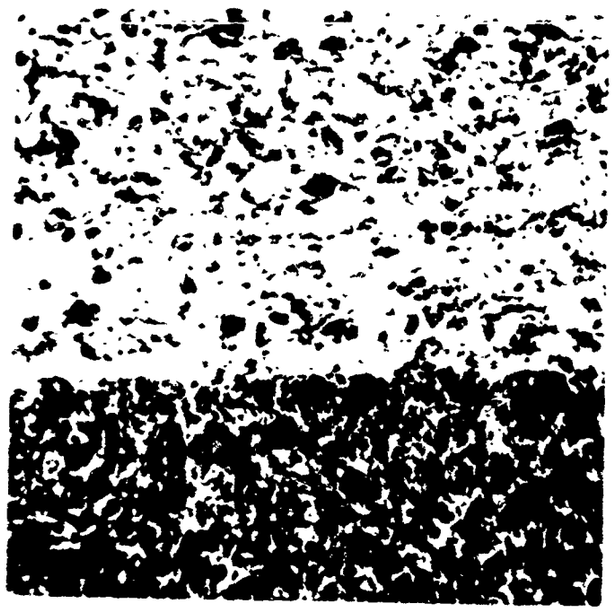

Figure 55. MCC 60-Graphite Junction, Unetched, 50X

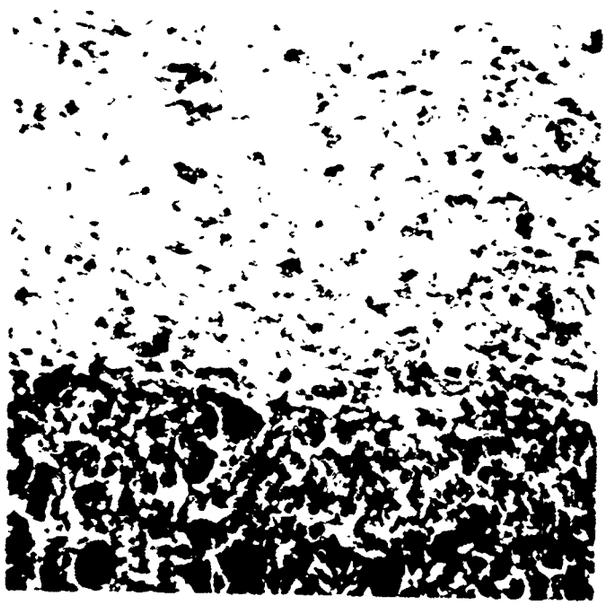

Figure 56. MCC 60-Graphite Junction, Unetched, 50X

a. n-Type, Tested 1000-hr. at a T_h of 950°C, T_c of 800°C

b. p-Type, Tested 1000-hr. at a T_h of 950°C, T_c of 800°C

c. n-Type, As-Pressed

d. p-Type, As-Pressed

Figure 57. MCC 40 Matrix, Etched with a Solution of 10 Parts, Nitric; 8 Parts, Hydrofluoric; and 79 Parts, Acetic Acids 50X

future. An appreciable amount of progress was made in the direction of explaining fundamental mechanisms responsible for the thermoelectric behavior of MCC-based materials. The primary significance of this progress is that it broadened the base of our knowledge of high-temperature thermoelectric phenomena.

E. PRELIMINARY INVESTIGATION OF SYSTEMS CONCEPTS

This section presents the results of a preliminary investigation of several high-temperature thermoelectric space power system concepts and considers nuclear, radioisotope, and solar-concentrating types of heat sources for thermoelectric generators that would utilize the properties of Monsanto Company high-temperature thermoelectric materials and components anticipated for 1964-1965. It also presents the projected performance of advanced high-temperature thermoelectric materials and components anticipated during 1971-1985.

Three types of nuclear reactor heat sources were considered for the thermoelectric space power system concepts investigated. The code name and descriptive title for each system studied are presented below:

1. HORSE (High Temperature Out-of-Pile Reactor-Powered System for Generation of Electricity)

2. TIGER (Thermoelectric In-Pile Generator of Electricity Utilizing a Reactor Heat Source)

3. SWIFT (System for Power Generation with In-Pile Fluid Thermoelectric Elements)

Additionally, eight radioisotopes were also considered as potential heat sources for thermoelectric space-type power units, with particular attention devoted to Cm^{242}, Cm^{244} and Sr^{90}. The performances of these three isotopes as heat sources are representative of those for the eight isotopes considered in this investigation. A thermoelectric space power system with a solar-concentrating type of heat source was also briefly considered.

In arriving at optimized performance figures for each of the systems investigated, separate FORTRAN optimization programs were prepared on an Air Force IBM 7094 computer. All computer programs were based on cylindrically shaped thermoelectric generators. Generators of spherical and flat configurations were judged to be too expensive and too difficult for present fabrication processes.

For purposes of this preliminary investigation the following thermoelectric and structural material properties, considered attainable during 1964-1965, were used as input to the computer programs for each of the systems investigated, with the exception of the solar-concentrating thermoelectric system. For the solar-heated system, a thermoelectric generator of 15 watt(e)/lb output was used to calculate system performance.

1964-1965 Material Characteristics*

Material	Application Temperatures, °C	Density, g/cc	Average Seebeck, μv/°C	Average ρ, ohm-cm	Average k, watt/cm°C
MCC 50	700-1200	2.34	+185	0.0045	0.0223
MCC 40 (p)	300-900	3.76	+240	0.0042	0.0336
MCC 60	900-1200	2.97	-125	0.0044	0.0430
MCC 40 (n)	300-950	3.99	-312	0.0046	0.0300
Graphite	500-1200	2.25	-	0.1135	1.0
Radiator, copper	500-700	8.9	-	0.0000	3.8
Insulation, thermal	500-1200	1.0	-	-	0.00064

Estimates of the average contact resistance per unit area of the thermoelements, used for the thermoelectric generator optimization studies, were selected on the basis of measurements made on representative hot-pressed 3/8-inch and 1/2-inch diameter segmented p- and n-type thermoelements. The resultant values were 0.0073 and 0.0131 ohms/cm^2 for p- and n-type thermoelements, respectively.

For purposes of projecting the performance of thermoelectric generators to the 1971-85 period, the following thermoelectric and structural material properties were used. H and M were used to signify improved high and medium temperature materials.

Predicted 1971-1985 Material Characteristics

Material	Application Temperatures, °C	Density, g/cc	Average Seebeck, μv/°C	Average ρ, ohm-cm	Average k, watt/cm°C
MCC H-p	700-1400	2.3	260	.0027	.022
MCC M-p	300-1050	3.7	340	.0025	.030
MCC M-n	900-1400	2.9	210	.0026	.037
MCC M-n	300-1050	4.0	350	.0027	.030

While advances will be made in techniques for reducing the resistance at junctions between contacts and thermoelectric materials, the 1964-65 values of contact resistance were used for the 1971-1985 performance predictions. If improved thermoelements with lower contact resistances are produced, the performance of future thermoelectric systems will be benefited accordingly.

*August 1964 material characteristics. These values supplant those used in the Third Quarterly Report, June 1964.

1. Nuclear Out-of-Pile and In-Pile Thermoelectric Space Power Systems

a. Introduction The results of preliminary investigations of nuclear out-of-pile systems and in-pile systems equipped both with and without heat transfer loops are herewith presented. The system coded HORSE utilizes a coolant loop to transport heat from a reactor to the hot junction of the thermoelements. The system coded TIGER requires no loop since the thermoelements are attached directly to the reactor and remove heat from the cold junctions by direct radiation. The system coded SWIFT utilizes a coolant loop to remove heat from the cold junctions of thermoelements. Calculations were done with both the 1964-65 and the 1971-85 sets of thermoelectric parameters for each of three different conceptual designs in order to determine the effect of these parameters on the performance of these systems.

The achievement of good Carnot efficiencies is aided by the use of MCC 50 and MCC 60 thermoelectric materials which permit the operation of thermoelectric generators at temperatures up to 1200-1400°C. However, thermoelectric generator operation at 1200-1400°C requires high-temperature reactors as heat sources.

Operating temperatures of 1200°C or higher preclude the use of hydrogen as a moderator in a nuclear reactor because it would diffuse out of the system. All other moderators are much less efficient than hydrogen. From the point of view of weight, the next best choice to hydrogen is beryllium, which would greatly increase the weight. Any moderated reactor not containing hydrogen would be heavier than one which did not contain a moderator. For this reason, a fast nuclear reactor was used in order to conserve weight.

During the study of the systems considered in this report, it was assumed that the payload had a diameter of 3 ft. and that it consisted of electronic equipment containing transistors. The radiation resistance of the transistors is the limiting factor which determines the reaction shielding requirements. Transistors can withstand approximately a 10^{13} neutron/cm^2 and 10^7 Rad (C)* of gamma rays over their lifetime. These limits were lowered to 5×10^{12} neutrons/cm^2 and 6×10^9 Rad (C) of gamma rays for systems containing coolant loops to allow for scattered radiation. Mission lifetime was assumed to be 10,000 hours in all cases.

*One Rad (C) is defined as the amount of radiation which produces 100 ergs in one gram of carbon.

b. Present State of the Art It is generally agreed that nuclear power will be the most likely source of power where quantities in excess of a few tens of kilowatts are needed for more than a few weeks' duration (Ref. 5). Nuclear systems based on thermoelectric energy conversion offer the following potential advantages:

1. Ruggedness and reliability
2. High power per unit area and volume
3. Elimination of orientation and deployment operations
4. Continuous power
5. Safety upon launch
6. Remote control start and stop

A large amount of development work has been done on three nuclear reactor-based space power systems: SNAP 10A, SNAP 2, and SNAP 8. These three systems utilize a zirconium hydride-moderated, thermal reactor as the heat source. Each of the three systems operates at temperatures well below 1200°C. SNAP 10A utilizes germanium-silicon thermoelectric elements located out-of-pile as the method of power generation. SNAP 2 and SNAP 8 produce power by means of alkali-metal, Rankine cycle turbines.

The expected electrical output, system performance, fuel cost, and system volumes are summarized for SNAP 10A, 2, and 8 in Table 28 (Ref. 6,7).

Table 28

EXPECTED PERFORMANCE OF PLANNED SPACE POWER SYSTEMS

System	Power Output, KW(e)	System Performance*, lbs./KW(e)	Fuel Cost, $/KW(e)	System Volume, ft.3/KW(e)
SNAP 10A	0.50	1300	96,000	-
SNAP 2	3.	400	16,000	-
SNAP 8	30.	>100	2,600	4.7

*unshielded

One other nuclear reactor-based, space power system is in the conceptual design stage. SNAP 50, based upon a ceramic-fueled, fast reactor, will use an alkali-metal turbine as the method of power generation. This system, having a 350 KW(e) output, has an estimated system performance of 15 lbs./KW(e), excluding the weight of shielding.

c. Out-of-Pile System (HORSE)

(1) Conceptual Design The proposed out-of-pile power system, as depicted in Figure 58, would consist of:

1. A reactor and controls.
2. A shadow shield for radiation attenuation.
3. A thermoelectric generator with integral radiators located between the shield and the payload.
4. A coolant system to transfer the heat from the reactor to the thermoelements.
5. Structural supports.

Placement of the thermoelements away from the reactor (out-of-pile) frees the reactor design from restrictions imposed by their presence, but necessitates the inclusion of a high-temperature coolant loop. This high-temperature, out-of-pile, reactor-based system for generation of electricity is coded HORSE.

The coolant used in these calculations was liquid lithium because it has a normal boiling point (1340°C) high enough to allow operation at a reasonable pressure at the required temperatures, and because it has excellent heat-transfer characteristics. The main disadvantage of lithium as a high-temperature coolant is that it is corrosive to almost all known materials of construction at 1200°C and hence it might be difficult to contain. An alternative to lithium would be an inert gas coolant, such as helium. Helium is expected to have good heat-transfer properties compared to other gases, but not as good as those of liquid lithium. It would not be corrosive, even at temperatures of 1200°C, but it would also be difficult to retain, since it can diffuse through solid materials as well as through minute cracks or holes at such high temperatures.

The fuels considered for the reactor were $U^{233}C$, $U^{235}C$, and $Pu^{239}C$. The 1200°C temperature eliminates metallic uranium or plutonium from consideration because of their low melting points.

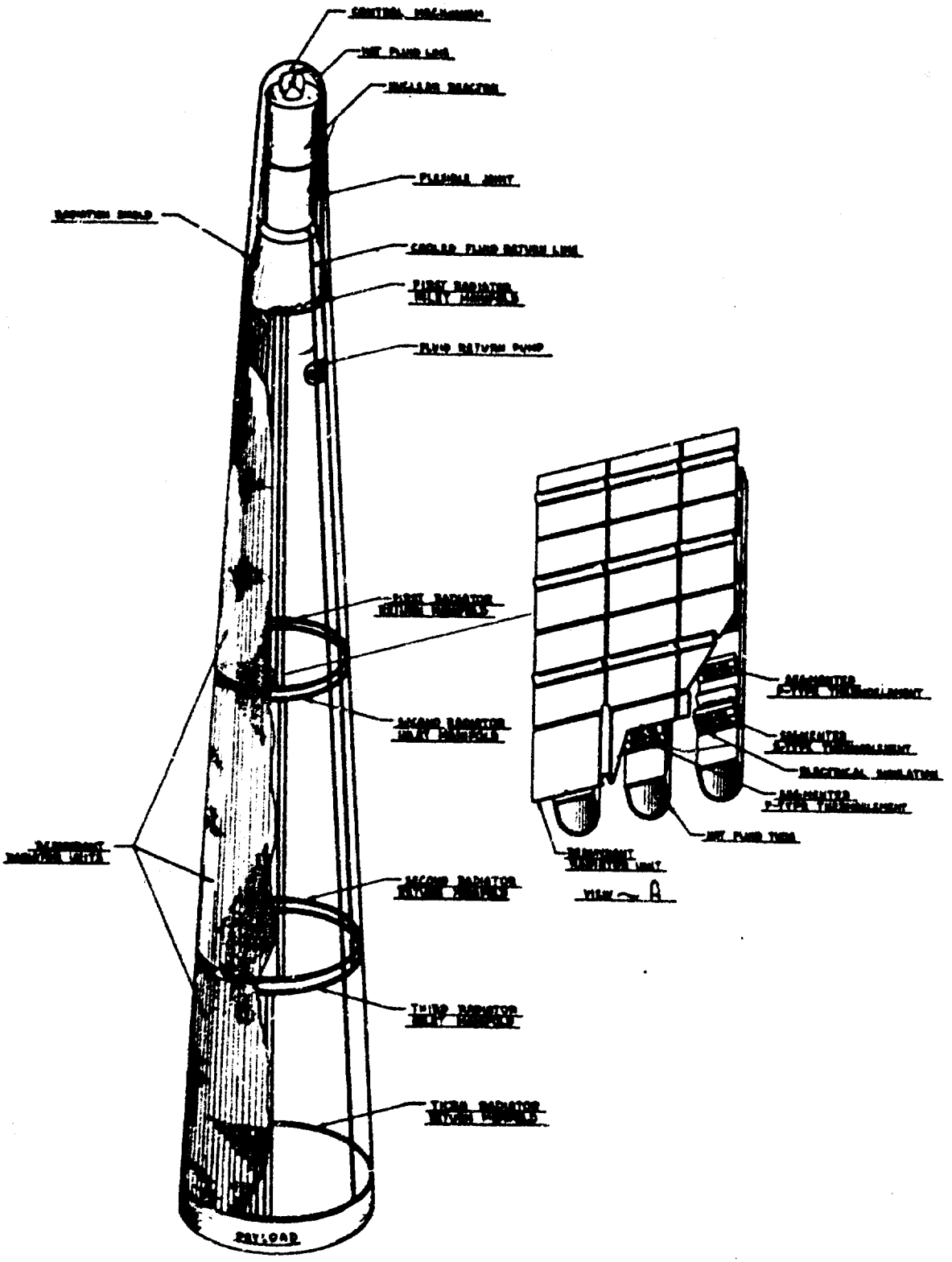

Figure 58. Conceptual Design of an Out-of-Pile Thermoelectric Space Power System with Coolant Loops (HORSE)

Both plutonium carbide (PuC) and uranium carbide (UC) have melting points well above 1200°C, and thermal conductivities which are higher than those of most other ceramic fuels.

The calculations were done on PuC rather than $U^{233}C$ or $U^{235}C$, because it has the most favorable nuclear properties and hence the smallest critical mass. The spherical critical masses of PuC, $U^{233}C$, and $U^{235}C$ were calculated to be 23.7 kg., 30.6 kg., and 101.3 kg., respectively, using multigroup neutron diffusion equations(Ref. 8). The plutonium was assumed to contain 4% Pu^{240}. The weights of reactors fueled with $U^{233}C$ would be slightly heavier than those fueled with $Pu^{239}C$. $U^{235}C$ reactors would be expected to be considerably heavier.

The present cost of plutonium, at $43 per gram, is high compared to the present cost of U^{235} at $11.32 per gram (or w/o U^{235})(Ref. 9). The price of plutonium, however, is expected to decrease to approximately $10 per gram as its supply becomes more plentiful as a byproduct from power reactors during the next four to eight years(Ref. 10). The figure of $10 per gram for plutonium fuel was used in these calculations rather than the present price of $43, since this is expected to be the prevailing price of plutonium by the time such systems are built in quantity.

The reactor core was designed in the shape of a cylinder which was split in half, radially (see Figure 58). The control of neutron leakage, and thus the reactor power level, is effected by moving the top and bottom halves of the cylindrical core closer together or farther apart. The control mechanism, located on top of the core, pushes against three support rods while the reactor is in weightless operation in space. The halves are held apart by shims during launch which can be removed once the generator is in a proper orbit or safely in space. This arrangement reduces the need for massive support rods.

The coolant tubes, made of high-temperature corrosion-resistant material, would pass through the reactor core parallel to its axis, but would fit loosely to allow movement of the halves relative to each other. Heat would be transmitted from the reactor core to the tube walls by radiation.

The distance from the lower face of the core to the payload was assumed to be 15 feet for the smaller units. This distance was lengthened for the larger units considered, in order to allow the larger number of thermoelectric elements and radiators to be positioned between the shadow shield and the payload. The generator and radiator were divided into redundant systems to increase the overall system reliability. The pumps were assumed to

be centrifugal ones that could be powered by interrupted DC currents with an assumed overall efficiency of 40%. The pumps would be placed in coolant return lines to the core.

A shadow shield in the shape of a frustrum of a cone was assumed. The shield consists of two parts, an inner portion of gamma ray shielding composed of depleted uranium and located adjacent to the core, and a neutron shield composed of lithium hydride encased in a stainless steel container 0.109 inches thick and located between the gamma shield and the payload.

(2) Performance Characteristics A computer program was written to facilitate the sizing of the HORSE system. The assumptions made and the equations used are given in Appendix I.

To calculate the performance characteristics, a core height, a coolant tube diameter, and a coolant fluid velocity were initially assumed. Based upon these input parameters the heat transfer taking place inside the reactor core was calculated and the number of tubes required was calculated. The pressure drop to the coolant tubes was calculated and the pump power was also calculated. Following these calculations, the reactor core was sized, based upon the amount of dilution included by introducing the coolant tubes. At this point the reactor shielding was designed. The thicknesses of the depleted uranium and lithium hydride were calculated by the removal cross-section method in a manner similar to that used in designing the shields for SNAP 10A, 2, and 8. The diameters of the shadow shield components were determined by geometrical considerations. Finally, the generator was sized. Initially, a separation distance of 15 feet was assumed between the back of the reactor core and the payload. However, if the radiator could not be fitted in the separation distance, the distance was lengthened.

Three sizes of units, namely, 3 KW(e), 30 KW(e) and 350 KW(e), were sized to correspond roughly to units presently being designed (SNAP 2, SNAP 8, and SNAP 50). Parameter runs were made using the program to determine the optimum core height, fluid velocity, and tube diameter for units of these sizes. Systems' performances and lbs/KW(e) were calculated for 3 KW(e) units with a core height of 0.75 feet, using tube diameters ranging from 0.25 to 1.50 inches and fluid velocities ranging from 5 to 50 ft./sec. The results of these calculations are shown in Table 29 . The best rating was attained with a tube diameter of 0.50 inch O.D. and a fluid velocity of 15 ft./sec. Similar runs were also made for 30 KW(e) and 350 KW(e) units each having a core height of 0.8 ft. The results of these calculations, recorded in Tables 30 and 31, also show the best performance using the 0.5-inch diameter tubes and the 15 ft./sec. velocity.

Table 29

EFFECT OF FLUID VELOCITY AND TUBE DIAMETER ON SYSTEM PERFORMANCE OF PuC-FUELED, 3 KW(e) UNITS

(No reflector, core height = 0.75 feet)

Fluid Velocity, ft./sec.	Tube OD, Inches: 0.25	0.50	0.75	1.00	1.25	1.50
	System Performance, lbs./KW(e)					
5	130	118	118	122	128	134
10	119	115	119	124	124	129
15	119	115	120	122	127	133
20	118	116	118	123	129	136
25	118	117	119	125	132	140
30	120	118	121	128	135	144
40	123	123	125	134	143	155
50	128	128	132	143	155	171

The effect of core height was then investigated. System performances were calculated for 3, 30 and 350 KW(e) units, assuming 0.50-inch OD tubes and 15 ft./sec. coolant velocity. The results of these calculations, presented in Table 32, show that the optimum performance for a 3 KW(e) unit was obtained with a core height of 0.6 ft. Similar runs for a 30 KW(e) unit indicated the optimum core height to be 0.8 ft. and for the 350 KW(e) unit, to be 0.9 ft.

The effect of reflector savings on system performance was also calculated. Table 33 shows that for each of the three system power levels considered, the best performance was attained when no reflector was added. In all of the subsequent calculations, however, 2 cm. of reflector were assumed in order to provide an insulation for the reactor core. The amount of decrease in system performance made by adding 2 cm. of beryllium oxide reflector would not be great, yet it would conserve a considerable amount of heat in the reactor core.

System performances were calculated for 3, 30, and 350 KW(e) units at six radiator temperatures (500, 550, 600, 650, 700, and 750°C) and for nine thermoelement lengths between 0.4 and 2.0 cm. Consideration was given to four thermoelement cross-sections: 1/16-inch x 1/16-inch square, 1/8-inch x 1/8-inch square, 3/16-inch diameter circular,

Table 30

EFFECT OF FLUID VELOCITY AND TUBE DIAMETER ON SYSTEM PERFORMANCE OF PuC-FUELED, 30 KW(e) UNITS

(No reflector, core height = 0.8 ft.)

Fluid Velocity, ft./sec.	Tube OD, Inches			
	0.25	0.50	0.75	1.00
	System Performance, lbs./KW(e)			
5	47	37	35	38
10	37	33	35	38
15	36	32	35	39
20	36	33	36	40
25	36	33	37	41

Table 31

EFFECT OF FLUID VELOCITY AND TUBE DIAMETER ON SYSTEM PERFORMANCE OF PuC-FUELED, 350 KW(e) UNITS

(No reflector, core height = 0.8 ft.)

Fluid Velocity, ft./sec.	Tube OD, Inches			
	0.25	0.50	0.75	1.00
	System Performance, lbs./KW(e)			
5	-	32	29	38
10	33	26	28	36
15	31	25	30	37
20	31	26	31	38
25	30	27	32	40

Table 32

EFFECT OF CORE HEIGHT ON SYSTEM PERFORMANCE OF PuC-FUELED UNITS*

Core Height, ft.	System Performance, lbs/KW(e)		
	3 KW(e)	30 KW(e)	350 KW(e)
0.3	143	-	-
0.4	121	-	-
0.5	114	33	-
0.6	111	32	26
0.7	113	31	-
0.8	117	31	24
0.9	121	32	-
1.0	125	33	25
1.2	-	34	26
1.4	-	-	28
1.6	-	-	29

*Fluid velocity = 15 ft/sec, 0.50" OD x 0.30" ID tubes, no reflector

Table 33

EFFECT OF REFIECTOR SAVINGS ON SYSTEM PERFORMANCE OF PuC-FUELED UNITS*

Reflector Thickness, cm.	System Performance, lbs/KW(e)		
	3 KW(e) (core height, 0.75 ft.)	30 KW (e) (core height, 1.0 ft.)	350 KW(e) (core height, 2.95 ft.)
0	113	33	42
2	119	34	43
5	136	36	45
10	192	-	50

*Fluid velocity = 15 ft/sec, 0.50" OD x 0.30" ID tubes

and 1/4 inch diameter circular cross-sections). The results for 3 KW(e) units are listed in Tables 34, 35, 36 and 37 for 1964-65 thermoelectric parameters and in Tables 38 and 39 for 1971-85 thermoelectric parameters. For 30KW(e) units the 1964-65 results are listed in Tables 40, 41, 42, and 43 and the 1971-85 values in Tables 44 and 45. For 350 KW(e) units the 1964-65 values are listed in Tables 46 and 47 and the 1971-85 values in Tables 48 and 49.

The maximum performance of the out-of-pile (HORSE) power system at different power outputs is summarized in Figure 59. This figure shows that the system performance utilizing 1964-65 thermoelectric technology improves rapidly from its 150 lbs/KW(e) value for 3 KW(e) units to approximately 50 lbs./KW(e) for very large units. Utilizing 1971-85 technology the possible system performances are considerably improved, showing promise of achieving approximately 20-25 lbs/KW(e) for large units.

The effect of power output and thermoelectric parameters on system volume of HORSE units is shown in Figure 60. The cubic feet of system volume required decrease rapidly as power level is increased from 3 to 30 KW(e). The 1971-85 technology would enable construction of significantly more compact units in the larger output ranges [350 KW(e)].

The effect of power output and thermoelectric parameters on fuel cost is shown in Figure 61. The fuel costs quoted are only for the raw material and do not include fabrication costs. Figure 61 shows a marked decrease in fuel cost per KW(e) with increasing system power level for both the 1964-65 and 1971-85 thermoelectric parameters, the latter giving slightly lower costs than the former.

The highest lbs./KW(e) ratings occurred for units with low to intermediate (500-650°C) radiator temperatures and with rather short thermoelements (0.60 - 1.00 cm.). The system performance seems little affected by thermoelement cross-sectional area. These calculations indicate that the most important variable for HORSE systems is element length and that more work should be expended on the production of short elements if this type of system were to be pursued.

The main advantage of the HORSE concept is that it gives very good performance in lb./KW(e) ratings, comparing very favorably with lb./KW(e) ratings estimated for SNAP 2 and SNAP 8. The 1971-85 technology would enable construction of significantly more compact units in the larger [350 KW(e)] output ranges.

Table 34

EFFECT OF RADIATOR TEMPERATURE AND ELEMENT LENGTH ON SYSTEM PERFORMANCE OF PuC-FUELED, 3 KW(e) HORSE UNITS WITH 1/16"x1/16" SQUARE THERMOELEMENTS (1964 THERMOELECTRIC PARAMETERS)

	System Performance, lbs./KW(e)								
Element Length, cm.	0.40	0.60	0.80	1.00	1.20	1.40	1.60	1.80	2.00
Radiator Temp., °C:									
500	-	160	150	150	150	150	170	180	190
550	170	160	160	160	150	170	180	190	210
600	170	160	170	170	180	190	200	210	230
650	170	170	170	170	190	210	220	240	260
700	190	190	190	210	220	240	260	280	310
750	240	210	220	230	250	270	290	320	350

Table 35

EFFECT OF RADIATOR TEMPERATURE AND ELEMENT LENGTH ON SYSTEM PERFORMANCE OF PuC-FUELED, 3 KW(e) HORSE UNITS WITH 1/8"x1/8" SQUARE THERMOELEMENTS (1964 THERMOELECTRIC PARAMETERS)

	System Performance, lbs./KW(e)								
Element Length, cm.	0.40	0.60	0.80	1.00	1.20	1.40	1.60	1.80	2.00
Radiator Temp., °C:									
500	-	-	-	-	160	160	170	180	180
550	-	-	200	160	160	160	160	170	190
600	-	220	160	160	160	170	170	180	190
650	-	160	160	160	170	180	180	190	210
700	180	170	170	170	170	180	190	210	220
750	180	170	170	180	190	200	210	220	240

Table 36

EFFECT OF RADIATOR TEMPERATURE AND ELEMENT LENGTH ON SYSTEM PERFORMANCE OF PuC-FUELED, 3 KW(e) HORSE UNITS WITH 3/16" DIAMETER CYLINDRICAL THERMOELEMENTS (1964 THERMOELECTRIC PARAMETERS)

	System Performance, lbs./KW(e)								
Element Length, cm.	0.40	0.60	0.80	1.00	1.20	1.40	1.60	1.80	2.00
Radiator Temp., °C									
500	-	-	150	150	160	160	170	180	190
550	-	160	160	160	170	170	180	190	210
600	-	160	160	170	180	190	200	210	240
650	180	170	180	180	200	210	230	240	260
700	190	190	200	210	220	240	260	280	300
750	210	220	230	250	270	290	320	350	380

Table 37

EFFECT OF RADIATOR TEMPERATURE AND ELEMENT LENGTH ON SYSTEM PERFORMANCE OF PuC-FUELED, 3 KW(e) HORSE UNITS WITH 1/4" DIAMETER CYLINDRICAL THERMOELEMENTS (1964 THERMOELECTRIC PARAMETERS)

	System Performance, lbs/KW(e)								
Element Length, cm.	0.40	0.60	0.80	1.00	1.20	1.40	1.60	1.80	2.00
Radiator Temp., °C:									
500	-	-	-	-	160	160	160	170	180
550	-	-	-	160	150	160	170	180	180
600	-	-	160	150	160	170	180	180	190
650	-	160	160	160	170	170	170	200	220
700	-	200	170	170	180	190	200	210	230
750	190	180	190	200	210	230	250	270	290

Table 36

EFFECT OF RADIATOR TEMPERATURE AND ELEMENT LENGTH ON SYSTEM PERFORMANCE OF PuC-FUELED, 3 KW(e) HORSE UNITS WITH 1/16"x1/16" SQUARE THERMOELEMENTS (1971-85 THERMOELECTRIC PARAMETERS)

	System Performance, lbs./KW(e)								
Element Length, cm.	0.40	0.60	0.80	1.00	1.20	1.40	1.60	1.80	2.00
Radiator Temp., °C:									
500	-	140	130	130	130	140	140	150	150
550	140	130	130	130	130	130	140	150	150
600	130	130	130	130	130	140	140	150	150
650	130	130	130	130	130	140	140	150	150
700	130	130	130	130	140	140	140	150	160
750	130	130	130	140	140	140	150	150	160

Table 39

EFFECT OF RADIATOR TEMPERATURE AND ELEMENT LENGTH ON SYSTEM PERFORMANCE OF PuC-FUELED, 3 KW(e) HORSE UNITS WITH 3/16" DIAMETER CIRCULAR THERMOELEMENTS (1971-85 THERMOELECTRIC PARAMETERS)

	System Performance, lbs./KW(e)								
Element Length, cm.	0.40	0.60	0.80	1.00	1.20	1.40	1.60	1.80	2.00
Radiator Temp., °C:									
500	-	-	-	130	130	130	130	140	150
550	-	-	130	120	120	130	130	140	140
600	-	130	120	120	130	130	140	140	150
650	160	120	120	120	130	140	130	140	150
700	130	120	120	130	130	140	130	140	150
750	-	130	130	130	140	130	140	140	150

Table 40

EFFECT OF RADIATOR TEMPERATURE AND ELEMENT LENGTH ON SYSTEM PERFORMANCE OF PuC-FUELED, 30 KW(e) HORSE UNITS WITH 1/16"x1/16" SQUARE THERMOELEMENTS (1964 THERMOELECTRIC PARAMETERS)

	System Performance, lbs./KW(e)								
Element Length, cm.	0.40	0.60	0.80	1.00	1.20	1.40	1.60	1.80	2.00
Radiator Temp., °C:									
500	-	63	61	63	68	74	81	91	100
550	69	60	61	64	71	80	91	100	120
600	63	59	64	72	82	84	110	120	140
650	67	68	76	86	99	110	130	150	170
700	80	84	95	110	120	140	160	190	210
750	100	110	130	140	170	190	220	250	280

Table 41

EFFECT OF RADIATOR TEMPERATURE AND ELEMENT LENGTH ON SYSTEM PERFORMANCE OF PuC-FUELED, 30 KW(e) HORSE UNITS WITH 1/8"x1/8" SQUARE THERMOELEMENTS (1964 THERMOELECTRIC PARAMETERS)

	System Performance, lbs./KW(e)								
Element Length, cm.	0.40	0.60	0.80	1.00	1.20	1.40	1.60	1.80	2.00
Radiator Temp., °C:									
500	-	-	-	-	69	70	78	88	89
550	-	-	110	63	65	73	79	90	97
600	-	120	60	63	70	74	81	92	100
650	-	61	59	65	73	81	88	100	110
700	71	63	66	71	77	89	100	110	120
750	70	67	71	81	90	100	110	130	140

Table 42

EFFECT OF RADIATOR TEMPERATURE AND ELEMENT LENGTH ON SYSTEM PERFORMANCE OF PuC-FUELED, 30 KW(e) HORSE UNITS WITH 3/16" DIAMETER CYLINDRICAL THERMOELEMENTS (1964 THERMOELECTRIC PARAMETERS)

	System Performance, lbs./KW(e)								
Element Length, cm.	0.40	0.60	0.80	1.00	1.20	1.40	1.60	1.80	2.00
Radiator Temp., °C.									
500	-	-	60	60	65	73	80	90	100
550	-	60	59	64	71	80	91	100	120
600	-	62	62	73	82	94	110	120	140
650	74	69	77	86	99	110	130	150	170
700	81	85	94	110	120	140	160	190	210
750	100	110	120	140	170	190	220	250	280

Table 43

EFFECT OF RADIATOR TEMPERATURE AND ELEMENT LENGTH ON SYSTEM PERFORMANCE OF PuC-FUELED, 30 KW(e) HORSE UNITS WITH 1/4" DIAMETER CYLINDRICAL THERMOELEMENTS (1964 THERMOELECTRIC PARAMETERS)

	System Performance, lbs./KW(e)								
Element Length, cm.	0.40	0.60	0.80	1.00	1.20	1.40	1.60	1.80	2.00
Radiator Temp., °C.									
500	-	-	-	-	63	69	73	82	92
550	-	-	-	60	62	69	77	88	81
600	-	-	59	60	66	75	85	91	100
650	-	61	60	68	74	83	95	110	120
700	63	64	69	79	89	100	120	130	150
750	77	77	88	100	110	130	150	170	200

Table 44

EFFECT OF RADIATOR TEMPERATURE AND ELEMENT LENGTH ON SYSTEM PERFORMANCE OF PuC-FUELED, 30 KW(e) HORSE UNITS WITH 1/16"x1/16" SQUARE THERMOELEMENTS (1971-85 THERMOELECTRIC PARAMETERS)

	System Performance, lbs./KW(e)								
Element Length, cm.	0.40	0.60	0.80	1.00	1.20	1.40	1.60	1.80	2.00
Radiator Temp., °C:									
500	-	46	42	42	46	52	59	61	64
550	53	39	40	42	44	49	55	63	66
600	42	38	40	42	48	51	54	62	66
650	38	38	40	42	47	51	58	62	68
700	39	38	42	45	48	53	57	65	71
750	39	39	41	46	48	55	61	67	72

Table 45

EFFECT OF RADIATOR TEMPERATURE AND ELEMENT LENGTH ON SYSTEM PERFORMANCE OF PuC-FUELED, 30 KW(e) HORSE UNITS WITH 3/16" DIAMETER CYLINDRICAL THERMOELEMENTS (1971-85 THERMOELECTRIC PARAMETERS)

	System Performance, lbs./KW(e)								
Element Length, cm.	0.40	0.60	0.80	1.00	1.20	1.40	1.60	1.80	2.00
Radiator Temp., °C:									
500	-	-	-	45	41	44	49	55	62
550	-	-	43	35	38	42	47	52	59
600	-	39	34	37	41	45	51	58	65
650	71	33	34	36	40	45	51	58	59
700	37	34	36	40	45	51	48	55	62
750	36	36	38	43	49	47	54	60	68

Table 46

EFFECT OF RADIATOR TEMPERATURE AND ELEMENT LENGTH ON SYSTEM PERFORMANCE OF PuC-FUELED, 350 KW(e) HORSE UNITS WITH 1/16"x1/16" SQUARE THERMOELEMENTS (1964 THERMOELEMENT PARAMETERS)

	System Performance, lbs./KW(e)								
Element Length, cm.	0.40	0.60	0.80	1.00	1.20	1.40	1.60	1.80	2.00
Radiator Temp., °C:									
500	-	61	60	62	67	73	80	92	100
550	71	60	61	63	71	81	93	110	120
600	66	60	66	74	84	97	110	130	140
650	76	74	81	91	100	120	140	160	180
700	100	97	110	120	140	160	180	-	-

Table 47

EFFECT OF RADIATOR TEMPERATURE AND ELEMENT LENGTH ON SYSTEM PERFORMANCE OF PuC-FUELED, 350 KW(e) HORSE UNITS WITH 3/16" DIAMETER CYLINDRICAL THERMOELEMENTS (1964 THERMOELECTRIC PARAMETERS)

	System Performance, lbs./KW(e)								
Element Length, cm.	0.40	0.60	0.80	1.00	1.20	1.40	1.60	1.80	2.00
Radiator Temp., °C:									
500	-	-	55	57	63	72	79	90	100
550	-	57	57	63	71	81	92	100	120
600	-	62	66	74	84	96	110	120	140
650	82	74	82	91	100	120	140	-	-
700	100	97	110	120	140	150	-	-	-

Table 48

EFFECT OF RADIATOR TEMPERATURE AND ELEMENT LENGTH ON SYSTEM PERFORMANCE OF PuC-FUELED, 350 KW(e) HORSE UNITS WITH 1/16"x1/16" SQUARE THERMOELEMENTS (1971-85 THERMOELECTRIC PARAMETERS

	System Performance, lbs./KW(e)								
Element Length, cm.	0.40	0.60	0.80	1.00	1.20	1.40	1.60	1.80	2.00
Radiator Temp., °C:									
500	-	42	37	37	42	48	55	57	60
550	48	33	36	37	39	45	51	59	63
600	37	33	36	38	44	46	50	58	62
650	33	34	35	37	43	47	54	59	64
700	35	34	38	41	45	49	54	62	63
750	34	34	37	43	45	52	58	64	67

Table 49

EFFECT OF RADIATOR TEMPERATURE AND ELEMENT LENGTH ON SYSTEM PERFORMANCE OF PuC-FUELED, 350 KW(e) HORSE UNITS WITH 3/16" DIAMETER CYLINDRICAL THERMOELEMENTS (1971-85 THERMOELECTRIC PARAMETERS)

	System Performance, lbs./KW(e)								
Element Length, cm.	0.40	0.60	0.80	1.00	1.20	1.40	1.60	1.80	2.00
Radiator Temp., °C:									
500	-	-	-	40	35	39	44	50	58
550	-	-	38	28	32	36	41	47	54
600	-	33	28	30	35	40	47	54	61
650	65	26	27	30	35	40	47	54	55
700	29	28	31	35	40	47	44	50	58
750	29	30	33	39	45	42	49	56	65

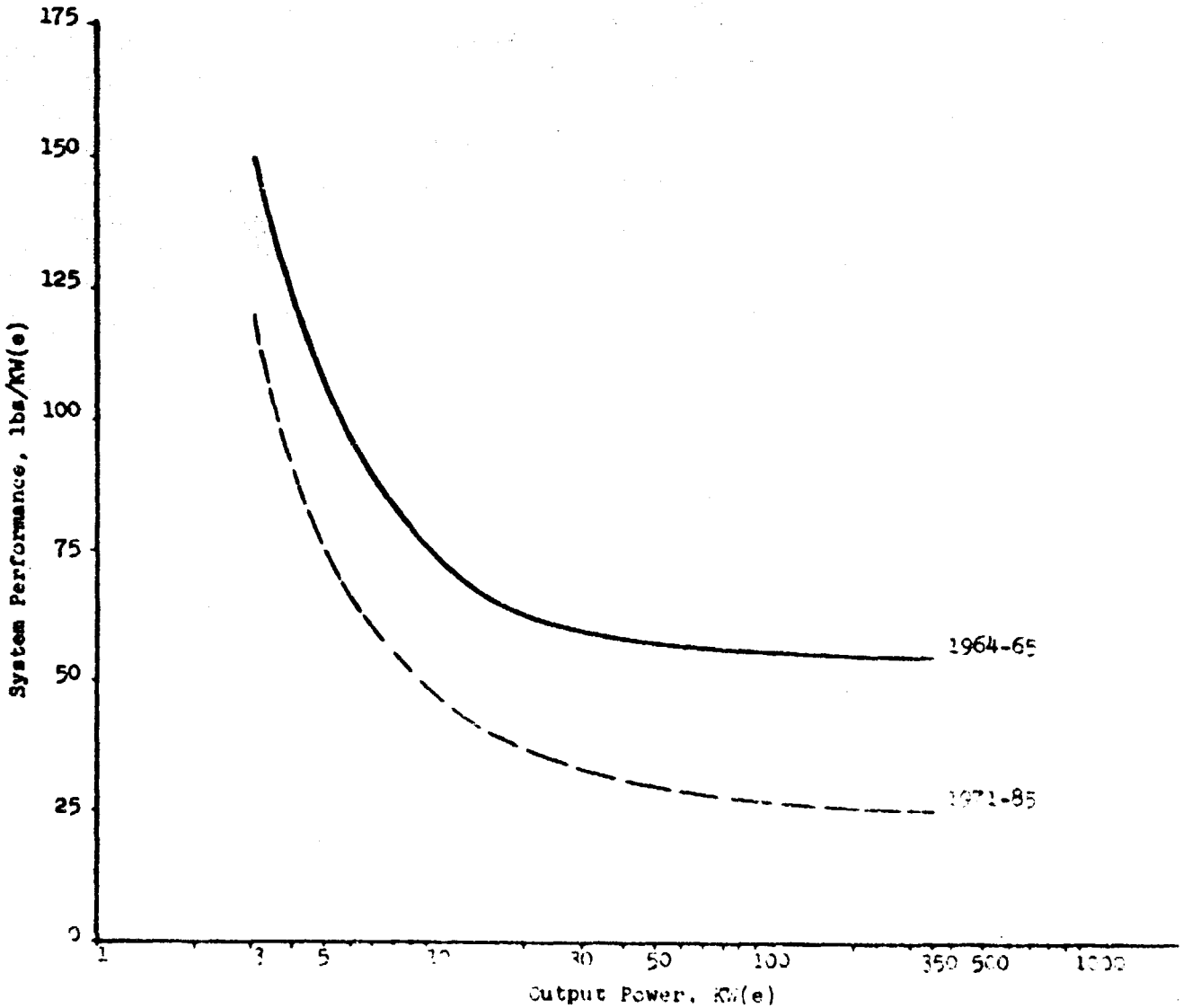

Figure 59. Maximum Performance vs. Output Power of the Out-of-Pile (HORSE) System

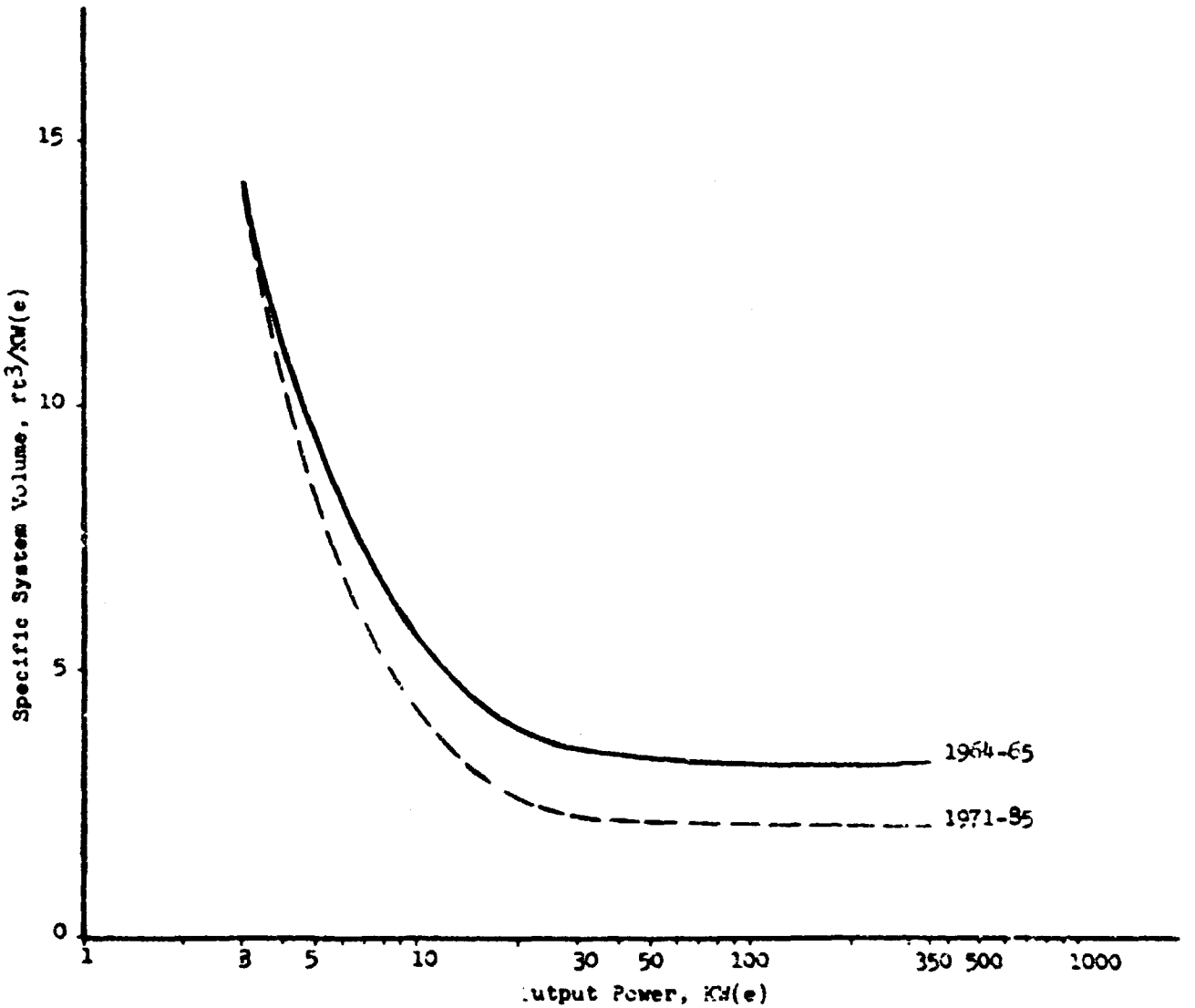

Figure 60. Specific System Volume vs. Output Power of the Out-of-Pile (HORSE) System

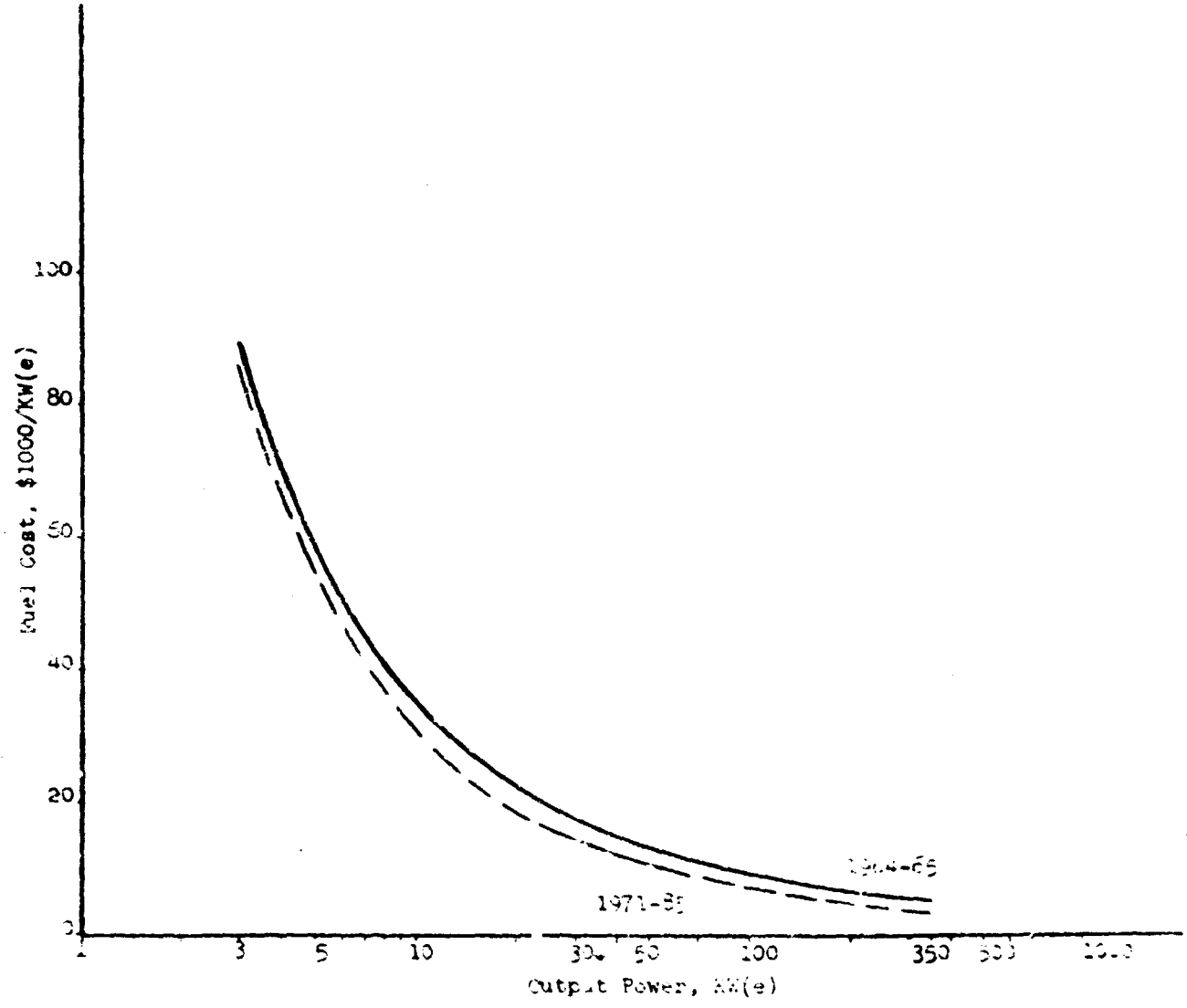

Figure 61. Fuel Cost vs. Output Power of the Out-of-Pile (HORSE) System

(3) Problem Areas Two major problems face the proposed HORSE power system concept:

- A fast reactor capable of 1200-1400°C sustained operation in space is needed.

- Liquid metal or other heat transfer loops capable of sustained operation at 1200-1400°C are required.

These same problems must be solved for any power system intended to utilize heat sources and liquid heat transfer loops at temperatures of 1200°C, or higher, to attain high specific performance in a space environment.

There are, of course, many additional problems that must be solved to make the HORSE concept practical. A partial list of problems to be solved includes:

- Development of suitably rugged, efficient, and long-lasting bonds between the materials of the liquid heat transfer loops and the thermoelements.

- Development of a complete safety program for fabrication, testing, launch, and operation in space.

- Integration of payload and power units.

- Development of long-lived fluid pumps. Since these pumps could be used to return cooled heat transfer media, they would operate at temperatures in the 500-700°C range.

- Verification that the thermoelectric properties of the thermoelectric materials, when operated at the proposed temperature, would not be seriously affected by radiation.

- Determination of micrometeorite-shielding requirements.

Here, again, solutions to most of the above and similar problems will be required for any space power system that would utilize a high-temperature nuclear energy heat source and liquid heat transfer loops.

(4) Probability of Success The probability of success for the HORSE space power system in the period 1965-70 is definitely dependent upon the availability of a fast reactor

and liquid heat transfer loops capable of extended operation at temperatures to 1200°C. The thermoelectric and component technology required could be established by 1967-68.

It is believed that fast reactor and structural materials technology is adequate to permit design and construction of a reactor capable of operating at the required temperatures in the 1965-70 period and there is a reasonable possibility that high-temperature loop materials could be developed to handle a liquid and/or evaporated lithium at 1200°C by 1970. It is believed that an immediate crash research and development program for the next 3-5 years could produce and ground-test a complete prototype system. It is estimated that the probability is not more than 35% for producing a successful HORSE type unit, ready for launching by 1970. On the assumption that advances in high-temperature materials technology will permit solution of the loop materials requirement problem in the 1971-85 period, it is estimated that the probability is 95-98% for successfully meeting the calculated system performance characteristics of this study.

d. In-Pile System Without Coolant Loop (TIGER)

(1) Conceptual Design The thermoelectric in-pile generator utilizing a reactor heat source (TIGER) consists of:

1. A reactor and controls.
2. A shadow shield for radiation attenuation.
3. Structural supports.
4. Thermoelectric elements.
5. Radiators attached directly to the surface of the reactor core.

Placement of the thermoelectric elements on the core and the radiators on the end of the elements eliminates the need for a coolant loop and its attendant probabilities for leaks, pump failure, line plugs and related difficulties. More importantly, elimination of these problem areas will significantly increase the reliability of the system.

A conceptual design for the TIGER space power system is shown in Figure 62. The reactor core differs from the cores used in HORSE in that it is not diluted by coolant tubes and often it is annular in shape. Annular cores have more surface area per unit of core weight than solid cores, allowing more

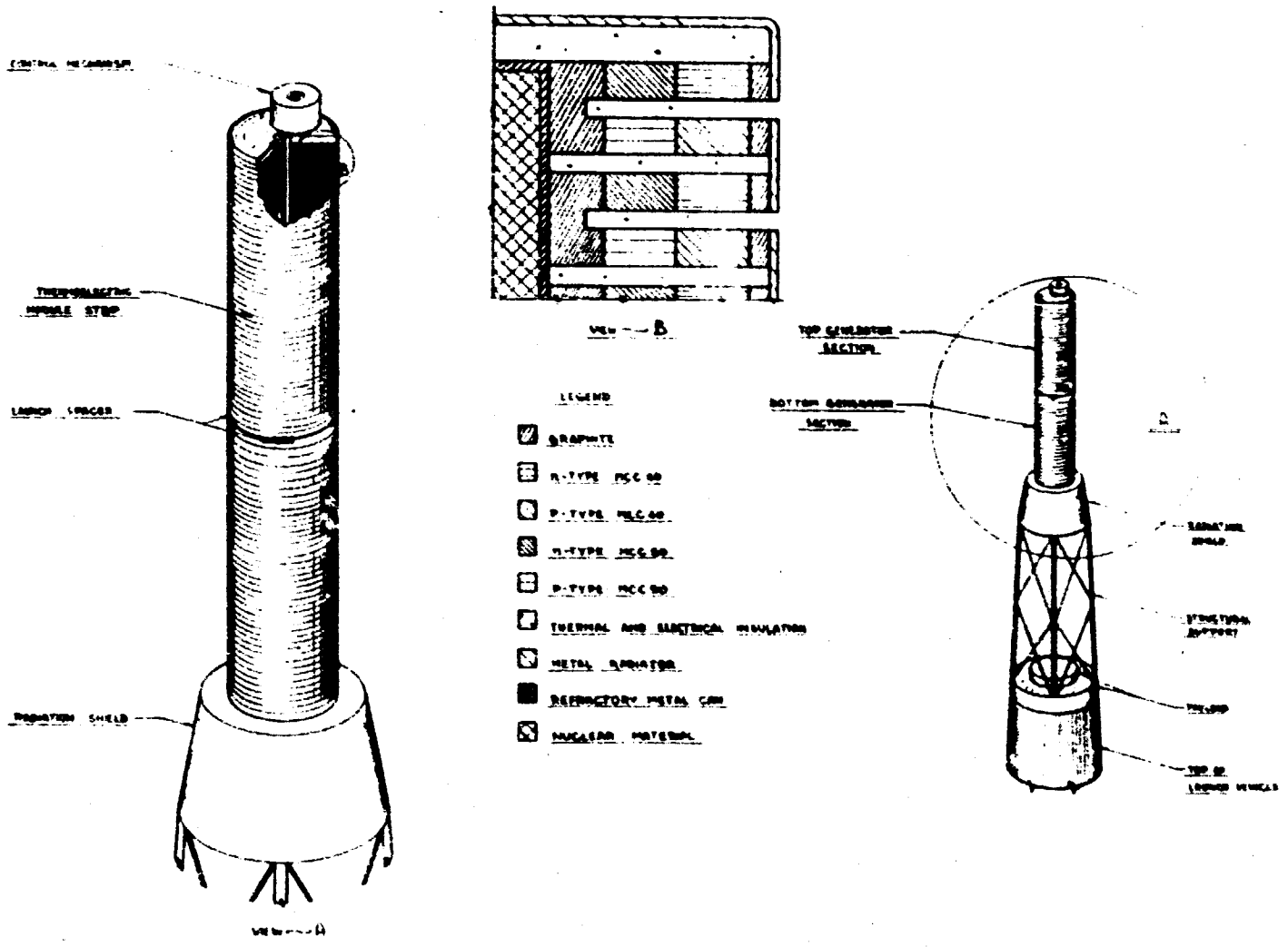

Figure 62. Conceptual Design of an In-Pile Thermoelectric Space Power System Without Coolant Loop (TIGER)

thermoelectric elements and higher power output per pound of fuel. Graphite shoes surround the reactor core. Segmented thermoelements are built around the graphite, as shown in views A and B. The thermoelements are surrounded by a metal radiator on which a highly emissive coating has been placed.

The core is split radially, as shown, into two halves. Control of the reactor takes place by changing the neutron leakage, which is adjusted by moving the top and bottom halves closer or farther apart. The interior of the annular reactor core is empty, so the neutron flux is not moderated in the annulus. The thermoelectric elements and graphite sections on the exterior of the core tend to act as a reflector, feeding the neutrons back into the core.

The derivation of the principal equations used to size the annular reactor cores assumes that the neutron flux is zero at the extrapolated outer radius of the reactor core and that the neutron current is zero at its inner radius. These assumptions have the effect of eliminating axial loss of neutrons by leakage through the annulus. Such assumptions generally hold for cores which have a ratio of height to diameter of ten or more and are approximately valid where the height-to-diameter ratio is as high as four or five.

The fuel used in the calculations was plutonium carbide, as in the HORSE system conceptual design. The fuel cost was again assumed to be $10.00 per gram. The temperature of the reactor was assumed to be hot enough to heat the hot junctions of the thermoelectric elements to 1200°C for the 1964-65 calculations and 1400°C for the 1971-85 calculations. In effect, the thermal conductivity of the reactor core was assumed to be infinite, and no calculations were made on the effect of thermal stress inside the core. For all of the calculations on the TIGER systems a constant distance of 15 feet between the core and the payload was used.

(2) Performance Characteristics A computer program was written to size these units. The equations and assumptions used are described in Appendix I.

The first major calculation in the program was sizing the reactor core, first assumed to be a solid cylinder. When the surface area on the solid cylinder proved to be insufficient, an annular type core was assumed. Next, gamma and neutron shadow shields composed of depleted uranium and lithium hydride, respectively, were sized as to thickness and diameter. Finally, the weight of structure necessary to support the reactor and shield was calculated.

Calculations were performed on units of two sizes, 3 KW(e) and 30 KW(e) with both the 1964-65 and 1971-85 sets of thermoelectric parameters. Parameter runs were made initially to determine the proper height to assume for the core. The results of parameter runs on both 3 KW(e) and 30 KW(e) units are shown in Tables 50 and 51, where system performance is tabulated as a function of core height. The numbers 9066 and 9110 refer to specific sets of thermoelectric generator parameters, the former with a high watt (e)/lb. of generator rating and the latter with a low rating. These tables reveal that system performance continually improves as core height is increased. In order to keep the core height from becoming unwieldy, however, it was decided to use a core height value of 6 ft. for the 3 KW(e) units and a value of 15 ft. as the core height for the 30 KW(e) units. Using these core heights, calculations of system performance were made for a large number of generators, and the results for 3 KW(e) units are recorded in Tables 52,53, and 54 for 1964-65 thermoelectric parameters and Tables 55,56 , and 57 for 1971-85 thermoelectric parameters. For 30 KW(e) units the 1964-65 results are listed in Tables 58,59 , and 60 and the 1971-85 results in Tables 61,62 , and 63 .

The system performance of TIGER units is shown in Figure 63 as a function of power level and thermoelectric parameters. The figure shows that power level has relatively little effect on system performance, but that changing from the 1964-65 set of thermoelectric parameters to the 1971-85 set improved the system performance from 290 lbs./KW(e) to 90 lbs./KW(e).

System volume/KW(e) is plotted as a function of power level and thermoelectric parameters in Figure 64. This figure shows that power level markedly influences system volume/KW(e) (21 ft.^{3}/KW(e) at 3 KW vs. 4.3 ft ^{3}/KW(e) at 30 KW(e) with 1964-65 thermoelectric parameters), and that improvement in thermoelectric parameters can improve system volume to a lesser extent.

The effect of power level and thermoelectric parameters on fuel cost is shown in Figure 65. As in the case of system performance, the fuel costs of TIGER units are affected markedly by the thermoelectric parameters and to a lesser extent by the power level. The sharp dependence of system performance and fuel cost on thermoelectric properties is to be expected since both of these criteria are determined by the amount of power obtainable per unit area of core external surface.

The best system performances for TIGER units are obtained with low-to-moderate length thermoelements (0.6 - 1.2 cm.) and low-to-moderate radiator temperatures (500-600°C) with 1/4-inch

Table 50

EFFECT OF CORE HEIGHT ON SYSTEM PERFORMANCE OF 3 KW(e) UNITS

Core Height, feet	System Performance, lbs/KW(e)	
	9066	9110
2.0	-	1300
4.0	560	1050
6.0	510	940
8.0	500	900
12.0	510	850
15.0	460	800

Table 51

EFFECT OF CORE HEIGHT ON SYSTEM PERFORMANCE OF 30 KW(e) UNITS

Core Height feet	System Performance, lbs/KW(e)	
	9066	9110
10	600	-
12	440	-
14	450	1780
16	440	1350
18	440	980
20	430	820
30	420	780
40	420	760

Table 52

EFFECT OF RADIATOR TEMPERATURE AND ELEMENT LENGTH ON SYSTEM PERFORMANCE OF PuC-FUELED, 3 KW(e), TIGER UNITS WITH 1/16" x 1/16" SQUARE THERMOELEMENTS (1964 THERMOELECTRIC PARAMETERS)

	System Performance, lbs./KW(e)								
Element Length, cm.	0.40	0.60	0.80	1.00	1.20	1.40	1.60	1.80	2.00
Radiator Temp., °C:									
500	-	390	450	-	450	490	520	550	590
550	440	-	480	510	550	590	630	670	710
600	500	530	580	620	670	720	-	830	890
650	610	660	720	780	850	920	990	1100	1100
700	770	850	930	1000	1100	1200	1300	-	1900
750	1000	1100	1200	-	1500	1600	1800	1900	-

Table 53

EFFECT OF RADIATOR TEMPERATURE AND ELEMENT LENGTH ON SYSTEM PERFORMANCE OF PuC-FUELED, 3 KW(e) TIGER UNITS WITH 3/16" DIAMETER CYLINDRICAL THERMOELEMENTS (1964 THERMOELECTRIC PARAMETERS)

	System Performance, lbs./KW(e)								
Element Length, cm.	0.40	0.60	0.80	1.00	1.20	1.40	1.50	1.80	2.00
Radiator Temp., °C:									
500	-	-	-	520	-	480	510	550	580
550	-	-	470	510	550	580	620	670	710
600	-	530	580	620	670	720	770	820	880
650	610	660	710	780	840	910	980	1100	1100
700	770	840	920	1000	1100	1200	1300	1400	1500
750	1000	1100	1200	-	1500	1600	1800	1900	2000

Table 54

EFFECT OF RADIATOR TEMPERATURE AND ELEMENT LENGTH ON SYSTEM PERFORMANCE OF PuC-FUELED, 3 KW(e) TIGER UNITS WITH 1/4" DIAMETER CYLINDRICAL THERMOELEMENTS (1964 THERMOELECTRIC PARAMETERS)

	System Performance, lbs./KW(e)								
Element Length, cm.	0.40	0.60	0.80	1.00	1.20	1.40	1.60	1.80	2.00
Radiator Temp., °C :									
500	-	-	-	-	-	-	350	380	420
550	-	-	-	-	360	390	440	490	540
600	-	-	370	410	460	520	590	-	-
650	-	430	-	-	490	530	560	600	640
700	470	500	550	590	640	690	740	800	840
750	610	670	720	800	860	930	1000	1100	1200

Table 55

EFFECT OF RADIATOR TEMPERATURE AND ELEMENT LENGTH ON SYSTEM PERFORMANCE OF PuC-FUELED, 3 KW(e) TIGER UNITS WITH 1/16"x1/16" SQUARE THERMOELEMENTS (1971-85 THERMOELECTRIC PARAMETERS)

	System Performance, lbs/KW(e)								
Element Length, cm.	0.40	0.60	0.80	1.00	1.20	1.40	1.60	1.80	2.00
Radiator Temp., °C:									
500	-	140	140	150	150	160	160	170	180
550	-	170	150	150	160	170	180	190	200
600	160	160	160	170	180	190	200	210	230
650	170	170	180	190	200	220	230	250	270
700	190	200	210	220	240	260	280	300	320
750	200	220	230	250	270	290	320	340	370

Table 56

EFFECT OF RADIATOR TEMPERATURE AND ELEMENT LENGTH ON SYSTEM PERFORMANCE OF PuC-FUELED, 3 KW(e) TIGER UNITS WITH 3/16" DIAMETER CYLINDRICAL THERMOELEMENTS (1971-85 THERMOELECTRIC PARAMETERS)

	System Performance, lbs/KW(e)								
Element Length, cm.	0.40	0.60	0.80	1.00	1.20	1.40	1.60	1.80	2.00
Radiator Temp., °C									
500	-	-	-	-	160	160	160	170	180
550	-	-	-	160	160	170	180	190	200
600	-	160	160	170	180	190	200	210	220
650	-	170	180	190	200	220	230	250	260
700	190	190	210	220	240	260	280	300	320
750	200	210	230	250	270	290	320	340	370

Table 57

EFFECT OF RADIATOR TEMPERATURE AND ELEMENT LENGTH ON SYSTEM PERFORMANCE OF PuC-FUELED, 3 KW(e) TIGER UNITS WITH 1/4" DIAMETER CYLINDRICAL THERMOELEMENTS (1971-85 THERMOELECTRIC PARAMETERS)

	System Performance, lbs./KW(e)								
Element Length, cm.	0.40	0.60	0.80	1.00	1.20	1.40	1.60	1.80	2.00
Radiator Temp., °C									
500	-	-	-	-	-	-	-	-	140
550	-	-	-	-	-	140	140	140	140
600	-	-	-	150	130	140	140	150	150
650	-	-	140	140	140	150	150	160	170
700	-	140	140	150	160	160	170	180	190
750	150	150	150	160	-	-	-	-	-

Table 58

EFFECT OF RADIATOR TEMPERATURE AND ELEMENT LENGTH ON SYSTEM PERFORMANCE OF PuC-FUELED, 30 KW(e) TIGER UNITS WITH 1/15"x1/16" SQUARE THERMOELEMENTS (1964 THERMOELECTRIC PARAMETERS)

Element Length, cm.	System Performance, lbs./KW(e)								
	0.40	0.60	0.80	1.00	1.20	1.40	1.60	1.80	2.00
Radiator Temp., °C									
500	-	330	350	390	430	460	490	540	580
550	350	390	430	460	510	560	570	660	710
600	420	460	520	570	630	-	-	-	-
650	530	590	660	-	-	-	-	-	-
700	640	-	-	-	-	-	-	-	-

Table 59

EFFECT OF RADIATOR TEMPERATURE AND ELEMENT LENGTH ON SYSTEM PERFORMANCE OF PuC-FUELED, 30 KW(e) TIGER UNITS WITH 3/16" DIAMETER CYLINDRICAL THERMOELEMENTS (1964 THERMOELECTRIC PARAMETERS)

Element Length, cm.	System Performance, lbs./KW(e)								
	0.40	0.60	0.80	1.00	1.20	1.40	1.60	1.80	2.00
Radiator Temp., °C									
500	-	-	-	390	420	460	490	540	580
550	-	-	420	460	500	550	590	650	660
600	-	460	520	560	610	-	-	-	-
650	540	-	640	870	-	-	-	-	-
700	650	-	-	-	-	-	-	-	-
750	-	-	-	-	-	-	-	-	-

Table 60

EFFECT OF RADIATOR TEMPERATURE AND ELEMENT LENGTH ON SYSTEM PERFORMANCE OF PuC-FUELED, 30 KW(e) TIGER UNITS WITH 1/4" DIAMETER CYLINDRICAL THERMOELEMENTS (1964 THERMOELECTRIC PARAMETERS)

	System Performance, lbs./KW(e)								
Element Length, cm.	0.40	0.60	0.80	1.00	1.20	1.40	1.60	1.80	2.00
Radiator Temp., °C:									
500	-	-	-	-	-	-	290	310	340
550	-	-	-	-	300	320	350	370	400
600	-	-	310	330	360	390	430	460	490
650	-	350	370	410	450	480	540	580	-
700	390	440	480	540	580	650	720	-	-
750	530	570	650	-	-	-	-	-	-

Table 61

EFFECT OF RADIATOR TEMPERATURE AND ELEMENT LENGTH ON SYSTEM PERFORMANCE OF PuC-FUELED, 30 KW(e) TIGER UNITS WITH 1/16"x1/16" SQUARE THERMOELEMENTS (1971-85 THERMOELECTRIC PARAMETERS)

	System Performance, lbs./KW(e)								
Element Length, cm.	0.40	0.60	0.80	1.00	1.20	1.40	1.60	1.80	2.00
Radiator Temp., °C:									
500	-	110	110	110	120	120	130	140	140
550	130	120	120	130	140	140	150	160	170
600	120	130	140	140	150	160	170	180	190
650	140	150	160	170	180	190	200	210	220
700	160	170	190	200	210	220	240	-	260
750	180	190	210	220	230	250	260	280	300

Table 62

EFFECT OF RADIATOR TEMPERATURE AND ELEMENT LENGTH ON SYSTEM PERFORMANCE OF PuC-FUELED, 30 KW(e) TIGER UNITS WITH 3/16" DIAMETER CYLINDRICAL THERMOELEMENTS (1971-85 THERMOELECTRIC PARAMETERS)

	System Performance, lbs./KW(e)								
Element Length, cm.	0.40	0.60	0.80	1.00	1.20	1.40	1.60	1.80	2.00
Radiator Temp., °C:									
500	-	-	-	-	130	120	130	140	140
550	-	-	-	130	-	140	150	160	160
600	-	130	-	140	150	160	170	180	190
650	-	150	160	170	180	190	200	210	220
700	170	170	180	200	210	220	230	-	260
750	180	190	200	220	230	-	260	280	300

Table 63

EFFECT OF RADIATOR TEMPERATURE AND ELEMENT LENGTH ON SYSTEM PERFORMANCE OF PuC-FUELED, 30 KW(e) TIGER UNITS WITH 1/4" DIAMETER CYLINDRICAL THERMOELEMENTS (1971-85 THERMOELECTRIC PARAMETERS)

	System Performance, lbs./KW(e)								
Element Length, m.	0.40	0.60	0.80	1.00	1.20	1.40	1.60	1.80	2.00
Radiator Temp., °C:									
500	-	-	-	-	-	-	-	-	120
550	-	-	-	-	-	-	-	90	90
600	-	-	-	100	90	90	100	100	110
650	-	-	100	100	100	110	110	120	130
700	-	110	110	110	120	130	140	140	150
750	110	110	120	130	-	-	-	-	-

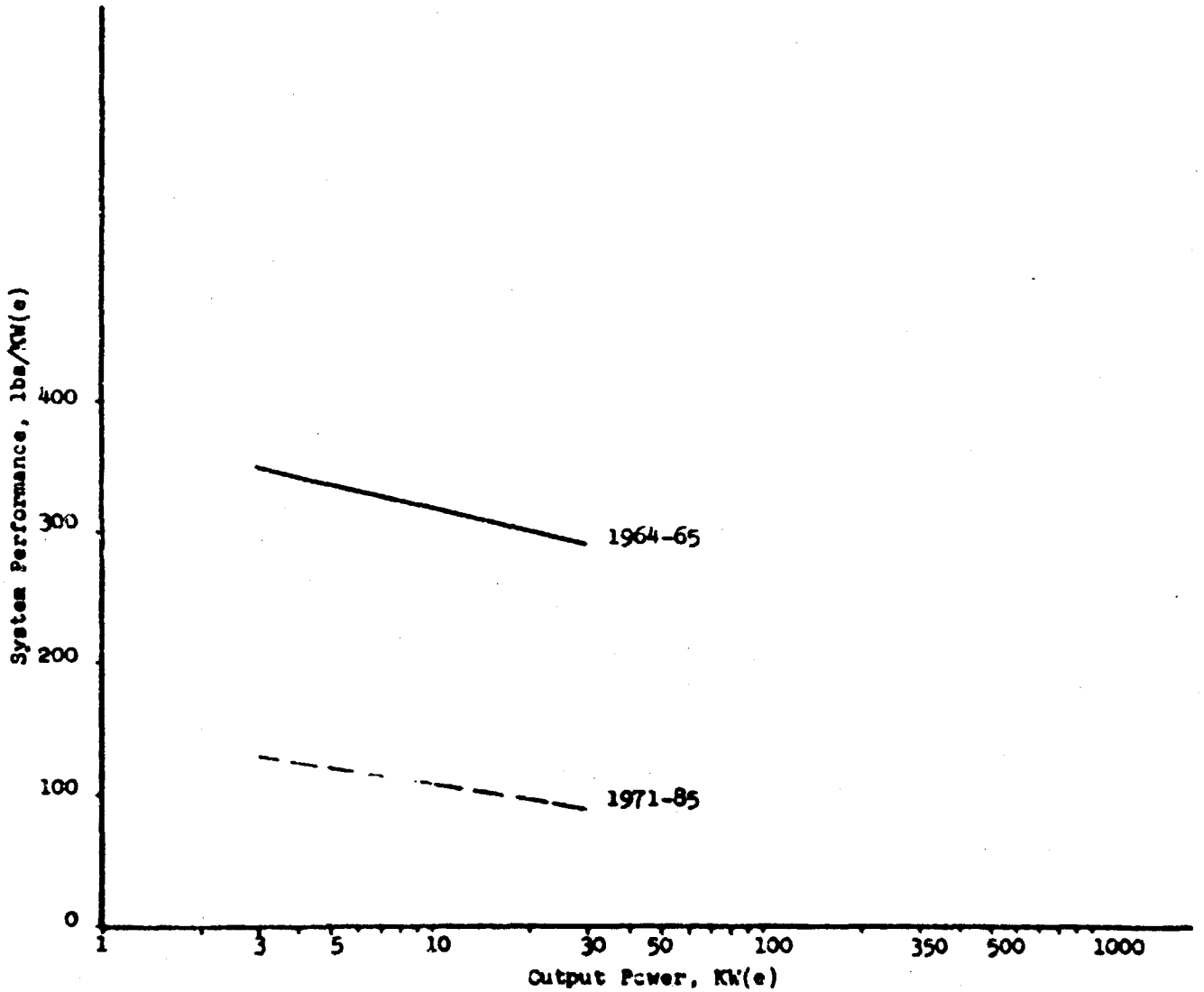

Figure 63. Effect of Electrical Output Level on Performance of PuC-Fueled TIGER System

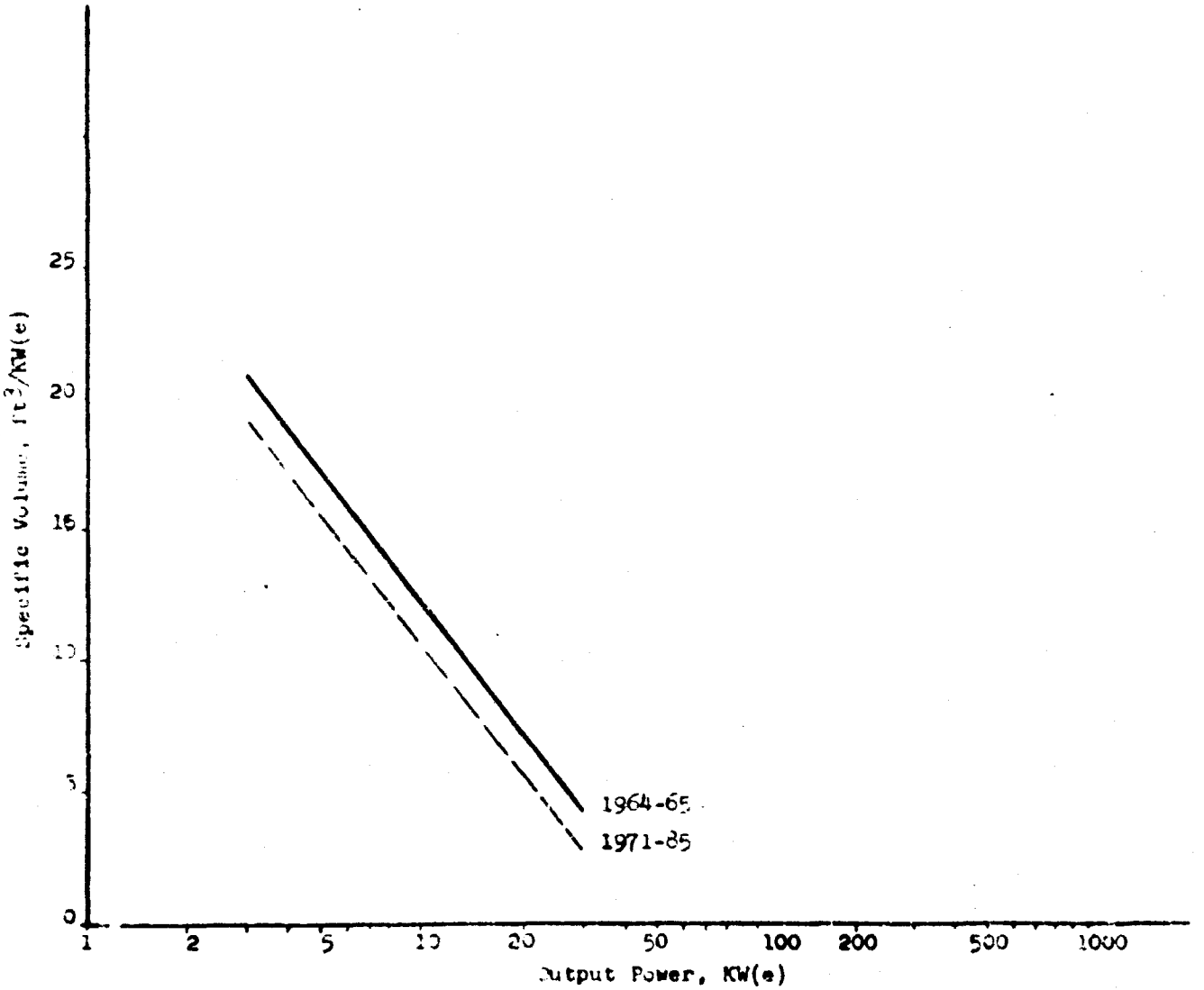

Figure 64. Effect of Electrical Output Level on Volume of PuC-Fueled TIGER System

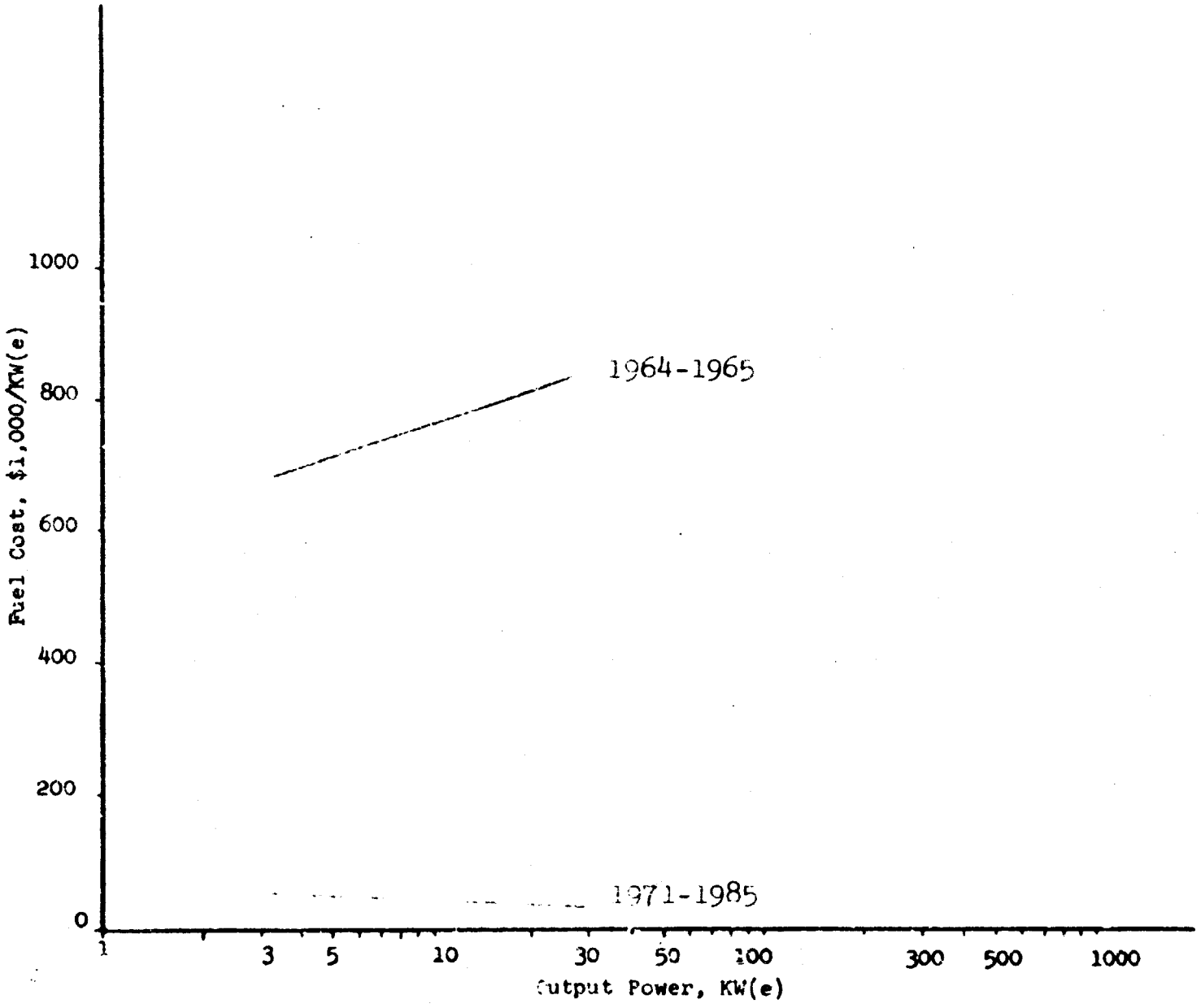

Figure 65. Fuel Cost vs. Electrical Output Level of PuC-Fueled TIGER Units

diameter cylindrical elements. The performance of these units, however, is considerably below that obtained with HORSE or SWIFT units.

The chief advantage of the in-pile (TIGER) system, with no coolant loop, is that it would have a higher reliability than other systems with liquid coolant loops. Systems containing coolant loops are subject to failure of many kinds: (1) loosening of fittings from vibration during takeoff; (2) leaks due to thermal stresses when putting system into operation; (3) puncturing of loop tubes by meteorites; (4) failure from corrosion; (5) pump failure; (6) plugging of tubes from deposition of products of corrosion; and, (7) freezing of lithium coolant with resultant failure of system. These problems are avoided in the TIGER conceptual design.

The use of redundant electrical circuits in the TIGER system concept would minimize meteorite damage to the electrical output of the system. Impacts from meteorites would likely have little effect on system performance, other than damage to those thermoelectric components suffering direct hits. The only moving part in the TIGER concept is the mechanism for moving the two halves of the reactor.

(3) Problem Areas A serious problem with the TIGER concept is that the amount of radiator area required is rather large per thermoelement. Anticipated improvements in the properties of available thermoelectric materials would directly increase the overall system efficiency and reduce the amount of heat which must be radiated per couple. Increasing the thermal efficiency of the couples would permit decreasing the radiator area proportionately and allow the electrical output of the system to be increased with no appreciable change in weight or cost of fuel material. Exceptionally large improvements in thermoelectric properties would have to be made, however, before TIGER units could successfully compete with HORSE or SWIFT units on the basis of system performance.

Another important problem for the TIGER type of unit is the lack of a fast reactor capable of operating at 1200-1400°C. It is believed that this type of reactor could be made available by 1970, if an intensified development program were begun immediately. The low system performance relative to a coolant loop system is a significant disadvantage of the present TIGER power system concept. Units of the HORSE type have much less weight per kilowatt(e) of output, which for a weight-limited mission could be a serious disadvantage.

(4) Probability of Success System reliability, and the probability of success in meeting mission requirements, are significantly enhanced because coolant loops are not used in the TIGER system concept. It is anticipated that thermoelectric materials of the desired properties will be available in 1966-67. These factors, coupled with the likelihood that design technology and materials of construction will be available for a fast reactor 1200°C heat source, give the TIGER concept quite a high (>90%) probability of research success in the 1965-70 period.

e. In-Pile Systems with Coolant Loops (SWIFT)

(1) Conceptual Design The system for power generation with in-pile fluid-cooled thermoelectric elements (SWIFT), as shown in Figure 66, consists of:

1. A reactor and controls.
2. Thermoelectric elements joined to the core.
3. A radiation shadow shield.
4. A section of radiator external to the reactor core.
5. A coolant loop.
6. Structural supports.

The coolant system runs over the cold ends of the thermoelements, removes heat from them, and then transports it to radiators located externally. The coolant used in the initial calculations was liquid lithium. The temperature of this coolant system, however, would be much lower than that used in HORSE, since the radiator temperature is far below the 1200-1400°C hot-junction temperature.

The reactor is equipped with spacers to prevent the top and bottom halves of the reactor from being driven together during launch. These are removed after the system is in orbit and has become weightless. The thermoelements radiate a small amount of heat directly from the cold junctions: then the coolant loop takes the remaining heat to be rejected and carries it back behind the shadow shield to a massive radiator area. The radiator area is divided into redundant units to aid system reliability. If additional radiator area is needed, more could be made available in the form of large, flat planes which could be extended radially from the reactor core. These wing-like projections could be quite large and would unfold after launch. Their radially

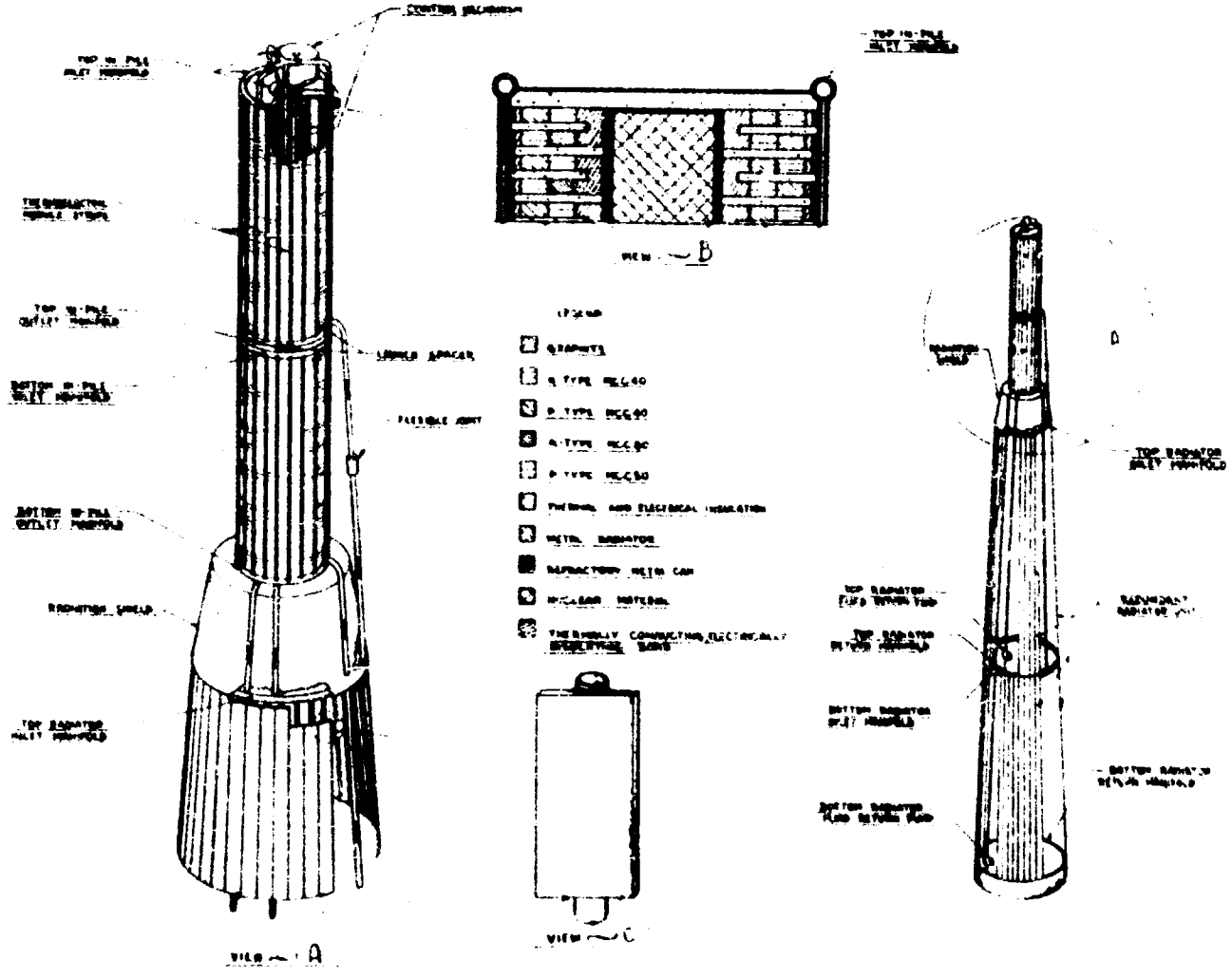

Figure 66. Conceptual Design of an In-Pile Thermoelectric Space Power System with Coolant Loops (SWIFT)

extended position would minimize the amount of scattered radiation which would be received by the payload.

The reactor core would be made in the shape of either an annular or solid cylinder. All of the elements are fixed on the exterior of a solid core, if possible. If not, then an annular core is used, and if the annulus is large enough, elements are placed on the inside of the annulus as well as on the outside. In the latter case, coolant tubes are fed through the inside of the annulus as well as around the outside. The shadow shield is composed of a layer of depleted uranium to absorb gamma rays and a layer of lithium hydride encased in stainless steel to absorb neutrons. The pumps used would be DC electromagnetic or thermoelectric pumps. The distance between the reactor core and the payload was fixed at 15 feet in all cases.

(2) Performance Characteristics A computer program was written to size SWIFT units for a given specified power output. The equations and assumptions used are described in Appendix I. The program starts by calculating a required surface area for the reactor core based upon the watts produced per couple and the cross-sectional area required per couple. Initially all of the elements were assumed to be attached to the exterior of a solid core up to 2.5 feet in length. If the surface area was insufficient, then annular core shape was assumed. The length of 2.5 feet was used because cores half as long, but annular in shape, would have an inside hole large enough to accommodate additional elements and yet the weight of fuel per centimeter of core length would be little changed. As a net result there would be almost twice as much core area per unit weight of core material. The correct ratio of core height to core diameter for annular-shaped cores was established by parameter runs. The results of calculations, shown in Table 64 , show that the most advantageous height-to-diameter ratio would be approximately 6.0 for 3 KW(e) units.

The effect of core height-to-diameter ratio on system performance for 30 KW(e) units is shown in Table 65 for a more favorable set of generator characteristics. This data indicates that the optimum core height-to-diameter ratio is about 5.0 for 30 KW(e) units. For 350 KW(e) units the optimum ratio is approximately 4.0 as shown in Table 66.

Calculations were run with thermoelements at different lengths and at different radiator temperatures. The element lengths used ranged from 0.2 cm to 2.0 cm, in increments of 0.2 cm. The radiator temperatures used were varied from 250°C to 750°C. These runs were made using 3/16-inch x 1/16-inch square and 3/16-inch diameter cylindrical thermoelements. Additional runs with 1/8-inch x 1/8-inch square and 1/4-inch diameter cylindrical thermo-

Table 64

EFFECT OF CORE HEIGHT-TO-DIAMETER RATIO ON SYSTEM PERFORMANCE FOR PuC-FUELED, 3 KW(e) SWIFT UNITS

Height-to-Diameter Ratio	System Performance, lbs/KW(e)
1.0	790
5.0	780
8.0	780
10.0	790
15.0	810

Table 65

EFFECT OF CORE HEIGHT-TO-DIAMETER RATIO ON SYSTEM PERFORMANCE FOR PuC-FUELED, 30 KW(e), SWIFT UNITS

Height-to-Diameter Ratio	System Performance, lbs/KW(e)
2.0	67
5.0	66
8.0	67
10.0	68
15.0	75

Table 66

EFFECT OF CORE HEIGHT-TO-DIAMETER RATIO ON SYSTEM PERFORMANCE FOR PuC-FUELED, 350 KW(e), SWIFT UNITS

Height-to-Diameter Ratio	System Performance, lbs/KW(e)
2.0	56
4.0	55
5.0	56
6.0	56
15.0	56

elements were made at the 350 KW(e) level.

The system performances for 3 KW(e) units are listed in Tables 67 and 68 with 1964-65 thermoelectric parameters and Tables 69 and 70 with 1971-85 thermoelectric parameters. For 30 KW(e) units the 1964-65 data is listed in Tables 71 and 72 and the 1971-85 data in Tables 73 and 74. For 350 KW(e) units the 1964-65 data is listed in Tables 75, 76, 77, and 78 and the 1971-85 data in Tables 79, 80, 81, and 82. The best system performances at each of the three power levels are plotted in Figure 67 for both sets of thermoelectric parameters. These data show that increasing power level and improvement in thermoelectric properties both markedly improve system performance of SWIFT units.

The specific volumes of SWIFT units are plotted as a function of power level and thermoelectric parameters in Figure 68. The specific volumes are shown to be strongly influenced by power level but to be virtually unaffected by the thermoelectric properties.

The fuel costs are plotted in Figure 69 against power level and thermoelectric parameters. Increasing values of both of these variables are shown to have a significant effect in decreasing fuel costs per KW(e).

The best system performances seem to result with the larger diameter thermoelements with short-to-moderate lengths (0.4-0.8 cm.) operated at 450 °C or 750 °C rather than at 250 °C. The performance value of 15 lbs./KW(e) calculated for a 350 KW(e) unit with 1971-85 thermoelectric parameters is the best performance calculated with any of the three nuclear-based systems investigated.

Another important advantage of SWIFT systems is that the coolant loop used with this concept would operate at much lower temperatures than the coolant loop in a HORSE system. The lower coolant temperature should markedly decrease corrosion problems experienced with the liquid metal or other heat transfer media used. It is quite likely that much of the hardware developed for other space power systems (e.g., SNAP 10A) could be readily adapted to the SWIFT concept.

(3) Problem Areas As with the HORSE and TIGER system concepts, a high-temperature (1200-1400 °C), fast reactor heat source is needed.

The favored annular or doughnut-shaped fast reactor core may offer some special problems over the more conventional solid core in reactor design, but it also offers the advantage of higher heat fluxes and more uniform heat transfer.

Table 67

EFFECT OF RADIATOR TEMPERATURE AND ELEMENT LENGTH ON SYSTEM PERFORMANCE OF 3 KW(e), PuC-FUELED, SWIFT UNITS WITH 1/16" x 1/16" SQUARE THERMOELEMENTS (1964 THERMOELECTRIC PARAMETERS)

	System Performance, lbs./KW(e)									
Element Length, cm.	0.20	0.40	0.60	0.80	1.00	1.20	1.40	1.60	1.80	2.00
Radiator Temp., °C:										
250	-	-	300	290	280	290	290	300	310	320
450	-	270	270	280	300	310	370	390	410	430
750	540	570	660	730	800	870	940	1000	1100	1200

Table 68

EFFECT OF RADIATOR TEMPERATURE AND ELEMENT LENGTH ON SYSTEM PERFORMANCE OF 3 KW(e), PuC-FUELED, SWIFT UNITS WITH 3/16" DIAMETER CYLINDRICAL THERMOELEMENTS (1964 THERMOELECTRIC PARAMETERS)

	System Performance, lbs./KW(e)									
Element Length, cm.	0.20	0.40	0.60	0.80	1.00	1.20	1.40	1.60	1.80	2.00
Radiator Temp., °C:										
250	-	-	160	160	170	180	190	200	210	220
450	-	210	220	240	260	280	300	300	340	360
750	270	320	370	430	490	550	620	700	770	850

Table 69

EFFECT OF RADIATOR TEMPERATURE AND ELEMENT LENGTH ON SYSTEM PERFORMANCE OF 3 KW(e), PuC-FUELED, SWIFT UNITS WITH 1/16" x 1/16" SQUARE THERMOELEMENTS (1971-85 THERMOELECTRIC PARAMETERS)

	System Performance, lbs./KW(e)									
Element Length, cm.	0.20	0.40	0.60	0.80	1.00	1.20	1.40	1.60	1.80	2.00
Radiator Temp., °C										
250	-	-	170	160	150	150	150	150	150	180
450	-	180	180	180	190	190	200	200	200	210
750	240	240	260	270	250	290	300	320	330	340

Table 70

EFFECT OF RADIATOR TEMPERATURE AND ELEMENT LENGTH ON SYSTEM PERFORMANCE OF 3 KW(e), PuC-FUELED, SWIFT UNITS WITH 3/16" DIAMETER CYLINDRICAL THERMOELEMENTS (1971-85 THERMOELECTRIC PARAMETERS)

	System Performance, lbs./KW(e)									
Element Length, cm.	0.20	0.40	0.60	0.80	1.00	1.20	1.40	1.60	1.80	2.00
Radiator Temp., °C										
250	-	-	160	160	170	170	180	180	180	180
450	-	-	-	110	110	110	110	110	110	110
750	110	110	100	110	120	130	140	150	160	170

Table 71

EFFECT OF RADIATOR TEMPERATURE AND ELEMENT LENGTH ON SYSTEM PERFORMANCE OF 30 KW(e), PuC-FUELED, SWIFT UNITS WITH 1/16" x 1/16" SQUARE THERMOELEMENTS (1964 THERMOELECTRIC PARAMETERS)

	System Performance, lbs./KW(e)									
Element Length, cm.	0.20	0.40	0.60	0.80	1.00	1.20	1.40	1.60	1.80	2.00
Radiator Temp., °C:										
250	-	-	200	200	190	190	190	200	210	210
450	-	170	170	180	190	210	220	240	250	270
750	410	320	450	510	580	640	700	730	770	870

Table 72

EFFECT OF RADIATOR TEMPERATURE AND ELEMENT LENGTH ON SYSTEM PERFORMANCE OF 30 KW(e), PuC FUELED, SWIFT UNITS WITH 5/16" DIAMETER CYLINDRICAL THERMOELEMENTS (1964 THERMOELECTRIC PARAMETERS)

	System Performance, lbs./KW(e)									
Element Length, cm.	0.20	0.40	0.60	0.80	1.00	1.20	1.40	1.60	1.80	2.00
Radiator Temp., °C										
250	-	-	80	90	100	110	120	130	140	140
450	-	60	70	85	100	110	130	140	160	180
750	90	130	180	230	270	330	400	440	500	560

Table 73

EFFECT OF RADIATOR TEMPERATURE AND ELEMENT LENGTH ON SYSTEM PERFORMANCE OF 30 KW(e), PuC-FUELED, SWIFT UNITS WITH 1/16" x 1/16" SQUARE THERMOELEMENTS (1971-85 THERMOELECTRIC PARAMETERS)

	System Performance, lbs./KW(e)									
Element Length, cm.	0.20	0.40	0.60	0.80	1.00	1.20	1.40	1.60	1.80	2.00
Radiator Temp., °C:										
250	-	-	92	84	81	80	80	81	83	85
450	-	71	68	68	71	74	77	81	85	90
750	110	110	110	120	120	130	140	150	160	170

Table 74

EFFECT OF RADIATOR TEMPERATURE AND ELEMENT LENGTH ON SYSTEM PERFORMANCE OF 30 KW(e), PuC-FUELED, SWIFT UNITS WITH 3/16" DIAMETER CYLINDRICAL THERMOELEMENTS (1971-85 THERMOELECTRIC PARAMETERS)

	System Performance, lbs./KW(e)									
Element Length, cm.	0.20	0.40	0.60	0.80	1.00	1.20	1.40	1.60	1.80	2.00
Radiator Temp., °C:										
250	-	-	36	37	39	41	43	46	48	51
450	-	25	26	30	33	36	40	44	48	52
750	24	34	42	50	58	66	75	84	92	100

Table 75

EFFECT OF RADIATOR TEMPERATURE AND ELEMENT LENGTH ON SYSTEM PERFORMANCE OF 350 KE(e), PuC-FUELED, SWIFT UNITS WITH 1/16" x 1/16" SQUARE THERMOELEMENTS (1964 THERMOELECTRIC PARAMETERS)

	System Performance, lbs./KW(e)									
Element Length, cm.	0.20	0.40	0.60	0.80	1.00	1.20	1.40	1.60	1.80	2.00
Radiator Temp., °C:										
250	-	-	190	160	160	-	180	-	180	200
450	-	160	150	-	-	-	-	-	-	-
750	-	-	-	-	-	-	-	-	-	-

Table 76

EFFECT OF RADIATOR TEMPERATURE AND ELEMENT LENGTH ON SYSTEM PERFORMANCE OF 350 KW(e), PuC-FUELED, SWIFT UNITS WITH 1/8" x 1/8" SQUARE THERMOELEMENTS (1964 THERMOELECTRIC PARAMETERS)

	System Performance, lbs./KW(e)									
Element Length, cm.	0.20	0.40	0.60	0.80	1.00	1.20	1.40	1.60	1.80	2.00
Radiator Temp., °C:										
250	-	-	68	75	81	90	96	105	110	-
450	-	43	54	63	79	-	90	110	130	180
750	56	95	-	-	-	-	-	-	-	-

Table 77

EFFECT OF RADIATOR TEMPERATURE AND ELEMENT LENGTH ON SYSTEM PERFORMANCE OF 350 KW(e) PuC-FUELED, SWIFT UNITS WITH 3/16" DIAMETER CYLINDRICAL THERMOELEMENTS (1964 THERMOELECTRIC PARAMETERS)

	System Performance, lbs./KW(e)									
Element Length, cm.	0.20	0.40	0.60	0.80	1.00	1.20	1.40	1.60	1.80	2.00
Radiator Temp., °C:										
250	-	-	74	79	86	94	98	110	115	-
450	-	48	59	70	74	75	86	130	210	240
750	76	100	-	-	-	-	-	-	-	-

Table 78

EFFECT OF RADIATOR TEMPERATURE AND ELEMENT LENGTH ON SYSTEM PERFORMANCE OF 350 KW(e) PuC-FUELED, SWIFT UNITS WITH 1/4" DIAMETER CYLINDRICAL THERMOELEMENTS (1964 THERMOELECTRIC PARAMETERS)

	System Performance, lbs./KW(e)									
Element Length, cm.	0.20	0.40	0.60	0.80	1.00	1.20	1.40	1.60	1.80	2.00
Radiator Temp., °C:										
250	-	-	89	92	98	100	110	115	120	120
450	-	63	70	80	-	-	140	160	-	190
750	160	-	-	-	-	-	-	-	-	-

Table 79

EFFECT OF RADIATOR TEMPERATURE AND ELEMENT LENGTH ON SYSTEM PERFORMANCE OF 350 KW(e), PuC-FUELED, SWIFT UNITS WITH 1/16" x 1/16" SQUARE THERMO-ELEMENTS (1971-85 THERMOELECTRIC PARAMETERS)

	System Performance, lbs./KW(e)									
Element Length, cm.	0.20	0.40	0.60	0.80	1.00	1.20	1.40	1.60	1.80	2.00
Radiator Temp., °C:										
250	-	-	81	73	69	67	66	66	67	69
450	-	57	54	55	57	59	61	63	67	70
750	68	73	82	91	93	170	220	-	240	-

Table 80

EFFECT OF RADIATOR TEMPERATURE AND ELEMENT LENGTH ON SYSTEM PERFORMANCE OF 350 KW(e), PuC-FUELED, SWIFT UNITS WITH 1/8" x 1/8" SQUARE THERMO-ELEMENTS (1971-85 THERMOELECTRIC PARAMETERS)

	System Performance, lbs./KW(e)									
Element Length, cm.	0.20	0.40	0.60	0.80	1.00	1.20	1.40	1.60	1.80	2.00
Radiator Temp., °C:										
250	-	-	24	25	27	29	32	34	35	38
450	-	-	15	18	21	24	27	30	34	37
750	-	17	23	30	36	45	49	57	65	-

Table 81

EFFECT OF RADIATOR TEMPERATURE AND ELEMENT LENGTH ON SYSTEM PERFORMANCE OF 350 KW(e), PuC-FUELED, SWIFT UNITS WITH 3/16" DIAMETER CYLINDRICAL THERMOELEMENT (1971-85 THERMOELECTRIC PARAMETERS)

	System Performance, lbs./KW(e)									
Element Length, cm.	0.20	0.40	0.60	0.80	1.00	1.20	1.40	1.60	1.80	2.00
Radiator Temp., °C:										
250	-	-	27	28	30	31	33	35	37	39
450	-	15	17	20	23	25	29	32	35	38
750	15	20	28	32	40	48	52	63	68	-

Table 82

EFFECT OF RADIATOR TEMPERATURE AND ELEMENT LENGTH ON SYSTEM PERFORMANCE OF 350 KW(e), PuC-FUELED, SWIFT UNITS WITH 1/4" DIAMETER CYLINDRICAL THERMOELEMENTS (1971-85 THERMOELECTRIC PARAMETERS)

	System Performance, lbs./KW(e)									
Element Length, cm.	0.20	0.40	0.60	0.80	1.00	1.20	1.40	1.60	1.80	2.00
Radiator Temp., °C:										
250	-	-	33	34	35	36	37	39	41	43
450	-	21	22	24	27	30	33	36	39	41
750	24	30	-	-	-	-	-	-	-	-

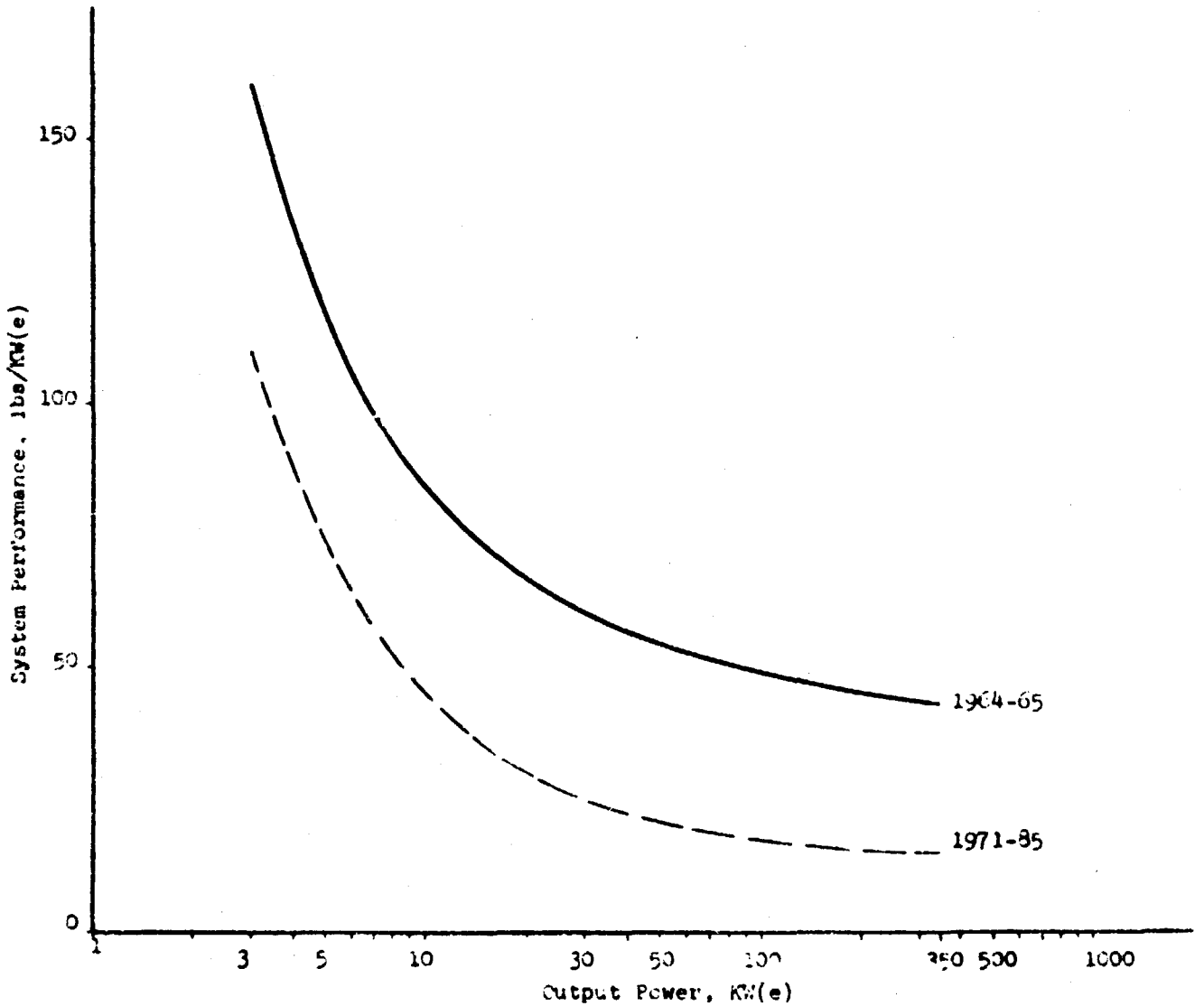

Figure 67. Effect of Output Power Level and Thermoelectric Parameters on System Performance of In-Pile, with Loop (SWIFT) Systems

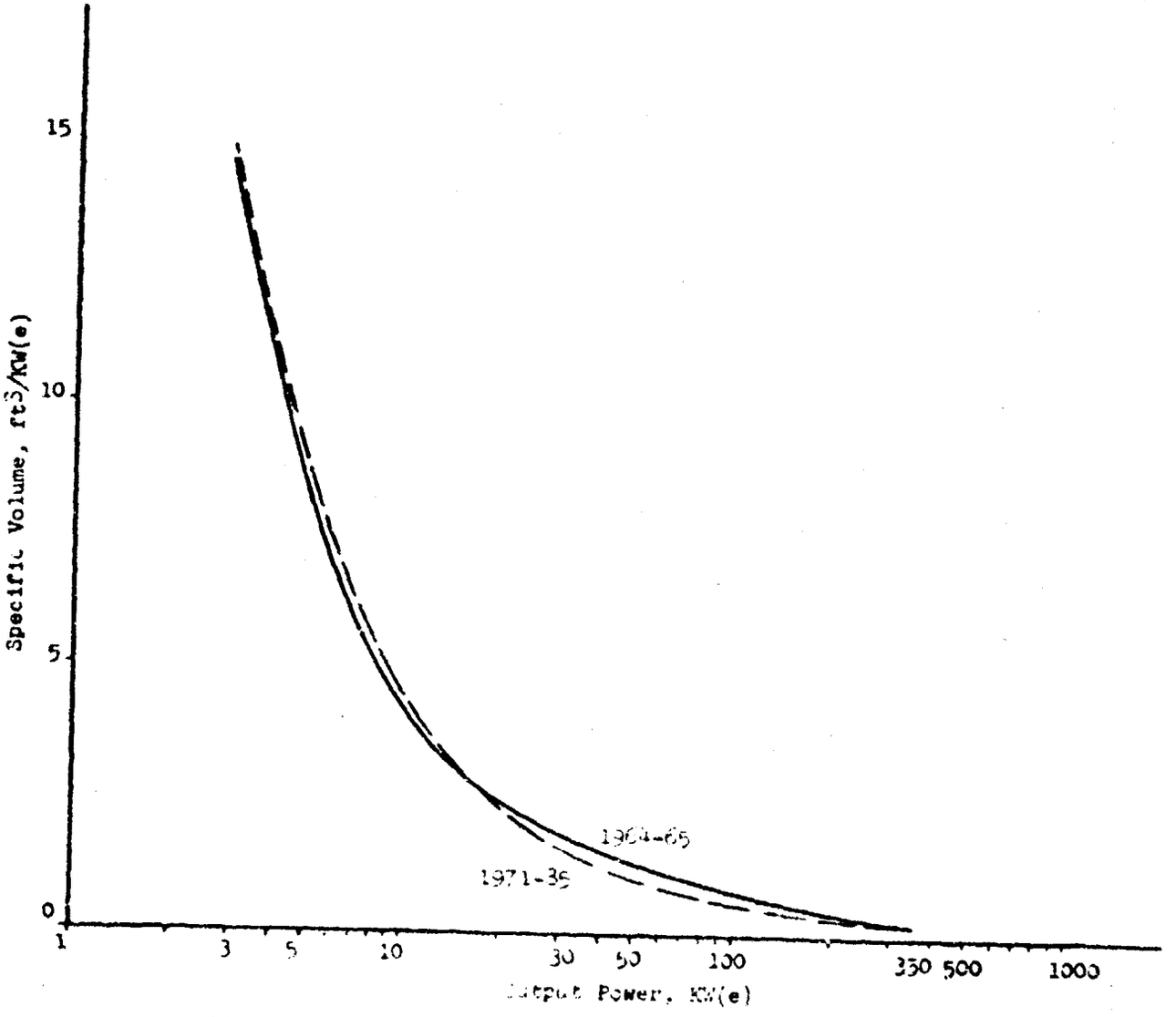

Figure 68. Effect of Output Power Level and Thermoelectric Parameters on Specific Volume of In-Pile, with Loop (SWIFT) Systems

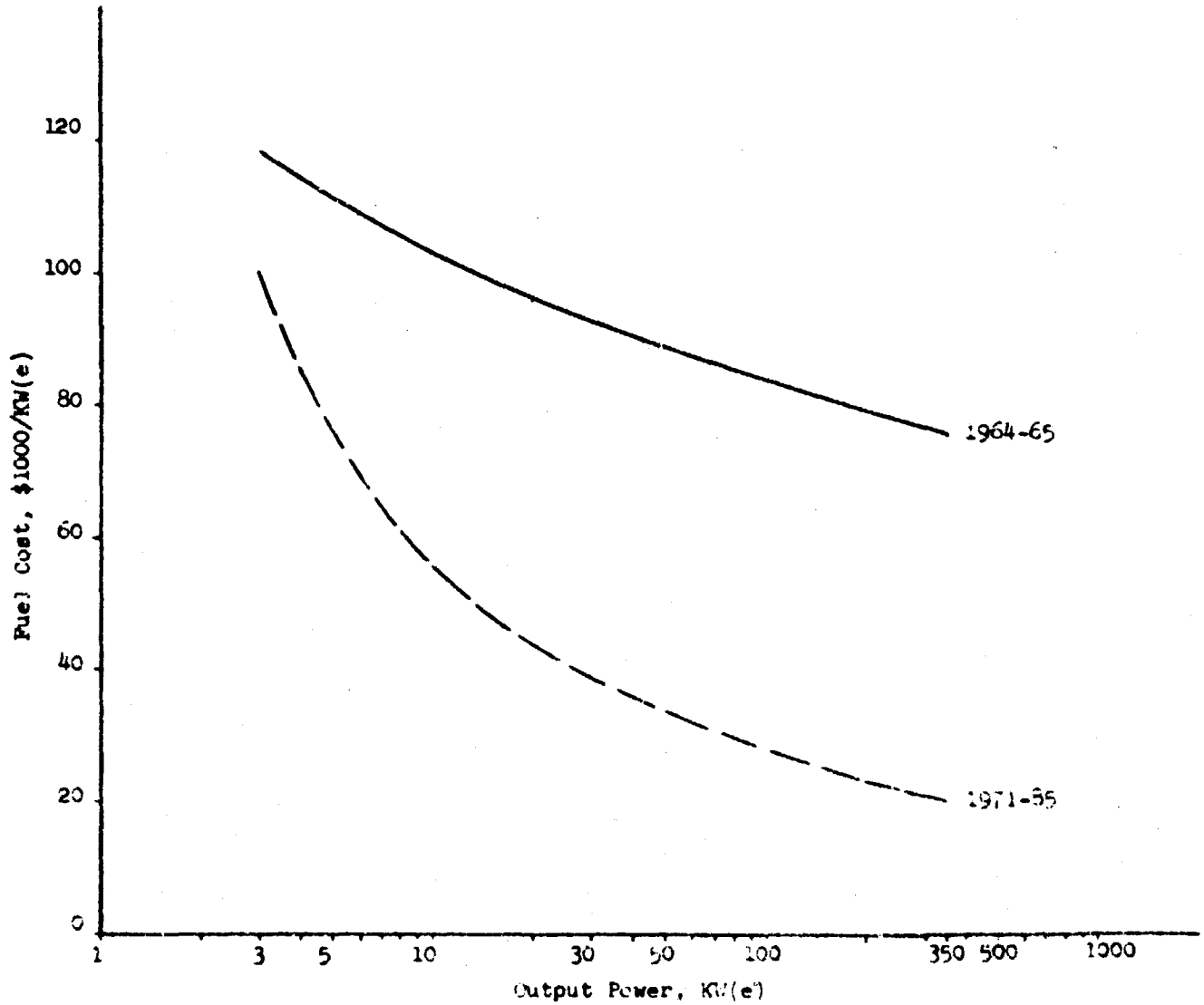

Figure 68. Effect of Output Power Level and Thermoelectric Parameters on Fuel Cost of In-Pile, with Loop (SWIFT) Systems

In addition to the need for a fast reactor heat source, problems that are common to most static and dynamic space power systems, such as those listed under the "Problem Areas" section of the discussion for the HORSE concept, would also require solutions.

(4) Probability of Success — On the promise that thermoelectric materials, with properties equal to those used in this study, would be available by 1966-67 and that design technology as well as structural materials will be available for construction of a fast reactor 1200°C heat source, the probability for developing a successful SWIFT type unit by 1970 is quite high, probably greater than 95%.

f. Comparison of Reactor-Based Power Systems — A comparison of the HORSE, TIGER, and SWIFT types of reactor-based power systems is recorded in Table 83. These data show that the SWIFT concept is superior to the HORSE, and that both the HORSE and SWIFT concepts are much superior to TIGER.

Table 83

SYSTEM PERFORMANCES OF REACTOR-BASED SPACE POWER UNITS

Space Power Concept	System Performance, lbs./KW(e)					
	3 KW(e)		30 KW(e)		350 KW(e)	
	1964-65	1971-85	1964-65	1971-85	1964-65	1971-85
HORSE	150	120	58	33	55	26
TIGER	350	130	290	90	-	-
SWIFT	160	110	60	24	43	15

The specific volumes required per KW(e) of output for each system concept are compared in Table 84. The large cores required for the TIGER concept prevent this system from having a low specific volume. The specific volume of the 350 KW(e) HORSE-type system could be decreased to approximately the 0.2 $ft.^3/KW(e)$ obtained for the 350 KW(e) SWIFT units by redesigning the large units of this type with the thermoelements on two large wing-like fins extending from the reactor, rather than placing all of the thermoelements between the shadow shield and the payload. If this were done, the HORSE and SWIFT units would exhibit approximately the same specific volumes at all power levels.

Table 84

SPECIFIC VOLUMES OF REACTOR-BASED SPACE POWER UNITS

Space Power Concept	Specific Volume, ft ^{3}/KW(e)					
	3 KW(e)		30 KW(e)		350 KW(e)	
	1964-65	1971-85	1964-65	1971-85	1964-65	1971-85
HORSE	14	14	3.5	2.2	3.2	2.2
TIGER	21	19	4.3	2.9	-	-
SWIFT	15	15	1.9	1.6	0.2	0.2

The fuel costs for the three types of systems are summarized in Table 85 . The fuel costs for HORSE systems are significantly lower than for either TIGER or SWIFT systems because HORSE permits more effective use of the fuel than the TIGER or SWIFT concepts. For large SWIFT-type systems the fuel utilization could possibly be improved by placing columns of thermoelements and cooling tubes within the nuclear core, as well as on its interior and exterior surfaces. This possibility was not investigated. The dilution of the core material in the SWIFT concept would be greater than in the case of HORSE-type systems, because the combined volume of thermoelements and coolant tubes would dilute the core more than the coolant tubes alone.

Table 85

FUEL COSTS FOR REACTOR-BASED SPACE POWER SYSTEMS

Space Power Concept	Fuel Cost, $/KW(e)					
	3 KW(e)		30 KW(e)		350 KW(e)	
	1964-65	1971-85	1964-65	1971-85	1964-65	1971-85
HORSE	89,000	86,000	17,000	14,000	4,800	3,400
TIGER	680,000	68,000	830,000	22,000	-	-
SWIFT	118,000	100,000	92,000	39,000	75,000	20,000

The fuel costs for TIGER-type systems, based upon annular-shaped cores, do not vary proportionately with increases in power output. For both the TIGER and SWIFT units, the efficiency of fuel utilization is low because the large radiator area required

per thermoelement severely limits the number of elements which can be attached to the core exterior.

A breakdown of the weight for the reactor-based space power systems by components is shown in Tables 86 and 87.

Table 86

WEIGHT DISTRIBUTION IN OPTIMIZED REACTOR-BASED SPACE POWER SYSTEMS USING 1964-65 THERMOELECTRIC PARAMETERS

Space Power Concept	Output, KW(e)	Portion of System Weight, %			
		Thermoelectric Generator	Reactor	Shielding	Structure
HORSE	3	33	34	20	13
	30	72	12	6	10
	350	79	2	1	18
TIGER	3	13	55	23	9
	30	15	69	7	9
SWIFT	3	31	38	22	9
	30	34	41	16	9
	350	42	41	8	9

Table 87

WEIGHT DISTRIBUTION IN OPTIMIZED REACTOR-BASED SPACE POWER SYSTEMS USING 1971-85 THERMOELECTRIC PARAMETERS

Space Power Concept	Output, KW(e)	Portion of System Weight, %			
		Thermoelectric Generator	Reactor	Shielding	Structure
HORSE	3	19	44	22	15
	30	57	20	11	12
	350	68	4	2	26
TIGER	3	8	37	46	9
	30	16	59	16	9
SWIFT	3	2	52	37	9
	30	15	52	24	9
	350	46	34	11	9

The ratio of reactor weight to total weight in the HORSE system drops with increase in power level, as does the shielding weight ratio, whereas the ratio of thermoelectric generator weight to total weight increases with an increase in power level. The fact that the thermoelectric portion of each of these systems increases with increased system power level emphasizes the importance of further improvements in the development of thermoelectric materials in minimizing system weights.

Increased thermal efficiency, which is possible with improved thermoelectric materials, would also decrease the size and weight of the reactor and hence the weight of the shielding. The large structural weight calculated for the 350 KW(e) HORSE-type unit could be reduced considerably by relocating some of the thermoelements on side panels or wings projecting from the reactor, rather than placing all of them on the conical structure between the shield and the payload.

Improvements in the system performance of TIGER-type systems are dependent upon decrease in radiator area per couple. Improvements of the order needed to compete with the performance of HORSE and SWIFT-type systems, however, would not be expected.

The weights of the thermoelectric generator and reactor are the factors controlling performance of the large SWIFT-type systems. Increased watt(e)/lb ratings for the thermoelectric generator significantly improve the system performance. In addition, improved thermoelectric materials would increase the power obtained per unit of reactor surface area, thus lowering the average weight of reactor per KW(e) output.

High-performance SWIFT-type systems would be attained by operating at cold-junction temperatures of 250-450 °C rather than at 750 °C. Hence, low-temperature thermoelectric materials, capable of being joined to the present doubly-segmented thermoelements now used at temperatures from 500 °C to 1200 °C, should be investigated. Since radiator and coolant loops could be operated at temperatures in the 250 °C-450 °C range, it is possible that overall system efficiency for the SWIFT concept could be significantly increased (to >20%) by utilizing a Rankine cycle-type power unit (steam or other low-temperature system). Such a Rankine-type power unit could receive its input power from the energy rejected at the 450 °C cold junctions of the thermoelectric generator, expand the working fluid through a turbine, and condense the resulting vapor in radiators operating at 250 °C. This would permit substantial reductions in the weight of the radiators.

Thermoelectric generator watt(e)/lb ratings beyond those postulated for 197 -85 could improve the system performance (including

shielding) of the 350 KW(e) HORSE-type units to below 20 lb/KW(e). Such low weight-to-power ratios would be quite attractive for large space propulsion needs. In addition, it is possible to combine the HORSE concept with a Rankine cycle-turbine power unit. The waste heat from the cold junctions of the thermoelectric elements could be absorbed by a second coolant loop containing a vaporizable coolant, such as water. The vaporized liquid could be superheated and then passed through a turbine to a condensing radiator. The system weight would be increased by the weight of the second coolant system and the turbine, but the system power output would be increased greatly by the overall 15+% efficiency output of the Rankine-turbine unit compared with the 3-5% efficiency of the thermoelectric generator. Computer studies optimizing the system performance of these hybrid static-dynamic systems should be made to determine the potentialities of these systems.

In summary, the watt(e)/lb rating and thermal efficiency of the thermoelectric generator are the most important factors affecting the performance of the three types of space power systems considered in this report. The size of the reactor cores for each of the three types of reactor-based space power systems is determined by heat transfer or thermoelectric thermal efficiency considerations, not energy limitations. In all cases, less than one atom percent burn-up would be required for a 10,000-hour mission, even at an assumed thermal efficiency of 4%. The shielding weight was determined by the reactor size, desired system power output, and thermal efficiency of the thermoelements. The system structure weight is determined by the weight and geometrical configuration of the major system components. Analysis of these observations shows that reactor, shielding, and structure weights are all strongly influenced, directly or indirectly, by thermoelectric properties. The importance of the thermoelectric properties in determining system performance indicates that further research could be profitable in terms of improved system performance for each of the concepts considered in this study. The possibilities of greatly improving system performance via hybrid static-dynamic systems should be further investigated.

2. Radioisotope Space Power Systems

a. Introduction Isotopes have several distinct advantages over other heat sources, particularly in systems with low and medium power requirements. Of primary importance is the fact that the isotope source can be designed to function in a manner completely independent of its environment. Also, sources are available in a wide range of specific power densities and lifetimes.

By combining radioisotope heat sources with high-temperature thermoelectric materials, it is possible to produce devices which are at once capable of high performance (high watt /lb. ratios) and also of the high component reliability inherent to all thermoelectric generators. The type of thermoelements developed by Monsanto Research Corporation should not encounter serious problems with regard to radiation, sublimation or solid-state diffusion types of damage when used in high-temperature generators. Neither should generators of this type be readily damaged by micrometeorite impact.

Generator and fuel-development programs are currently under way, or planned, to investigate the use of isotopes such as Po^{210}, Cm^{242}, Cm^{244}, Pu^{238}, Pm^{147}, and Sr^{90} as power sources for use in outer space. While satisfactory techniques have been developed for encapsulation of most radioisotopic heat sources in ways to insure safety in handling on the ground or in the event of launch pad accidents, additional work is necessary to lower the cost of encapsulation and to perfect capsules which will either remain intact or burn up completely during reentry. By the proper choice of radioisotopes, a generator may be designed to meet almost any mission duration, including those lasting several years.

The principal disadvantage of isotope heat sources for generators is their relatively high cost. In almost all cases, however, it is believed that an increase in demand will result in larger scale production facilities and in resultant lowering of production costs.

A second disadvantage of the isotope-heated generator is the presence of radiation resulting from the process of isotope decay. Not only can this direct radiation present a biological hazard and/or be detrimental to the payload, but it can also induce secondary radiation with equally hazardous properties. For those isotopes which emit only α-particles, radiation from isotope decay is absorbed in the materials containing the isotope heat source and surrounding generator. An induced secondary radiation may necessitate minor shielding. Beta (β) emission, however, is not easily absorbed, and the resultant Bremsstrahlung requires either

shielding or considerable separation between the generator and the payload. Neutron and γ-emissions are present for some isotopes, and, like the β-emissions, require protection of the payload either by shielding or by separation. For all but the α-emitting isotopes, heavy biological shielding is required for ground handling and launch pad operations.

With the above considerations in mind, preliminary investigation of several conceptual designs for radioisotope-powered thermoelectric generators was undertaken. This investigation was concerned with utilizing high-temperature segmented p- and n-type thermoelements produced by Monsanto Research Corporation with short, medium, and long half-life isotope heat sources. Estimates were made of the performance characteristics, cost, and probability of success in achieving the design goals for selected generators.

The results of a preliminary investigation on radioisotope-powered thermoelectric generators have been previously reported in the Third Quarterly Progress Report of Contract No. AF 33(615)-1084. These initial studies were based upon the use of light-weight isotope containers such as might be considered for the wide dispersal type of reentry mode. For this report the studies have been changed and are now based upon the use of heavy-walled containers such as are necessary for total containment of the isotope on impact after reentry or after a launch abort. Another change was the choice of a somewhat higher intermediate temperature at the interfaces between the MCC 60 and MCC 40 (n-type) and the MCC 50 and MCC 40 (p-type) materials. This temperature was increased from 850°C, used in the previous report, to 900°C to reflect the proven higher temperature capability of the MCC 40 materials. Finally this report will summarize some of the results of a performance study for isotope power thermoelectric generators based upon extrapolated material values for the period 1971-1985.

b. Characteristics and Selection of Isotopes An isotope must possess several important characteristics in order to meet the requirements for utilization as a fuel for high-temperature thermoelectric power generation systems. These are:

1. It must have a sufficiently long half-life to sustain adequate power generation throughout the mission.

2. It must have a high thermal density.

3. Preferably, its emittance will constitute only α-radiation.

4. It should be available at relatively low cost.

Although no one isotope can meet all of the prerequisites ideally, eight candidates stand out as possible choices. They are presented in Table 88.

Table 88

RADIOISOTOPES SUITABLE FOR SPACE POWER GENERATION (Ref. 11)

Isotope	Half-life, year	Decay Produc.	Power Density, watts/g.	Useful Mission Life, yr.
Po^{210}	0.38	Alpha, Neutron	140	0.5
Cm^{242}	0.44	Alpha, Neutron	120	0.5
Ce^{144}	0.78	Beta, Gamma	2.3	1.0
Pm^{147}	2.60	Beta, Gamma	0.18	2.5
Cm^{244}	18	Alpha, Neutron	2.3	10
Cs^{137}	27	Beta, Gamma	0.07	10
Sr^{90}	28	Beta, Gamma	0.2	10
Pu^{238}	86	Alpha, Neutron	0.48	10

For design purposes, these eight candidate isotopes will be considered in two groups of four members each. The first four isotopes listed in Table 88 are of use for short-duration missions only, since their rate of decay is too rapid to provide stable power output over long periods of time. The latter four have half-lives ideally suited for missions lasting up to and beyond ten years.

Ranking second in importance to half-life as a factor in the choice of an isotope fuel is its power density (watts/g. or watts/cc.). More than any other factor, this property governs the performance ratio (watts/lb.) of the generator. The higher the power density, the less the fuel itself weighs; of even greater significance is the reduction in weight possible in the isotope fuel container and surrounding generator.

A further characteristic which must be taken into consideration is the melting point. It is necessary to provide a heat source capable of operation at high temperature in order to make use of the advantages of the high-temperature thermoelectric materials. For the Monsanto Research Corporation thermoelements, this temperature is 1200°C. Thus the melting point of any isotope compound should be higher than the 1200°C level. Table 89 lists high-temperature properties for several forms of radioisotopes.

(1) Biological Shielding From the standpoint of safety, any thermoelectric generator with radioisotope power must have some form of biological shielding. All eight isotopes considered for generator power for outer space produced γ-emission as part of their natural decay schemes. Also, those with β-emission can produce a Bremsstrahlung flux (Ref. 13). Moreover, four of the eight isotopes are characterized by neutron emission, the neutrons coming from spontaneous fission or from α-neutron reactions in the fuel material. If material shielding only is used, shield weights can be quite high, but fortunately shield weight penalties can often be largely avoided if, for example, shielding by separation, rather than material shielding, is relied upon for protection. For most of the isotopes under consideration, the necessary separation distances between source and payload are entirely feasible in view of the integration of both the isotope-heated generator and the payload in the launch vehicle.

Table 89

RADIOISOTOPE CHARACTERISTICS (Ref. 12)

Radioisotope Component	Half-Life	Melting Point, °C	Initial Power Density, watts/cc	Specific Power, watts/g
Strontium-90 titanate	28 yrs.	1910	0.99	0.22
Strontium-90 oxide	28 yrs.	2430	1.4	0.38
Cesium-137 polyglass	30 yrs.	>1000	0.21	0.067
Promethium-147 oxide	2.7 yrs.	>2000	2.34* 0.73+ to 1.4	0.284* 0.15+ to 0.27
Polonium-210 gadolinium polonide	138 days	1600	550	71.4
Plutonium-238 metal	89.6 yrs.	639	7.43-7.91	0.45-48
Plutonium-238 dioxide	89.6 yrs.	~2250	3.5	0.39
Curium-242 sesquioxide	163 days	1950	150	12.7
Curium-244 sesquioxide	18.4 yrs.	~1950	26.4++	2.49**
Cerium-144	.78 yrs.	2680	13.8	2.3

*Theoretical
+As specified by ORNL Isotopes Production Division
**98 percent isotopic purity
++80 percent of theoretical density

An indication of the relative γ and neutron dose rates from a 200 watt(t) power source is given in Table 90.

From Table 90 it is evident that for isotopes which emit α-particles (Po^{210}, Cm^{242}, Cm^{244}, Pu^{238}), very little γ-emission is present. Also, in the cases of Po^{210} and Pu^{238}, neutron emission is quite low. The two curium isotopes show significant neutron dose rates. It was recently reported (Ref. -5) that research tests have shown that the shielding requirements for Cm^{244} are disappointingly high.

Table 90

DOSE RATES* FROM 200 THERMAL WATT POWER SOURCE (Ref. 12)

Isotope	Gamma	Neutron
Po^{210}	.044	.0003
Cm^{242}	.022	.020
Ce^{144}	770.	-
Pm^{147}	.033	-
Cm^{244}	.11	.24
Cs^{137}	3900.	-
Sr^{90}	130.	-
Pu^{238}	.005	.0083

*Rads/hr. at 50 cm. from lightly shielded right cylinder sources with length equal to diameter, unshielded except for the equivalent of 1 cm. of lead.

It has been assumed in this initial study on radioisotopes that the necessary protection for adequate biological shielding would be achieved by separation of payload and generator and thus no shielding weights have been included.

(c) Costs and Availability of Isotopes The availability and costs of isotopes represent the two greatest unknowns encountered in the preliminary study. It has been concluded after examination of all available data that whereas present production is low and costs are very high, almost any future demand could be satisfied, given a lead time of several years. In all likelihood the costs will remain high. In Table 91 the projected production capacity on the basis KWH(t) is summarized as reported by Davies(Ref.11). Table 92 is a tabulation of isotopes presently being produced, planned, or that can be produced(Ref.14).

From the following tables it is apparent that Cm^{242} and Cm^{244}, in addition to Po^{210}, are presently in least supply, in terms of the 1965-70 period. It also appears that, if required, appreciable quantities of all the isotopes could be obtained by 1971-85.

Table 93 lists the projected cost for the radioisotopes from three sources. It is likely that projected cost estimates from the March 1964 column of Table 93 are more representative of future costs than the figures of the other columns. There is an apparent trend, therefore, of lowering radioisotope costs as time increases.

c. Design of Thermoelectric Generator

(1) Generator Configuration Three conceptual designs of generator configurations, namely, cylindrical, spherical, and sandwich, were chosen for study with radioisotope heat sources. In each case the heat source was contained at the center with segmented thermoelements radiating outwards and terminating with finned radiators.

(a) Cylindrical In the cylindrical concept the isotope is encapsulated in a relatively long cylindrical container or can, with the hot ends of the segmented thermoelements thermally coupled to the surface of the can. The thermoelements extend outwards from the surface of the can and are connected at their cold ends to finned radiators. A major advantage of this design is that the cylinders may be stacked to yield units of higher power levels.

(b) Spherical In the second or spherical design the isotope is contained in a spherically shaped can with the ends of the thermoelements thermally coupled to the surface of the can and with the cold ends terminated with finned radiators.

PROJECTED PRODUCTION CAPACITY OF CANDIDATE RADIOISOTOPE HEAT SOURCES (Ref.11)

Isotope	Production Capacity, KWH (t)/yr 1963	1967	1970	1980
Po^{210}	3	14	14	14
Cm^{242}	-	9.5	9.5	9.5
Ce^{144}	25	700	1330	4900
Pm^{147}	0.01	11	25	111
Cm^{244}	-	41	129	134
Cs^{137}	5	48	110	458
Sr^{90}	19	63	157	693
Pu^{238}	1.5	11	35.8	73

Table 92

PROJECTED PRODUCTION CAPACITY OF CANDIDATE RADIOISOTOPE HEAT SOURCES (Ref.8)

Isotope	Present	Planned	"Capacity Could Be"
Po^{210}	50 grams	300-500 grams	1000 to 10,000 grams
Cm^{242}	100 grams	100 grams	1,000+ grams
Ce^{144}	as needed	1,100 grams	30,000+ grams
Pm^{147}	300 grams	500 grams	30,000+ grams
Cm^{244}	200 grams	1,500 grams	many KG
Cs^{137}	11,500 grams	40,000 grams	115,000 grams
Sr^{90}	21,000 grams	35,000 grams	70,000+ grams
Pu^{238}	4,000 grams	10,000 grams	40,000 grams

Table 93

PROJECTED RADIOISOTOPE COSTS

Isotope	$/Thermal Watt March 1963 (Ref.11)	Nov. 1963 (Ref.16)	March 1964 (Ref.14)
Po^{210}	190	188	50
Cm^{242}	165	17	150
Ce^{144}	5	1	1
Pm^{147}	485	91	86
Cm^{244}	435	357	1000
Cs^{137}	194	21	21
Sr^{90}	77	19	20
Pu^{238}	1040	894	1000

(c) The sandwich type of configuration utilizes a flat fuel can in which the thermoelements contact each of the flat sides. This type of construction permits close spacing and ease of thermal insulation between adjacent thermoelements, a gain made at the expense of providing less radiator surface for each thermoelement with a resultant decrease in efficiency due to the higher radiator temperature produced. However, the lower efficiency may more than offset reduction of heat loss.

d. Initial Calculation Methods The computer program for the optimization of calculations was written in IBM FORTRAN II language. A copy of the detailed computer program was supplied to the Air Force Task Engineer. Basically the program is divided into two parts. The first section of the program is concerned with optimization of the thermoelectric elements themselves, whereas the second determines the optimum performance of an integrated unit (heat source, thermoelements, and radiator). The mathematics employed in the thermoelement optimization is based on the well-known article by Swanson, Somers, and Heikes(Ref.17), and yields segment lengths, area ratios, and load resistance to obtain maximum thermocouple efficiency. The first portion of the program was used for the spherical, sandwich, and cylindrical design configurations. The portion concerned with generator optimization determines the total number of couples required to meet voltage and power requirements. At this point the size of the isotope heat source, with the thermal power requirements and design configuration, is calculated. Spacing of the elements over the surface of the isotope container is computed if the available radiator area is calculated. In this preliminary study the available radiator area was equated to the total cold strap area and the effect of the fin structure was not taken into account. Information pertaining to the heat transfer of finned structures could not be incorporated in this study in time. However, it was felt that the results obtained from a study not considering the fin structure could be meaningful and that they could be extrapolated to include the effects of the fin structure. The subsequent steps in the calculation are: (a) if the radiator area is insufficient, the calculations for that particular set of input data are terminated, and(b) if the radiator area is sufficient, the performance characteristics of the generator are determined.

For the spherical and sandwich configurations there are no further calculations. The cylindrical configuration, however, undergoes a further calculation for determination of optimum performance. The cylindrical unit would consist of a number of rings of thermoelements stacked around and in thermal contact with the central isotope fuel containers (see Figure 70. In the optimization calculations, the number of rings for thermoelements is reduced by one, and the configuration calculations are repeated

until a maximum watts/lb. ratio is obtained. Thus, from an initial given length, the cylindrical generator is reduced in length and increased in diameter until an optimum geometry is found.

The preliminary generator performance calculations are quite complete and fairly accurate with exception of those for isotope fuel temperature and radiator configuration. It was felt at the time that to include these design considerations would prevent the timely conclusion of this study. However, both design factors are of importance to the isotope fuel temperature because of decay gas pressure and vapor pressure considerations, and the radiator configuration because of the reduction in volume and weight of the device that can be achieved with a proper design of the radiator (fin structures). Consequently, it was decided to modify the computer program to account for these considerations.

Up to this time it had been mandatory to contain completely the helium produced by the decay of the less harmful α-emitting isotopes for the expected life of the container. It is technically possible to produce strong, porous, refractory materials capable of containing the isotope totally while allowing the helium to escape through micropores in the walls of the container.

e. Optimization Studies It was beyond the scope of this phase of the project to prepare a complete analysis of all the design factors influencing the optimization of the generator. Therefore, for the initial study it was decided to consider several generator configurations at one power level, 25 watts(e).

The 25-watt power level was chosen because it was felt that the first operational, high-temperature thermoelectric generators based on segmented thermoelements would be in this power range. This choice seemed justified by the high cost and limited availability of most of the isotopes for the near future.

(1) 25-Watt(e) Power Level Study The property of an isotope which most affects the performance of a generator is its power density. In the interest of economy it was decided to make a complete systems evaluation for only one isotope but to enlarge the study with a comparison of the performances of systems powered by different isotopes at one radiator temperature. The isotope which was fully evaluated is Cm^{242}, a high-density radioisotope with a half-life of 163 days. Although Po^{210} is a better representative of the group of high density, short-life isotopes, both with respect to cost and availability, it was not chosen since at the initiation of this study not enough information was available.

For the comparative study, three radioisotopes were used: Po^{210} (gadolinium polonide), Cm^{242} (curium sesquioxide), and Cm^{244} (curium sesquioxide). An attempt was made to include Pu^{238} (plutonium oxide) in the study but this could not be done efficienctly without modifying the computer program. Some preliminary computations were made for Pu^{238} and the results showed the performance of a Pu^{238}-heated generator system to be lower than that of a Cm^{244}-heated one, but not enough to outweigh the advantages of Pu^{238} with respect to shielding and availability. Sr^{90} (strontium titanate) was also studied, but this isotope proved itself to be a very poor candidate for powering space devices - both the weight of isotope required and the weight of its container are very high.

One thermoelement diameter was used throughout this study. An element diameter of 3/8" was chosen, since this diameter was used for the 50-watt laboratory model generator.

Six cold-junction temperatures were chosen, because the radiator temperature has a great effect on the performance of a generator. The lower the radiator temperature, the better the efficiency of the thermoelectric conversion, but the lesser the ability of the radiator to reject heat. Values selected were 500, 550, 600, 650, 700 and 750°C. For the parameter runs only the values of 500, 600, and 700°C were used.

Total thermoelement length was the final factor studied. For the larger thermoelements, a total of 27 lengths were used. These ranged from 0.1 cm. to 2.7 cm. This number was chosen because previous calculations for the 50-watt laboratory model generator demonstrated that in the short element length region the device performance was best for any one set of conditions until the inability of the radiator to remove sufficient heat became controlling. It seems appropriate to draw attention to the fact that this study is a preliminary one and that, for example, it does not take into account the actual radiator configuration. The actual performance values are somewhat higher than those shown in Figures 71, 72, and 73, but also the maxima in the performance curves are going to occur at smaller element lengths.

The hot ends of the thermoelements were placed as close as possible to one another, leaving only sufficient space between thermoelements to permit fabrication. The ratio of the hot-strap area not covered by the thermoelements to the total available hot-strap area, defined here as the stack factor parameter, was not varied in this investigation. For the diameter elements used, the thermoelements covered from 50-60% of the available space (stack factors from 0.5 to 0.4). With the plasma-spray techniques, this factor could be decreased further.

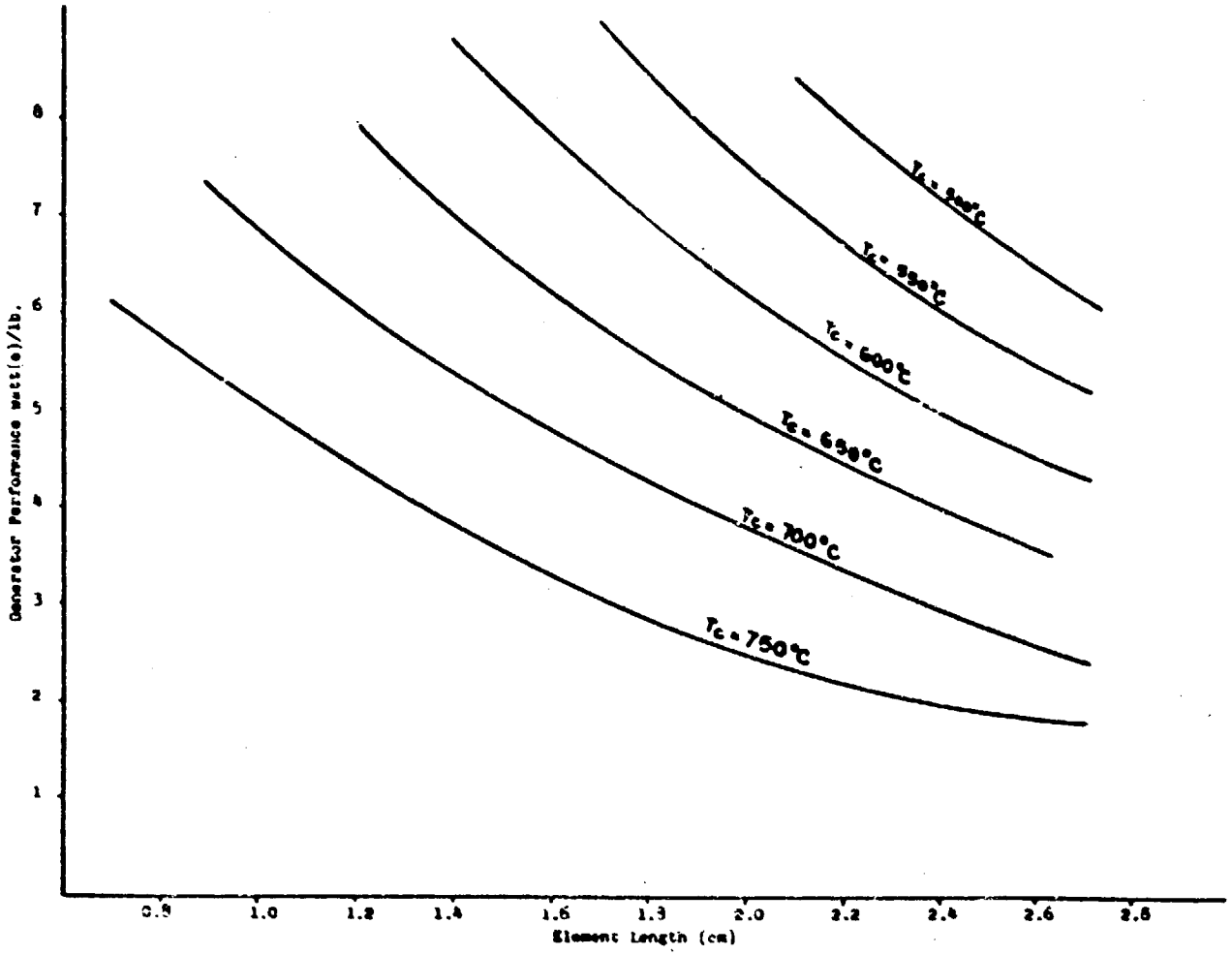

Figure 71. Performance $\sqrt{\text{watt(e)/lb.}}$ vs. Length of 3/8-inch Diameter Segmented Thermoelements in a 25-watt(e) Cylindrical Generator with Cm^{242} as the Heat Source, T_h of 1200°C and Various Cold Junction (T_c) Temperatures

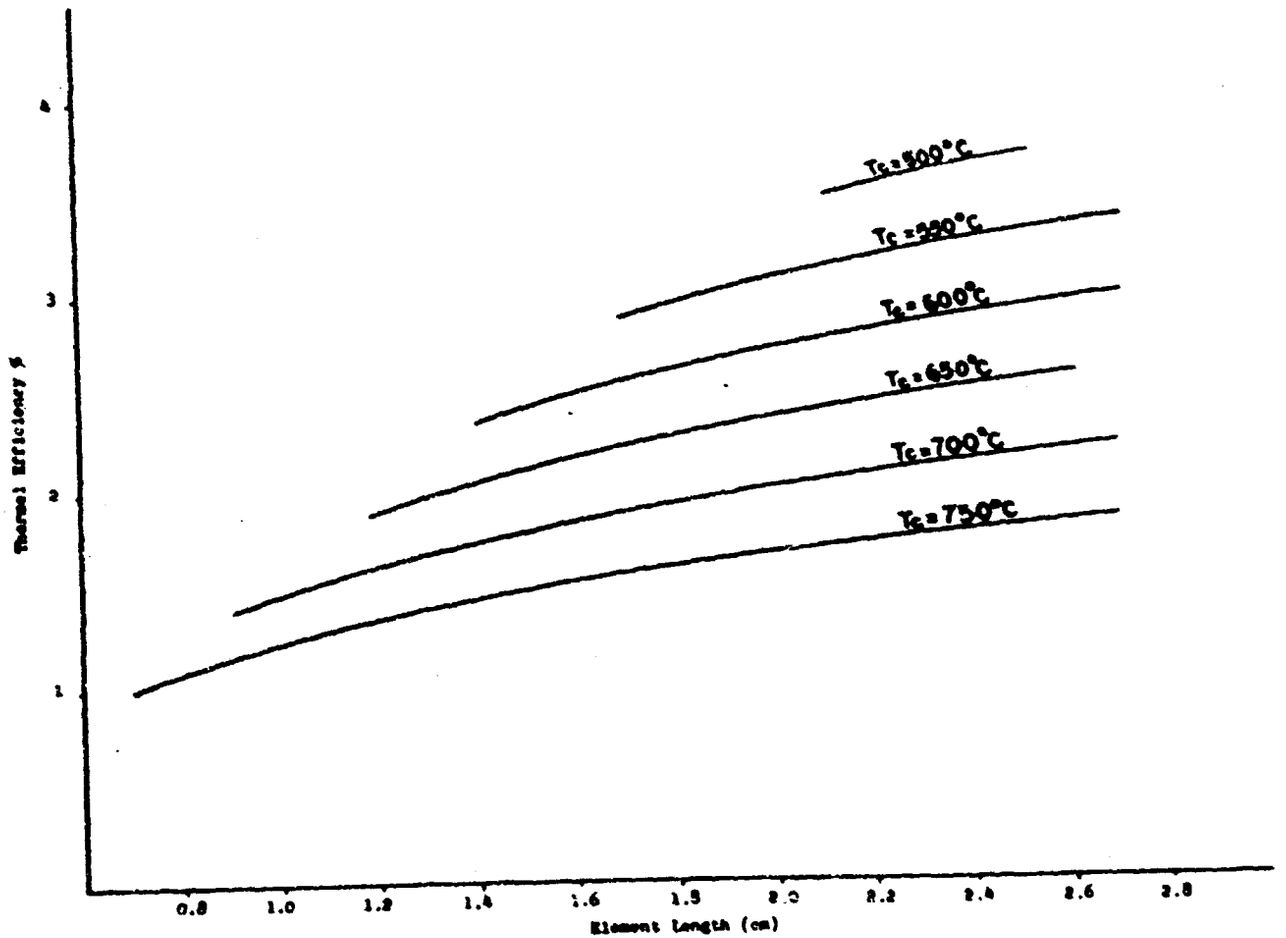

Figure 72. Thermal Efficiency vs. Length of 3/8-inch Diameter Segmented Thermoelements in a Cylindrical 25-watt(e) Generator with Cm^{242} as the Heat Source, T_h of 1200°C and Various Cold Junction (T_c) Temperatures

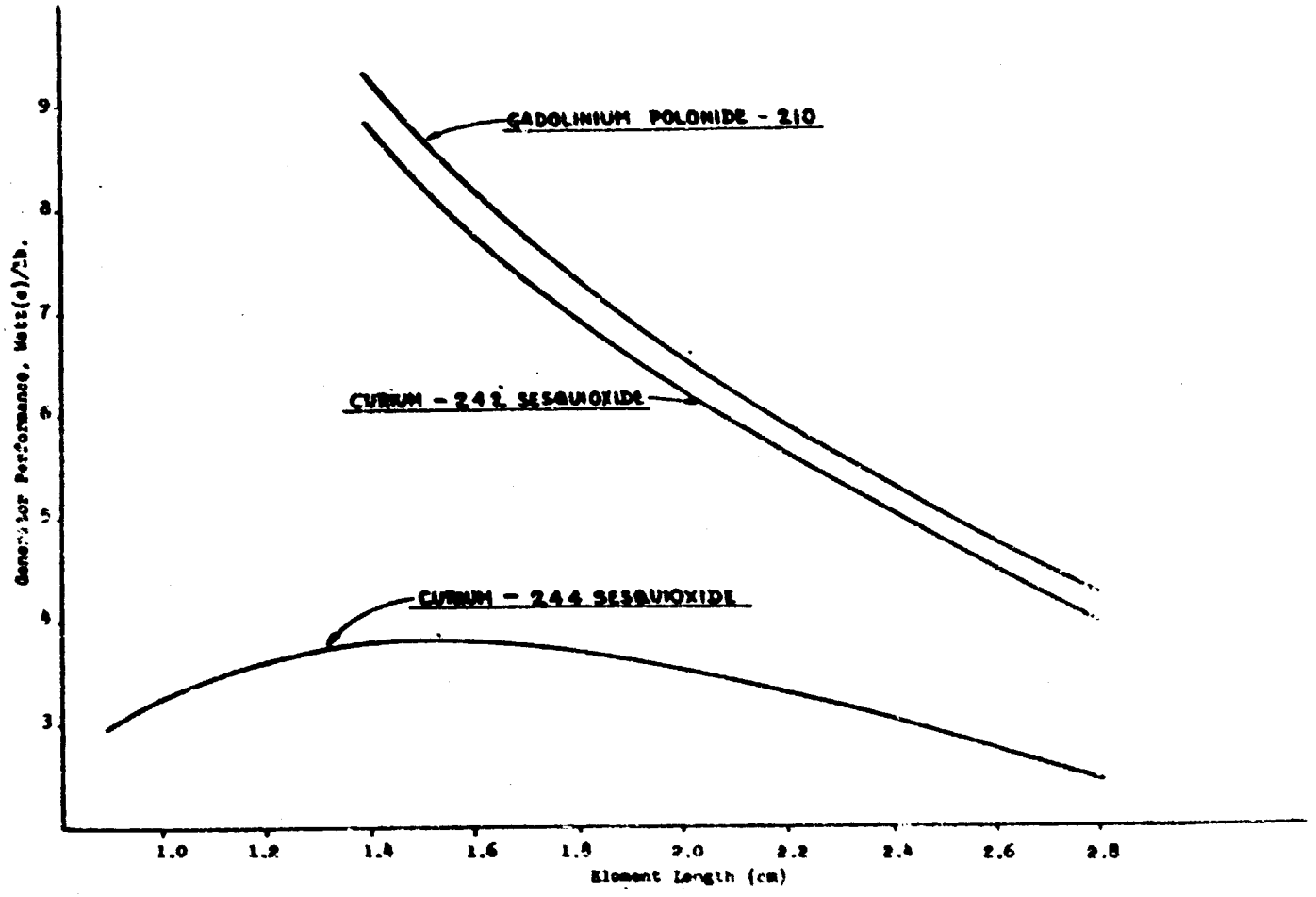

Figure 73. Performance [watt(e)/lb.] vs. Length of 3/8-inch Diameter Segmented Thermoelements for a 25-watt(e) Cylindrical Generator with Various Isotope Heat Sources (T_h = 1200°C, T_c = 600°C)

The isotope capsule wall thicknesses were computed utilizing a procedure outlined in Ref. 18. The capsule material used in all cases was Moly TZM with a 0.1" of Hastelloy C cladding to prevent oxidation of the molybdenum alloy. A 30% void volume was taken into account for the α-emitting isotopes. The containers were designed for impact(Ref. 18) and the effects of the helium pressure build-up. The effect of reentry heating was neglected. Additional study will be necessary to arrive at a calculational procedure that duly takes into account all factors governing capsule wall thickness. However, it is felt at the present time that the use of the impact criterion yields a good first approximation of the wall thickness. While internal pressures due to radioisotope decay, vapor pressure, and possibly additional thicknesses of oxidation-resistant coatings may result in an increase of capsule wall thickness, and thus of capsule weight, it may also be that the approach of Ref. 18 is actually a bit too conservative and that a correction of the approach may tend to compensate for the effects mentioned above or it may even result in a decrease of the wall thickness.

The relative physical positions of segmented thermoelements, insulation, and radiators in the cylindrical-type generator may best be understood by referring to Figure 70. In Figure 70 the high-temperature thermoelectric segments of both the p- and n-type legs are connected to the graphite hot shoes. MCC 50 is the designation of the high-temperature p-material and MCC 60 is the designation of the high-temperature n-material.

To each of these high-temperature materials is bonded the appropriate p- and n-type MCC 40, Monsanto Research Corporation's intermediate-temperature thermoelectric materials. A thin copper radiator is attached at the cold end of each leg. Thermal and electrical insulation fills the remaining spaces of the thermopile.

The isotope heat source for this proposed generator design is shown in the center within a welded inner and outer can. The outer can, of course, also takes the form of an oxidation-resistant cladding of the inner can. As portrayed in Figure 13, a void was used to limit the pressure of the helium that would be released during decay of the α-emitting isotope. If the use of the micropore containers we have proposed ultimately proves to be feasible, and is accepted by both the Air Force and the AEC, this void would not be required and can weights would be much lower.

The doubly-segmented thermoelements in concentric ring form shown in the cutaway view in Figure 70 would be produced by flame- and arc-plasma spray techniques, now under investigation. These techniques show considerable promise for producing segmented thermoelements in a variety of shapes and performance characteristics.

The two conically shaped thermal radiation heat shields shown at the lower end of support rod of the cylindrical generator in Figure 70 serve as thermal shadow shields for the payload. The support rod would preferably be long enough to permit adequate separation of the generator from the payload, minimizing damage by radiation from the isotope heat source.

The physical properties used for the initial optimization studies of the conceptual cylindrical unit shown in Figure 70 were presented in Section I of this report.

For all reported calculations on the state-of-the-art systems (1964-1965), constant values of the hot-junction and interface temperature of 1200°C and 900°C, respectively, were used. In each case these temperatures represent the limit of safety at which, at the present time, the respective materials appear to be operable for periods of more than a year. The reported calculations on the 1971-1985 systems use hot-junction and interface temperatures of 1400°C and 1050°C, respectively, temperatures which we feel can be safely utilized by our materials once their development has been completed.

On the basis of performance and life tests made to date of generators constructed with doubly-segmented Monsanto Company thermoelectric materials, it is possible to develop approximately 12 volts at 25 watts(e), or higher voltages at larger generator capacity. For example, more than 24 volts are obtainable under matched load conditions for generator power outputs in excess of 100 watts. Accordingly, no effort was made to include any form of power-conditioning equipment in this study period for the longer half-life heat source. It is possible that power conditioning would not be required, depending upon the missile power profile. Mechanical methods of dissipating unused heat, such as the shutter used on the SNAP 11 generator, may be necessary when shorter half-life isotopes are employed.

Figure 71 portrays a typical relationship between the watts/lb. performance ratio and the total element length of segmented thermoelements for a cylindrical configuration utilizing thermoelements of 3/8-inch diameter and an isotope fuel consisting of Cm^{242}. The cold-junction temperature represents the parameter. The optimum performance is noted at approximately 9 watt(e)/lbs. for a total element length of 1.7 cm and a cold-junction temperature of 550°C. As shown in Figure 72, the conversion efficiency would be about 4.8% for this element length and cold-junction temperature. It is also noted from Figure 71 that a somewhat lower performance of, for example, 7.5 watt(e)/lb. can be attained for a fairly wide range of element lengths and radiator temperatures.

The general shape of the curves shown in Figure 71 illustrates the effect of obtaining improved generator performance by decreasing the overall element length. However, it is apparent that there is a practical limitation on improving the generator performance by decreasing the element length, because as the length decreases the resistance decreases, thus permitting an increase in current and losses. Also, the heat flux through each element increases, necessitating the rejection of more heat per unit radiator area. The maximum points on each curve in Figure 71 represent the cases where radiator size becomes the controlling factor and a further increase in heat throughput reduces the generator performance drastically.

In Figure 72 the overall generator efficiency associated with each of the cases shown in Figure 71 is demonstrated. The effect of changing the cold-junction temperature on generator efficiency is quite apparent.

Figure 73 illustrates the importance of a high-power density isotope for a 25 watt(e) cylindrical generator, fabricated with segmented thermoelements and operating between 1200°C and 600°C. In this case the only parameter varied was the isotope. Of the isotopes considered, Po^{210} is the most attractive heat source. Cm^{244} offers a relatively good performance, but other considerations such as cost, ground handling and payload shielding make Pu^{238} a more attractive, medium-density, long-life fuel. The performance values for Sr^{90} were calculated but they have not been plotted. The Sr^{90} performance values are quite low and it seems that Sr^{90} should only be utilized for terrestrial applications where weight is not such an overriding design criterion as it is in space power applications.

The maximum performance calculated for a 25-watt(e), cylindrical, isotope-heated generator, using 3/8-inch diameter thermoelements, are:

9.3 watt(e)/lb., using Po^{210} as a fuel
8.8 watt(e)/lb., using Cm^{242} as a fuel
3.8 watt(e)/lb., using Cm^{244} as a fuel

In Figure 74 is presented the comparison of the various designs of cylindrical, spherical, and sandwich conceptual designs for the 25-watt(e) generators utilizing Cm^{242} as the heat source.

The results of calculations based upon the 1200°C hot-junction and the 600°C cold-junction temperatures and 3/8-inch diameter segmented elements reveal that the spherical configuration has a slightly better performance than the cylindrical. In view of the fabrication complexity of a spherical configuration, it is

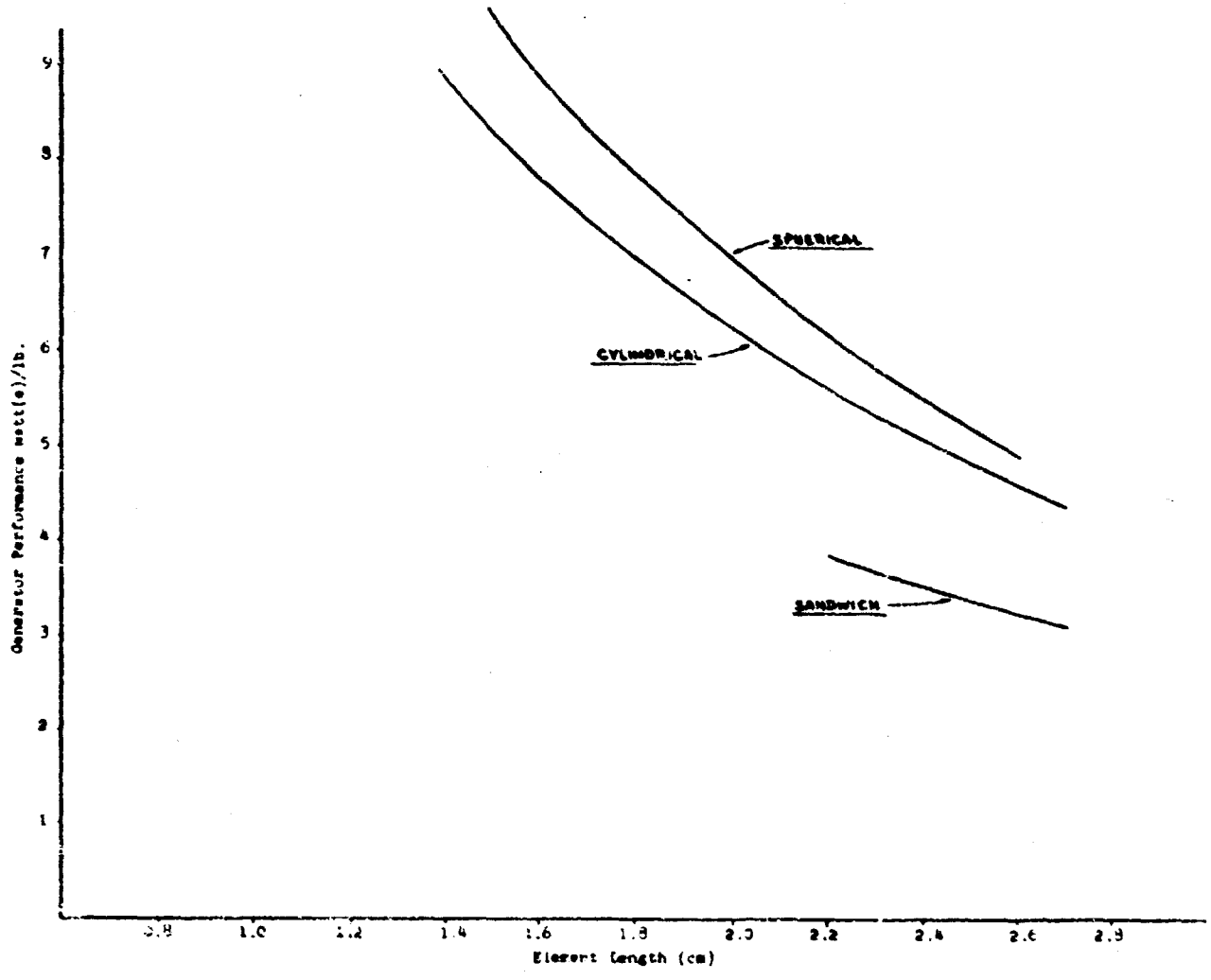

Figure 74. Comparison of Cylindrical, Spherical and Sandwich Generator Configurations of 25-watt(e) Output, T_h of 1200°C and T_c of 600°C with a Cm^{242} Heat Source

felt that the cylindrical configuration is to be preferred in almost all cases. The sandwich configuration compares very unfavorably with both the cylindrical and spherical design. It is again to be noted that the increased heat-rejection capacities of the radiators, due to the fin structures mounted on them, have not been taken into consideration and that further study will reveal that the actual performance values are in all cases somewhat larger and extend somewhat more into the range of shorter element lengths. However, it is felt that the conclusions with respect to the superiority of the cylindrical design still hold.

The figures for isotope costs under the November 1963 (Ref. 16) column were used at the time this part of the study was made, and, therefore, Cm^{242} was selected to show the typical dependencies of thermal efficiency and performance on element lengths for various element cross sections, radiator temperatures and generator configurations. However, Po^{210} is, on the basis of Ref. 14, lower in cost than Cm^{242} and, since it has also better performance (see Figure 73) and less shielding requirements than Cm^{242} has, Po^{210} would be the right choice for any short mission application. It is to be noted that the conclusions drawn from the Cm^{242} study are equally valid for Po^{210}.

In the medium-power density area, the initial fuel costs of Cm^{244} are identical with those for safe but low power density Pu^{238}. On a short-term basis, i.e., 1-5 year life, costs would remain the same, but if it were possible to use a generator to the half-life of Cm^{244} and Pu^{238}, then Pu^{238} would be the more economical fuel. Certainly Pu^{238} presents much less in the way of shielding and ground handling problems and costs than does Cm^{244} and would be much more economical to use.

Further revisions are anticipated to the projected costs of the eight isotopes listed in Table 93. Such changes in costs are dependent upon demand and type of usage involved in commercial developments. For the immediate future, isotope power density, availability, and mission safety factors will probably govern their selection for space power systems.

The results reported on the previous pages were based on the properties of the Monsanto Research Corporation MCC 60, MCC 50 and MCC 40 materials established for the period 1964-1965. A table of these properties is shown on page 168 of Section E. On the same page the thermoelectric property values considered to be feasible once the development of the MRC materials is completed

have been tabulated. It is felt that these material values a valid for the period 1971-1985. A preliminary study based upon these material values showed that a 1400°C hot-junction temperature, 1050°C interface-temperature, and 550 °C cold-junction temperature, a systems thermal efficiency of 9.0% can be reached, while a performance of better than 20 watts(e)/lb. can be achieved for a wide range of element lengths and cold-junction temperatures. A 25 watt(e) thermoelectric space power system using a gadolinium-polonide-210 heat source can have a performance better than 25 watts(e)/lb. based upon these 1971-1985 material property predictions.

f. Problem Areas In any discussion of anticipated problem areas for isotope-heated space power systems, the problem of safety during launch, abort, orbit, and reentry is paramount. Any new design would undoubtedly require an extensive safety analysis and test program. It should be feasible to solve such problems, since they are, in general, quite similar to those that were faced and solved during the several successful SNAP missions.

Additionally, problems will have to be solved in the production of the optimized but very small thermoelements needed, and in joining of the thermoelectric generator and isotope-container interfaces. Also important are the problems of when, where, and at what cost the desired quantities of isotopes can be obtained. Present indications are that the AEC could produce sufficient quantities of each of the isotopes considered here, if the mission is important enough to obtain project funding, and if sufficient lead time is allowed to provide the needed facilities.

Containment of isotopes, for use at 1200-1300°C in a vacuum or space environment, is at hand, and rugged functional and efficient junctions between the isotope-container and the thermoelectric generator components can be developed.

g. Probability of Success On the above bases, it is estimated that there is a high (up to 95%) probability of success for producing Cm^{242} (or Po^{210})-heated generators of 25-100 watts(e) capable of from 140 lbs./KW(e) performance during the 1965-1970 period.

3. Solar-Concentrating Thermoelectric Systems

a. Introduction Because of budget restrictions, this investigation was limited to estimating the performance of a typical solar-concentrating, high-temperature, thermoelectric generator module in space power systems, operating in a 130-mile terrestrial orbit at a solar flux of 135 watts/ft.^{2}.

Considerations of various solar-concentrator type space power systems (Ref. 17, 19, 20, 21) showed that:

1. Collectors of high (preferably >0.7) calorimetric efficiency and concentration ratios are needed to provide hot-junction temperatures of 1200°C in a near-earth orbit.

2. Only expensive one-piece, highly accurate, concentrating mirrors are likely to provide the necessary calorimetric efficiency.

3. Precise mirror-orienting mechanisms are required to keep the collector accurately aimed at the sun if constant 1200°C temperatures are to be maintained.

4. The maximum diameter of one-piece collectors capable of the high calorimetric efficiency and concentration ratios required is not likely to exceed 9 ft. This also appears to be about the maximum mirror diameter to permit stowability in launch vehicles to about 1970.

5. There is no reliable information on the life or performance of thermal storage systems that would work at temperatures to 1200°C.

6. The unit weights of advanced (1965-1970) one-piece collectors with appropriate deployment and orientation hardware were estimated to be about 0.5 lb./ft.^{2}.

b. Conceptual Design With regard to the performance of a thermoelectric generator to utilize the thermal energy from a solar collector, it was assumed that a 250-watt(e) unit of the design shown in Figure 75, capable of 4% thermal efficiency and 100 lbs./KW(e), could be available in the 1965-1970 period. Such a generator, shown without a thermal storage component, would consist of stacked rings of concentric layers of thermoelectric, contact, and radiator materials fabricated by plasma-spray or hot-pressed techniques. The conceptual designs presented in

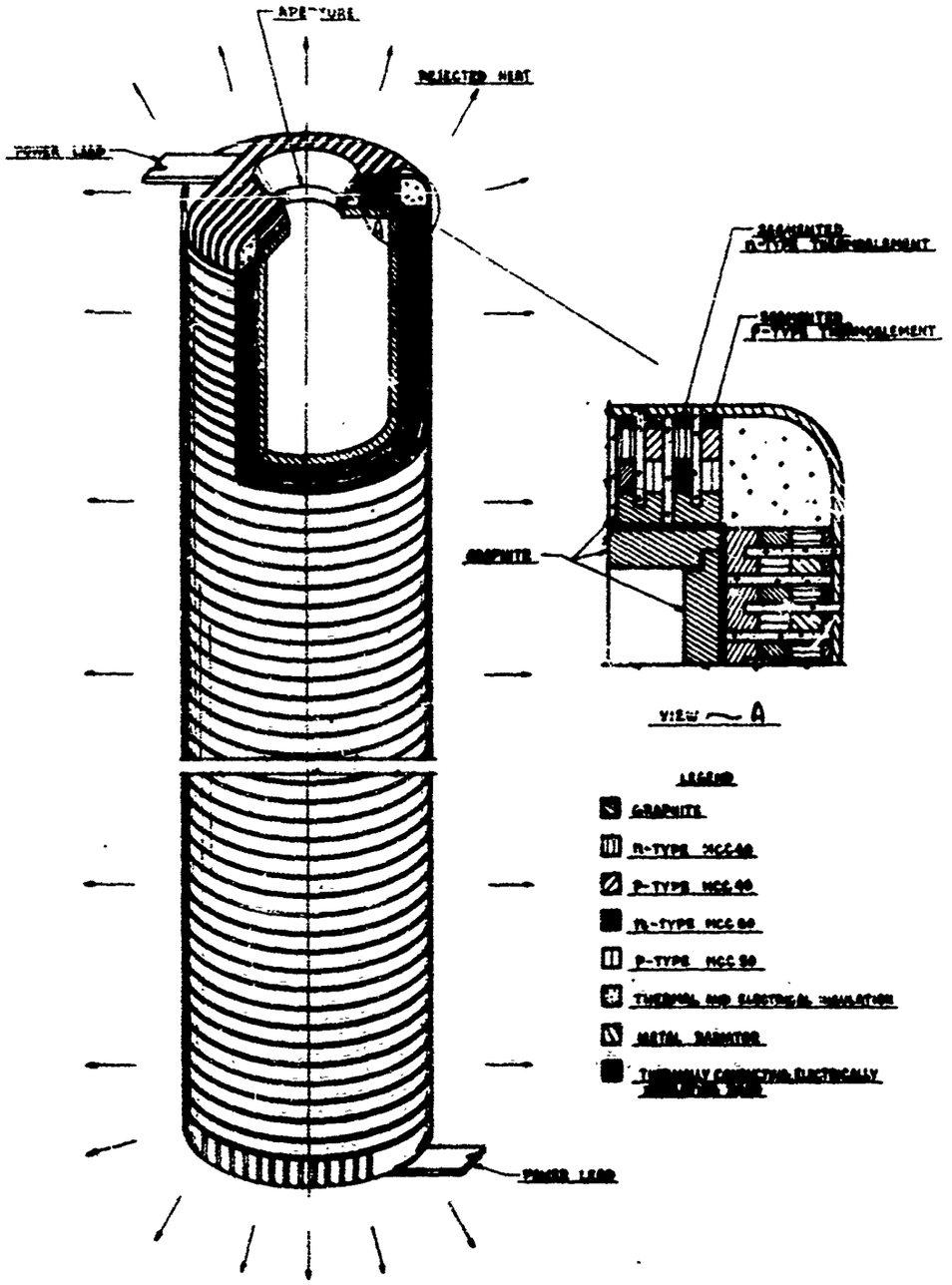

Figure 75. Conceptual Design of a 250-watt(e) Cavity-Type Thermoelectric Generator Made by Plasma-Spray Techniques

Figures 75 and 76 show only the plasma-sprayed type of thermoelement which we anticipate being available by 1970.

The central black body cavity of the generator of Figure 75 would consist of graphite. The ends of the generator would be produced from p- and n-type layers, also produced by plasma-spraying. As shown in the enlarged cross-section view "A", the stacked rings of thermoelements would be alternately p- and n-type, joined at their outer edges by a copper radiator and at their hot ends by graphite. The surface of the radiators would be treated with a highly emissive coating for maximum heat rejection. Each concentric-layered thermoelement ring or disc offers, in effect, many parallel thermal and electrical connection between its hot and cold ends with each two-segment p-type thermoelement ring joined in series to an adjacent n-type ring.

Current and voltage characteristics of this type of generator could be modified by slicing each disc to provide thin or thick thermoelement discs. Thin discs would yield thermoelements with higher length/area ratios, higher temperature drops across each ring, and higher voltage, with reduced Joule heating losses compared to thick discs. Accordingly, such a generator concept could be used to provide a large variety of power characteristics.

The thermoelectric generator concept of Figure 75 is shown in combination with a 9-ft. diameter high-quality collector in Figure 76. This collector-generator module, similar to designs proposed by others (Ref. 22), is equipped with a semicircular yoke which permits the collector to pivot toward the sun once the launch vehicle is in orbit and the stowed modules are deployed.

c. Performance Characteristics A brief examination was made of the possibility of using either heat-of-fusion or vapor-phase types of thermal storage components to provide energy during a dark orbit period of 35 minutes. It was found that for a 250-watt(e) generator, as shown in Figure 75, operated at a T_h of 1200°C, the available thermal storage cavity (23 inches long by 2.5-inches diameter) is not large enough to handle the volume of thermal storage materials that would be required.

As an alternative, silver-cadmium batteries rated at about 400 watt-min./lb. (1965-1970 technology) for 50% discharge depths were assumed as the source of energy during the dark orbiting period. A 10% additional energy allowance was assumed for these batteries.

No power conditioning equipment was assumed, since it is possible to produce directly about 100 volts with a 250 watt(e)

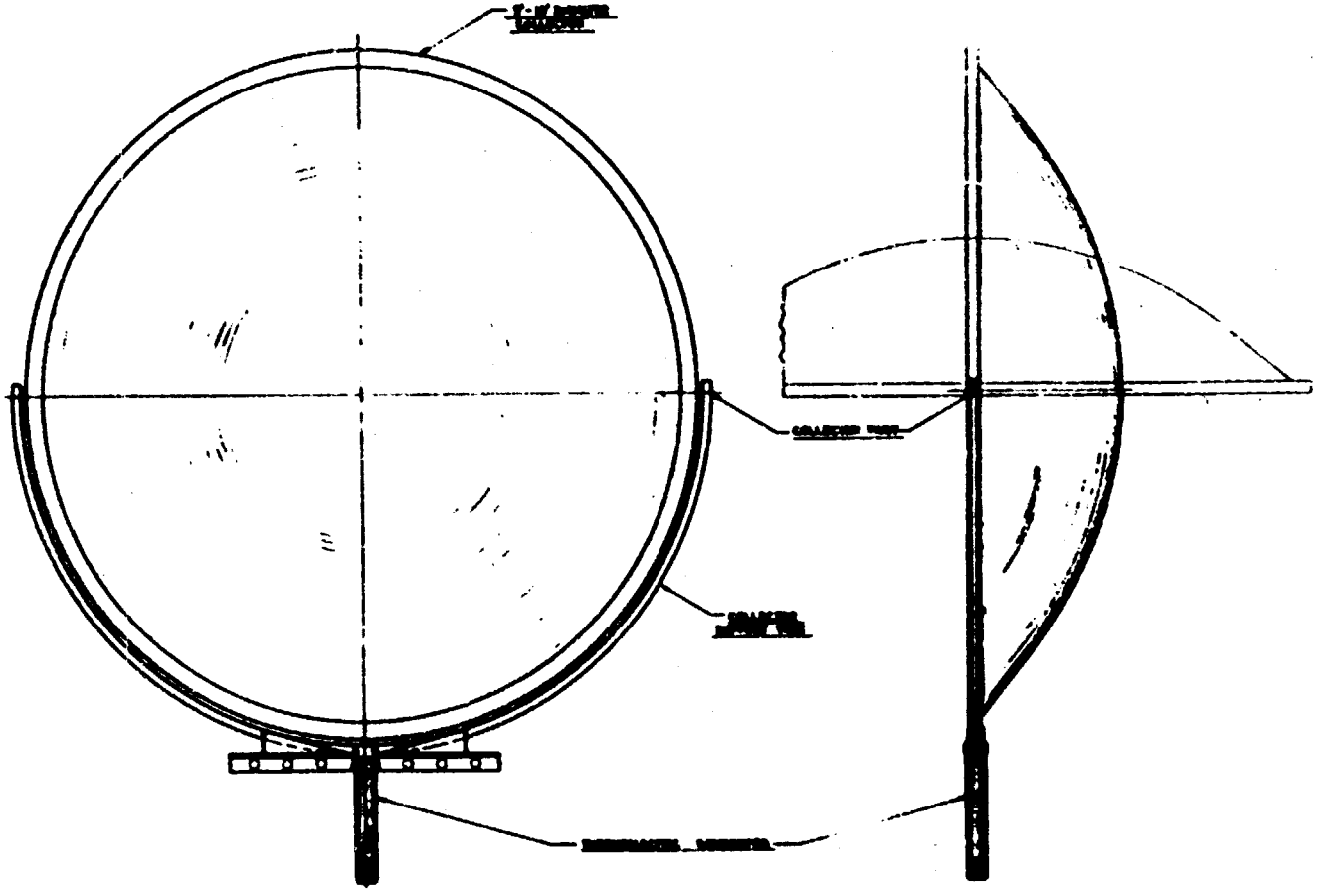

Figure 76. Conceptual Design of a Solar Collector Cavity-Type High-Temperature Thermoelectric Space Power Module

Module Component	Weight/Module, lbs
Mirror with deployment and orientation hardware	35.2
Batteries	23.5
Thermoelectric generator	25
Total Weight	83.7 lbs

The specific performance of a 250 watt(e) mirror-generator module based on the above weight is 335 lb/KW(e). Based on an estimated volume of 60 ft^3/module (complete with battery storage), the specific volumetric performance for this type of system would be 240 ft^3/KW(e). Assuming a length/diameter ratio of 2:1, for stowage chambers required to house such solar-concentrating thermoelectric power systems during launch, the following relation exists between stowage chamber diameters and power output:

System Power Output, KW(e)	Stowage Chamber Diameter, ft.	Weight of System, Without Stowage Chamber, lbs
1	5.4	335
3	7.7	1,000
10	11.6	3,350
20	14.6	6,700
30	16.6	10,000
350	37.6	117,000

As indicated by the above performance numbers, it is not anticipated that the stowed volume per module or the lb/KW(e) performance will decrease with increasing output levels for solar-concentrating thermoelectric space power systems. For this reason there is nothing to be gained in system performance by increasing the power level. As indicated above, large vehicles would be required to launch power systems of more than a few KW(e) output.

d. Problem Areas Mirror fabrication techniques appear to have progressed to the point where one-piece parabolic units up to 9 ft in diameter, capable of 0.73% thermal efficiency, could be produced. However, the situation is not as good with respect to deployment and orientation mechanisms capable of properly and reliably manipulating more than one or two of the proposed modules in a space environment. It is our opinion that considerable effort will be required to develop deployment-orientation hardware that will be suitable for attainment and maintenance of the needed 1200°C hot-junction temperatures in a space environment for the thermoelectric component.

Battery technology appears adequate for providing the energy storage needs involved in near-earth orbits and for reasonable time periods. However, problems will have to be solved in integrating electrical characteristics of the thermoelectric generator with those for the batteries and the duty cycles imposed by missions. It may be advisable to use power conditioning equipment, which will further increase the lb/KW(e) ratio and lower the performance of the system.

With regard to the thermoelectric generator, it is likely that hot-pressed rather than plasma-sprayed thermoelements would be available by 1964-1965. While it is anticipated that the thermoelectric properties of individual thermoelectric materials used in this investigation will be available by 1964-65, there are difficult problems to be solved in producing high-performance, short, segmented thermoelements of less than 1/4-inch diameter.

Solutions for each of the above problem areas are technically feasible.

e. Probability of Success On the premise that the state of the art on one-piece solar-concentrators is presently adequate, and that hot-pressed thermoelements capable of 7.5-10 watts(e)/lb performance will be available by 1964-1965, the probability of success should be quite high (>95%) for producing a practical, solar-concentrating, thermoelectric space power module of the predicted performance during the 1965-1970 period.

IV. RECOMMENDATIONS

The key to improved performance (watts/lb. or watts/ft.^{2}) of all space power systems is heat source temperature. Since advancement in performance must be paced by the availability of the materials technology required for high-temperature operation, our progress on thermoelectric elements during the past year, coupled with the inherent reliability of thermoelectric systems, now leads us to recommend further effort in the following areas.

A. FUNDAMENTAL INVESTIGATIONS

It is recommended that attempts be made to identify important solid-state components found in the MCC thermoelectric materials after their fabrication at high temperatures. Attainment of this difficult goal could appreciably extend the state of the art of high-temperature thermoelectric materials and lead to the establishment of meaningful physical models of these unique materials.

B. FABRICATION TECHNIQUES

It is recommended that additional effort be directed to developing further improvements in methods for measuring R, S, k, and ρ to 1200°C. Production of improved thermoelements by means of hot-pressing, isostatic hot-pressing and arc-plasma spraying techniques should be investigated. Additionally, efforts should be made to improve the reproducibility of thermoelements to be used in thermoelectric generators.

C. MATERIAL CHARACTERISTICS

Since the performance of thermoelectric generators is highly dependent upon the thermal conductivity of the thermoelectric materials, it is recommended that further attempts be made to measure this property up to 1200°C in a vacuum. Additionally, important mechanical properties such as the elastic modulus, modulus rigidity, compressive and impact strengths, expansion coefficients, and density should be measured to permit more meaningful mechanical system designs.

D. COMPONENT RESEARCH

It is recommended that studies be made to consider maximum utilization of available thermal flux area, radiator fin effectiveness, element electrical interconnections, and thermal shunt losses of high-temperature thermoelectric generators. Additionally, it would be helpful to determine the effect of radiation on the performance of the four MCC materials being investigated.

E. LABORATORY MODEL

Since meaningful design and operating data can be more economically obtained using 5-10 watt generators, rather than 25-100 watt units, it is recommended that future evaluation of thermoelectric elements, modules and designs be confined to small generators. Vibration, shock, and acceleration tests on representative generators, or generator sections, should be made. Differences in the cost of large vs. small generators should be applied to laboratory studies of various types of thermal insulation needed to minimize thermal shunt losses in space power units.

F. RADIOISOTOPE SYSTEM CONCEPTS

Radioisotope subsystem concepts, with respect to probable designs, characteristics, problem areas, and methods of problem circumvention should be studied in greater detail, taking into account the latest thermoelectric properties. Additionally, the performance of such systems should be made on the basis of projected material properties and mission areas of interest to the Air Force.

V. REFERENCES

1. Power Sources Draw Attention at Geneva, C and EN, p. 56-57 Sept 21, 1964.

2. Henderson, C. M., et al, High Temperature Thermoelectric Generator, ASD-TDR-62-896, Part II, Oct 1963, p. 115.

3. Ibid.,p.130-132

4. Ibid.,p. 121-132

5. Szego, G. C., Space Power Systems, XIVth Congress of The International Astronautical Federation, Part IV, Paris, September 1963.

6. Dieckamp, H., Nuclear Space Power Systems, Atomics International, Report AI-Memo-7585, Revision 1 (1963).

7. Johnson, C. E. and Goetz, C. A., "SNAP 8 Reactor and Shield AIAA Journal, Vol. 1, 1963, p. 2355.

8. MacFarlane, D. R., A 200-watt Conduction-Cooled Reactor Power Supply for Space Application, Argonne National Laboratory Report ANL-6694, March 1963.

9. Miscellaneous Notices, United States Federal Register, October 15, 1962.

10. McAlduff, Harold, AEC Materials Leasing Officer, Oak Ridge, Tennessee, private communication.

11. Davis, H. L., Nucleonics, Vol. 21, No. 3, March 1963, p.61.

12. Hittman Associates, Inc., Task 9, Radioisotopes for Power Production, AEC Contract AT(30-1)-3165, Baltimore, Maryland September 1963.

13. Nichols, J. D. and Arnold, E. D., Nucleonics, Vol. 22, February 1964, p.52.

14. A. E. C. Clearing House Report No. 11, Vol. 10, March 16, 1964.

15. Anon, Nucleonics, Vol. 21, October 1963, p. 74.

16. Hanford Laboratory Report, No. HW-76323, Revision 1, p.52.

17. Swanson, B. W., Somers, E. V., Heikes, R. R., Journal of Heat Transfer, February 1961, p.77.

18. W. E. Kortier, The Analysis and Design of a High Temperature Thermoelectric Conversion Device, June 1964. BAT-5-3697-1.

19. Szego, G. C., Space Power Systems, XIVth Congress of The International Astronautical Federation, Part III, Paris, September 1963.

20. Heath, A. R., Status of Solar Energy Collector Technology, Space Power Systems Conference, Santa Monica, California, September 25-28, 1962.

21. McClelland, D. H., Solar Concentrator and Absorbers, Space Power Systems Course, George Washington University, 1 September 1963.

22. Batutis, E. F. and Purdy, D. L., Thermal Energy Storage For Thermionic Conversion, Space Power Systems Course, George Washington University, 1 September 1963.

APPENDIX I

COMPUTER PROGRAMS FOR PARAMETER STUDIES OF NUCLEAR REACTOR-THERMOELECTRIC SPACE POWER GENERATION SYSTEMS

Three programs were written to describe nuclear reactor-based thermoelectric space power systems: 1) an out-of-pile system, 2) an in-pile system without coolant loop, and 3) an in-pile system with coolant loop. The code names for these three computer programs are HORSE, TIGER, and SWIFT, respectively. In each of the three cases, the objective was to mathematically describe the important parameters in the system and evaluate the total weight, system volume, and fuel cost for a given set of parameters. The main components in each system were the reactor, the reactor shielding, the radiator-generator, and the structural weight.

I. PROGRAM HORSE (High-Temperature, Out-of-Pile, Reactor-Powered System for Generation of Electricity

Program HORSE was written to describe an out-of-pile thermoelectric space power system which utilizes a fast nuclear reactor as its heat source. Coolant circulating through the reactor core carries heat to the thermoelectric elements located between the reactor shield and the payload. The thermoelectric elements are cooled by radiation from radiators attached to their cold ends. Location of the elements away from the reactor prevents them from directly affecting the reactor design, but it does introduce the need for a heat transfer loop.

Program HORSE consists of the following parts:

1. Executive Routine
2. Subroutine 1--heat transfer in reactor core
3. Subroutine 2--for sizing nuclear reactor core
4. Subroutine 3--reactor shielding calculations
5. Subroutine 4--generator calculation
6. Subroutine 5--input data
7. Subroutine 6--thermoelectric element data
8. Subroutine Exit

The subroutines are discussed as they enter into the program.

Executive Routine Few calculations are carried out in the Executive Routine. Its main function is to control the logic flow of the program. The statements describing what output is to be printed and the form in which it is to be printed are also located in the Executive Routine.

Subroutine 6 The first subroutine called by the Executive Routine is Subroutine 6, which controls the reading in of the thermoelectric element data onto a scratch tape. This data was calculated via another computer program and the results punched onto cards for use as input data to program HORSE. The following data is given for elements of various diameters: the computer run number, the thermal efficiency, the power per couple, the radiator area required per couple, the watts per pound, the element length, and the radiator temperature. This data is read into the computer and stored until actually needed in the calculations. The number of cards read in at this time may number in the hundreds. Subroutine Exit erases and rewinds this tape after the data has been used.

Subroutine 5 After the thermoelectric element data has been read in, the Executive Routine calls Subroutine 5 to read in the rest of the input data. The input data consists of the following:

Fuel density
Fuel atomic weight
Fuel molecular weight
Critical mass
Cost per gram of fuel
Fission cross-section of fuel
Absorption cross-sections of fuel
Thermal expansion coefficient
Extrapolation distance
Reflector savings
Reflector thickness
Reflector density
Number of neutrons emitted per fission
Molecular weight of tubing material
Tube wall thickness
Tube diameter
Density of tubing material

Absorption cross-section of tubing
Density of gamma shielding material
Density of neutron shielding material
Density of shield container material
Neutron cross-section of neutron and gamma absorbing materials
Gamma cross-sections of the neutron and gamma absorbing materials
Neutron and gamma absorbing properties of fuel
Shield container thickness
Allowable neutron dosage to payload
Allowable gamma dosage to payload
Coolant density
Coolant thermal conductivity
Coolant specific heat
Coolant viscosity
Coolant molecular weight
Coolant absorption cross-section
Log mean temperature difference between coolant and reactor core
Approximate core temperature
Temperature of the coolant leaving reactor
Reactor core height
Distance between payload and reactor core
Diameter of payload
Fluid velocity
Watt output desired from system
Length of time system is to operate
Run number.

After these numbers are read, the calculations are begun in Subroutine 1.

Subroutine 1 Using the assumed values of fluid velocity and tube inside diameter, the weight rate of flow per tube is calculated.

$$WTFLOW = 1560\ (CSATUB)\ (FLDVEL)\ (DNSCOL) \qquad \text{Eq. 1}$$

WTFLOW = weight rate of coolant flow, lbs/hr/tube
CSATUB = inside cross sectional area of tube, in^2.
FLDVEL = fluid velocity, ft/sec.
DNSCOL = coolant density, gms/cc

The next step is to calculate the heat transfer coefficient inside the core based upon the Seban-Shimazaki equation (Ref. 1).

$$HTTRCO = 12 \frac{(THKCOL)}{(TUBEID)} \left[4.8 + 0.030 \left(\frac{WTFLOW \times SPHTCL}{TUBEID \times THKCOL}\right)^{0.8}\right] \quad \text{Eq. 2}$$

als

HTTRCO = heat transfer coefficient, Btu/hr/ft^2/°F
THKCOL = thermal conductivity of coolant, Btu/hr/ft/°F
TUBEID = inside diameter of coolant tube, inches
SPHTCL = specific heat of coolant, Btu/lb/°F

The heat transfer per tube is then calculated using equation 3.

$$QPRTUB = (HTTRCO)\ (PRAPTB)\ (DELT) \quad \text{Eq. 3}$$

QPRTUB = heat transferred per tube, Btu/hr/tube
PRAPTB = peripheral area inside tube, ft.^{2}
DELT = temperature difference between coolant and tube wall, °F

DELT across the coolant film is initally assumed to be 300°F.

Next, the temperature increase of the coolant as it passed through the core is calculated using equation 4. This increase is

$$TEMPDR = QPRTUB/(WTFLOW \times SPHTCL) \quad \text{Eq. 4}$$

TEMPDR = temperature rise, °F

assumed to be equal to the temperature drop as the coolant passes through the generator. All of this heat is assumed to pass through either the elements or the insulation surrounding them. If TEMPDR exceeds 100°F, DELT is lowered and QPRTUB and TEMPDR are recalculated until TEMPDR is equal to or less than 100°F.

The total electrical output required is calculated next in equation 5.

$$TWATTE = WATTSE + WATTEC + WATTEP \quad \text{Eq. 5}$$

TWATTE = total power generated by system, watts
WATTSE = electrical output of system, watts
WATTEC = electrical power needed for reactor control, watts
WATTEP = electrical power needed to run pump, watts

Initially, the pump power is assumed to be zero.

Next, the total reactor heat load is calculated in equation 6.

$$TOHTLD = 100\ (TWATTE)/EFFGEN \qquad \text{Eq. 6}$$

TOHTLD = total heat load, watts
EFFGEN = generator efficiency, percent

The number of coolant tubes required inside the reactor core is calculated from equation 7. Since the number of tubes used

$$NUMTUB = 3.413\ (TOHTLD/QPRTUB) \qquad \text{Eq. 7}$$

NUMTUB = number of tubes, dimensionless

must be an integer, NUMTUB is rounded off to the next highest integer.

The next major step is to calculate the actual amount of pump power required. To do this, the friction factor for the coolant tubes is first calculated using equation 8.

$$FFACT = 0.00140 + 0.125 \left[\frac{(2.42)(VISCOL)(CSATUB)}{(12)(TUBEID)\ (WTFLOW)}\right]^{0.32} \qquad \text{Eq. 8}$$

FFACT = friction factor, dimensionless
VISCOL = coolant viscosity, centipoise

The pressure drop across the reactor core is calculated using equation 9.

$$PDROP = (6.0) \left[\frac{4.275 \times 10^{-6}(FFACT)(HEIGHT + 15)\ (WTFLOW)^2}{32.17\ (TUBEID)\ (CSATUB)^2\ \ (DNSCOL)}\right] \qquad \text{Eq.}$$

PDROP = pressure drop across reactor core, psi
HEIGHT = reactor core height, cm
DNSCOL = coolant density, gm/cc

A distance of 15 cm was added to the core height in order to allow for tubing connections to the core. The calculated pressure drop

was multiplied by 6 to allow for pressure drop through the rest of the coolant system. The pump power requirement was then calculated using equation 10.

$$WATTEP = 1.356\ (PDROP)\ (CSATUB)\ (FLDVEL)\ (NUMTUB)/E\ FFPMP \quad \text{Eq. 10}$$

EFFPMP = pump efficiency, fraction

The pump efficiency used in the initial calculation was 0.40, assuming the use of a DC electromagnetic pump. These pumps are noted for their simplicity of construction, minimum insulation problems, and achievement of long periods of operation at high (1472°F) temperature (Ref. 2). The total electrical power generated is then recalculated using equation 5 and compared with the amount previously calculated. The program recycles through equations 5 through 10 until successive values of TWATTE agree within one percent.

Subroutine 2 The purpose of this subroutine is to size the cylindrical reactor core of HORSE. The first step is to take the spherical critical mass of the fuel and modify it for the effects of thermal expansion (Eq. 11) and control allowances (Eq. 12).

8

$$DNSFS2 = DNSFS1 / [1 + ALPHA\ (TCORE-75)] \quad \text{Eq. 11}$$

DNSFS1 = density of fissionable atoms at room temperature, gm/cc
DNSFS2 = density of fissionable atoms at operating temperature, gm/cc
ALPHA = volumetric thermal expansion coefficient for fuel, cc/cc°F
TCORE = temperature of reactor core, °F

Eq. 9

$$DNSFS3 = DNSFS2\ (1-ALLOW) \quad \text{Eq. 12}$$

DNSFS3 = density of fissionable atoms with temperature and control allowances, gm/cc
ALLOW = control allowance, dimensionless

w

The control allowance was assumed to be equivalent to a 4 percent decrease in fuel density.

The next major step is to calculate the effect of coolant tube dilution on the fissionable atom density. The volume of the spherical critical mass undiluted for effects of thermal expansion or control allowance is calculated using equation 13.

$$VOLSPH = CTMASS/DNSFUL \qquad \text{Eq. 13}$$

VOLSPH = volume of the undiluted mass, cc
CTMASS = critical mass of fuel, grams
DNSFUL = density of the fuel at room temperature, grams/cc

The relationship between critical masses and densities of fissionabel atoms is shown in equation 14 where it is indicated that the critical mass is inversely proportional to the density of the fissionable atoms squared.

$$\frac{CMASS_2}{CMASS_1} = \left(\frac{DNSFL_1}{DNSFL_2}\right)^2 \qquad \text{Eq. 14}$$

$CMASS_{1,2}$ = critical masses of fissionable atoms, gms
$DNSFL_{1,2}$ = densities of fissionable atoms, gm/cc

Since mass is equal to volume x density, equation 14 can be modified to equation 15 where the quantities VOLDIL minus TUBVOL and VOLDIL are proportional to the fissionable atom densities.

$$VOLDIL = VOLSPH \left(\frac{VOLDIL-TUBVOL}{VOLDIL}\right)^3 \qquad \text{Eq. 15}$$

VOLDIL = diluted critical volume, cm^3
TUBVOL = volume of tube, cm^3

The volume of the tubing is calculated using equation 16.

$$TUBVOL = \frac{\pi}{4}\left[(TUBDIA)^2 \ (HEIGHT) \ (NUMTUB)\right] \qquad \text{Eq. 16}$$

TUBDIA = tube diameter, cm
HEIGHT = core height, cm
NUMTUB = number of tubes in core, dimensionless

The tubes and coolant are treated as additional moderator absorbing neutrons.

Having calculated TUBVOL and VOLDIL, one can then calculate the density of the reactor core diluted by thermal expansion, control allowance, and inclusion of coolant tubes using equation 17.

$$DILDNS = DNSFS3 \left(1 - \frac{TUBVOL}{VOLDIL}\right) \qquad \text{Eq. 17}$$

DILDNS = density of diluted core, gms/cc

The critical mass of the diluted core can be calculated using equation 18.

$$CTMSDL = CTMASS \left(\frac{DNSFS1}{DILDNS}\right)^2 \qquad \text{Eq. 18}$$

CTMSDL = critical mass of diluted core, gms/cc
CTMASS = critical mass of core undiluted, gms/cc

Next, the critical radius of the diluted sphere is calculated using equation 19.

$$CTRAD = \left(\frac{VOLDIL \times 3}{4\pi}\right)^{1/3} \qquad \text{Eq. 19}$$

CTRAD = critical radius of diluted sphere, cms

CTRAD is used to calculate the buckling for the fuel material using equation 20.

$$BUCSPH = \left(\frac{\pi}{CTRAD + DELEXT + DELSAV}\right)^2 \qquad \text{Eq. 20}$$

BUCSPH = buckling for material, cm^{-2}
DELEXT = extrapolation distance, cms
DELSAV = reflector savings, cms

The extrapolation distances used were 1.5 cm for $Pu^{239}O$, 1. cm for $U^{233}O$, and 2.. cms for [illegible]. The reflector savings for BeO or Be are listed below (Ref. 3).

Reflector Thickness, cms	Reflector Savings, cms		
	PuC	$U^{233}C$	$U^{235}C$
0	0	0	0
2	1.2	1.4	1.8
5	2.1	2.4	3.0
10	2.7	3.3	4.5

The next step is to calculate the radius of the cylindrical reactor core using equations 21 and 22.

$$B_G^2 = B_M^2 = \text{BUCSPH} \qquad \text{Eq. 21}$$

$$B_G^2 = \left(\frac{2.405}{\text{CYLRAD} + \text{DELEXT} + \text{DELSAV}}\right)^2 + \left(\frac{\pi}{\text{HEIGHT} + 2\ \text{DELEXT} + 2\ \text{D}}\right.$$

Eq. 22

B_M^2 = material buckling, cm^{-2}
B_G = geometrical buckling, cm^{-2}
CYLRAD = radius of cylindrical reactor core, cm

The volume of fuel material is calculated from equation 23.

$$\text{FULVOL} = \pi\ (\text{CYLRAD})^2\ (\text{HEIGHT}) - \text{TUBVOL} \qquad \text{Eq. 23}$$

FULVOL = volume of the fuel, cc

The weight of the fissionable atoms is then calculated from equation 24, and the weight of the fuel is calculated by equation 25.

$$\text{WTFISS} = (\text{FISVOL})\ (\text{DNSFS3}) \qquad \text{Eq. 24}$$

WTFISS = weight of fissionable atoms, gms

$$\text{WTFUEL} = \text{WTFISS}\ (\text{FMOLWT}/\text{FATMWT}) \qquad \text{Eq. 25}$$

WTFUEL = weight of fuel, grams
FMOLWT = molecular weight of fuel
FATMWT = atomic weight of fissionable atoms

Reactor core weight. including reflector weight, is calculated from equation 26.

$$WTCORE = WTFUEL + [\pi (CYLRAD + REFTHK)^2 * (HEIGHT + 2*REFTHK) - (FISVOL + TUBVOL (HEIGHT + 2 REFTHK)/HEIGHT)] REFDNS \quad \text{Eq. 26}$$

REFTHK = reflector thickness, cm
REFDNS = density of reflector material, gms/cc
WTCORE = gross weight of core, grams

WTCORE is converted to pounds; 100 pounds is added as allowance for reactor controls.

Subroutine 3 Having calculated the coolant tubes needed in the reactor core, the amount of shielding is next calculated. Payload was assumed to be an instrument payload with transistors able to withstand radiation levels of 10^7 Rad carbon of gamma radiation and 10^{13} neutrons/sq cm over their lifetime. Payload has a 3-ft. diameter and is located 15 plus feet from the nearest point of the reactor core. Attenuation of gamma radiation occurs by the inverse square law with distance and by absorption. Absorption within the core and materials between payload and core was usually enough to absorb almost all gamma radiation, so that the gamma shielding usually was not heavy. In contradistinction, neutron shielding was heavy, where lithium hydride encased in stainless steel containers 0.109 inches thick was used. When gamma shielding was needed, depleted uranium was used.

The first step in calculating shielding requirements is to calculate the numbers of atoms of various types present in the reactor core in atoms/cc. Volume of the fissionable part of the core is calculated by equation 27.

$$CORVOL = \pi (CYLRAD)^2 (HEIGHT) \quad \text{Eq. 27}$$

CORVOL = volume of reactor core, cm^3

The atoms/cc of fissionable material are then calculated from equation 28.

$$APCCFS = WTFISS \times 6.02 \times 10^{23}/(FATMWT \times CORVOL) \quad \text{Eq. 28}$$

APCCFS = atoms of fissionable materials per cc

The volume of tubing material in the core is calculated from equation 29.

$$VTUBWL = \pi/4 \ (TUBEOD^2 - TUBEID^2) \ (HEIGHT) \ (NUMTUB) \quad \text{Eq. 29}$$

VTUBWL = volume of tubing atoms, cm^3

The average number of tubing atoms/cc of core volume is calculated from equation 30.

$$APCCTB = VTUBWL \times DNSTUB \times 6.02 \times 10^{23}/(TMOLWT \times CORVOL) \quad \text{Eq. 30}$$

APCCTB = atoms of tubing material, cc
TMOLWT = molecular weight of tubing
DNSTUB = density of tubing material, gm/cc

For the initial calculations on HORSE, molybdenum tubing with a specific gravity of 10.2 grams/cc and a molecular weight of 95.95 was assumed.

Next, the volume of coolant in the core is calculated from equation 31.

$$VOLCOL = \pi/4 \ (TUBEID)^2 \ (HEIGHT) \ (NUMTUB) \quad \text{Eq. 31}$$

VOLCOL = volume of coolant, cm^3

The atoms of coolant per cu cm of the reactor core are calculated from equation 32.

$$APCCCL = VOLCOL \times DNSCOL \times 6.02 \times 10^{23}/(CMOLWT \times CORVOL) \quad \text{Eq. 32}$$

APCCCL = atoms of coolant per cc of core volume
DNSCOL = density of coolant, grams/cc
CMOLWT = coolant molecular weight

In the initial calculations liquid lithium was used as the coolant.

Next, the macroscopic neutron capture cross-sections were calculated for the fuel, coolant, and the tubing material using equation 33.

. 28 $$SGMAFS = APCCFS \times FCRS \times 10^{-24} \qquad \text{Eq. 33}$$

SGMAFS = macroscopic fission cross-section of fissionable atoms, cm^{-1}
APCCFS = fissionable atoms/cc
FCRS = fission cross-section, barns

. 29 Next, the infinite multiplication factor for neutrons was calculated from equation 34.

lated $$FINFMT = \frac{FISNEU \times SGMAFS}{(SGMAFS + SGMAF1 + SGMAF2 + SGMATC + SGMACC)} \qquad \text{Eq. 34}$$

Eq. 30

FINFMT = infinite multiplication factor, dimensionless
FISNEU = average number of neutrons emitted per fission
SGMAF1 and SGMAF2 = neutron capture cross-section of fuel and fuel anion, cm^{-1}
SGMATC = neutron capture cross-section of tubing material, cm^{-1}
a .95 SGMACC = neutron capture cross-section of coolant, cm^{-1}

The average number of fission neutrons per fission for uranium 233 is equal to 2.65, for uranium 235 = 2.52, for plutonium = 2.98. Since an average of 1.0 neutrons per fission is needed to cause Eq. 31 other atoms to fission and sustain the chain reaction, the excess neutrons which must be shielded against are calculated by taking the number of fissions which occur per second and multiplying this by the infinite multiplication factor minus 1 as in equation 35.

$$TNUSEC = (FINFMT - 1.0) (FISSEC) \qquad \text{Eq. 35}$$

Eq. 3[illegible]

TNUSEC = total neutrons per sec to be shielded against
FISSEC = fissions occurring per second

Since 3.3×10^{10} fissions/sec are required in order to yield one thermal watt, the total number of fissions taking place per second can be calculated from equation 36.

lant. $$FISSEC = 3.3 \times 10^{10} (TOHTLD) \qquad \text{Eq. 36}$$

1-

TOHTLD = total heat load, watts

The total number of neutrons given off during the mission lifetime is calculated from equation 37.

$$TNUMIS = 3600 \times TNUSEC \times TIME \qquad \text{Eq. 37}$$

TNUMIS = total number of neutrons given off during the mission lifetime
TIME = mission lifetime, hours

The amount of neutron attenuation required for shielding is calculated from equation 38.

$$ATTNEU = 4\pi\ (DISTCP)^2\ (DOSEN)/TNUMIS \qquad \text{Eq. 38}$$

ATTNEU = required neutron attenuation
DISTCP = distance between core and instrument payload, cm
DOSEN = allowable total number of neutrons per cm^2 which the payload can tolerate over its lifetime

Neutron cross-sections used in the above calculations were read at 3 MEV. The gamma rays emitted were also assumed to all be at 3 MEV. An average of 5.67 of these gamma rays was assumed to be emitted per fission. See equation 39.

$$TGMSEC = 5.67 \times FISSEC \qquad \text{Eq. 39}$$

TGMSEC = total gamma rays emitted per second

The total amount of gamma rays emitted per mission is calculated using equation 40.

$$TGAMIS = 3600 \times TGMSEC \times TIME \qquad \text{Eq. 40}$$

TGAMIS = total number of gamma rays emitted per mission

The necessary gamma attenuation is then calculated from equation 41.

$$ATTGAM = 4\pi\ (DISTCP)^2\ (2.08 \times 10^7\ DOSEG)/TGAMIS \qquad \text{Eq. 41}$$

ATTGAM = required gamma attenuation
DOSEG = allowable gamma ray dose at payload, Rad carbon

Next, the thickness of gamma shielding material is calculated using equation 42.

$$TSHLDG = \left[CSNLIH(\ln_e ATTG4M) - GCSLIH(\ln_e ATTNEU) + CONTHK \times (GCRSSS \times CSNLIH - GCSLIH \times CSNSS) + CSNLIH \times GCSFUL \times \frac{DNSFS3}{DNSFS1} \times \frac{FISVOL}{FISVOL + TUBVOL} \times \frac{HEIGHT}{2}\right] \div (GCSLIH \times CSNDPU - GCSDPU \times CSNLIH)$$

Eq. 42

TSHLDG = gamma shield thickness, cm
CSNLIH = neutron removal cross-section for lithium hydride, cm^{-1}
CONTHK = container thickness, cm
GCRSSS = gamma removal cross-section for stainless steel container, cm^{-1}
CSNSS = neutron removal cross-section for container, cm^{-1}
GCSLIH = gamma removal cross-section for lithium hydride, cm^{-1}

Next, the neutron shield thickness is calculated from equation 43.

$$TSHLDN = - \frac{(\ln_e ATTNEU + CSNDPU \times TSHLDG + CSNSS \times CONTHK)}{CSNLIH} \div$$

Eq. 43

TSHLDN = thickness of neutron shielding material, cm

Having established the thicknesses of the neutron and gamma shielding materials, the next step is to establish their diameters. The equations below assume that the reactor core diameter is smaller than the payload diameter, that the gamma shielding material is adjacent to the core, and that the neutron shielding material is between the gamma shielding material and the payload.

An extrapolation distance is calculated to aid in sizing the diameters of the shadow shields. See equation 44.

$$EXDIST = \frac{2 \times CYLRAD\ (HEIGHT + DISTCP)}{(PAYDIA - 2\ CYLRAD)} \qquad \text{Eq. 44}$$

EXDIST = extrapolation distance, cm
PAYDIA = payload diameter, cm

The diameter of the gamma shadow shield adjacent to the reactor core (DSHLD1) is found from equation 45.

$$DSHLD1 = 2(CYLRAD)\ \ (EXDIST + HEIGHT)/EXDIST \qquad \text{Eq. 45}$$

The other diameter of the frustrum of the cone forming the gamma shadow shield (DSHLD2) is found from equation 46.

$$DSHLD2 = 2\ (CYLRAD)\ (EXDIST + HEIGHT + TSHLDG)\ \div EXDIST \qquad \text{Eq. 46}$$

The smaller diameter of the neutron shadow shield is assumed equal to the larger diameter of the gamma shadow shield. The larger diameter of the neutron gamma shield (DSHLD3) has been calculated from equation 47.

$$DSHLD3 = 2(CYLRAD)\ (EXDIST + HEIGHT + TSHLDG + TSHLDN) \div EXDIST \qquad \text{Eq. 47}$$

The weight of the gamma shadow shield is then calculated from equation 48.

$$WTGMSD = \pi/12\ \ (DNSHDG)\ \ [(DSHLD2)^2\ (EXDIST + HEIGHT + TSHLDG) - (DSHLD1)^2\ (EXDIST + HEIGHT)] \qquad \text{Eq. 48}$$

The weight of the neutron shadow shield is calculated from equation 49.

$$WTNTSD = \pi/12\ (DNSHDN)\ [(DSHLD3)^2\ (EXDIST + HEIGHT + TSHLDG + TSHLDN) - (DSHLD2)^2\ (EXDIST + HEIGHT + TSHLDG)] \qquad \text{Eq. 49}$$

WTNTSD = point of neutron shield, gms

:q. 44 The weight of the neutron shield material container has been calculated from equation 50.

$$WTSHCR = \pi/4\ (DNSCON)\ (CONTHK)\ \left[(DSHLD2)^2 + (DSHLD3)^2 + 2(DSHLD2 + DSHLD3) \times \left[(TSHLDN)^2 + \left(\frac{DSHLD3 - DSHLD2}{2}\right)^2\right]^{0.50}\right] \qquad \text{Eq. 50}$$

tor

q. 45 WTSHCR = weight of shield container material, gms

amma

Subroutine 4: Generator Calculations The total radiator area required for the thermoelectric elements is calculated from equation 51.

ST

q. 46 $$TOTSFA = TWATTE \times RAPCPL/PWRCPL \qquad \text{Eq. 51}$$

e
n

TOTSFA = total surface area, cm^2
TWATTE = total watts output
RAPCPL = radiator area per couple, cm^2
PWRCPL = power per couple, watts

The total generator length necessary to provide this area has been calculated from equation 52.

q. 47

m

$$TGNLGT = \left[\frac{(2 \times TOTSFA)}{\pi\ (DIAPAY + DSHLD3)^2} - \frac{(PAYDIA - DSHLD3)^2}{2}\right]^{1/2} \qquad \text{Eq. 52}$$

q. 48

The generator weight is then calculated from equation 53.

$$GENWT = TWATTE/WATPLB \qquad \text{Eq. 53}$$

GENWT = generator weight, pounds
TWATTE = total watts required
. 49 WATPLB = watts per pound

If the generator length required, TGNLGT, is greater than the 15 feet minus the shielding thicknesses which are allowed, then this allowance must be increased. This is done in the Executive Routine, and the calculations in Subroutines 3 and 4 are then

repeated until an adequate allowance is made for this length. Finally, the Executive Routine prints out the answers which have been calculated.

The average running time is 1.8 seconds per case.

REFERENCES

1. Lyon, R. M., Liquid Metals Handbook, 2nd Edition, U. S. Govt. Printing Office, Washington, D. C., (1954) p. 187.

2. Jackson, C. B., Liquid Metals Handbook, Na(NaK) Supplement, U. S. Govt. Printing Office, Washington, D. C., (1955) p. 304.

3. MacFarlane, D. R., "A 200-watt Conduction-cooled Reactor Power Supply for Space Application," ANL-6694, March 1963, p. 17.

11. TIGER (Thermoelectric In-Pile Generator of Electricity Utilizing Reactor Heat Source

The TIGER type of thermionic space power generation system consists of a reactor core to which thermoelectric elements are directly attached, reactor shielding, and structure. The thermoelectric elements radiate heat from the end not attached to the reactor. This concept has maximum simplicity, since no fluid loops are needed, but it is limited by the number of elements that can be placed on the surface of the reactor core.

Routine TIGER consists of the following:

1. Executive Routine
2. Subroutine 1 - generation and core calculation
3. Subroutine 2 - shielding
4. Subroutine 3 - miscellaneous calculations
5. Subroutine 4 - data input
6. Subroutine 6 - thermoelectric data input
7. Subroutine Exit
8. Function $J_0(x)$
9. Function $J_1(x)$
10. Function $Y_1(x)$
11. Function $Y_0(x)$

Executive Routine The Executive Routine calls the subroutines in proper order and specifies what data is to be printed out. It also controls the logic flow of the program.

Subroutine 6 Subroutine 6, the first subroutine called by the Executive Routine, directs the computer to read data cards that describe the thermoelectric elements to be used in the subsequent calculations. The information on each card is as follows:

Run number
Thermal efficiency, percent
Power obtained per couple, watt
Radiator area required per couple, cm^2
Watts obtained per lb
Element length, cm
Radiator temperature, °K

This information is generated and punched into cards by another program. The information is stored on a scratch tape during the calculation. Subroutine Exit clears the scratch tape at the

conclusion of the calculations.

Subroutine 4 The next subroutine called is Subroutine 4, which controls the data input for TIGER. The following reactor and systems parameters are read in Subroutine 4.

Distance between payload and reactor core, ft
Payload diameter, ft
Density of the fuel, gm/cc
Atomic weight of fuel
Molecular weight of fuel
Thermal expansion coefficient, cc/cc°C
Approximate core temperature, °C
Control allowance, dimensionless
Spherical critical mass of fuel, gms
Extrapolation distance, cm
Reflector savings, cm
System electrical output, watts
Power needed to control the reactor, watts
Fuel costs in dollars/gram
Fuel fission cross-section, barns
Fuel absorption cross-sections for neutrons, barns
Density of gamma shielding material, gm/cc
Neutron emitted per fission, dimensionless
Mission length, hours
Allowable neutron dose to payload, neutrons/cm^2
Allowable gamma ray dose to payload, Rad carbon
Neutron and gamma ray absorption coefficient for neutron absorbing material, cm^{-1}
Neutron shielding material container thickness, in
Neutron and gamma absorption coefficients of neutron container material, cm^{-1}
Gamma absorption coefficient of fuel, cm^{-1}
Neutron and gamma absorption coefficients for gamma ray absorption material, cm^{-1}
Density of container for neutron absorbing material, gm/cc
Density of neutron absorbing material, gm/cc
Core height, ft
Run number.

This subroutine selects the first set of reactor and system parameters , calculates the system properties for each of the thermoelectric data cards, and then selects the next set of reactor and system properties.

Subroutine 2 ... maximum allowable core height of a solid right circular cylindrical reactor core is assumed. Based upon this core height and the thermal expansion and control allowances, the buckling of the fuel material is calculated as described under Subroutine 7 of HPSE. A core outside radius is then calculated using equation 1.

$$BUCSPH = \left(\frac{2.405}{RADCYL + DELEXT + DELSAV}\right)^2 + \left(\frac{\pi}{HEIGHT + 2(DELEXT + 2(DELSAV}\right)^2 \qquad \text{Eq. 1}$$

BUCSPH = buckling of fuel material, cm^{-2}
RADCYL = radius of cylindrical core, cm
HEIGHT = core height, cm
DELEXT = core extrapolation distance, cm
DELSAV = reflector savings, cm

The core surface area is then calculated from equation 2.

$$RADARA = 2(RADCYL + ELLGTH)(HEIGHT) \qquad \text{Eq. 2}$$

RADARA = radiator area, cm^2
ELLGTH = element length, cm

The electrical output required is the sum of the output from the system plus the power needed to control the reactor (see equation 3).

$$TWATTE = WATOUT + WATCON \qquad \text{Eq. 3}$$

TWATTE = total electrical watts producted by system
WATOUT = electrical output of system, watts
WATCON = electrical power needed to control reactor, watts

Then the radiator area required for the system is calculated using equation 4.

$$RADSFA = (TWATTE)(RAPCPL/PWRCPL) \qquad \text{Eq. 4}$$

RADSFA = required surface area, cm^2
RAPCPL = radiator area required per couple, cm^2
PWRCPL = power output per couple, watts

If the available radiator area (RADARA) is equal or greater than the required surface area (RADSFA), this core sizing is used. If not, then it is assumed that an annular-shaped, cylindrical reactor core will be used in order to increase the available surface area. The outer radius of the core is calculated by using the assumed core height in equation 5.

$$OUTRAD = \frac{RADSFA}{2\ \pi\ (HEIGHT)} - ELLGTH \qquad \text{Eq. 5}$$

The basic equations used to calculate the dimensions of annular reactor cores were taken from the report by Schuske and Bidinger (Ref. 1) and are listed below as equations 6 and 7.

$$J_o(BR_1) + C\ Y_o(BR_1) = 0 \qquad \text{Eq. 6}$$

$$J_1(BR_2) + C\ Y_1(BR_2) = 0 \qquad \text{Eq. 7}$$

R_2 = inner radius of core, cm

R_1 = outer radius of core including extrapolation distance plus reflector savings, cm

B = square root of the material buckling, cm^{-1}

C = a constant

J_o = Bessel function of first kind, zero order (BESZRO)

J_1 = Bessel function of first kind, first order (BES1)

Y_o = Bessel function of second kind, zero order (YZERO)

Y_1 = Bessel function of second kind, first order (YONE)

Equations 6 and 7 were derived by assuming the neutron flux equal to zero at the extrapolated outer radius, and the neutron current equal to zero at the inner radius.

The Bessel functions were calculated as separate functions in the program. The equations for the four Bessel functions used are listed below as equations 8-11.

$$J_o(x) = 1 - \frac{x^2}{2^2} + \frac{x^4}{(2^2)(4^2)} - \frac{x^6}{(2^2)(4^2)(6^2)} + \ldots\ldots \qquad \text{Eq. 8}$$

$$J_1(x) = \frac{x}{2}\left[1 - \frac{x^2}{(2)(2)} + \frac{x^4}{(8)(24)} - \frac{x^6}{(48)(192)} + \ldots\ldots\right] \qquad \text{Eq. 9}$$

$$Y_o(x) = J_o(x) \ln x + \frac{x^2}{(2^2)} - \frac{x^4\,\Omega_2}{(2^2)(4)^2} + \frac{x^6\,\Omega_3}{(2^2)(4^2)(6^2)} \ldots\ldots \qquad \text{Eq. 10}$$

where $\Omega_k = 1 + 1/2 + 1/3 + \ldots\ldots \frac{1}{k}$

$$Y_1(x) = \frac{1}{\pi}\left[J_1(x) \ln \frac{x}{2} - \sum_{k=0}^{\infty} \frac{(-1)^k}{(2)^{2k+1}} \frac{(x)^{2k+1}}{(k!)(k+1)!}\right. \qquad \text{Eq. 11}$$

$$\left.[\,\psi(k+1) + \psi(k)\,]\right]$$

where $\psi(k) = 0.57722 + 1 + 1/2 + 1/3 \ldots\ldots + \frac{1}{k}$

Using the material buckling and the calculated reactor outer radius in equation 6, the constant C is calculated, and then the reactor buckling and C are used in equation 7 to solve for the inner core radius. Once the inner radius, outer radius, and height of the core are known, the weight of the fuel can be calculated using equation 12.

$$\text{FUELWT} = \pi\,(\text{OUTRAD}^2 - \text{COREIR}^2)\,(\text{HEIGHT})\,\text{DNSFS3}) \qquad \text{Eq. 12}$$

OUTRAD = the outer radius of the core, cm
COREIR = core inner radius, cm
FUELWT = weight of fissionable atoms, gms

The weight of the reactor core is calculated from equation 13.

COREWT = FUELWT (FMOLWT/FATMWT) Eq.

COREWT = weight of core, gms

The fuel cost is calculated from equation 14.

FULCST = (FUELWT) (CSTPGM) Eq.

FULCST = cost of fuel, dollars
CSTPGM = cost of fuel, $ per gram

Finally, the weight of the radiator and of the generator elements is calculated with equation 15.

WTRDGN = TWATTE/WATPLB Eq.

WTRDGN = weight of radiator and generator, lbs
WATPLB = specific power of radiator-generator, watts/lb

Subroutine 2 Shielding Calculations Subroutine 2 is very similar to the shielding subroutine in HORSE. The equations are virtually identical with the exception that the allowance for self-shielding of the core from the gamma rays generated within it is only equal to the core height divided by four, rather than the core height divided by two for cases where the reactor has an internal annulus.

Subroutine 3 Miscellaneous Calculations In Subroutine 3 miscellaneous calculations are done; the core weight is converted to pounds, and the weight of the reactor is specified by adding 100 lbs miscellaneous equipment. See equation 16.

WTREAC = COREWT + 100 Eq. 1

WTREAC = weight of reactor, pounds
COREWT = weight of reactor core, pounds

The weight of the structure is found from equation 17.

$$WTSTRT = \frac{0.10\ (DISTCP)}{15}\ (WTREAC + WTRDGN + WTSHLD)$$ Eq. 1

WTSTRT = weight of structure, pounds
DISTCP = distance between reactor core and paylod,ft
WTSHLD = total weight of shielding, pounds

The overall system performance in pounds/KW is calculated in equation 18.

$$PDSPKW = 1000\ (WTREAC + WTSHLD + WTSTRT + WTRDGN/WATOUT \qquad \text{Eq. 18}$$

PDSPKW = system performance, pounds/KW

The following information is printed out on a summary sheet for each run:

Run numbers for the system properties and for the thermoelectric properties
Watts/lb for the system
Watt output of the system
Core height, cm
Core diameter, cm
Thermoelectric element length, cm
Distance between core and payload, cm
Core weight, pounds
System performance, pounds/KW
Total shield weight, pounds
Efficiency of thermoelectric elements, percent
Fuel weight, gms
Fuel cost, dollars
Reactor weight, pounds
Cold-junction temperature of radiator, °K

The following information calculated in Subroutine 1 is printed out:

Run numbers
Fuel density - cold
Fuel density after thermal expansion
Fuel density after thermal expansion and with control allowance
Critical mass of the sphere with these allowances, gm
Critical radius of spherical mass, cm
Buckling for sphere, cm^{-2}
Contribution of height of cylinder to buckling, cm^{-2}
Cylinder radius, cm
Core outside diameter, cm
Radiator diameter, cm
Available radiator area on solid core, cm^2
Total electrical output of system, watts
Required surface area, cm^2
Buckling of cylindrical core in radial direction, cm^{-2}

Core inner radius, cm
Quantities BR_1, BR_2, from the solution of the Bessel equations
Core weight, gms
Radiator-generator weight, lbs
Fuel weight, gms
Fuel cost, $

The information printed out from Subroutine 2 includes:

Number of atoms per cc of fuel inside the reactor core
Macroscopic cross-sections of the fuel for fission and neutron absorption, barns
Infinite multiplication factor
Fissions per sound
Total neutrons emitted per second
Total neutrons emitted per mission
Required neutron attenuation
Gamma rays emitted per second
Total gamma rays emitted per mission
Necessary gamma ray attenuation
Thickness of gamma shielding, cm
Thickness of neutron shielding, cm
Extrapolation distance, cm
Shielding diameter at the core gamma shield interface, cm
Shielding diameter at gamma neutron shield interface, cm
Shielding diameter at the rear of the neutron shield, cm

The information printed out from Subroutine 3 is as follows;

System performance, lbs/KW
Core weight
Weight of reactor, lbs
Weight of neutron shield, lbs
Weight of total shielding material, lbs
Weight of the neutron shielding container, lbs
Weight of the gamma shield, lbs
Weight of the structure, lbs
Watts per lb rating for system.

The average running time per case is slightly over two seconds each.

REFERENCES

1. Schuske, C. L., and Bidinger, G. H., "An Empirical Interpretation of Annuli Critical Mass Data," Dow Chemical Co., RFP-149, (Oct. 1959), pp. 25-26.

III. SWIFT (System for Power Generation With In-Pile Fluid-Cooled Thermoelectric Elements)

Routine SWIFT is an evaluation of a nuclear space power system in which the thermoelectric elements are located on the outside and in some cases on the inside of the reactor core, but the heat is removed from the elements via coolant loop and transported to radiator elements located elsewhere. The principal components of this system are the reactor core, the thermoelectric elements, the reactor shielding, the structure weight, and the weight of the radiator. Routine SWIFT consists of the following:

1. Executive Routine
2. Subroutine 1 - generator and core calculations
3. Subroutine 2 - shielding calculation
4. Subroutine 3 - miscellaneous calculation
5. Subroutine 4 - input data
6. Subroutine DUMBO - external ear radiator fin calculation
7. Subroutine 6 - thermoelectric input data
8. Subroutine Exit
9. Function J_o (x)
10. Function J_1^o (x)
11. Function Y_1 (x)
12. Function Y_1^o (x).

Executive Routine The Executive Routine calls the other subroutines in the proper sequence, controls the logic flow, and dictates the printout of desired information.

Subroutine 6 The first subroutine called, Subroutine 6, dictates that the data cards containing information on the thermoelectric elements be read onto a scratch tape. The information read in consists of the following:

Run number
Generator efficiency in percent
Power produced per couple in watts
Cross-sectional area of per couple in sq cm
Watts per lb
Element length in cm
Radiator temperature, °K.

Subroutine Exit erases the scratch tape after the calculations are finished.

Subroutine 4 The next subroutine called is Subroutine 4, which directs the input of data. The following data are read in:

Distance between reactor core and payload, ft
Diameter of payload, ft
Density of fuel, gm/cc
Fuel atomic weight
Fuel molecular weight
Volumetric thermal expansion coefficient of fuel, cc/cc °C
Approximate core temperature, °C
Control allowance
Critical mass for sphere of fuel, gm
Extrapolation distance, cm
Reflector savings, cm
Power needed to control the reactor, watts
Fuel cost, $ per gram
Fission and absorption cross-section of fuel, barns
Number of neutrons given off per average fission
Mission length, hrs
Allowable neutron dose to payload, neutrons/cm^2
Allowable gamma ray dose to payload, Rad
Neutron and gamma absorption coefficients for neutron shielding material, cm^{-1}
Thickness of neutron shielding container, inches
Neutron and gamma cross-sections of neutron shield container, cm^{-1}
Gamma cross-section of fuel, cm^{-1}
Neutron and gamma cross-sections for gamma shielding material, cm^{-1}
Density of shield container material, gm/cc
Density of neutron shield material, gm/cc
Core height, ft
Run number
Electrical output of system, watts
Density of gamma shielding material, gm/cc
Ratio of core height to diameter.

Subroutine 1 Next, Subroutine 1 is called to size the reactor core and generator. The core and generator for SWIFT could have one of three configurations: 1) the elements could all be on the exterior of a solid cylindrical core; 2) the elements could all be on the exterior of an annular cylindrical core; 3) the elements could be mounted on both the exterior and the interior of an annular cylindrical core. The procedure followed in Subroutine 1 is to investigate the possibility of placing all of the elements on the exterior of a solid cylindrical

core. The equations used in doing this consist of the buckling equation and the equations which modify the density of the fuel materials for thermal volumetric expansion and for control allowance, as given in Routine HORSE. The core height is assumed and the radiator area available on its exterior is calculated. The cross-sectional area allowed for elements is equal to the cross-sectional area per element times 1.25 to allow for close spacing. The required surface area is computed from equations 1 and 2.

$$TWATTE = WATOUT + WATCON + WATTEP \qquad \text{Eq. 1}$$

$$RADSFA = 1.25\ (CSACPL)\ (TWATTE)/PWRCPL \qquad \text{Eq. 2}$$

TWATTE = total power produced, watts
WATOUT = electrical output from system, watts
WATCON = electric power to control reactor, watts
WATTEP = power required for pumping coolant through system, watts
RADSFA = radiator surface area required, cm^2
CSACPL = cross-sectional areas/couple, cm^2
PWRCPL = electrical output/couple, watts.

A constant factor of 100 watts was used for WATCON. WATTEP was assumed to be 5% of the output from the system.

When the element area available on the exterior of the solid core exceeds that required, the core height is shortened by the ratio of required surface area to actual surface area and the calculations are repeated. If the required surface area exceeds that available on the exterior of the solid core, then an annular solution is tried.

The equations for annular reactor cores used are described in Routine TIGER. If the radius of the annulus exceeds the element length plus 0.6 centimeter (radius of a coolant tube), then elements can be placed both on the exterior and the interior of the reactor core. If the core inner radius is less than this figure, then elements are placed only on the core exterior. The fuel weight, core weight, fuel cost, and weight of thermoelectric elements are calculated as in previous routines.

Subroutine 2 The shielding equations used for SWIFT are virtually identical with those used for Routine TIGER.

Subroutine 3 Subroutine 3 calculates core weight, reactor weight, weight of gamma shield, weight of neutron shield, weight of shield container, total shield weight, and weight of structure in pounds. The weight of the structure differs from the previous equations in that the weight of the radiator is included as a separate item. See equation 3.

$$WTSTRT = \frac{(0.10\ DISTCP)}{15}\ (WTREAC + WTRDGN + WTSHLD + WTRAD) \qquad \text{Eq. 3}$$

WTSTRT = weight of structure, pounds
DISTCP = distance between core and payload, ft
WTREAC = weight of reactor, pounds
WTRDGN = weight of thermoelectric elements exclusive of radiator, pounds
WTSHLD = weight of shield components, pounds
WTRAD = weight of radiator, pounds.

The weight of the reactor is equal to the core weight plus the 100-lb allowance for controls and miscellaneous instruments. The weight of the radiator is calculated from Subroutine DUMBO.

Subroutine DUMBO All the radiator area that can be placed between the reactor shielding and the payload is mounted on the surface of the truncated frustrum of a cone. Additional radiator area is available on the cylindrical surface of the core. Calculation of this surface area using equations 4, 5 and 6 is done to determine if this amount of radiator area is sufficient.

$$SEP = DISTCP - (TSHLDN + TSHLDG) \qquad \text{Eq. 4}$$

$$SIDE = [(SEP)^2 + (PAYDIA - DSHLD3)^2]^{1/2} \qquad \text{Eq. 5}$$

$$AREA = \pi \left[DSHLD3 + \frac{(PAYDIA - DSHLD3)}{2}\right] (SIDE) + 2\pi\ (HEIGHT)\ (RADIUS + ELLGTH) \qquad \text{Eq. 6}$$

SEP = separation between neutron shield and payload, cm
TSHLDN = thickness of neutron shield, cm
TSHLDG = thickness of gamma shield, cm
SIDE = length of side of frustrum, cm
DSHLD3 = diameter of neutron shield, cm

AREA = surface area available for radiator between shield and payload and on core, cm^2
RADIUS = radius of reactor core, cm
ELLGTH = element length, cm
HEIGHT = core height, cm.

Next, the radiator temperature is assumed to be 10°C lower than the cold-junction temperature punched into the cards. See equation 7.

$$TRAD = TC-10 \qquad \text{Eq. 7}$$

TRAD = temperature radiator, °K
TC = cold-junction temperature of thermo-electric elements, °K.

Next, the heat radiated by this area is calculated using equation 8.

$$QRAD = 5.672 \times 10^{-12} (0.88) (AREA) (TRAD)^4 \qquad \text{Eq. 8}$$

QRAD = total amount of heat radiated, watts.

0.88 is the emittance of the radiator material. The amount of heat which must be radiated for the system is calculated from equation 9.

$$QREQ = \frac{TWATTE \times 100}{EFFGEN} \qquad \text{Eq. 9}$$

QREQ = heat which is required to be radiated, watts
EFFGEN = generator efficiency, percent.

The total radiator area required is calculated from equation 10.

$$AREA = AREA \frac{(QREQ)}{(QRAD)} \qquad \text{Eq. 10}$$

Volume of radiator materials is calculated from equation 11.

$$VOL = AREA \times 0.127 \qquad \text{Eq. 11}$$

VOL = volume radiator volume material, cc.

The thickness of the radiator is assumed to be 0.127 cm. In cases where the radiator will not fit in the space between the shielding and the payload, then additional area is assumed to be available on two large, wing-shaped projections extending radially from the reactor core. These large projections can radiate heat from both sides; hence, the volume of radiator material in these projections is assumed to be only 0.0635 times the radiator area. The weight of radiator is then calculated from equation 12.

$$WTRAD = VOL \times 8.0 \qquad \text{Eq.}$$

WTRAD = weight of radiator, gm.

The specific gravity of the radiator material is assumed to be 8.0 gms/cc.

Executive Routine The Executive Routine prints out the following information from Subroutine 1:

Run numbers
Densities of fuel, gm/cc
Material with and without thermal expansion and control effects, gm/cc
Modified spherical critical mass of fuel, gms
Radius of the spherical critical mass, cm
Material buckling
Height contribution to buckling of the cylinder, cm^{-2}
Cylindrical radius, cm
Core outside diameter, cm
Radiator area, cm^2
Total watts produced by system
Radiator surface area required
Cylinder buckling minus the height contribution, cm^{-2}
Core inside radius, cm
The quantities BR_1, BR_2, and constant used in the Bessel equation solutions
Core weight
Weight of thermoelectric elements
Fuel weight
Fuel cost
Watts required per pump
Cross-sectional area per couple, cm^2
Inner and outer annular radii, cm.

The printout for Su routine 4 includes:

Atoms per cc of fuel in core
Macroscopic cross-sections for fission and absorption by fuel, barns
Infinite multiplication factor
Fissions occurring per second
Total neutrons emitted from core per second
Total neutrons emitted per mission
Required neutron attenuation
Eq. 12
Total gamma rays emitted per second
Total gamma rays emitted per mission
Required gamma ray attenuation
Thickness of gamma shielding, cm
Thickness of neutron shielding, cm
Extrapolation distance, cm
The three shields' diameters, cm.

Calculated information printed out from Subroutine 3 includes:

System performance, lbs/KW
Watt/lb rating
Core weight
Weight of radiator, lbs
Weight of reactor, lbs
Weight of neutron shield, lbs
Total shield weight, lbs
Weight of shield container, lbs
Weight of gamma shield, lbs
Weight of structure, lbs.

The following information is printed out on a summary sheet:

Run number
Watts/lb
System performances, pounds/KW
Core height, cm
Diameter core, cm
Element length, cm
Distance between core and payload, cm
Core weight, lbs
Weight of shield, lbs
Thickness of neutron shield, cm
Generator efficiency, percent
Fuel weight, lbs
Fuel cost, dollars
Core inner radius, cm
Radiator temperature, °K.

IV. PROPERTY VALUES USED

A. General Properties

The following general properties have been selected or assumed for use in calculations on HORSE, TIGER, and SWIFT.

1. System Parameters

Payload diameter - 3 ft
Minimum distance between core and payload - 15 ft
Mission life - 10,000 hours
Control allowance - 4 atom percent
Maximum allowable temperature drop through system - 100°F
Maximum allowable log mean Δt inside core - 300°F.

2. Reactor Material Properties

Fuel		plutonium carbide
Atomic weight		239
Molecular weight		251
Density of fuel		13.6 gms/cc
Spherical critical mass		23,700 gms
Thermal expansion coefficient		18.9×10^{-6} cc/cc°F
Gamma absorption cross-section		0.593 cm^{-1}
Fuel extrapolation distance		1.5 cm
Fuel cost		$10.00/gram
Reflector material		BeO
Density of reflector		2.8 gm/cc
Allowable neutron dose to payload	total	1×10^{13} neutron/cm^2
	direct	5×10^{12} neutron/cm^2
	scattered	5×10^{12} neutron/cm^2
Allowable gamma dose to payload	total	1×10^{7} rad(c)
	direct	9×10^{6} rad(c)
	scattered	1×10^{6} rad(c)
Average number of neutrons/fission		2.98
Fission cross-section		1.78 barns
Neutron absorption cross-section		0.153 barns.

3. Coolant System Properties

Coolant	liquid lithium
Atomic weight	6.94
Density	0.48 gms/cc
Specific heat	1.0 Btu/lb °F
Thermal conductivity	28.2 Btu/ft hr °F
Viscosity	0.20 centipoise
Neutron absorption cross-section	0.0301 barns
Tubing material	molybdenum
Atomic weight	95.95
Density	10.2 gm/cc
Neutron absorption coefficient	0.0 barns.

4. Shielding Properties

Gamma shielding material	depleted uranium
Density	18.7 gm/cc
Gamma absorption cross-section	0.62 cm^{-1}
Neutron removal cross-section	0.170 cm^{-1}
Neutron shielding material	lithium hydride
Density	0.710 gm/cc
Gamma absorption cross-section	0.0241 cm^{-1}
Neutron removal cross-section	0.110 cm^{-1}
Neutron shielding container	stainless steel
Thickness	0.109 inches
Density	7.9 gm/cc
Gamma absorption coefficient	0.279 cm^{-1}
Neutron absorption coefficient	0.167 cm^{-1}.

B. Specific Parameters

The following specific parameters have been obtained by means of preliminary calculations for use in HORSE, TIGER, and SWIFT.

1. HORSE

Reactor Parameter

Power levels	3, 30, and 350 KW
Coolant tube outside diameter	0.50 inches
Coolant tube wall thickness	0.050 inches
Fluid velocity	15 feet/sec
Reflector thickness	20 cm
Core height (3 KW)	0.60 ft
(30 KW)	0.80 ft
(350 KW)	0.90 ft.

Generator Data

Element diameter, inches	3/16	3/16	3/16
Run number	9102	9048	9118
Generator efficiency, %	2.52	4.46	2.84
Power/couple, watts(e)	0.331	0.340	0.0757
Radiator area/couple, cm^2	1.41	1.64	0.880
Watts(e)/lb	59.4	31.8	6.31
Element length, cm	0.40	1.00	2.00
Radiator temperature, °K	1023	873	1023.

2. TIGER

Reactor Parameters

Power levels	3, 30 KW
Core height (3 KW)	8.0 ft
(30 KW)	15.0 ft

Generator Data

Element diameter, inches	3/16	3/16	3/16
Run number	9102	9048	9118
Thermal efficiency, %	2.53	4.60	2.85
Power/couple, watts	0.331	0.340	0.0757
Radiator area/couple, cm^2	1.40	1.56	0.880
Watts(e)/lb	71.1	50.8	8.87
Element length, cm	0.40	1.00	2.00
Radiator temperature, °K	1023	873	1023

3. SWIFT

Reactor Parameters

Power levels	3, 30, and 350 KW
Core height to diameter ratio	6.0 for 3 KW 5.0 for 30 KW

Generator Data

Element diameter, inches	3/16	3/16	3/16
Run number	9102	9048	9118
Thermal efficiency, %	2.56	4.66	2.88
Power/couple, watts	0.331	0.341	0.0757

Cross-sectional area/couple, cm^2	0.356	0.356	0.356
Watts/lb	137.6	83.0	11.44
Element length, cm	0.40	1.00	2.00
Radiator temperature, °K	1023	873	1023.

DISTRIBUTION LIST

CYS	ACTIVITIES AT WPAFB
2	SEPIR (Library)
1	SEPI
1	APX
1	APE
1	API
1	APP
1	APIP-1
1	APIP-3
6	APIP-2 (Capt. R. Morrow)
	OTHER DOD ACTIVITIES
1	Lt. Col. Lew Allen ODD R and E OSD - The Pentagon Washington 25, D. C.
1	Mr. Henry Randall Office of Asst. Secty. of Defense Research and Engineering Washington 25, D. C.
1	Office of Asst. Secty. of Defense for R and D Attn: Physical Sciences Div. Dr. J. T. Holloway Washington 25, D. C.
26	DDC Cameron Station Alexandria, Virginia 22314

DISTRIBUTION LIST (Cont'd)

CYS	ARMY
1	Office of the Secretary of the Army, R and D Attn: Dr. J. B. Edson Washington 25, D. C.
1	Commanding Officer Attn: Mr. Phil Youngblood ABMA Guidance and Control Lab Redstone Arsenal, Alabama
1	U. S. Army Research Office (Durham) Attn: Dr. Wilhelm Jorgenson Box CM, Duke Station Durham, North Carolina
1	U. S. Army Electronics R and D Labs. Power Sources Div. (SEIRA/PSA) Ft. Monmouth, N. J. 07703
1	U. S. Army Engineer R and D Labs. Electrical Power Branch (SMOFB-EP) Ft. Belvoir, Va. 22060
	NAVY
1	Chief, Bureau of Ships Department of the Navy Attn: Cdr. P. G. Beirl (Code 450) Washington 25, D. C.
1	Director U. S. Naval Research Lab. Attn: Code 2027 Washington 25, D. C.
1	Naval Research Laboratory (Code 5230) Attn: Mr. B. James Wilson Washington 25, D. C.
1	Bureau of Naval Weapons (Code RAAE-511) Department of the Navy Attn: Mr. Milton Knight Washington 25, D. C.
1	Naval Research Laboratory Attn: Dr. Paul Egli Washington 25, D. C.

DISTRIBUTION LIST (Cont'd)

CYS	OTHER U. S. GOVERNMENT AGENCIES (Cont'd)
1	Oak Ridge National Lab Attn: Mr. A. J. Miller P. O. Box Y Oak Ridge, Tennessee
2	Scientific and Technical Information Facility Attn: NASA Representative (SAK/DL) P. O. Box 5700 Bethesda, Maryland 20014
1	NASA-Manned Spacecraft Center Attn: Mr. J. Cioni (Ep 21) 2101 Webster-Seabrook Rd. Houston, Texas 77058
1	NASA-Goddard Space Flt. Ctr. Attn: Mr. J. Epstein (Code 636) Greenbelt, Maryland
1	NASA Attn: Mr. Walter Scott 1512 H Street, NW Washington 25, D. C.
1	NASA-Lewis Research Center Nuclear Power Technology Branch Attn: Mr. R. A. Lindberg 21000 Brookpark Cleveland 35, Ohio
1	Mr. James F. Morris NASA Lewis Research Center 21000 Brookpark Road Cleveland 35, Ohio
100	Chief, Input Section Clearinghouse for Federal Scientific and Technical Information (CFSTI) Sills Building 5285 Port Royal Road Springfield, Virginia 22151
1	ARPA Attn: Dr. J. H. Huth Pentagon, Rm. 3E-147 Washington 25, D. C.

DISTRIBUTION LIST (Cont'd)

CYS	AIR FORCE (Cont'd)
1	AFCRL (CPRSCP, Dr. A. D. Johnson) L G Hanscom Field Bedford, Mass.

OTHER U. S. GOVERNMENT AGENCIES

1	USAEC Division of Reactor Development Auxiliary Power Branch Attn: Mr. Robert T. Carpenter Washington 25, D. C.
1	USAEC Division of Reactor Development Attn: Cdr. W. A. Schoenfeld, Chief, Direct Conversion Branch Washington 25, D. C.
1	U. S. Atomic Energy Commission Office of Technical Information Extension Attn: M. L. Pfluger P. O. Box 62 Oak Ridge, Tennessee
1	Lt. Col. Kenneth R. Chapman, USAF U. S. Atomic Energy Commission SNAP Reactor Branch, DRD Washington, D. C. 20545
1	Dr. J. D. Lafleur, Jr. Auxiliary Power Branch Div. of Reactor Development USAEC Washington 25, D. C.
1	Mr. T. W. McIntosh Advanced Space Reactor Branch Division of Reactor Development USAEC Washington 25, D. C.
1	LDCR J. P. Culwell Isotopic Power Branch Div. of Reactor Development USAEC Washington 25, D. C.

DISTRIBUTION LIST (Cont'd)

CYS	NAVY (Cont'd)
1	Bureau of Ships (Code 342B) Department of the Navy Attn: Mr. Bernard B. Rosenbaum Washington 25, D. C.
1	Commanding Officer and Director U. S. Naval Marine Engineering Lab. Attn: Library (J. F. Williams) Annapolis, Md.
1	Dr. James B. Friauf Bureau of Ships (Code 660) Department of the Navy Washington 25, D. C.

AIR FORCE

1	SSD (SSTRE, Maj. Iler) AF Unit Post Office Los Angeles, Calif. 90045
1	SSD (SSZAE-3) AF Unit Post Office Los Angeles, Calif. 90045
1	SSD (SSZME, Capt. Origer) AF Unit Post Office Los Angeles, Calif. 90045
1	SSD (SSZAS) AF Unit Post Office Los Angeles, Calif. 90045
1	AFRD (CRZAP, Dr. N. Rosenberg) L G Hanscom Field Bedford, Mass.
1	Rome Air Development Center Attn: RASSM (Mr. F. J. Mellura) Griffiss AFB, N. Y.
1	AFWL (WLDN-2) Kirtland AFB New Mexico 87117
1	RADC (RCVGM) Griffiss AFB, N. Y.
1	RADC (RACGP, Mr. Richards) Griffiss AFB, N. Y.

DISTRIBUTION LIST (Cont'd)

CYS	NON-GOVT INDIVIDUALS AND ORGANIZATIONS
1	Aerospace Corporation Attn: Library Technical Documents Cp. P. O. Box 95085 Los Angeles, Calif. 90045
1	Jet Propulsion Laboratory Calif. Institute of Technology Attn: Mr. Paul Goldsmith 4800 Oak Grove Drive Pasadena, California
1	Mr. Owen S. Merrill Jet Propulsion Laboratory 4800 Oak Grove Drive Pasadena 3, California
1	General Atomic Division General Dynamics Corporation P. O. Box 608 San Diego 12, California
1	Power Information Center Moore School Building 200 S. 33rd Street Philadelphia 4, Pa.
1	Martin-Marietta Corp. Nuclear Division Baltimore, Maryland
1	Battelle Memorial Institute 505 Columbus Ave. Columbus, Ohio
1	Atomics International P. O. Box 309 Canoga Park, California
1	Minnesota Mining and Mfg. Co. 2301 Hudson Road St. Paul 19, Minnesota
1	Melpar Inc. 3000 Arlington Blvd. Falls Church, Va.

DISTRIBUTION LIST (Cont'd)

CYS	NON-GCVT INDIVIDUALS AND ORGANIZATIONS (Cont'd)
1	Radio Corporation of America Attn: Mr. R. L. Klem 415 S. Fifth St. Harrison, N. J.
1	Advanced Technology Laboratory General Electric Company Schenectady, New York
1	Thermoelectric Division General Instrumer Corporation Attn: Mr. R. Rush 65 Gouverneur St. Newark 5, New Jersey
1	Westinghouse Electric Corp. Aerospace Electrical Div. Attn: Mr. D. Naumer Lima, Ohio
1	Space Technology Laboratory Attn: Lt. Col. G. Austin, Ret. 1 Space Park Redondo Beach, California
1	Dr. George C. Szego Institute for Defense Analyses Research and Engineering Support Div. 1666 Connecticut Ave., NW Washington 9, D. C.
1	Dr. Robert C. Hamilton Research and Engineering Support Div. Institute for Defense Analyses 1666 Connecticut Ave., NW Washington 9, D. C.
1	Monsanto Dayton Laboratory Attn: Mr. C. M. Henderson 1515 Nicholas Road Dayton 7, Ohio